DISSERTATION

# ENGINEERING A BIOMIMETIC PERIOSTEUM ON CORTICAL BONE ALLOGRAFTS FOR THE RECONSTRUCTION OF CRITICAL-SIZED BONE DEFECTS IN MICE

Submitted by

Raimundo Romero

Graduate Degree Program in Bioengineering

In partial fulfillment of the requirements

For the Degree of Doctor of Philosophy

Colorado State University

Fort Collins, Colorado

Fall 2017

Doctoral Committee:

Advisor: Matt J. Kipper
Co-Advisor: Nicole P. Ehrhart

John D. Kisiday
Alan R. Schenkel

ABSTRACT

ENGINEERING A BIOMIMETIC PERIOSTEUM ON CORTICAL BONE ALLOGRAFTS FOR THE RECONSTRUCTION OF CRITICAL-SIZED BONE DEFECTS IN MICE

Load bearing bone allografts suffer from clinical failure due to low allograft-host tissue integration. Removal of the periosteum, a thin tissue layer on bone with a high regenerative capacity, is responsible for bone allografts' decreased clinical performance. This interdisciplinary project addressed this problem by creating multiple engineered periostea on mice bone allografts. Using a polysaccharide biomaterial, chitosan, tissue engineering scaffolds constructed on these bone allografts were modified with the glycosaminoglycan, heparin, and a chitosan derivative, trimethyl chitosan, to create periostea with different scaffold morphologies yet similar surface chemistries. Cell instructive cues such as growth factors fibroblast growth factor-2 (FGF-2) and transforming growth factor-β1 (TGF-β1) were adsorbed onto the engineered periostea and found to release up to 14 and 7 days *in-vitro*, respectively. Engineered allografts were found to support adipose-derived stem cell (ASC) adhesion and proliferation. FGF-2 and TGF-β1 delivered from the engineered allografts to ASC supported an osteoprogenitor phenotype in ASC and did not inhibit alkaline phosphatase and receptor activator of nuclear factor-kappaB (RANKL) protein expression. From *in vitro* results, the nanofiber engineered periosteum was found to be the most cytocompatible scaffold and was selected for subsequent implantation in a pre-clinical mouse critical-sized femoral defect model. We assessed the engineered periosteum's efficacy on modulating allograft healing and incorporation. We confirmed the engineered allografts successfully delivered ASC, FGF-2, and

TGF-β1 to the femur defect and found ASC persisted in the femur defect for at least 7 days, similar to other reports in the literature. At week 6, microcomputed tomography results of excised femurs showed no statistical difference in new bone volume formation between experimental groups. However, treatment groups containing ASC showed a trend of at least 24% more bone volume compared to their respective cell-free controls suggesting possible therapeutic effects of ASC. Union ratio and histological analysis both confirmed the nanofiber engineered periosteum did not degrade at 6 weeks and inhibited allograft incorporation. Subsequent relative gene expression experiments showed that ASC maintained an undifferentiated phenotype in response to FGF-2 and TGF-β1 delivered from chitosan nanofibers. Overall, this project developed a novel polysaccharide-based engineered periosteum for delivering growth factors and progenitor cells to a bone defect for regenerative medicine applications.

# ACKNOWLEDGMENTS

Numerous individuals made this work possible. I will attempt to express my sincere gratitude to all, knowing that as a fallible human, I will surely miss some.

First, I would like to recognize my advisor Dr. Matt J. Kipper for his exceptional role as a mentor, colleague, and friend. His keen intellect is a wonderful resource to have for all things research and life. Our many discussions have formed me to be the scientist I am today and I am forever grateful. I am inspired by Matt's approach to science and only hope I can emulate his excitement for discovery in my future career. Thank you for being a patient mentor when I was exploring and developing new research protocols or writing (which always took longer than I anticipated).

Second, I would like to thank my committee members, Dr. Nicole P. Ehrhart, Dr. John Kisiday, and Dr. Alan Schenkel, who provided countless suggestions on my experimental designs and challenged me to always look deeper into the data. Nicole, thank you being wonderful co-advisor and collaborator and for always making time for meetings even with your busy clinical schedule. John, thank you for your input and advice on designing my PCR experiments. Alan, thank you for your insightful critiques and for recommending I take a grant writing class, even when I didn't want to.

Third, I thank my research colleagues past and present who assisted with the research or gave feedback on research presentations including Dr. Laura Place and Hasan Hedayati. I would especially like to thank John Travers, Emilie Ashbury, and Attie Pennybaker who performed sample and data collection as well as data analysis which was crucial for the papers published from this work. Dr. Ruth Rose, Dr. Megan Aanstoos, and Laura Chubb of the Ehrhart lab are

recognized for their help with the *in vivo* animal work. In addition, Laura Chubb's assistance with cell culture and lab ordering made this research go smoother.

Fourth, I thank my colleagues in the School of Biomedical Engineering, Dr. Susan P. James and Dr. Melissa Reynolds for the opportunity to rotate through their research labs in my first year of the program which helped me get my feet wet in research. School of Biomedical Engineering staff members Sara Mattern and Brett Beal are recognized for creating a welcoming friendly department culture and for their administrative assistance in remembering when and which forms to turn in and answering my countless e-mails.

Fifth, several CSU faculty and staff are recognized for equipment training, use, and discussions which were invaluable to obtaining the data presented in this work. These include: Drs. Pat McCurdy, Chris Rithner, and Karolien Denef from the Central Instrument Facility in the Department of Chemistry; Dr. Ketul Popat from the Department of Mechanical Engineering; Dr. Christine Peebles and Tim Gonzalez from the Department of Chemical and Biological Engineering; Dr. Susan Delong from the Department of Civil and Environmental Engineering; Dr. Dawn Duval from the Clinical Sciences Department. Also, the following faculty and staff located at other institutions are also recognized for their assistance during this project including: Sara Gookin, Dr. Snehal Shetye, Dr. Salman Khetani, and Dr. Hani Awad, specifically for providing the union ratio algorithm.

I would be remiss to not mention my funding sources which supported me during my time in graduate school which included the Alliances for Graduate Education and the Professoriate (AGEP) Fellowship, Musculoskeletal Transplant Foundation, and Bioscience Discovery Evaluation Grant Program.

Finally, I would like to acknowledge my friends and family whose social, emotional, and spiritual support saw me through the adventure of graduate school. In particular, I thank my parents, who may not have directly taught me about science growing up but instilled in me an appreciation for the education and opportunities I have received in my life. They have loved me and supported me every step of the way and for that, I am truly thankful. To my sister Jacqueline, who has always believed in me and challenged me to aim higher personally and professionally. To Erin, whose compassionate and adventurous spirit keeps me grounded and provided crucial support during the last years of grad school. I love you babe!

# DEDICATION

*Para mi familia, que me ha apoyado toda mi vida.*

TABLE OF CONTENTS

# CHAPTER 1 INTRODUCTION

## 1.1. Motivation

Significant bone injuries such as traumatic bone loss or osteosarcoma resection can lead to the formation of a critical-sized, or non-healing, defect in the remaining bone. Clinical intervention strategies may include the transplantation of a bone graft. Bone autografts are regarded as the gold standard treatment, often resulting in union and healing between the graft and native bone tissue.[1] This healing is facilitated by native bone architecture of the autograft being left intact, including the periosteum. The periosteum actively participates in the healing of injured bone by providing necessary osteoprogenitors and osteoinductive factors.[2,3] However, bone autografts possess inherent limitations due to limited autograft size and complications such as donor site morbidity. In contrast, bone allografts overcome these limitations by using cadaveric bone tissue. However, risks such as disease transmission, infection, rejection, and suboptimal healing are valid concerns for bone allografts. Fortunately, these risks can be mitigated by stringent donor screening and allograft processing. Tissue procurement organizations subject aseptically harvested bone allografts to cleansing procedures which may include: antibiotic and chemical washes to minimize bacterial contamination and cellular material removal, respectively; allograft freezing to minimize allograft antigenicity; and terminal sterilization via ethylene oxide exposure or gamma irradiation.[4,5] Unfortunately, removing the periosteum from bone allografts discards a rich reservoir of extracellular matrix (ECM), osteoinductive growth factors, and osteoprogenitors involved the bone healing process.[3,6,7] Mimicking bone autograft healing through a tissue engineered periosteum is a logical strategy to improve the osseointegration of bone allografts. Periosteum-inspired approaches that emulate the

native bone fracture healing cascade in bone allografts could have a significant impact on alleviating the global burden of bone fractures.

## 1.2. Project description

### 1.2.1. Hypothesis and research aims

The work presented herein ultimately aims to create an engineered periosteum on the surface of cortical bone allografts which can deliver osteoprogenitor cells and heparin binding growth factors to a bone fracture site. This proposal will investigate the hypothesis that modifying bone allografts with an engineered periosteum delivering FGF-2, TGF-β1 and adipose-derived stem cells can modulate bone allograft healing and integration with the host bone tissue.

This will be accomplished through the three objectives found below:

**Objective 1:** Engineer periostea on mouse cortical bone allografts.

**Objective 2:** Determine *in vitro* effects of engineered periosteum on mouse adipose-derived stem cells.

**Objective 3:** Determine *in vivo* effects of engineered periosteum in a critical-sized mouse femoral defect model.

### 1.2.2. Organization of dissertation

Subsequent sections contain a literature review of materials, adult stem cell sources, and growth factor approaches used in engineering periosteum substitutes. Chapters that follow address the objectives mentioned above. A final chapter including conclusions and future directions culminates this work. A brief description of each chapter follows.

Chapter 2 investigates objective 1 and focuses on the creation of a periosteum-mimetic scaffolds on cortical bone allografts. These scaffolds were engineered to conformally coat the murine bone allografts. First, a procedure previously described by Almodovar *et al.* to create polyelectrolyte multilayers using layer-by-layer deposition of *N,N,N*-trimethyl chitosan and heparin on ovine bone was translated to murine bone.[8] Second, a chitosan freeze-dried porous scaffold on the bone allografts was made. Lastly, electrospun chitosan nanofibers were adhered onto the bone allograft surface. Creating three scaffold structures aided in creating diverse nanoscale topographies. Surface chemistry modifications were made on the freeze-dried scaffolds and electrospun nanofibers to incorporate heparin as well. Seeding the scaffolds with mouse adipose-derived stem cells (mASC) incorporated an osteoprogenitor cell source. Initial cytotoxicity and osteogenic protein expression studies were performed to evaluate mASC response to the engineered periosteum-mimetic scaffolds and informed studies planned for objective 2 and 3.

Chapter 3 investigates objective 3 and the *in vivo* performance of one engineered periosteum-mimetic scaffold delivering FGF-2, TGF-β1, and mASC to a murine critical-sized femoral defect. FGF-2 and TGF-β1 release from the engineered periosteum was investigated via ELISA. New bone mineralization in the bone callus was analyzed by microCT and union ratio analysis. Blinded histological analysis was used to characterize allograft incorporation using common histological criteria.

Chapter 4 investigates objective 2 and characterized the *in vitro* mASC response to engineered periosteum. Heparin incorporation into engineered periosteum-mimetic scaffolds facilitated FGF-2 and TGF-β1 binding and released FGF-2 and TGF-β1 from all three engineered periostea were quantified through ELISA. The viability and proliferative response of

mASC seeded on engineered periostea were tracked using bioluminescence imaging. Osteogenic differentiation of mASCs was examined by Western Blot analysis using common osteoblast protein markers. Multipotent gene expression studies of mASC seeded on FGF-2 and TGF-β1 coated PEM-modified nanofibers were also conducted to investigate mASC differentiation.

Chapter 5 is the final chapter of this dissertation and contains a summary of the work performed. Conclusions drawn from experimental work and potential future studies are listed.

## 1.3. Bone structure and fracture healing

### 1.3.1. Cancellous and cortical bone: structure and function

The human skeletal system has many functions in the human body including serving as a mineral reservoir, mechanical support and is a protective structure for internal organs and soft tissues. Skeletal bone is a composite of a dense mineral phase made of hydroxyapatite and an organic protein phase mainly made of collagen. The combination of the rigid mineral phase and elastic protein phase in an optimized hierarchical structure contributes to the viscoelastic behavior of bone.[9] Skeletal bone is classified into two types—cancellous and cortical bone. Cancellous bone participates in distributing mechanical loads on skeletal tissue and is characterized by its trabeculae, which create a porous structure.[10] The voids within cancellous bone are filled with bone marrow, which contain progenitor cells for hematopoietic tissue.

In contrast to porous cancellous bone, cortical bone is a dense compact form of bone with a hierarchical structure that provides the majority of the skeletal system's compressive strength as shown in Figure 1.1.[9] At a macroscopic tissue scale, cortical bone makes the outside dense shell of many bones. Within cortical bone at a microscopic level, osteons are present and are the basic functional units of bone.[11,12] Osteons are concentric layers of bone lamellae with Haversian

canals containing blood vessels and nerve tissue.[12] Within osteons, bone lacunae exist containing osteoblasts mineralizing the underlying extracellular matrix.[13] Osteoclasts are also present in bone resorption pits and are responsible for the breakdown of osseous tissue.[13] At the subcellular scale, the bone extracellular matrix collagen fibers are comprised of multiple collagen fibrils which contain individual collagen molecules with hydroxyapatite plate crystals periodically interspersed.[14] Normal bone physiology constantly undergoes a balanced remodeling process of bone tissue formation and resorption. It is estimated the entire human skeleton is resorbed and replaced approximately three to five times over an individual's lifetime.[15] Interestingly, bone is the only tissue in the body that can heal itself without forming a fibrous scar and undergoes a well-characterized healing process during bone fractures.[3,16]

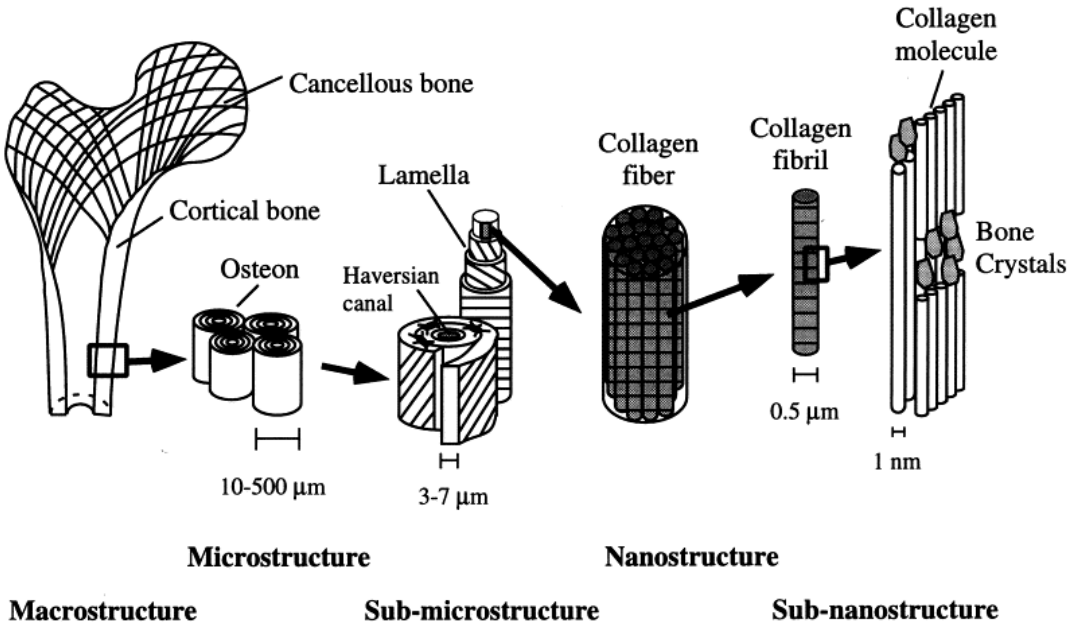


**Figure 1.1** Example of hierarchical structure of bone. From left to right: 1) cancellous and cortical bone; 2) osteons with Haversian systems; 3) lamellae; 4) collagen fibers made of collagen fibrils; 5) bone hydroxyapatite crystals, collagen molecules, and non-collagenous proteins. (Reprinted from Medical Engineering & Physics, 20/2, J.Y. Rho, L. Kuhn-Spearing, P. Zioupos, Mechanical properties and the hierarchical structure of bone, 92-102., Copyright 1998, with permission from Elsevier.)

### 1.3.2. Periosteum structure and function

The periosteum is a soft tissue multilayer structure on the outside of non-articulating regions of bone and tendon insertion points on cortical bone surfaces.[17] The periosteum is composed of an inner cambial layer of osteoprogenitors directly in apposition with cortical bone and an outer fibrous extracellular matrix layer containing pericytes and fibroblasts as seen in Figure 1.2.

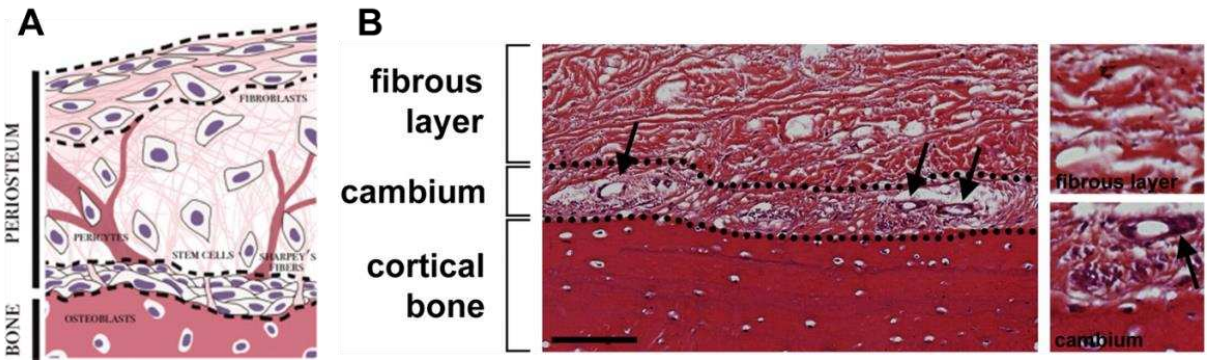


**Figure 1.2** Structure of periosteum. (A) Schematic of multilayer periosteum structure showing cell populations present in periosteum. (B) H&E stained section of the human fibula showing an inner cambium layer and outer fibrous ECM layer. Arrows show blood vessels. Scale bar = 100 µm. (Adapted from Stem Cells Translational Medicine, 1/6, C. Hana, M.L.K Tate, Concise Review: The Periosteum: Tapping into a Reservoir of Clinically Useful Progenitor Cells, 480-491., Copyright 2012, and Bone, 70, S.J. Roberts, N.G. Gastel, G. Carmeliet, F.P. Lyten, Uncovering the periosteum for skeletal regeneration: The Stem Cell that Lies Beneath. 10-18., Copyright 2015, with permission from John Wiley and Sons and Elsevier, respectively)

Anchored to cortical bone via Sharpey's fibers, the periosteum is a well-vascularized and innervated structure.[18-21] The periosteum's structure and the cell populations contained within are conducive to its function as a regenerative reservoir that provides several important functions during bone fracture healing.[3,22]

Animal studies have shown that the periosteum contributes skeletal progenitor cells to the bone fracture callus and that removal of the periosteum impairs fracture healing.[23-25] In addition to the periosteum's biological functionality in fracture repair, the periosteum contributes to the

biomechanical strength of long bones, with periosteum-covered rat fermora showing improved ultimate strength ,stiffness, absorbed energy, and deflection compared to periosteum-free contralateral femurs.[26] The periosteum acts as a bounding membrane around bone and has been shown to have direction- and flow rate-dependent permeability leading to tissue level mechanical signaling that may induce signals at the cellular level to begin fracture healing.[27,28] In sum, the biological and biomechanical function of the periosteum leads to beneficial properties for bone fracture healing.

### 1.3.3. Bone fracture healing and complications

Bone fracture healing is generally characterized in four main phases outlined in Figure 1.3. First, within minutes to hours of fracture, an initial hematoma forms at the site of injury creating a hypoxic environment and inflammatory cells are recruited to rid the callus of necrotic tissue.[16] Second, ruptured blood vessels and the intramedullary hematopoietic compartment provide a myriad of cytokines to begin the fracture healing process by recruiting and activating osteoprogenitors in the periosteum.[3] Third, after a period of a few days, granulation tissue is deposited by invading progenitor cells producing a soft cartilaginous matrix.[29] Concurrent with soft callus formation, new blood vessel recruitment occurs as well as initial mineralization.[30] Eventually, the soft callus comprised of an immature woven bone intermediate is fully remodeled into mature lamellar bone via osteoblast- and osteoclast-mediated mechanisms.[16]

In several ways, bone fracture healing replicates elements of bone tissue morphogenesis.[31] Bone tissue is formed via two main pathways: intramembranous and endochondral formation. These two bone formation pathways in fracture healing differ mainly in whether or not a cartilaginous template is used to pattern new bone formation.[29] While an in-

depth description of bone tissue morphogenesis is outside the scope of this review, it is important to note that emulating native bone fracture healing or bone tissue morphogenesis may inform periosteum-inspired strategies to augment bone fracture healing.

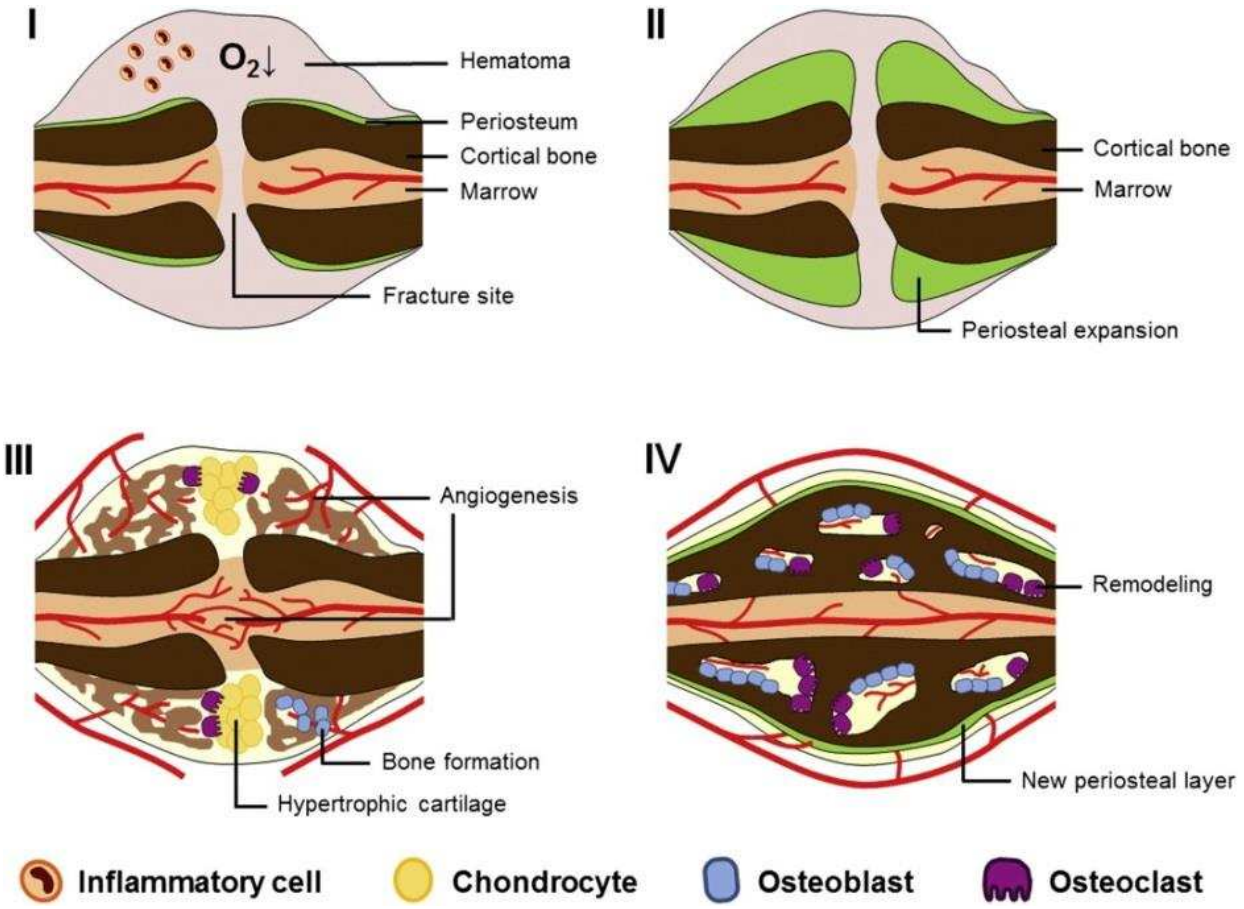


**Figure 1.3** Phases of fracture healing. (I) Initial hematoma formation after bone fracture leading to inflammation, pain, and hypoxia due to ruptured blood vessels. (II) Periosteal cell expansion due to growth factors present in hematoma. (III) Periosteal cells differentiate into chondrocytes and osteoblasts producing soft callus (IV) Remodeling of woven bone into mature bone through osteoblast- and osteoclast-mediated mechanisms. (Reprinted from Bone, 70, S.J. Roberts, N.G. Gastel, G. Carmeliet, F.P. Lyten, Uncovering the periosteum for skeletal regeneration: The Stem Cell that Lies Beneath. 10-18., Copyright 2015, with permission from Elsevier)

### 1.4. Brief history of bone graft transplantation and periosteum tissue engineering

Unfortunately, certain musculoskeletal injuries are unable to heal through natural processes requiring clinical intervention. The modern age of bone graft transplantation began in 1668 when Job van Meekeren, a surgeon, reported the first heterologous bone graft transplantation where a xenogenic dog skull fragment was implanted into an injured soldier's skull and graft incorporation occurred.[32] Later, the periosteum's osteogenic potential was initially hypothesized by Henri Louis Duhamel in 1742 and eventually, by 1867, Louis Leopold Ollier confirmed the periosteum could become osteogenic under the proper conditions.[32] Around 1880, the first human bone allograft transplantation occurred when Sir William MacEwen reconstructed the humerus of a 3 year old boy.[33]

Since then, advances in bone biology such as the discovery of bone morphogenetic proteins, mesenchymal stem cells, and the hematopoietic niche have informed strategies to improve the clinical performance of bone grafts through tissue engineering.[15,34-37] While bone autografts are still the current clinical gold standard, challenging indications such as large traumatic bone loss or osteosarcoma resections require the use of bone allografts. However, bone allograft potential risks such as non-union, fracture, infection, and immune response lead to sub-optimal graft healing compared to bone autografts. It has been hypothesized that engineering a periosteum on bone allografts could improve bone allograft clinical performance.[38] In recent years, increased publications on periosteum tissue engineering (Figure 1.4) shows rising interest in replicating and translating the periosteum's regenerative properties.[39] In subsequent sections, the periosteum tissue engineering literature will be reviewed with an emphasis on the material, adult stem cells, and growth factors used in the context of bone defect healing and is visually outlined in Figure 1.5.

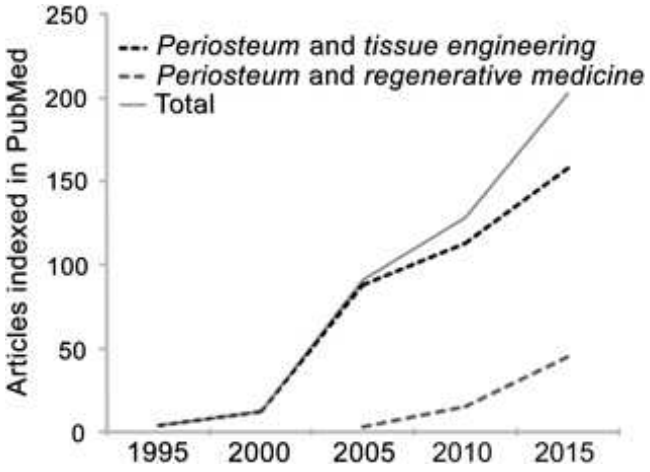


**Figure 1.4** Increased number of published articles indexed in PubMed on periosteum tissue engineering. Search keywords used were "periosteum and tissue engineering" and "periosteum and regenerative medicine". By 2015, articles on periosteum tissue engineering and regenerative medicine more than doubled compared to 2005. (Reprinted from STEM CELLS Translational Medicine, 5/12, S.R. Moore, C. Heu, N.Y. Yu, R.M. Whan, U.R. Knothe, S. Milz, M.L. Knothe Tate, Translating Periosteum's Regenerative Power: Insights from Quantitative Analysis of Tissue Genesis with a Periosteum Substitute Implant.1739-1749., Copyright 2016, with permission John Wiley and Sons)

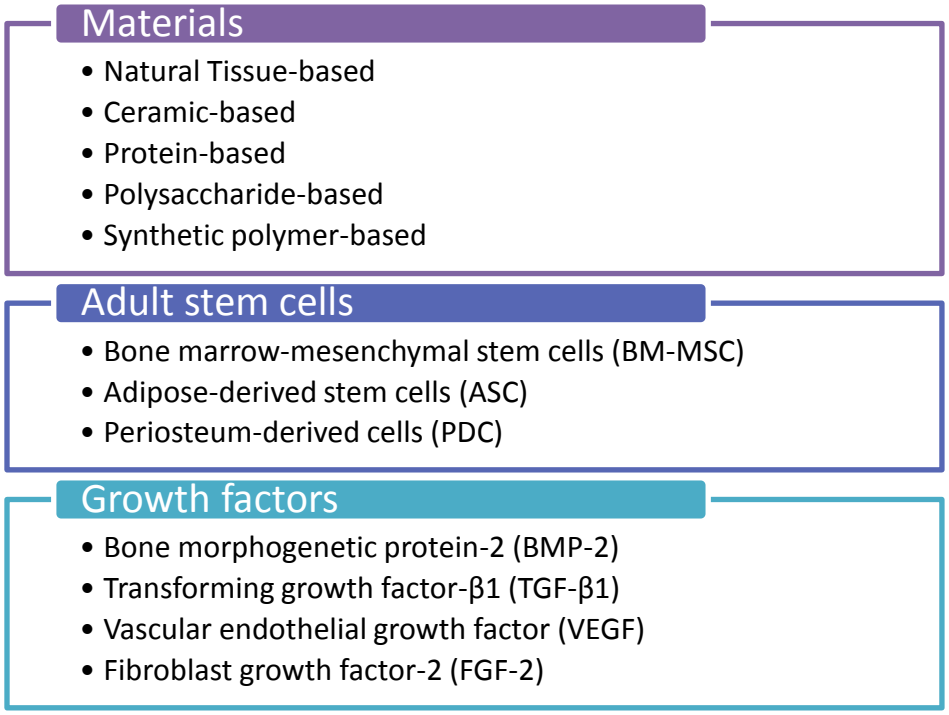


**Figure 1.5** Overview of materials, adult stem cells, and growth factors used in periosteum inspired approaches to mimic bone graft healing.

### 1.5. Periosteum mimicking strategies to improve bone graft healing

#### 1.5.1. Natural tissue approaches

Recognizing the periosteum's regenerative capacity, it is logical to use the periosteum or a periosteum-like structure to augment large bone defect fracture healing. In 2000, Masquelet and co-authors reported reconstructing 35 large diaphyseal defects between 1986 and 1999 via a two-stage process.[40]In the first stage, a cement spacer was inserted into the defect site, which induced a pseudosynovial membrane to form around the cement spacer. After 6 to 8 weeks, in the second stage, the induced membrane was opened and the cement spacer removed. Then the void within the induced membrane was filled with autologous cancellous bone or another bone substitute and sutured closed. The induced membrane was shown to be biologically active by secreting vascular and osteoinductive growth factors and preventing resorption of cancellous bone graft filling while being structurally similar to the periosteum.[41-44] In 2005, Stevens and colleagues showed that hydraulic elevation of periosteum in a rabbit tibia could be used to create bone tissue *in situ*.[45] By filling the void between the periosteum and tibia periosteal surface with a calcium – alginate gel, new bone was formed after 6 weeks showing ECM histological markers of native bone and osteons. Stevens *et al.* found that the newly formed bone could be harvested without compromising the native bone tissue and when implanted into a contralateral rabbit tibial defect, the new bone was remodeled and integrated into the surrounding bone. This study illustrated that bone could be formed *in situ* without cell or growth factor transplantation using intrinsic periosteum tissue albeit with limited bone tissue formation.

Perhaps recognizing the need for a one-stage clinical intervention to repair long bone defects, Knothe and Springfield pioneered a novel surgical procedure using an *in situ* elevated periosteum sleeve to enclose long bone defects and regenerate bone.[46,47] However, this technique

is limited by the amount of healthy periosteum available. Addressing this limitation, Knothe Tate and colleagues developed a modular surgical membrane-based periosteum substitute. The periosteum substitute consisted of a bi-layer silicone elastomer sheeting with suture seams to create pockets, which could be filled with different autologous materials. Maximal defect bridging and greatest bone tissue generation was observed in experimental groups receiving the pocketed surgical membrane containing strips of periosteal tissue compared to control groups receiving the surgical membrane alone or with other material including periosteum-derived cells or a commercially available absorbable collagen membranes.[48] Recent work by Moore *et al.* showed progenitor cells present in the periosteal tissue strips along with intrinsic biological and mechanobiological factors were responsible for potentiation of the periosteum's regenerative ability.[39]

The studies mentioned above are limited by multiple surgical interventions or require healthy periosteum to be present in the bone defect site to regenerate bone. This has led to strategies modifying bone allografts with a periosteum-mimicking structure to enhance bone allograft healing and incorporation with native bone tissue. The following subsections discuss material-based approaches to augment bone defect healing with engineered periosteum.

### 1.5.2. Ceramic-based approaches

The mineral phase of cortical bone is estimated to comprise approximately 70 % of bone tissue mass. Consequently, investigating calcium phosphate biomaterials with a similar mineral composition to the hydroxyapatite in bone tissue is a logical approach to augment bone fracture healing. Calcium phosphate materials, such as β-tricalcium phosphate (β-TCP) and hydroxyapatite, provide an osteoconductive surface, form bone apatite-like structures on scaffold

surfaces, and can form a strong bone-CaP interface.[49] β-TCP and hydroxyapatite mixtures can also be effective carriers of osteoprogenitors like bone marrow-derived mesenchymal stem cells (BM-MSC). Bruder *et al.* showed effective bone regeneration and bridging in critical-sized femur defects in athymic mice and canine femur using a fibronectin-coated porous β-TCP and hydroxyapatite scaffold seeded with BM-MSC.[50,51]

In more recent work, cell sheet technology was used to create a periosteum-like cell layer on the outside of β-TCP scaffolds.[52] BM-MSC and human umbilical vascular endothelial cell sheets were combined into a dual layer wrapping on a porous β-TCP cylinder to create a vascularized bone tissue construct. Subcutaneous implantation of the construct into the dorsum of nude mice showed that the β-TCP graft had significant vascularization and osteogenic potential compared to the cell sheet-free β-TCP graft.[52] This study further supports the benefit of vascularized bone tissue engineering strategies. While this study shows promising results, it has not been examined in a clinically relevant bone defect to test whether the engineered periosteum can to regenerate bone tissue. On the other hand, Nau *et al.* tested a β-TCP scaffold combined with a vascularized periosteal flap and bone marrow-derived mononuclear cells in a rat femur defect.[53] β-TCP scaffolds augmented with vascularized periosteal flaps or bone marrow-derived mononuclear cells led to increased bone mass in the femur defects compared to β-TCP scaffolds only.[53] While β-TCP scaffolds are similar to the bone mineral phase and can show improved bone defect healing, β-TCP scaffolds lack the protein phase of bone tissue, which is conducive to cell attachment, provides inherent growth factor sequestration, and is important for the elastic strength of bone tissue. Protein-based approaches to improve bone graft healing will be discussed in the next section.

### 1.5.3. Protein-based approaches

The second largest constituent of cortical bone tissue is the protein phase, estimated to account for ~20% of bone tissue.[54] This protein phase is made of several ECM proteins including collagen I, elastin, fibronectin, and non-collagenous proteins. With collagen I being the most abundant protein in bone tissue, researchers have pursued collagen-based matrices to augment bone fracture healing.[9] Various collagen matrices have been used in many forms and have been derived from many sources such as collagen sponges, decellularized dermal or periosteal tissue structures, and templated collagen sheets. In 2005, Hattori *et al.* reported using a collagen sponge seeded with rat BM-MSC to reconstruct a critical-sized rat calvarial defect.[55] While the seeded BM-MSC plus collagen sponge did not significantly improve calvarial bone formation compared to a cell-free collagen sponge, rats treated with collagen sponge or BM-MSC seeded collagen sponge had significantly increased bone density compared to an empty defect, showing a therapeutic effect of the implanted collagen sponge.[55] A similar study used a collagen I sheet to deliver cobalt dichloride treated BM-MSC to a SCID mouse calvarial defect.[56] Cobalt dichloride has been shown to activate angiogenic genes in BM-MSC.[57] The BM-MSC angiogenic activation led to increased blood vessel density and new bone formation in the defect showing that progenitor cell pretreatment can lead to improved therapeutic effects of transplanted cells in a periosteum-like carrier.[56]

A limitation on collagen sponge scaffolds is the loss of the native ECM architecture and the absence of other ECM proteins. *In vitro* studies have shown that precise topographical cues exist on native periosteum tissue can modulate cell response supporting the use of decellularized matrices.[58] Schonmeyr *et al.* used an acellular dermis seeded with mouse BM-MSC to create a periosteum-like material.[59] BM-MSC cultured on the acellular dermis retained their ability to

proliferate and differentiate *in vitro.* When the periosteum-like material seeded with bone morphogenetic protein 2 (BMP-2) expressing BM-MSC was implanted into a rat mandibular critical-sized bone defect, accelerated defect bridging was observed by 4 weeks compared to no bridging in all other groups at the same time point.[59] Researchers have also used allogeneic decellularized periosteal matrices to serve as carriers for progenitor cells. Rapp *et al.* used bovine decellularized periosteum to deliver adipose-derived stem cells (ASC) or periosteum-derived stem cells (PDC) into a rat calvarial defect filled with cancellous bone chips.[60] ASC treated groups showed increased mineralization in the defect compared to PDC treated groups in the calvarial defect.[60] Chen *et al.* used rabbit decellularized periosteum to show that PDC infiltrated the decellularized periosteum and did not produce an immunogenic response when implant subcutaneously in the backs of rabbits.[61] However, this study did not test the osteogenic potential or bone forming capabilities of the engineered periosteum tissue. Taken together, acellular or decellularized substrates provide a more complete ECM-like microenvironment for progenitor cells compared to collagen sponges, and can deliver progenitor cells *in vivo*. Importantly, the studies conducted by Schonmeyr *et al.*, Rapp *et al.*, and Chen *et al.* did not test their periosteum mimics in appendicular bone defects. Their bone regeneration performance in long bone defects remains to be investigated.

One other common acellular ECM-like biological material investigated is small intestine submucosa (SIS). SIS is available in several commercially available products commonly used in many different applications ranging from surgical meshes to a bioscaffold for the regeneration of various tissues.[62,63] SIS contains most ECM components and even has been shown to retain growth factors such as fibroblast growth factor-2, transforming growth factor-β1, and vascular endothelial growth factor.[64] Xie *et al.* used SIS-wrapped bone allografts to deliver transfected

C3H10T1/2 MSC cells to a mouse femur defect.[65] The SIS-wrapped allografts showed no improved healing compared to SIS-free allografts leading researchers to conclude that the delivered C3H10T1/2 MSC cells expressing BMP-2 were responsible for increased new bone formation compared to cell-free allografts.[65] Similarly, Zhao *et al*. found that SIS alone could not guide bone regeneration in a critical-sized rabbit tibial defect but the addition of osteoinduced BM-MSC enhanced defect bridging compared to allograft only treated groups.[66]

These studies using protein-based approaches to augment bone fracture healing indicate that delivering only ECM material to a bone defect is likely insufficient for guided bone regeneration. Recent innovations including a platelet rich plasma-gel carrier or an elastin-like material to engraft MSCs into a bone defect expand the options when using a protein-based material approach.[67,68] In all, protein-based approaches show promise in augmenting bone graft healing when used in combination with a progenitor cell source but concerns over incomplete removal of cellular debris and pathogenic transmission is a concern that can lead to clinical complications.[69]

### 1.5.4. Polysaccharide-based approaches

#### 1.5.4.1. Chitosan

In addition to the presence of several proteins in the ECM, there exists several proteoglycans and glycosaminoglycans (GAGs). GAGs have been shown to have important functions in mammalian tissues such as providing compressive strength in cartilage,[70] providing lubrication on articulating cartilage,[71] and mediating protein signaling by binding proteins like growth factors.[72,73] Chitin, the second most abundant polysaccharide in the world after cellulose, can be deacetylated to form chitosan, which has a similar chemical structure to GAGs. Chitosan

is a linear polysaccharide made of *N*-acetylated glucosamine and *N*-glucosamine units linked by β(1-4) glycosidic bonds as seen in Figure 1.6. Chitosan has been extensively investigated for tissue engineering applications due to several of its attractive characteristics, such as biocompatibility, biodegradability, and antibacterial activity.[74-79] Chitosan also has favorable characteristics for bone tissue engineering, such as osteoconductivity and the ability to be blended with currently used orthopedic materials.[79-82]

In the context of engineering a periosteum substitute, few studies using chitosan have been reported. Guo *et al.* used a chitosan composite with β-TCP and gelatin to deliver ASC to a rabbit radius defect.[83] The addition of β-TCP improved mechanical strength of the implant while the wrapped chitosan and gelatin membrane reinforced the β-TCP phase.[83] The addition of ASC to the chitosan-gelatin-β-TCP composite resulted in improved bone healing in the radius defect compared to the cell-free composite scaffold or a chitosan-only membrane.[83] Almodovar and co-authors deposited chitosan and heparin polyelectrolyte multiplayers (PEM) on ovine cortical bone and found the PEM-modification on bone imparted antimicrobial properties against *S. aureus* and *E. Coli*.[84] Chitosan used to make free-standing membranes with alginate possesses osteoinductive properties when loaded with BMP-2 and subcutaneously implanted in the backs of nude mice.[85]

One of chitosan's strengths as a material for tissue engineering scaffolds is its diverse processability including phase separation techniques, polymer blends, and cationic nature in acidic solutions.[86-88] Chitosan's primary amines have a pKa of approximately 6.3, which are positively charged in acidic solutions. This property can be exploited when chitosan is exposed to polyanionic GAGs, such as heparin, in solution to easily incorporate heparin into a chitosan containing scaffold.

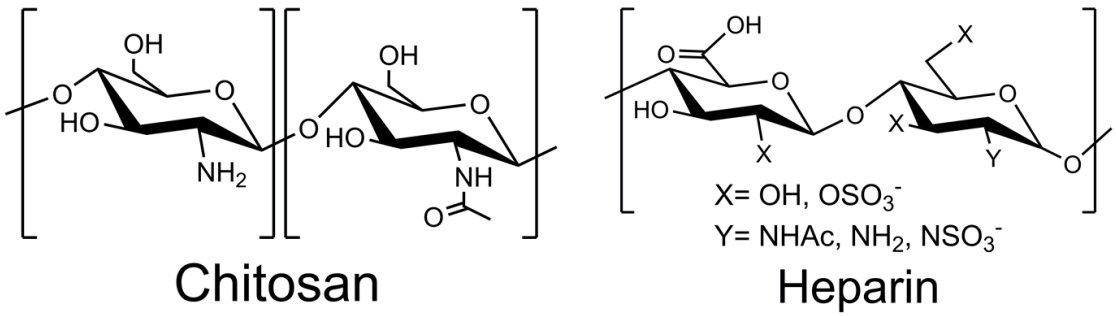


**Figure 1.6** Chemical structures of chitosan and heparin

### 1.5.4.2. Heparin

Heparin, a GAG structurally similar to heparan sulfate, (Figure 1.6) is a well-studied polysaccharide most known for its anticoagulant properties.[72] Due to its inherent ability to bind heparin binding growth factors, it has been used in growth factor delivery applications as part of composite scaffolds.[89-92] The electrostatic complexation between chitosan and heparin can be used to drive assembly of different nanostructures.[93] Heparin-containing periosteum-mimetic scaffolds may allow localized and targeted therapeutic delivery of heparin-binding growth factors to osteoprogenitor cells. While Almodovar *et al.* incorporated heparin on PEM-modified cortical bone, the periosteum-mimic's ability to deliver heparin-binding growth factors *in vitro* or *in vivo* has not been investigated.[8] As few periosteum-like substitutes have incorporated heparin, there is need to further investigate heparin's advantageous growth factor binding property when incorporated into a periosteum-like substitute.

Naturally derived polymeric materials, such as polysaccharides or protein-based matrices, suffer from similar limitations including manufacturing lot-to-lot variability and the potential for pathogen contamination that could activate an organism's immune response. In contrast, synthetic polymer materials are chemically well defined and are reproducibly manufactured. A

brief overview of synthetic polymer approaches to creating an engineered periosteum substitute follows in the subsequent section.

### 1.5.5. Synthetic polymer based approaches

Synthetic polymers possess some advantages compared to naturally derived materials in a biomaterial context including consistent chemical structures, lack of pathogenic transmission, and a higher degree of processing flexibility. Various synthetic biodegradable polymers have been investigated in bone tissue engineering applications, yet relatively few have been investigated to create a periosteum-like structure. Oest *et al.* investigated a porous poly(L-lactide-co-D,L-lactide 7:3) (PLDL) scaffold in a rat critical-sized femur defect.[94] The PLDL scaffold was coated with fibronectin to improve cell adhesion and BMP-2 and transforming growth factor-β3 were added to the scaffold via a calcium crosslinked alginate carrier.[94] The growth factor containing PLDL scaffold resulted in significantly increased bone volume in the defect compared to the PLDL scaffold alone or an empty defect.[94] However, the growth factors delivered to the femur defect did not improve torsional strength of the defect compared to the PLDL scaffold group alone, demonstrating that the PLDL material was insufficient in rebuilding the bone defect.[94]

Polyethylene glycol (PEG) hydrogels are another well-investigated synthetic polymer used in tissue engineering applications due to its naturally hydrated structure, bioinertness, and flexible chemical modifications. Hoffman *et al.* was able to use a photopolymerizable PEG solution to homogenously encapsulate BM-MSC around the periosteal surface of decellularized bone allografts.[95] Localized delivery of BM-MSCs to a mouse femur defect was achieved using a tuned scaffold degradation time of approximately 14 days.[95] This resulted in enhanced

vascularization, bone callus formation, and torsional strength by week 16 compared to an untreated allograft .[95] Further work showed that altering the transplanted cell population to more closely mimic the native periosteum cell population led to enhanced allograft healing and integration, due to paracrine factor production by the transplanted cells.[96] The PEG hydrogel material did not contribute significantly to bone callus formation, which was attributed to the transplanted cells.[95] Similarly, Baldwin *et al.* used a multilayer composite scaffold of polycaprolactone (PCL) and a multi-arm PEG hydrogel covalently crosslinked with heparin to deliver human BM-MSC and human umbilical vein endothelial cells (HUVEC) to a mouse non-critical sized femur defect.[97] They investigated BM-MSC and HUVEC effects on healing and terminal cell fate in a novel orthotopic xenograft model.[97] Human BM-MSC were found to maintain a precursor phenotype and secrete collagen I matrix. HUVEC-treated groups had increased vascularization compared to HUVEC-free or cell-free scaffolds and formed capillary-like networks that connected to host vascularization that was eventually replaced by host cells.[97] These studies show that PEG hydrogels can be used as a periosteum-like substitute with beneficial *in vivo* results.

Recent innovative work with hydroxyapatite (HA) mixed with poly(lactide-*co*-glycolide)-*b*-poly(ethylene glycol)-*b*- poly(lactide-*co*-glycolide) (PELGA) composites created a material that stiffens upon hydration due to enhanced PEG crystallization and has temperature-sensitive shape memory facilitating cell-seeded sheet transfer onto bone allografts.[98] BM-MSC and periosteum-derived stem cells were found to adhere onto the HA-PELGA scaffold and supported the proliferation and osteogenesis of periosteum-derived stem cells. However, synthetic polymers also do not emulate the native bone or periosteum tissue architecture requiring modifications to produce porous structures to facilitate cell invasion and adhesion.[99] Synthetic

polymers' flexible processing has led to extensive study into many tissue engineering applications.[99] The wide range of synthetic polymers allows for selection of a material with the appropriate characteristics for a given tissue engineering application.

A common theme emerges when comparing and contrasting ceramic, protein, polysaccharide, and synthetic polymer material approaches to periosteum tissue engineering. While each material type has its advantages and limitations, it is striking to observe that most of the materials in the articles discussed above do not inherently significantly contribute to the formation of new bone in several different pre-clinical animal models and bone defects when used as a periosteum-like substitute. Generally, most of the materials studied in the periosteum tissue engineering context require some biological augmentation by incorporating one or more cell populations and/or proteins such as growth factors or fibronectin. This observation is in line with the traditional tissue engineering paradigm first canonized in Langer and Vacanti's seminal publication in 1993 that effective tissue replacements would consist of a combination of material matrices, replacement cells, and tissue signaling molecules such as growth factors.[100] Therefore, proper selection of progenitor cell populations and growth factors used in a periosteum tissue engineered substitute is important to create an engineered periosteum with physiologically relevant properties. Common adult stem cell populations and growth factors used in periosteum tissue engineering are briefly discussed in the subsequent sections.

## 1.6. Adult stem cell sources in periosteum tissue engineering

### 1.6.1. Bone marrow mesenchymal stem cells

Precursors of bone cells were originally discovered by Alexander Friedenstein and Maureen Owen in the mid 1960's when studying the kinetics of bone cell proliferation *in*

*vivo*.[15,36] These bone marrow-derived stromal stem cells were later renamed mesenchymal stem cells in 1991 by Arnold L. Caplan.[35] Bone marrow mesenchymal stem cells (BM-MSC) have been extensively investigated in tissue engineering and regenerative medicine applications originally due to their multipotent differentiation capacity when given the correct environmental stimuli.[101,102] BM-MSC have also been found to possess immunomodulatory effects, injury homing capabilities, and trophic activity.[101,103,104] BM-MSC are bone cell precursors and their application to regenerate bone tissue is a natural choice. BM-MSC have also been used therapeutically in several studies in bone defect reconstruction.[50,105,106]

In general, delivery of BM-MSC cultured on a periosteum-like substitute and transplanted to a bone defect typically results in enhanced mineralization and sometimes bone tissue formation in multiple types of bone defects in different animal models.[55,66,67,95,96] This is consistent with reports in the literature of BM-MSC robust osteogenic potential with the proper stimuli and is promising for translational clinical intervention.[106,107] However, BM-MSC do suffer from low cell numbers in bone marrow tissue, requiring *ex vivo* culture expansion before implantation and delaying therapeutic intervention.[108] Even with extensive investigation into using BM-MSC for tissue engineering applications for the past two and a half decades, there is still no tissue engineered product initiated with BM-MSC used medically.[107] Clinical translational hurdles to overcome include clinical trial failures involving BM-MSC, limited transient cell engraftment, a lack of public funding or venture capital to acquire the necessary regulatory data for clinical trials, and prohibitively expensive scale-up of cell manufacturing.[109-111] The lack of translated BM-MSC tissue engineered products suggest more is to be learned about how to harness the effective therapeutic capabilities of BM-MSC to make a safe, efficacious, and clinically viable tissue engineered product.

### 1.6.2. Adipose-derived stem cells

Another adult stem cell source in adipose tissue was discovered in 2001 by Zuk *et al.*[112] ASC have potential to differentiate into cells types of mesodermal, ectodermal, and endodermal lineages.[113] Human ASC are easily harvested from adipose tissue and are found in greater abundance in adipose stromal tissue compared to BM-MSC in bone marrow. While differences exist between ASC and BM-MSC, these differences are negligible in the osteogenic differentiation of the two human cell sources.[114,115] Thus, ASCs do possess the ability to be used in autogenic or allogenic orthopedic tissue engineering applications.[116-118] ASC isolation from the stromal vascular fraction is a well-accepted technique that can be done in a variety of mammalian organisms including humans, monkeys, mice, and dogs.[112,119] However, ASCs have some variation depending on species of origin, gender, and even choice of fat depot used in the isolation.[119-121] These variations must be considered by researchers when interpreting experimental results and attempting to extrapolate results using ASC isolated from one species and applying those conclusions to another species.

While ASC have been investigated to reconstruct bone defects and have shown promising results, few studies have specifically studied ASC delivery from an engineered periosteum.[116,122] Rapp *et al.* found ASC produced greater calcified material within rat calvarial defects compared to periosteum-derived stem cells when delivered from an acellular allo-periosteum scaffold.[60] Guo *et al.* found that osteoinduced ASC delivery with a chitosan reinforced β-TCP periosteum substitute led to increased trabecular bone area in a rabbit radial defect compared to a cell-free scaffold according to histomorphometric analysis.[83] There is a lack of studies using ASC as the progenitor cell source when studying periosteum-like substitutes for bone defect repair. This area

is ripe for investigation, especially delivering ASC to segmental bone defects to elucidate ASC effectiveness in regenerating bone in a clinically challenging bone defect.

### 1.6.3. Periosteum-derived cells

In engineering periosteum-like substitutes, using periosteum-derived cells (PDC) as a progenitor cell source is a logical choice. PDC are present in the periosteum and are known to participate in bone fracture healing differentiating into chondrocytes or osteoblasts to regenerate bone tissue.[3,123] This has led to investigating PDC as an alternative mesenchymal stem cell for bone tissue engineering applications. PDC can be harvested from periosteum tissue present on discarded femoral heads during joint replacement surgery or periosteum tissue from other locations during surgery.[123] PDC are obtained by cell migration out of periosteal tissue or enzymatic degradation of periosteum to release PDC.[3] PDC can be stably culture expanded over many passages, attributed to their long telomeres, and retain differentiation potential for over 10 passages.[124,125]

Similar to BM-MSC and ASC, PDC have been shown to possess multipotent differentiation capabilities down adipogenic, chondrogenic, and osteogenic lineages.[125-127] However, when PDC are directly compared to other mesenchymal stem cell sources, differences are observed. Hayashi *et al.* found evidence that PDC were less osteogenic compared to BM-MSC.[128] Sakaguchi *et al.* found human PDC colonies had a higher mineralization capacity compared to ASC suggesting a stronger osteogenic potential in PDC.[129] Confirming PDC osteogenic potential has led to using PDC as a progenitor cell source to create engineered bone tissue. Several studies have shown PDC to enhance mineralization in several *in vivo* bone defects.[130-132] Surprisingly, few studies have investigated PDC as a cell source in tissue

engineered periosteum. Rapp *et al.* compared ASC or PDC cultured on decellularized bovine periosteum to reconstruct a rat calvarial defect and found that ASC led to higher calcification within the defect compared to PDC.[60] The lack of studies investigating PDC in tissue engineered periosteum may be due to the limitation of needing native periosteum tissue to isolate cells from which is not a clinically relevant scenario when dealing with a large segmental bone defect due to traumatic injury.

In all, several adult stem cell sources exist to use in a tissue engineered periosteum. BM-MSC, ASC, and PDC can be isolated *ex vivo* and culture expanded for therapeutic use. All three progenitor cells have shown osteogenic potential *in vitro* and *in vivo* albeit with some minor differences.[133,134] They can be seeded on multiple types of carrier materials to be delivered to a bone defect. Ultimately, in the context of a tissue engineered periosteum, more work should be done to assess ASC and PDC performance in regenerating bone tissue particularly in a challenging indication such as a load bearing segmental defect. Optimal therapeutic cell dose, pretreatment cell conditions, and efficient cell seeding on a periosteum mimic need to be determined prior to clinical translation.

## 1.7. Growth factors in periosteum tissue engineering

### 1.7.1. General growth factor characteristics and involvement in bone fracture healing

A second type of biological augmentation for materials used in periosteum tissue engineering is the incorporation of signaling cytokines such as growth factors. Several growth factors participate in bone fracture healing and can potentially help enhance the bone healing process.[16,29,135] Unfortunately, growth factors have been found to be very unstable in organisms due to degradation or serum inactivation that results in short serum half-lives requiring

engineered localized delivery systems.[136] Growth factor instability, high cost of production, and unknown optimal therapeutic dosages have thus far limited the therapeutic value of growth factors in tissue engineering applications. Previous strategies have been limited to systemic delivery or supraphysiological dosages.[137] Fortunately, recent materials innovation allow for localized delivery of growth factors to take advantage of their potent signaling in cell-based therapeutics or to recruit endogenous progenitor cells in a bone defect environment for bone tissue regeneration. The subsequent sections will give an overview of select growth factors that participate in bone fracture healing and are used in engineered periosteum.

### 1.7.2. Bone morphogenetic protein-2

The concept of an osteoinductive factor in bone was discovered in 1965 when Urist *et al.* implanted demineralized bone into a rat muscle pouch and observed bone ossicle formation.[34] Soon after, the bone inductive substance was named bone morphogenetic protein (BMP).[138] Eventually, multiple isoforms of BMP were discovered as well as their participation in regulating bone formation.[139,140] Of the various BMP isoforms now known, BMP-2 is one of the most investigated BMPs, with BMP-2 approved for clinical use in humans to help repair single-level anterior lumbar interbody fusion, tibial nonunions, and oral maxillofacial reconstructions.[141,142] Due to BMP-2's potent osteoinductive effect, BMP-2 is a popular growth factor to use in bone tissue engineering applications.

Several animal studies report increased bone formation with direct administration of BMP-2 supporting its osteoinductive properties.[137] Oest *et al.* delivered 200 ng of BMP-2 and 20 ng of transforming growth factor-β3 within an alginate and PLDL scaffold to a rat femoral defect and found increased bone volume compared to an empty defect or growth factor free scaffold at

weeks 4 and 16.[143] However, the addition of growth factors did not contribute to a statistically different effect in mechanical testing.[143] Rapp *et al.* found that 0.1 ng BMP-2 in 10 µl dripped into rat calvarial defect with covered with a decellularized periosteum seeded with ASC or PDC resulted in the most mineralization in the defect compared to no growth factor control groups and with vascular endothelial pretreated ASC or PDC.[60] Caridade *et al.* used free-standing chitosan and alginate membranes to deliver 60 and 100 µl $ml^{-1}$ dosages of BMP-2 in a ectopic bone assay.[85] Ectopic bone was only formed in the membrane loaded with 100 µl $ml^{-1}$ BMP-2 and was visible beginning at day 21 and continued to grow until day 52.[85] These studies show that direct addition of BMP-2 to periosteum-like substitutes can modulate the bone healing response and further studies are needed to elucidate optimal therapeutic dosages.

In contrast to direct delivery, BMP-2 can be indirectly delivered to a bone defect through genetically engineered transplanted cells expressing BMP-2. Zhang *et al.* found that BMP-2 producing BM-MSC on bone allografts showed increased in bone graft incorporation and neovascularization in a critical-sized mouse femoral defect compared to acellular allografts or control transfected cells.[22] Similarly, Xie *et al.* implanted C9 cells from the C3H10T1/2 MSC line transfected to express BMP-2 in a critical-sized mouse femoral defect and found increased bone formation around the allograft compared to live isograft.[65] Yet delayed allograft resorption was observed.[65] Lieberman *et al.* found that BMP-2 expressing BM-MSC could heal a rat segmental defect.[144] These studies support the use of genetically engineered cell populations to indirectly deliver potent growth factors to augment bone graft healing.

Although BMP-2 is a potent bone forming growth factor, recent discoveries about clinical complications associated with BMP-2 is concerning.[142] Several other growth factors such as transforming growth factor-β, vascular endothelial growth factors or fibroblast growth factors

are involved in the bone fracture healing process and their potential to augment bone graft healing has been investigated.[16,29,31,135] These growth factors delivered alone or in combination with other growth factors may lead to even more effective therapeutic approaches if optimal delivery and dosing can be confirmed.

### 1.7.3. Transforming growth factor-β1

Originally discovered in the context of cancer biology around 1980, transforming growth factor-β (TGF-β) proteins are now known to be involved in many physiological processes ranging from embryonic development, adult tissue homeostasis, disease states, and cell differentiation.[145-148] The discovery of multiple TGF-β isoforms and their context dependent roles in cell differentiation have shown that TGF-β1 can enhance mesenchymal differentiation towards chondrocytes.[149,150] In addition, TGF-β1 regulates chondrocyte and osteoblast phenotype expression *in vivo*.[151,152] TGF-β1 also has chemotactic effects, recruiting preosteoblasts and has been shown to increase matrix synthesis.[153,154] Not surprisingly, TGF-β1 is involved in bone fracture healing and is constitutively expressed in a mouse tibia fracture callus for up to 28 days.[155] TGF-β1's involvement in bone fracture healing and its highly conserved structure in mammals make it a candidate for use as a bone-forming agent.[156]

Indeed, studies have shown exogenous TGF-β1 administration promotes bone formation *in vivo* in a long bone fracture healing environment.[156] Moxham *et al.* reported 750 µg of TGF-β1 added to demineralized bone matrix and implanted in a sheep tibial defect resulted in complete bony bridging in a sheep tibial defect compared to incomplete bridging in defects treated with only demineralized bone matrix. Tieline *et al.* found TGF-β1 released from a polylactide fixation pin near a femur defect filled with a cellulose sponge led to more fibroblast-

rich mesenchymal tissue inside a cellulose sponge and at week 3, increased periosteal bone compared to defects treated with TGF-β1-free pins.[157] However, histological examination showed no increased bone formation within the cellulose sponge at any time point examined.[157] Ehrhart *et al.* found TGF-β1 delivered by a gelatin hydrogel to an irradiated critical-sized rabbit tibial defect resulted in radiographic evidence for increased bone formation at 8 weeks compared to an untreated defect or TGF-β1-free gelatin treated defect.[158] To date, no studies delivering TGF-β1 from a tissue engineered periosteum exist and may be an approach to augment bone allograft healing in a long bone defect.

One explanation why TGF-β1 has not been more thoroughly investigated as an osteoinductive factor is due to its lesser osteoinductive quality compared to BMP-2.[156] While TGF-β1 is involved in bone fracture healing, BMP-2 has usually shown more robust osteoinductive and mineralization responses in a bone defects compared to TGF-β1.[156] However, it is unknown whether TGF-β1 can work synergistically with other growth factors to overcome its limited osteoinductive nature. This remains an unaddressed question in the TGF-β1 literature.

### 1.7.4. Vascular endothelial growth factor

An alternate growth factor strategy for bone defect reconstruction is to deliver an angiogenic growth factor from the vascular endothelial growth factor (VEGF) family. Angiogenesis and osteogenesis are interconnected processes during bone tissue formation and fracture healing.[159] VEGF-mediated formation of new vasculature within a bone defect improves fracture healing by restoring transport of oxygen, nutrients, and cells involved in the fracture healing cascade.[135,160,161] Direct VEGF delivery to a mouse femur defect was found to enhance blood vessel formation and new bone callus maturation.[161] In the same study but a separate

experiment, VEGF administration to a rabbit radial defect promoted bony bridging compared to defects not receiving VEGF treatment.[161] Clarke *et al.* showed that VEGF in combination with autologous BM-MSC delivered to a critical-sized rabbit ulnar defect was necessary to promote bone bridging as BM-MSC delivered alone to the ulnar defect was insufficient bridge the defect. Thus, delivery of VEGF to a bone defect environment can modulate the fracture healing response for improved bone tissue regeneration.

Surprisingly, not many engineered periosteum studies have investigated direct VEGF delivery to enhance bone graft healing. El Backly *et al.* implanted a VEGF-releasing PRP membrane with encapsulated BM-MSC into a rabbit ulnar defect which was responsible for new bone formation in the defect compared to little or no bone formation to VEGF-free BM-MSC seeded membranes or cell-free PRP, respectively.[67] Most studies have focused on indirect delivery of VEGF through cell engraftment on bone allografts or gene therapy approaches. Hoffman *et al.* measured *in vitro* VEGF release from mouse BM-MSC photoencapsulated in a PEG-based engineered periosteum and found increased callus bone formation, graft-host integration, and biomechanics compared to all other experimental groups.[96] However, *in vivo* delivery of VEGF was not confirmed as only VEGF gene expression was confirmed in green fluorescent protein labeled BM-MSC.[96] Ito *et al.* delivered VEGF indirectly to a mouse femoral defect by freeze-drying recombinant adeno-associated virus vectors (rAAV) for VEGF and receptor activator of nuclear factor kappaB ligand (RANKL) onto the allograft cortical surface.[162] New live bone was found on the periosteal allograft surface treated with both rAAV+VEGF and rAAV+RANKL compared to no new bone formation when allograft bone was treated with only one of the rAAV.[162] Geiger *et al.* found in two separate studies that VEGF gene therapy delivered either through a transfection plasmid via collagen sponge or genetically

engineered BM-MSC to a rat radial defect increased defect healing and vascularization compared to their control groups.[163,164]

While direct and indirect VEGF delivery to bone defects has shown to augment bone fracture healing, there is still no clinically approved VEGF therapies to heal human bone fractures. Clinical translation limitations include a short in vivo half-life of 6-8 hours and the potential of an excessive VEGF dose putting patients at risk for tumor malignancy.[165,166] Thus, a safe and effective VEGF clinical dose regime in humans to improve bone graft healing has eluded researchers so far. However, advances in growth factor delivery technology combined with further elucidation of bone graft healing molecular mechanisms may one day lead to an effective VEGF therapy to improve bone graft healing.

### 1.7.5. Fibroblast growth factor-2

Similar to VEGF, fibroblast growth factor-2 (FGF-2), a member of the fibroblast growth factor family, is known to be involved in angiogenesis.[167] FGF-2 is a potent mitogen for endothelial cells and can stimulate the capillary formation *in vivo*.[167] In fact, FGF-2 has mitogenic effects on other cell types including osteoprogenitors and adipose derived stem cells.[168,169] FGF-2 is also known to be expressed early in bone callus formation and was found to be responsible for triggering periosteal cell proliferation and subsequent increase in BMP-2 secrection.[3,170,171] Therefore, FGF-2 is candidate growth factor to explore augmenting bone graft healing.

While no tissue engineered periosteum approaches have used FGF-2 delivery (direct or indirect) to improve bone graft healing, several *in vivo* studies support FGF-2 enhancing bone formation. As early as 1996, FGF-2 delivered from a hyaluronate gel induced bone growth into a

rat bone conduction chamber.[172] Komaki *et al.* found that 200 µg of FGF-2 combined with β-TCP granules and collagen I implanted in a rabbit tibial defect resulted in complete healing and at 12 weeks compared to incomplete healing in FGF-2 free control groups.[173] Kawaguchi *et al.* reported local injection of 0.8 or 2.4 mg FGF-2 in a gelatin hydrogel accelerated tibial shaft fractures in humans.[174] Ueno *et al.* used a modified FGF-2 containing an engineered collagen binding motif to deliver FGF-2 to a mouse femoral defect .[175] The collagen sheet wrapped bone allograft bound modified FGF-2 which accelerated callus bridging and increased callus volume by week 3 compared to collagen sheet wrapped allografts delivering unmodified FGF-2.[175] However, the authors did not speculate whether sustained delivery of modified FGF-2 or an increased FGF-2 dose compared to unmodified FGF-2 was responsible for the accelerated defect healing.

However, conflicting studies on FGF-2 enhancing bone fracture healing exists. Nakajima *et al.* found that a single injection of FGF-2 contained in a fibrin gel at the site of a rat femoral fracture led to increased cartilage production in the fracture callus but ultimately did not induce more rapid healing.[176] Niedhart *et al.* FGF-2 delivered via β-TCP scaffolds to a rat femur defect had neither a positive or negative effect on bone formation.[177] Nevertheless, sufficient evidence exists to investigate FGF-2's effect to potentially increase bone allograft incorporation either through a mitogenic effect on osteoprogenitor cells or angiogenic stimuli within the bone defect.

To summarize, growth factors such as BMP-2, TGF-β1, VEGF, and FGF-2 present opportunities to augment periosteum-like substitutes to improve bone allograft healing. In the greater context of bone tissue engineering, BMP-2 and VEGF are the more investigated growth factors due to their potent osteoinductive and angiogenic effects, respectively, compared to TGF-β1 and FGF-2.[137] However, combined growth factor delivery strategies should ultimately

outperform single growth factor delivery strategies in enhancing bone fracture healing as this will more closely mimic the natural bone fracture healing cascade.[178,179] Table 1.1 summarizes the main results of research studies using the periosteum as a template to improve bone defect healing and lists the material, cells, and growth factors used in each study.

**Table 1.1 Summary table of periosteum-inspired studies to improve bone defect healing.**

| Material Approach | Author | Scaffold material used | Exogenous cell source | Growth factor addition | *In vivo* model used | Main result(s) |
|---|---|---|---|---|---|---|
| Natural tissue-based | Masquelet *et al*. | PMMA bone cement spacer and cancellous bone autograft | N/A | N/A | Human segmental defects | Reported repair of large segmental defect where an induced membrane formed over a bone cement spacer which was later removed and filled with bone autograft.[40] |
| | Stevens *et al.* | Ca-alginate hydrogel | N/A | N/A | Rabbit tibial periosteal void | Used hydraulically elevated periosteal void as *in situ* reactor to create bone tissue without exogenous cell or growth factor supplementation.[45] |
| | Knothe-Tate *et al.* | Silcone membrane containing periosteal tissue | PDC | N/A | Critical sized ovine femur defects | Greatest tissue generation and defect bridging detected in groups receiving autologous periosteal strips compared to controls containing collagen and PDC.[39,48] |
| Ceramic-based | Bruder *et al.* | Fibronectin-coated HAp/β-TCP porous cylinders | BM-MSC | N/A | Athymic rat and canine femoral defects | BM-MSC loaded ceramic cylinders showed radiographic and histological evidence of increased bone formation compared to cell-free ceramic cylinders.[50,51] |
| | Kang *et al.* | Cell sheet wrapped β-TCP scaffold | BM-MSC, HUVEC | N/A | Dorsal subcutaneous implantation in nude mice | BM-MSC and HUVEC cell sheet wrapped β-TCP scaffolds facilitated enhanced angiogenesis and bone matrix production compared to cell-free groups.[52] |
| | Nau *et al.* | β-TCP with vascularized periosteal flap | BM-MNC | N/A | Critical-sized rat femur defect | A vascularized periosteal flap combined with BM-MNCs seeded on β-TCP granules resulted in increased bone mineral density, vascularization, and strength compared to cell-free groups.[53] |

| | | | | | | |
|---|---|---|---|---|---|---|
| Protein-based | Hattori *et al.* | Collagen sponge | BM-MSC | N/A | Rat calvarial defect | Collagen sponge improved bone mineralization in rat calvarial defect compared to empty defect.[55] |
| | Schomeyr *et al.* | Acellular human dermis | BM-MSC | Transfected cells to express BMP-2 | Critical-sized mandibular defects in nude rats | After 6 weeks, bone defects treated with BMP-2 transfected BM-MSC delivered via acellular human dermis were healed compared to no healing in defects receiving non-transfected BM-MSC.[59] |
| | Rapp *et al.* | Fibronectin coated decellularized periosteum, xenograft bone | PDC, ASC | BMP-2, VEGF | Rat calvarial defect | Micro-CT results showed ASC supported greater mineralization compared to PDC-seeded decellularized periosteum. Addition of VEGF or BMP-2 with periosteum substitute increased bone formation in defect site.[60] |
| | Xie *et al.* | SIS-wrapped bone allograft | BM-MSC | Transfected cells to express BMP-2 | Mouse femur defect | SIS provided no benefits over BMP-2 expressing BM-MSC. Increased new bone formation torsional strength and stiffness were found in defects treated with BMP-2 expressing BM-MSC compared to untreated allografts.[65] |
| | Zhao *et al.* | SIS | BM-MSC | N/A | Critical sized rabbit radial defect | Pure SIS did not bridge bone defect. Osteoinduced BM-MSC delivered via SIS to bone defect enhanced defect bridging compared to the allograft only group.[66] |
| Polysaccharide-based | Guo *et al.* | Chitosan-TCP-gelatin scaffold | ASC | N/A | Critical sized rabbit radial defect | Addition of osteoinduced ASC improved bone healing compared to cell-free composite scaffold or a chitosan-only membrane. Chitosan stabilized ceramic scaffold phase.[83] |

| | | | | | | |
|---|---|---|---|---|---|---|
| | Almodovar *et al.* | Chitosan, heparin | BM-MSC | N/A | N/A | Chitosan-heparin polyelectrolyte multilayers showed antibacterial activity against *S. aureus* and *E. Coli* and facilitated BM-MSC attachment.[8] |
| | Caridade *et al.* | Chitosan, alginate | N/A | BMP-2 | Dorsal subcutaneous implantation in nude mice | BMP-2 on chitosan-alginate membranes induced ectopic bone nodule formation in mice at 21 days.[85] |
| Synthetic polymer-based | Oest *et al.* | PLDL | N/A | BMP-2, TGF-β3 | Critical-sized rat femur defect | BMP-2 & TGF-β3 increased bone volume formation in defect compared to PLDL scaffold only or untreated defect but did not increase torsional strength compared to defects treated with PLDL scaffold only group.[94] |
| | Hoffman *et al.* | Photopolymerizable PEG | BM-MSC | N/A | Critical-sized mouse femur defect | BM-MSC resulted in enhanced vascularization, bone callus formation in BM-MSC treated allografts compared to untreated allografts. PEG hydrogel alone found to minimally contribute to therapeutic effect.[95,96] |
| | Baldwin *et al.* | PCL, PEG, heparin hydrogel | BM-MSC, HUVEC | N/A | 0.5 mm femur cortical windows (NOD-SCID gamma mice) | Co-transplantation of HUVEC with BM-MSC in mice didn't increase BM-MSC viability but did increase vascularization compared to cell-free scaffolds. BM-MSC remained undifferentiated in implantation site for up to 30 days.[97] |

PMMA = polymethyl methacrylate, PDC = periosteum-derived cells, Hap= hydroxyapatite, β-TCP = tricalcium phosphate, BM-MSC = bone marrow mesenchymal stem cells, HUVEC = human umbilical vein endothelial cell, BM-MNC = bone marrow-derived mononuclear cells, BMP-2 = bone morphogenetic protein-2, ASC = adipose-derived stem cell, VEGF = vascular endothelial growth factor, SIS = submucosa intestinal scaffold, PLDL = poly(L-lactide-co-D,L-lactide), TGF-β3 = transforming growth factor-β3, PEG= polyethylene glycol, PCL = polycaprolactone, N/A = not applicable

# REFERENCES


1. Sen MK, Miclau T. Autologous iliac crest bone graft: should it still be the gold standard for treating nonunions? Injury 2007;38 Suppl 1:S75-80.
2. Zhang X, Xie C, Lin AS, Ito H, Awad H, Lieberman JR, Rubery PT, Schwarz EM, O'Keefe RJ, Guldberg RE. Periosteal progenitor cell fate in segmental cortical bone graft transplantations: implications for functional tissue engineering. J Bone Miner Res 2005;20(12):2124-37.
3. Roberts SJ, van Gastel N, Carmeliet G, Luyten FP. Uncovering the periosteum for skeletal regeneration: The stem cell that lies beneath. Bone 2015;70:10-18.
4. Boyce T, Edwards J, Scarborough N. Allograft bone. The influence of processing on safety and performance. Orthop Clin North Am 1999;30(4):571-81.
5. McAllister DR, Joyce MJ, Mann BJ, C. Thomas Vangsness J. Allograft Update: The Current Status of Tissue Regulation, Procurement, Processing, and Sterilization. The American Journal of Sports Medicine 2007;35(12):2148-2158.
6. Zhang X, Awad HA, O'Keefe RJ, Guldberg RE, Schwarz EM. A perspective: engineering periosteum for structural bone graft healing. Clin Orthop Relat Res 2008;466(8):1777-87.
7. Colnot C, Zhang X, Knothe Tate ML. Current insights on the regenerative potential of the periosteum: molecular, cellular, and endogenous engineering approaches. Journal of Orthopaedic Research 2012;30(12):1869-1878.
8. Almodovar J, Mower J, Banerjee A, Sarkar AK, Ehrhart NP, Kipper MJ. Chitosan-heparin polyelectrolyte multilayers on cortical bone: Periosteum-mimetic, cytophilic, antibacterial coatings. Biotechnology and Bioengineering 2013;110(2):609-618.
9. Rho JY, Kuhn-Spearing L, Zioupos P. Mechanical properties and the hierarchical structure of bone. Med Eng Phys 1998;20(2):92-102.
10. Ashman RB, Rho JY. Elastic modulus of trabecular bone material. J Biomech 1988;21(3):177-81.
11. Van. Leeuwenhoek A. An extract of a letter from Mr. Anth. Van. Leeuwenhoek, containing several observations on the texture of the bones of animals compared with that of wood: On the bark of trees: On the little scales found on the cuticula, etc. Philisophical Transactions 1693;17:838-843.
12. Buckwalter JA, Glimcher MJ, Cooper RR, Recker R. BONE BIOLOGY .1. STRUCTURE, BLOOD-SUPPLY, CELLS, MATRIX, AND MINERALIZATION. Journal of Bone and Joint Surgery-American Volume 1995;77A(8):1256-1275.
13. Datta HK, Ng WF, Walker JA, Tuck SP, Varanasi SS. The cell biology of bone metabolism. Journal of Clinical Pathology 2008;61(5):577-587.
14. Reznikov N, Shahar R, Weiner S. Bone hierarchical structure in three dimensions. Acta Biomater 2014;10(9):3815-26.
15. Bianco P. Stem cells and bone: a historical perspective. Bone 2015;70:2-9.
16. Einhorn TA, Gerstenfeld LC. Fracture healing: mechanisms and interventions. Nat Rev Rheumatol 2015;11(1):45-54.
17. Allen MR, Hock JM, Burr DB. Periosteum: biology, regulation, and response to osteoporosis therapies. Bone 2004;35(5):1003-1012.

18. Aaron JE. Periosteal Sharpey's fibers: a novel bone matrix regulatory system? Front Endocrinol (Lausanne) 2012;3(98):1-10.
19. Hirashima S, Ohta K, Kanazawa T, Uemura K-i, Togo A, Yoshitomi M, Okayama S, Kusukawa J, Nakamura K-i. Anchoring structure of the calvarial periosteum revealed by focused ion beam/scanning electron microscope tomography. Scientific Reports 2015;5(17511).
20. Hohmann EL, Elde RP, Rysavy JA, Einzig S, Gebhard RL. Innervation of periosteum and bone by sympathetic vasoactive intestinal peptide-containing nerve fibers. Science 1986;232(4752):868-71.
21. Ellender G, Feik SA, Carach BJ. Periosteal structure and development in a rat caudal vertebra. J Anat 1988;158:173-87.
22. Zhang X, Xie C, Lin ASP, Ito H, Awad H, Lieberman JR, Rubery PT, Schwarz EM, O'Keefe RJ, Guldberg RE. Periosteal progenitor cell fate in segmental cortical bone graft transplantations: implications for functional tissue engineering. Journal of Bone and Mineral Research 2005;20(12):2124-2137.
23. Colnot C. Skeletal cell fate decisions within periosteum and bone marrow during bone regeneration. J Bone Miner Res 2009;24(2):274-82.
24. Ozaki A, Tsunoda M, Kinoshita S, Saura R. Role of fracture hematoma and periosteum during fracture healing in rats: interaction of fracture hematoma and the periosteum in the initial step of the healing process. J Orthop Sci 2000;5(1):64-70.
25. Zhang XP, Xie C, Lin ASP, Ito H, Awad H, Lieberman JR, Rubery PT, Schwarz EM, O'Keefe RJ, Guldberg RE. Periosteal progenitor cell fate in segmental cortical bone graft transplantations: Implications for functional tissue engineering. Journal of Bone and Mineral Research 2005;20(12):2124-2137.
26. Yiannakopoulos CK, Kanellopoulos AD, Trovas GP, Dontas IA, Lyritis GP. The biomechanical capacity of the periosteum in intact long bones. Arch Orthop Trauma Surg 2008;128(1):117-20.
27. Evans SF, Chang H, Knothe Tate ML. Elucidating Multiscale Periosteal Mechanobiology: A Key to Unlocking the Smart Properties and regenerative capacity of the Periosteum? Tissue Engineering. Part B 2013;19:147-159.
28. Evans SF, Parent JB, Lasko CE, Zhen X, Knothe UR, Lemaire T, Knothe Tate ML. Periosteum, Bone's "smart" bounding membrane, exhibits direction dependent permeability. Journal of Bone and Mineral Research 2013;28 608-617.
29. Marsell R, Einhorn TA. The biology of fracture healing. Injury 2011;42(6):551-5.
30. Carano RAD, Filvaroff EH. Angiogenesis and bone repair. Drug Discovery Today 2003;8(21):980-989.
31. Gerstenfeld LC, Cullinane DM, Barnes GL, Graves DT, Einhorn TA. Fracture healing as a post-natal developmental process: molecular, spatial, and temporal aspects of its regulation. J Cell Biochem 2003;88(5):873-84.
32. Hernigou P. Bone transplantation and tissue engineering. Part II: bone graft and osteogenesis in the seventeenth, eighteenth and nineteenth centuries (Duhamel, Haller, Ollier and MacEwen). International Orthopaedics 2015;39(1):193-204.
33. Donati D, Zolezzi C, Tomba P, Vigano A. Bone grafting: historical and conceptual review, starting with an old manuscript by Vittorio Putti. Acta Orthop 2007;78(1):19-25.
34. Urist MR. Bone: Formation by Autoinduction. Science 1965;150(3698):893-899.

35. Caplan AI. Mesenchymal stem cells. Journal of orthopaedic research : official publication of the Orthopaedic Research Society 1991;9(5):641-50.
36. Owen M, Friedenstein AJ. Stromal stem cells: marrow-derived osteogenic precursors. Ciba Found Symp 1988;136:42-60.
37. Schofield R. The relationship between the spleen colony-forming cell and the haemopoietic stem cell. Blood Cells 1978;4(1-2):7-25.
38. Zhang X, Awad HA, O'Keefe RJ, Guldberg RE, Schwarz EM. A perspective: Engineering periosteum for structural bone graft healing. Clinical Orthopaedics and Related Research 2008;466(8):1777-1787.
39. Moore SR, Heu C, Yu NYC, Whan RM, Knothe UR, Milz S, Tate MLK. Translating Periosteum's Regenerative Power: Insights From Quantitative Analysis of Tissue Genesis With a Periosteum Substitute Implant. Stem Cells Translational Medicine 2016;5(12):1739-1749.
40. Masquelet AC, Fitoussi F, Begue T, Muller GP. [Reconstruction of the long bones by the induced membrane and spongy autograft]. Ann Chir Plast Esthet 2000;45(3):346-53.
41. Pelissier P, Masquelet AC, Bareille R, Pelissier SM, Amedee J. Induced membranes secrete growth factors including vascular and osteoinductive factors and could stimulate bone regeneration. J Orthop Res 2004;22(1):73-9.
42. Giannoudis PV, Faour O, Goff T, Kanakaris N, Dimitriou R. Masquelet technique for the treatment of bone defects: tips-tricks and future directions. Injury 2011;42(6):591-8.
43. Cuthbert RJ, Churchman SM, Tan HB, McGonagle D, Jones E, Giannoudis PV. Induced periosteum a complex cellular scaffold for the treatment of large bone defects. Bone 2013;57(2):484-492.
44. Wang X, Wei F, Luo F, Huang K, Xie Z. Induction of granulation tissue for the secretion of growth factors and the promotion of bone defect repair. Journal of Orthopaedic Surgery and Research 2015;10.
45. Stevens MM, Marini RP, Schaefer D, Aronson J, Langer R, Shastri VP. In vivo engineering of organs: The bone bioreactor. Proceedings of the National Academy of Sciences of the United States of America 2005;102(32):11450-11455.
46. Knothe UR, Springfield DS. A novel surgical procedure for bridging of massive bone defects. World J Surg Oncol 2005;3(1):7.
47. Knothe Tate ML, Ritzman TF, Schneider E, Knothe UR. Testing of a new one-stage bone-transport surgical procedure exploiting the periosteum for the repair of long-bone defects. J Bone Joint Surg Am 2007;89(2):307-16.
48. Tate MLK, Chang H, Moore SR, Knothe UR. Surgical Membranes as Directional Delivery Devices to Generate Tissue: Testing in an Ovine Critical Sized Defect Model. Figshare 2011.
49. LeGeros RZ. Properties of osteoconductive biomaterials: Calcium phosphates. Clinical Orthopaedics and Related Research 2002(395):81-98.
50. Bruder SP, Kraus KH, Goldberg VM, Kadiyala S. The effect of implants loaded with autologous mesenchymal stem cells on the healing of canine segmental bone defects. J Bone Joint Surg Am 1998;80(7):985-96.
51. Bruder SP, Kurth AA, Shea M, Hayes WC, Jaiswal N, Kadiyala S. Bone regeneration by implantation of purified, culture-expanded human mesenchymal stem cells. J Orthop Res 1998;16(2):155-62.

52. Kang YQ, Ren LL, Yang YZ. Engineering Vascularized Bone Grafts by Integrating a Biomimetic Periosteum and beta-TCP Scaffold. ACS Applied Materials & Interfaces 2014;6(12):9622-9633.
53. Nau C, Henrich D, Seebach C, Schroeder K, Fitzsimmons S-J, Hankel S, Barker JH, Marzi I, Frank J. Treatment of Large Bone Defects with a Vascularized Periosteal Flap in Combination with Biodegradable Scaffold Seeded with Bone Marrow-Derived Mononuclear Cells: An Experimental Study in Rats. Tissue Engineering Part A 2016;22(1-2):133-141.
54. Brett E, Flacco J, Blackshear C, Longaker MT, Wan DC. Biomimetics of Bone Implants: The Regenerative Road. Biores Open Access 2017;6(1):1-6.
55. Hattori K, Yoshikawa T, Takakura Y, Aoki H, Sonobe M, Tomita N. Bio-artificial periosteum for severe open fracture - An experimental study of osteogenic cell/collagen sponge composite as a bio-artificial periosteum. Bio-Medical Materials and Engineering 2005;15(3):127-136.
56. Fan W, Crawford R, Xiao Y. Enhancing in vivo vascularized bone formation by cobalt chloride-treated bone marrow stromal cells in a tissue engineered periosteum model. Biomaterials 2010;31(13):3580-3589.
57. Pacary E, Legros H, Valable S, Duchatelle P, Lecocq M, Petit E, Nicole O, Bernaudin M. Synergistic effects of CoCl(2) and ROCK inhibition on mesenchymal stem cell differentiation into neuron-like cells. J Cell Sci 2006;119(Pt 13):2667-78.
58. Shi XT, Chen S, Zhao YH, Lai C, Wu HK. Enhanced Osteogenesis by a Biomimic Pseudo-Periosteum-Involved Tissue Engineering Strategy. Advanced Healthcare Materials 2013;2(9):1229-1235.
59. Schonmeyr B, Clavin N, Avraham T, Longo V, Mehrara BJ. Synthesis of a tissue-engineered periosteum with acellular dermal matrix and cultured mesenchymal stem cells. Tissue Eng Part A 2009;15(7):1833-41.
60. Rapp SJ, Jones DC, Gerety P, Taylor JA. Repairing critical-sized rat calvarial defects with progenitor cell-seeded acellular periosteum: A novel biomimetic scaffold. Surgery 2012;152(4):595-605.
61. Chen K, Lin X, Zhang Q, Ni J, Li J, Xiao J, Wang Y, Ye Y, Chen L, Jin K and others. Decellularized periosteum as a potential biologic scaffold for bone tissue engineering. Acta Biomaterialia 2015;19:46-55.
62. Hodde J. Naturally occurring scaffolds for soft tissue repair and regeneration. Tissue Eng 2002;8(2):295-308.
63. Crapo PM, Gilbert TW, Badylak SF. An overview of tissue and whole organ decellularization processes. Biomaterials 2011;32(12):3233-43.
64. Shi L, Ronfard V. Biochemical and biomechanical characterization of porcine small intestinal submucosa (SIS): a mini review. Int J Burns Trauma 2013;3(4):173-9.
65. Xie C, Reynolds D, Awad H, Rubery PT, Pelled G, Gazit D, Guldberg RE, Schwarz EM, O'Keefe RJ, Zhang X. Structural bone allograft combined with genetically engineered mesenchymal stem cells as a novel platform for bone tissue engineering. Tissue engineering 2007;13(3):435-445.
66. Zhao L, Zhao J, Wang S, Wang J, Liu J. Comparative study between tissue-engineered periosteum and structural allograft in rabbit critical-sized radial defect model. Journal of Biomedical Materials Research Part B-Applied Biomaterials 2011;97B(1):1-9.

67. El Backly RM, Zaky SH, Muraglia A, Tonachini L, Brun F, Canciani B, Chiapale D, Santolini F, Cancedda R, Mastrogiacomo M. A Platelet-Rich Plasma-Based Membrane as a Periosteal Substitute with Enhanced Osteogenic and Angiogenic Properties: A New Concept for Bone Repair. Tissue Engineering Part A 2013;19(1-2):152-165.
68. Tejeda-Montes E, Klymov A, Nejadnik MR, Alonso M, Rodriguez-Cabello JC, Walboomers XF, Mata A. Mineralization and bone regeneration using a bioactive elastin-like recombinamer membrane. Biomaterials 2014;35(29):8339-8347.
69. Zheng MH, Chen J, Kirilak Y, Willers C, Xu J, Wood D. Porcine small intestine submucosa (SIS) is not an acellular collagenous matrix and contains porcine DNA: possible implications in human implantation. J Biomed Mater Res B Appl Biomater 2005;73(1):61-7.
70. Kiani C, Chen L, Wu YJ, Yee AJ, Yang BB. Structure and function of aggrecan. Cell Res 2002;12(1):19-32.
71. Swann DA, Radin EL, Nazimiec M, Weisser PA, Curran N, Lewinnek G. Role of hyaluronic acid in joint lubrication. Ann Rheum Dis 1974;33(4):318-26.
72. Rabenstein DL. Heparin and heparan sulfate: structure and function. Natural Product Reports 2002;19:312-31.
73. Mulloy B, Rider CC. Cytokines and proteoglycans: an introductory overview. Biochem Soc Trans 2006;34(Pt 3):409-13.
74. Bhattarai N, Edmondson D, Veiseh O, Matsen FA, Zhang M. Electrospun chitosan-based nanofibers and their cellular compatibility. Biomaterials 2005;26(31):6176-84.
75. Aiba S. Studies on chitosan: 4. Lysozymic hydrolysis of partially N-acetylated chitosans. Int J Biol Macromol 1992;14(4):225-8.
76. Tomihata K, Ikada Y. In vitro and in vivo degradation of films of chitin and its deacetylated derivatives. Biomaterials 1997;18(7):567-575.
77. Freier T, Koh HS, Kazazian K, Shoichet MS. Controlling cell adhesion and degradation of chitosan films by N-acetylation. Biomaterials 2005;26(29):5872-8.
78. Senel S, McClure SJ. Potential applications of chitosan in veterinary medicine. Adv Drug Deliv Rev 2004;56(10):1467-80.
79. Levengood S, Zhang M. Chitosan scaffolds for bone tissue engineering. Journal of Materials Chemistry B 2014.
80. Shin SY, Park HN, Kim KH, Lee MH, Choi YS, Park YJ, Lee YM, Ku Y, Rhyu IC, Han SB and others. Biological evaluation of chitosan nanofiber membrane for guided bone regeneration. Journal of Periodontology 2005;76(10):1778-1784.
81. Florczyk SJ, Leung M, Li Z, Huang JI, Hopper RA, Zhang M. Evaluation of three-dimensional porous chitosan-alginate scaffolds in rat calvarial defects for bone regeneration applications. J Biomed Mater Res A 2013;101(10):2974-83.
82. Costa-Pinto AR, Reis RL, Neves NM. Scaffolds Based Bone Tissue Engineering: the Role of Chitosan. Tissue Engineering Part B: Reviews 2011;17(5):331-347.
83. Guo H, Li X, Yuan X, Ma X. Reconstruction of radial bone defects using the reinforced tissue-engineered periosteum: An experimental study on rabbit weight-bearing segment. Journal of Trauma and Acute Care Surgery 2012;72(2):E94-E100.
84. Almodóvar J, Mower J, Banerjee A, Sarkar AK, Ehrhart NP, Kipper MJ. Chitosan-heparin polyelectrolyte multilayers on cortical bone: Periosteum-mimetic, cytophilic, antibacterial coatings. Biotechnology and Bioengineering 2013;110(2):609-618.

85. Caridade SG, Monge C, Almodovar J, Guillot R, Lavaud J, Josserand V, Coll J-L, Mano JF, Picart C. Myoconductive and osteoinductive free-standing polysaccharide membranes. Acta Biomaterialia 2015;15:139-149.
86. Jiang T, Deng M, James R, Nair LS, Laurencin CT. Micro- and nanofabrication of chitosan structures for regenerative engineering. Acta Biomaterialia 2014;10(4):1632-1645.
87. Madihally SV, Matthew HW. Porous chitosan scaffolds for tissue engineering. Biomaterials 1999;20(12):1133-42.
88. Ohkawa K, Cha D, Kim H, Nishida A, Yamamoto H. Electrospinning of Chitosan. Macromolecular Rapid Communications 2004;25(18):1600-1605.
89. Macdonald ML, Samuel RE, Shah NJ, Padera RF, Beben YM, Hammond PT. Tissue integration of growth factor-eluting layer-by-layer polyelectrolyte multilayer coated implants. Biomaterials 2011;32(5):1446-53.
90. Macdonald M, Rodriguez NM, Smith R, Hammond PT. Release of a model protein from biodegradable self assembled films for surface delivery applications. Journal of controlled release : official journal of the Controlled Release Society 2008;131(3):228-34.
91. Volpato FZ, Almodóvar J, Erickson K, Popat KC, Migliaresi C, Kipper MJ. Preservation of FGF-2 bioactivity using heparin-based nanoparticles, and their delivery from electrospun chitosan fibers. Acta biomaterialia 2012;8(4):1551-1559.
92. Almodóvar J, Bacon S, Gogolski J, Kisiday JD, Kipper MJ. Polysaccharide-based polyelectrolyte multilayer surface coatings can enhance mesenchymal stem cell response to adsorbed growth factors. Biomacromolecules 2010;11(10):2629-39.
93. Boddohi S, Kipper MJ. Engineering nanoassemblies of polysaccharides. Advanced materials (Deerfield Beach, Fla.) 2010;22(28):2998-3016.
94. Oest ME, Dupont KM, Kong HJ, Mooney DJ, Guldberg RE. Quantitative assessment of scaffold and growth factor-mediated repair of critically sized bone defects. J Orthop Res 2007;25(7):941-50.
95. Hoffman MD, Xie C, Zhang X, Benoit DSW. The effect of mesenchymal stem cells delivered via hydrogel-based tissue engineered periosteum on bone allograft healing. Biomaterials 2013;34(35):8887-8898.
96. Hoffman MD, Benoit DSW. Emulating native periosteum cell population and subsequent paracrine factor production to promote tissue engineered periosteum-mediated allograft healing. Biomaterials 2015;52:426-440.
97. Baldwin JG, Wagner F, Martine LC, Holzapfel BM, Theodoropoulos C, Bas O, Savi FM, Werner C, De-Juan-Pardo EM, Hutmacher DW. Periosteum tissue engineering in an orthotopic in vivo platform. Biomaterials 2017;121:193-204.
98. Zhang B, Filion TM, Kutikov AB, Song J. Facile Stem Cell Delivery to Bone Grafts Enabled by Smart Shape Recovery and Stiffening of Degradable Synthetic Periosteal Membranes. Advanced Functional Materials 2017;27(5).
99. Nair LS, Laurencin CT. Polymers as biomaterials for tissue engineering and controlled drug delivery. Adv Biochem Eng Biotechnol 2006;102:47-90.
100. Langer R, Vacanti JP. Tissue engineering. Science 1993;260(5110):920-6.
101. Caplan AI. Adult mesenchymal stem cells for tissue engineering versus regenerative medicine. J Cell Physiol 2007;213(2):341-7.

102. Pittenger MF. Multilineage Potential of Adult Human Mesenchymal Stem Cells. Science 1999;284(5411):143-147.
103. Haynesworth SE, Baber MA, Caplan AI. Cytokine expression by human marrow-derived mesenchymal progenitor cells in vitro: effects of dexamethasone and IL-1 alpha. J Cell Physiol 1996;166(3):585-92.
104. Beyth S, Borovsky Z, Mevorach D, Liebergall M, Gazit Z, Aslan H, Galun E, Rachmilewitz J. Human mesenchymal stem cells alter antigen-presenting cell maturation and induce T-cell unresponsiveness. Blood 2005;105(5):2214-9.
105. Barry FP, Murphy JM. Mesenchymal stem cells: clinical applications and biological characterization. International Journal of Biochemistry & Cell Biology 2004;36(4):568-584.
106. Bruder SP, Fink DJ, Caplan AI. Mesenchymal stem cells in bone development, bone repair, and skeletal regeneration therapy. J Cell Biochem 1994;56(3):283-94.
107. Caplan AI. Mesenchymal Stem Cells: Time to Change the Name! Stem Cells Translational Medicine 2017;6(6):1445-1451.
108. Caplan AI. Review: mesenchymal stem cells: cell-based reconstructive therapy in orthopedics. Tissue Eng 2005;11(7-8):1198-211.
109. Dimmeler S, Ding S, Rando TA, Trounson A. Translational strategies and challenges in regenerative medicine. Nat Med 2014;20(8):814-21.
110. Trounson A, McDonald C. Stem Cell Therapies in Clinical Trials: Progress and Challenges. Cell Stem Cell 2015;17(1):11-22.
111. Morrow D, Ussi A, Migliaccio G. Addressing Pressing Needs in the Development of Advanced Therapies. Front Bioeng Biotechnol 2017;5:55.
112. Zuk PA, Zhu M, Mizuno H, Huang J, Futrell JW, Katz AJ, Benhaim P, Lorenz HP, Hedrick MH. Multilineage cells from human adipose tissue: implications for cell-based therapies. Tissue Engineering 2001;7(2):211-228.
113. Zuk P. Adipose-Derived Stem Cells in Tissue Regeneration: A Review. ISRN Stem Cells 2013;2013(1):1-35.
114. Izadpanah R, Trygg C, Patel B, Kriedt C, Dufour J, Gimble JM, Bunnell BA. Biologic properties of mesenchymal stem cells derived from bone marrow and adipose tissue. J Cell Biochem 2006;99(5):1285-97.
115. Kern S, Eichler H, Stoeve J, Kluter H, Bieback K. Comparative analysis of mesenchymal stem cells from bone marrow, umbilical cord blood, or adipose tissue. Stem Cells 2006;24(5):1294-301.
116. Cowan CM, Shi YY, Aalami OO, Chou YF, Mari C, Thomas R, Quarto N, Contag CH, Wu B, Longaker MT. Adipose-derived adult stromal cells heal critical-size mouse calvarial defects. Nat Biotechnol 2004;22(5):560-7.
117. Cowan CM, Aalami OO, Shi YY, Chou YF, Mari C, Thomas R, Quarto N, Nacamuli RP, Contag CH, Wu B and others. Bone morphogenetic protein 2 and retinoic acid accelerate in vivo bone formation, osteoclast recruitment, and bone turnover. Tissue Engineering 2005;11(3-4):645-658.
118. Halvorsen YD, Franklin D, Bond AL, Hitt DC, Auchter C, Boskey AL, Paschalis EP, Wilkison WO, Gimble JM. Extracellular matrix mineralization and osteoblast gene expression by human adipose tissue-derived stromal cells. Tissue Eng 2001;7(6):729-41.
119. Levi B, Nelson ER, Brown K, James AW, Xu D, Dunlevie R, Wu JC, Lee M, Wu B, Commons GW and others. Differences in Osteogenic Differentiation of Adipose-Derived

Stromal Cells from Murine, Canine, and Human Sources In Vitro and In Vivo. Plastic and Reconstructive Surgery 2011;128(2):373-386.
120. Levi B, James AW, Glotzbach JP, Wan DC, Commons GW, Longaker MT. Depot-specific variation in the osteogenic and adipogenic potential of human adipose-derived stromal cells. Plast Reconstr Surg 2010;126(3):822-34.
121. Levi B, Longaker MT. Osteogenic differentiation of adipose-derived stromal cells in mouse and human: in vitro and in vivo methods. J Craniofac Surg. United States; 2011. p 388-91.
122. Levi B, James AW, Nelson ER, Vistnes D, Wu B, Lee M, Gupta A, Longaker MT. Human adipose derived stromal cells heal critical size mouse calvarial defects. PLoS One 2010;5(6):e11177.
123. Chang H, Tate MLK. Concise Review: The Periosteum: Tapping into a Reservoir of Clinically Useful Progenitor Cells. Stem Cells Translational Medicine 2012;1(6):480-491.
124. Ball MD, Bonzani IC, Bovis MJ, Williams A, Stevens MM. Human periosteum is a source of cells for orthopaedic tissue engineering: a pilot study. Clin Orthop Relat Res 2011;469(11):3085-93.
125. De Bari C, Dell'Accio F, Vanlauwe J, Eyckmans J, Khan IM, Archer CW, Jones EA, McGonagle D, Mitsiadis TA, Pitzalis C and others. Mesenchymal multipotency of adult human periosteal cells demonstrated by single-cell lineage analysis. Arthritis Rheum 2006;54(4):1209-21.
126. Wang Q, Huang C, Zeng F, Xue M, Zhang X. Activation of the Hh Pathway in Periosteum-Derived Mesenchymal Stem Cells Induces Bone Formation in Vivo Implication for Postnatal Bone Repair. American Journal of Pathology 2010;177(6):3100-3111.
127. Nakahara H, Dennis JE, Bruder SP, Haynesworth SE, Lennon DP, Caplan AI. In vitro differentiation of bone and hypertrophic cartilage from periosteal-derived cells. Exp Cell Res 1991;195(2):492-503.
128. Hayashi O, Katsube Y, Hirose M, Ohgushi H, Ito H. Comparison of osteogenic ability of rat mesenchymal stem cells from bone marrow, periosteum, and adipose tissue. Calcif Tissue Int 2008;82(3):238-47.
129. Sakaguchi Y, Sekiya I, Yagishita K, Muneta T. Comparison of human stem cells derived from various mesenchymal tissues: superiority of synovium as a cell source. Arthritis Rheum 2005;52(8):2521-9.
130. Breitbart AS, Grande DA, Kessler R, Ryaby JT, Fitzsimmons RJ, Grant RT. Tissue engineered bone repair of calvarial defects using cultured periosteal cells. Plast Reconstr Surg 1998;101(3):567-74; discussion 575-6.
131. Bakker AD, Schrooten J, van Cleynenbreugel T, Vanlauwe J, Luyten J, Schepers E, Dubruel P, Schacht E, Lammens J, Luyten FP. Quantitative screening of engineered implants in a long bone defect model in rabbits. Tissue Eng Part C Methods 2008;14(3):251-60.
132. Perka C, Schultz O, Spitzer RS, Lindenhayn K, Burmester GR, Sittinger M. Segmental bone repair by tissue-engineered periosteal cell transplants with bioresorbable fleece and fibrin scaffolds in rabbits. Biomaterials 2000;21(11):1145-53.
133. Stockmann P, Park J, von Wilmowsky C, Nkenke E, Felszeghy E, Dehner JF, Schmitt C, Tudor C, Schlegel KA. Guided bone regeneration in pig calvarial bone defects using

autologous mesenchymal stem/progenitor cells - a comparison of different tissue sources. J Craniomaxillofac Surg 2012;40(4):310-20.
134. Yoshimura H, Muneta T, Nimura A, Yokoyama A, Koga H, Sekiya I. Comparison of rat mesenchymal stem cells derived from bone marrow, synovium, periosteum, adipose tissue, and muscle. Cell Tissue Res 2007;327(3):449-62.
135. Hankenson KD, Gagne K, Shaughnessy M. Extracellular signaling molecules to promote fracture healing and bone regeneration. Advanced Drug Delivery Reviews 2015;94:3-12.
136. Tessmar JK, Göpferich AM. Matrices and scaffolds for protein delivery in tissue engineering. Advanced Drug Delivery Reviews 2007;59(4):274-291.
137. Gothard D, Smith EL, Kanczler JM, Rashidi H, Qutachi O, Henstock J, Rotherham M, El Haj A, Shakesheff KM, Oreffo RO. Tissue engineered bone using select growth factors: A comprehensive review of animal studies and clinical translation studies in man. Eur Cell Mater 2014;28:166-207; discussion 207-8.
138. Urist MR, Strates BS. Bone morphogenetic protein. J Dent Res 1971;50(6):1392-406.
139. Wozney JM, Rosen V, Celeste AJ, Mitsock LM, Whitters MJ, Kriz RW, Hewick RM, Wang EA. Novel regulators of bone formation: molecular clones and activities. Science 1988;242(4885):1528-34.
140. Grgurvic L, Pecina M, Vukicevic S. Marshall R. Urist and the discovery of bone morphogenetic proteins. International Orthopaedics 2017;41(5):1065-1069.
141. Fisher DM, Wong JM, Crowley C, Khan WS. Preclinical and clinical studies on the use of growth factors for bone repair: a systematic review. Curr Stem Cell Res Ther 2013;8(3):260-8.
142. James AW, LaChaud G, Shen J, Asatrian G, Nguyen V, Zhang X, Ting K, Soo C. A Review of the Clinical Side Effects of Bone Morphogenetic Protein-2. Tissue Eng Part B Rev 2016.
143. Oest ME, Dupont KM, Kong H-J, Mooney DJ, Guldberg RE. Quantitative assessment of scaffold and growth factor-mediated repair of critically sized bone defects. Journal of Orthopaedic Research 2007;25(7):941-950.
144. Lieberman JR, Daluiski A, Stevenson S, Wu L, McAllister P, Lee YP, Kabo JM, Finerman GA, Berk AJ, Witte ON. The effect of regional gene therapy with bone morphogenetic protein-2-producing bone-marrow cells on the repair of segmental femoral defects in rats. J Bone Joint Surg Am 1999;81(7):905-17.
145. de Larco JE, Todaro GJ. Growth factors from murine sarcoma virus-transformed cells. Proc Natl Acad Sci U S A 1978;75(8):4001-5.
146. Moses HL, Branum EL, Proper JA, Robinson RA. Transforming growth factor production by chemically transformed cells. Cancer Res 1981;41(7):2842-8.
147. Roberts AB, Anzano MA, Lamb LC, Smith JM, Sporn MB. New class of transforming growth factors potentiated by epidermal growth factor: isolation from non-neoplastic tissues. Proc Natl Acad Sci U S A 1981;78(9):5339-43.
148. Moses HL, Roberts AB, Derynck R. The Discovery and Early Days of TGF-β: A Historical Perspective. Cold Spring Harb Perspect Biol 2016.
149. Seyedin SM, Thomas TC, Thompson AY, Rosen DM, Piez KA. Purification and characterization of two cartilage-inducing factors from bovine demineralized bone. Proc Natl Acad Sci U S A 1985;82(8):2267-71.

150. Morikawa M, Derynck R, Miyazono K. TGF-β and the TGF-β Family: Context-Dependent Roles in Cell and Tissue Physiology. Cold Spring Harbor Perspectives in Biology 2016;8:a021873.
151. Joyce ME, Roberts AB, Sporn MB, Bolander ME. Transforming growth factor-beta and the initiation of chondrogenesis and osteogenesis in the rat femur. The Journal of Cell Biology 1990;110(6).
152. Tuli R, Tuli S, Nandi S, Huang X, Manner PA, Hozack WJ, Danielson KG, Hall DJ, Tuan RS. Transforming Growth Factor-β-mediated Chondrogenesis of Human Mesenchymal Progenitor Cells Involves N-cadherin and Mitogen-activated Protein Kinase and Wnt Signaling Cross-talk. The Journal of Biological Chemistry 2003;278:41227-36.
153. Pfeilschifter J, Department of Medicine I E, University of Heidelberg, Luisenstrasse 5, 6900 Heidelberg, Federal Republic of Germany, Department of Medicine I EUoHLDH, Federal Republic of Germany, Wolf O, Department of Medicine I E, University of Heidelberg, Luisenstrasse 5, 6900 Heidelberg, Federal Republic of Germany, Naumann A, Department of Medicine I E, University of Heidelberg, Luisenstrasse 5, 6900 Heidelberg, Federal Republic of Germany, Minne HW, Department of Medicine I E, University of Heidelberg, Luisenstrasse 5, 6900 Heidelberg, Federal Republic of Germany, Mundy GR and others. Chemotactic response of osteoblastlike cells to transforming growth factorÎ². Journal of Bone and Mineral Research 1990;5(8):825-830.
154. Marcelli C, Yates AJ, Mundy GR. In vivo effects of human recombinant transforming growth factor beta on bone turnover in normal mice. J Bone Miner Res 1990;5(10):1087-96.
155. Cho TJ, Gerstenfeld LC, Einhorn TA. Differential temporal expression of members of the transforming growth factor beta superfamily during murine fracture healing. J Bone Miner Res 2002;17(3):513-20.
156. Janssens K, ten Dijke P, Janssens S, Van Hul W. Transforming growth factor-beta 1 to the bone. Endocrine Reviews 2005;26(6):743-774.
157. Tieline L, Puolakkainen P, Pohjonen T, Rautavuori J, Tormala P, Rokkanen P. The effect of transforming growth factor-beta1, released from a bioabsorbable self-reinforced polylactide pin, on a bone defect. Biomaterials 2002;23(18):3817-23.
158. Ehrhart NP, Hong L, Morgan AL, Eurell JA, Jamison RD. Effect of transforming growth factor-beta 1 on bone regeneration in critical-sized bone defects after irradiation of host tissues. American Journal of Veterinary Research 2005;66(6):1039-1045.
159. Das A, Botchwey E. Evaluation of angiogenesis and osteogenesis. Tissue Eng Part B Rev 2011;17(6):403-14.
160. Kanczler JM, Oreffo RO. Osteogenesis and angiogenesis: the potential for engineering bone. Eur Cell Mater 2008;15:100-14.
161. Street J, Bao M, deGuzman L, Bunting S, Peale FV, Jr., Ferrara N, Steinmetz H, Hoeffel J, Cleland JL, Daugherty A and others. Vascular endothelial growth factor stimulates bone repair by promoting angiogenesis and bone turnover. Proc Natl Acad Sci U S A 2002;99(15):9656-61.
162. Ito H, Koefoed M, Tiyapatanaputi P, Gromov K, Goater JJ, Carmouche J, Zhang XP, Rubery PT, Rabinowitz J, Samulski RJ and others. Remodeling of cortical bone allografts mediated by adherent rAAV-RANKL and VEGF gene therapy. Nature Medicine 2005;11(3):291-297.

163. Geiger F, Bertram H, Berger I, Lorenz H, Wall O, Eckhardt C, Simank HG, Richter W. Vascular endothelial growth factor gene-activated matrix (VEGF165-GAM) enhances osteogenesis and angiogenesis in large segmental bone defects. J Bone Miner Res 2005;20(11):2028-35.
164. Geiger F, Lorenz H, Xu W, Szalay K, Kasten P, Claes L, Augat P, Richter W. VEGF producing bone marrow stromal cells (BMSC) enhance vascularization and resorption of a natural coral bone substitute. Bone 2007;41(4):516-22.
165. Kasten P, Beverungen M, Lorenz H, Wieland J, Fehr M, Geiger F. Comparison of Platelet-Rich Plasma and VEGF-Transfected Mesenchymal Stem Cells on Vascularization and Bone Formation in a Critical-Size Bone Defect. Cells Tissues Organs 2012;196(6):523-533.
166. Kaigler D, Wang Z, Horger K, Mooney DJ, Krebsbach PH. VEGF scaffolds enhance angiogenesis and bone regeneration in irradiated osseous defects. J Bone Miner Res 2006;21(5):735-44.
167. Montesano R, Vassalli JD, Baird A, Guillemin R, Orci L. Basic fibroblast growth factor induces angiogenesis in vitro. Proc Natl Acad Sci U S A 1986;83(19):7297-301.
168. Quarto N, Longaker MT. FGF-2 inhibits osteogenesis in mouse adipose tissue-derived stromal cells and sustains their proliferative and osteogenic potential state. Tissue Eng 2006;12(6):1405-18.
169. Radomsky ML, Thompson AY, Spiro RC, Poser JW. Potential role of fibroblast growth factor in enhancement of fracture healing. Clin Orthop Relat Res 1998(355 Suppl):S283-93.
170. Du XL, Xie YL, Xian CJ, Chen L. Role of FGFs/FGFRs in skeletal development and bone regeneration. Journal of Cellular Physiology 2012;227(12):3731-3743.
171. Schmid GJ, Kobayashi C, Sandell LJ, Ornitz DM. Fibroblast growth factor expression during skeletal fracture healing in mice. Dev Dyn 2009;238(3):766-74.
172. Wang JS, Aspenberg P. Basic fibroblast growth factor enhances bone-graft incorporation: dose and time dependence in rats. J Orthop Res 1996;14(2):316-23.
173. Komaki H, Tanaka T, Chazono M, Kikuchi T. Repair of segmental bone defects in rabbit tibiae using a complex of beta-tricalcium phosphate, type I collagen, and fibroblast growth factor-2. Biomaterials 2006;27(29):5118-26.
174. Kawaguchi H, Oka H, Jingushi S, Izumi T, Fukunaga M, Sato K, Matsushita T, Nakamura K. A local application of recombinant human fibroblast growth factor 2 for tibial shaft fractures: A randomized, placebo-controlled trial. J Bone Miner Res 2010;25(12):2735-43.
175. Ueno M, Uchida K, Saito W, Matsushita O, Yogoro M, Nishi N, Ogura T, Hattori S, Inoue G, Tanaka K and others. Acceleration of bone union after structural bone grafts with a collagen-binding basic fibroblast growth factor anchored-collagen sheet for critical-size bone defects. Biomedical Materials 2014;9(3).
176. Nakajima F, Ogasawara A, Goto K, Moriya H, Ninomiya Y, Einhorn TA, Yamazaki M. Spatial and temporal gene expression in chondrogenesis during fracture healing and the effects of basic fibroblast growth factor. J Orthop Res 2001;19(5):935-44.
177. Niedhart C, Maus U, Miltner O, Graber HG, Niethard FU, Siebert CH. The effect of basic fibroblast growth factor on bone regeneration when released from a novel in situ setting tricalcium phosphate cement. J Biomed Mater Res A 2004;69(4):680-5.

178. Mehta M, Schmidt-Bleek K, Duda GN, Mooney DJ. Biomaterial delivery of morphogens to mimic the natural healing cascade in bone. Advanced Drug Delivery Reviews 2012;64(12):1257-1276.
179. Richardson TP, Peters MC, Ennett AB, Mooney DJ. Polymeric system for dual growth factor delivery. Nature Biotechnology 2001;19(11):1029-1034.

# CHAPTER 2: COATING CORTICAL BONE ALLOGRAFTS WITH PERIOSTEUM-MIMETIC SCAFFOLDS MADE OF CHITOSAN, TRIMETHYL CHITOSAN, AND HEPARIN[1]

## 2.1. Summary

Bone allografts have very limited healing leading to high rates of failure from non-union, fracture, and infection. The limited healing of bone allografts is due in large part to devitalization and removal of the periosteum, which removes osteogenic cells and osteoinductive signals. Here we report techniques for directly coating cortical bone with tissue scaffolds, and evaluate the scaffolds' capacity to support osteoprogenitor cells. Three types of coatings are investigated: *N*,*N*,*N*-trimethyl chitosan-heparin polyelectrolyte multilayers, freeze-dried porous chitosan foam coatings, and electrospun chitosan nanofibers. The freeze-dried and electrospun scaffolds are also further modified with polyelectrolyte multilayers. All of the scaffolds are durable to subsequent aqueous processing, and are cytocompatible with adipose-derived stem cells. Alkaline phosphatase and receptor activator of nuclear factor kappa-B ligand expression at days 7 and 21 suggest that these scaffolds support an osteoprogenitor phenotype. These scaffolds could serve as periosteum mimics, deliver osteoprogenitor cells, and improve bone allograft healing.

[1] Portions of this chapter appear in the following:
Romero, R., Chubb, L., Travers, J.K., Gonzalez, T., Ehrhart, N.P., Kipper, M.J. "Coating Cortical Bone Allografts with Periosteum-Mimetic Scaffolds made of Chitosan, Trimethyl Chitosan and Heparin" *Carbohydrate Polymers.* 2015. (122). 144-151. Used with permission.

## 2.2. Introduction

Estimates of the number of bone graft procedures performed annually in the U.S. range from 500,000 to 600,000 (in 2002) to 1.5 million (in 2008)[1,2]. Bone autografts are considered the gold standard treatment due to superior clinical performance attributed to the preservation of the periosteum. The periosteum is a critical component of bone healing due to its high vascularization, osteogenic progenitor cells, osteoinductive growth factors, and an osteoconductive structure[3,4]. However, bone autografts are not without limitations. Bone autografts suffer from graft size availability, and donor site morbidity associated with the autograft harvest can lead to further complications such as pain and infection. Bone allografts have thus become a viable clinical alternative as they overcome some of autografts' limitations. However, to mitigate an immune response and disease transmission, bone allografts must undergo rigorous cleansing and sterilization steps before implantation, which includes removal of the periosteum. Devitalized allografts have a severely diminished osteogenic potential compared to live autografts[5]. Cortical bone allografts experience limited remodeling through a creeping substitution mechanism due to their dense bone structure, which ultimately limits allografts' osteointegration[6]. This limited healing often results in premature failure of allografts. Large segmental bone allografts have 10-year failure rates as high as 60 %[7]. A recent retrospective study of 20 cases by Ogilvie et al. found that allograft fractures occurred 45 % of the time[8]. Unfortunately, 10 % of the reviewed cases developed an infection due to revision surgeries associated with poor integration of the allograft with host tissue[8]. Clearly, strategies for improving the osteogenic and osteoinductive characteristics of bone allografts are needed.

One strategy to improve bone allografts is through the creation of a biomimetic periosteum[9]. An ideal biomimetic periosteum would provide delivery strategies for

osteoprogenitor cells and osteoinductive growth factors, restore angiogenic potential, and help inhibit microbial infection on the allograft surface, to allow better host allograft union[9,10]. Recent efforts to improve allografts include revitalization through the use of multiple osteoprogenitor cell types,[11-14], gene therapy[6,7,15], and coatings with tissue engineering scaffolds[10,16,17] that can incorporate osteoinductive factors, such as growth factors involved in the bone healing and remodeling process. To date, there is not one strategy that appears to improve the clinical performance of bone allografts to the level of autografts in terms of healing and integration[17].

A biomimetic strategy to improve bone allografts leads one to evaluate the use of natural materials as tissue engineering scaffolds. Chitosan, a deacetylated derivative of the naturally abundant polysaccharide chitin, is a material with many interesting properties for bone tissue engineering[18]. Chitosan is biocompatible for a number of tissue engineering applications[19-21], biodegradable[22-24], has antibacterial activity,[10,25,26], and promotes wound healing[27-29]. Furthermore, it can be readily processed into various tissue engineering scaffolds and surface coatings[30]. Chitosan's attractive material properties and versatility make it a prime candidate to be used to construct a biomimetic periosteum on bone allografts.

Our group has recently demonstrated that nanomaterials including ultra-thin coatings and nanoparticle complexes based on polyelectrolyte multilayers (PEMs) of chitosan and polyanionic glycosaminoglycans (e.g. heparin) can be used to bind, stabilize, and deliver heparin-binding growth factors[31-35]. Furthermore, we have shown that these ultra-thin conformal coatings can be applied directly to cortical bone surfaces, and we have demonstrated their cytocompatibility and antimicrobial properties[10]. The purpose of this work is to combine these ultra-thin PEM coatings with porous chitosan scaffolds to create porous cortical bone allograft coatings that may serve as a biomimetic periosteum. Three engineered allograft coatings were evaluated to determine their

cytocompatibilty and whether they supported the osteogenic differentiation of murine adipose-derived stem cells.

## 2.3. Materials and methods

### 2.3.1. Materials

Heparin sodium from porcine intestinal mucosa (14.4 kDa, 12.5% sulfur) was purchased from Celsus Laboratories (Cincinnati, OH). Chitosan (80 kDa, 9 % acetylated confirmed through $^1$H NMR) was acquired from Novamatrix (Sandvika, Norway). Chitosan was methylated to make *N*,*N*,*N*-trimethyl chitosan (TMC) following a previously reported method[36]. A detailed synthesis and characterization of TMC by $^1$H NMR can be found in Appendix A1 and Figure A1.1. The degree of quaternization (DQ) of TMC was calculated to be 71 %. Aqueous solutions were made by dissolving heparin or TMC in water at 0.01 M solutions (based on a saccharide unit basis). 11-Phosphonoundecanoic acid (PUA), glutaraldehyde, retinoic acid, dexamethasone, L-ascorbic acid-2-phosphate, β-glycerophosphate and sucrose were obtained from Sigma-Aldrich (St. Louis, MO). Hexamethyldisilazane was purchased from Alfa Aesar (Ward Hill, MA). Sodium cacodylate trihydrate was purchased from Polysciences Inc. (Warrington, PA). Dimethyl sulfoxide was purchased from EMD Chemicals Inc. (Gibbstown, NJ). Dichloromethane (DCM) and trifluoroacetic acid (TFA) were purchased from Acros Organics (New Jersey, US). Aqueous solutions were made using ultrapure water (18.2 MΩ·cm water from a Millipore Synthesis water purification unit). Polyvinyldifluoride (PVDF) 0.22 µm filters were obtained from Fisher-Scientific (Pittsburgh, PA). Dulbecco's Modification of Eagle's Medium-low glucose (DMEM), Hank's Balanced Salt Solution (HBSS), MEM vitamins, MEM nonessential amino acids,

antibiotic-antimycotic solution were obtained from Corning Cellgro (Manassas, VA). Fetal bovine serum was obtained from Atlas Biologics (Fort Collins, CO).

### 2.3.2. Bone tissue harvest and cleaning

Murine femurs and humeri allografts (4 mm) were harvested from C3H mice (Age 7-9 weeks) sacrificed for another study. All mice used in this study were cared for under Colorado State University's Institutional Animal Care Review Board protocol. The allografts were rinsed with saline and frozen at −80 °C for a minimum of 2 weeks. They were then thawed, rinsed with ultrapure water. The allografts were cleansed by removal of residual bone marrow from the intramedullary cavity, mechanically scraped with a razor to remove any remaining soft tissue, and then sonicated with 70 % ethanol for 3 hours and dried under vacuum.

### 2.3.3. Luciferase-expressing adipose-derived stem cell isolation and expansion

Luciferase-expressing adipose-derived mesenchymal stem cells (Luc-ASCs) were isolated from abdominal adipose tissue of (FVB/NTsv-Tg(svyb-luc)-Xen) mice from Taconic (Hudson, NY). Adipose tissue underwent a collagenase digestion for 30 minutes. Luc-ASCs were then plated for 24 hours, and plastic-adherent cells were selected by rinsing and aspirating to remove non-adherent cells. Luc-ASCs were cryopreserved at −80 °C until ready to be used. Thawed Luc-ASCs were expanded in growth media consisting of DMEM, 15% FBS, 1% antibiotic and antimycotic and supplemented with MEM vitamin solution and non-essential amino acids at 37°C and 5% $CO_2$. Passage 4 Luc-ASCs were used in the cytocompatibility study and to evaluate osteogenic differentiation of Luc-ASCs by western blotting.

### 2.3.4. Cortical bone allografts coatings

Allografts' diaphyseal surfaces were coated with one of three tissue engineering scaffolds—polyelectrolyte multilayers (PEMs), freeze dried chitosan (FD), and electrospun chitosan nanofibers (NF). In order to adhere the PEMs to the bone surface, allografts were first treated with PUA. The allografts were immersed overnight in a 10 mM solution of PUA in dimethyl sulfoxide[10]. The treated allografts were then subjected to layer-by-layer (LbL) deposition of alternating solutions of TMC and heparin with TMC being the first layer deposited. TMC and heparin solutions were made by dissolving TMC and heparin at a 0.01 M concentration on a per saccharide basis in ultrapure water. The solutions were filtered with a 0.22 µm PVDF filter. Bone allografts were placed in a 48-well plate and subjected to an initial 5 minute rinse with ultrapure water. The rinse water was aspirated and the appropriate PEM solution was pipetted into each well plate containing each bone allograft. Five minute adsorption steps were used for each polyelectrolyte solution with a 5-minute rinse step with ultrapure water between PEM adsorption steps. All steps were performed under gentle agitation using a Barnstead Labline titer plate shaker 4625 (Dubuque, IA). Six-layer PEMs were deposited directly on the allograft surface resulting in a terminal heparin layer.

To create a porous chitosan scaffold, allograft bone was cast in a custom cylindrical mold with a 6 % (w/v) chitosan in 0.34 M acetic acid solution and frozen at −20 °C for 24 hours. The custom mold assembly was then subsequently lyophilized for 48 hours, after which the chitosan scaffold on the allograft was mechanically shaved with a razor and neutralized with a 5 M $NH_4OH$ solution for 6 hours. We refer to this as the "FD" (freeze-dried) scaffold. After neutralization, the FD chitosan scaffold was ready for surface modification with TMC and heparin PEMs (described below).

To create a porous chitosan scaffold with an alternative structure, chitosan nanofiber scaffolds were directly electrospun onto the bone diaphyseal surface using a custom rotating collector apparatus. A 1/16-inch copper plate covered with grounded aluminum foil served as a collection plate. A rotating shaft with a custom allograft holder was placed in front of the grounded plate. A syringe pump containing a glass syringe and 18-gauge blunt-tip needle was placed across from the grounded collector. The needle tip–to-collector distance was 7 inches. Chitosan was dissolved as a 7 % (w/v) solution in a 7:3 TFA:DCM ratio for 24 hours before electrospinning. The chitosan solution was supplied at a volumetric flow rate of 1 mL/hr using a Kent Scientific Genie Plus syringe pump (Torrington, Connecticut). The solution was electrospun at 18 kV using a high voltage DC power supply (Gama High Voltage Research Ormond Beach, FL). The nanofibers were then stabilized by neutralizing in a 5 M NH4OH solution for 6 hours, as we have previously reported [33]. We refer to this as the "NF" (nanofiber) scaffold. After neutralization, the NF scaffold was ready for subsequent surface modification with TMC and heparin PEMs (described below).

### 2.3.5. Surface modification of freeze-dried and nanofiber scaffolds with heparin and *N,N,N*-trimethyl chitosan polyelectrolyte multilayers

The chitosan NF and FD scaffold-coated allografts were subjected to LbL deposition of TMC and heparin following the same procedure described above for modifying the bone surfaces with PEMs. However, for the NF and FD scaffolds, heparin was used as the initial layer. Seven layers were deposited to achieve a terminal heparin layer.

### 2.3.6. Macroscopic characterization

PEM-modified and NF-modified allografts were coated with 10 nm of gold and FD-modified allografts were coated with 20 nm of gold before imaging with a scanning electron microscope (SEM; JEOL JSM-6500F, Tokyo, Japan). Micrographs were taken of the unmodified bone surface, unmodified scaffolds on bone, the scaffolds' intermediate processing step, and scaffolds after PEM deposition.

### 2.3.7. X-ray photoelectron spectroscopy of surface modified scaffolds

Surface chemistry of the modified bones was obtained using a Phi Electronics 5800 Spectrometer (Chanhassen, MN). Spectra were obtained with a monochromatic Al Kα x-ray source ($hv$ = 1486.6 eV), a hemispherical analyzer, and multichannel detector. High resolution spectra were obtained using a 23.5 eV analyzer pass energy with 0.1 eV steps and an X-ray spot of 800 µm. All spectra were obtained with a photoelectron takeoff angle of 45°. A low energy electron gun was used for charge neutralization. Spectra curve fitting was done using Phi Electronics Multipak version 9.3 (Chanhassen, MN). Curve fitting of all spectra used a Shirley background. Gaussian peaks were fit according to expected functional groups. The height of each peak was fit first while keeping each peaks' position, full width half max (fwhm), and percent Gaussian fixed. Then the fwhm, percent Gaussian, and finally position were fit while minimizing the chi squared value[37].

### 2.3.8. In-vitro culture of luciferase expressing adipose-derived stem cells on engineered scaffolds

Passage 4 Luc-ASCs were seeded onto allografts or allografts coated with either PEM, FD, and NF scaffolds ($n$ = 5 per scaffold type) using a highly concentrated cell solution (500,000 cells in 30 ml of ASC media) and were allowed to attach onto allografts for 2 hours at 37 °C, 5% $CO_2$. After initial attachment, cells were transferred to new wells and the appropriate cell culture media was added. Engineered allografts were cultured in osteogenic supplemented media (OSM), defined as ASC growth media plus 20 mM β-glycerophosphate and 50 μM L-ascorbic acid-2-phosphate with no induction hormone. Control samples, Luc-ASCs on TCPS, were cultured in osteogenic induction media (OIM), defined as osteogenic supplemented media with 10 nM dexamethasone. Samples were cultured at 37 °C and 5 % $CO_2$ in a humidified incubator for 21 days with media changes every 2-3 days.

### 2.3.9. Cytocompatibility assay

Luc-ASCs were cultured on modified allografts for 21 days. At days 1, 4, 7, 14, and 21, firefly luciferin substrate was added to each well plate at a concentration of 0.6 mg $mL^{-1}$, incubated for approximately 5 minutes at room temperature. Bioluminescent readings were taken on an IVIS-100 *in vivo* imaging system from PerkinElmer (Waltham, MA) using a humidified chamber. Images were thresholded and the total photon flux was calculated for each scaffold. The average total flux of each scaffold was calculated and then normalized to each scaffolds' day 1 reading. After 13 days of culture, ASC-seeded allografts were fixed using a 2 % glutaraldehyde solution prepared in 0.2 M sodium cacodylate and 0.1 M sucrose buffer solution. The ASC-seeded allografts were then dehydrated using an increasing concentration ethanol series with a

final hexamethyldisilazane dehydration step. Allografts were then imaged by scanning electron microscopy after being sputter coated with gold as mentioned above.

### 2.3.10. Luciferase expressing adipose-derived stem cells osteogenic differentiation evaluation by western blot

Luc-ASCs cultured on modified allografts were evaluated for osteogenic differentiation after 7 and 21 days of *in-vitro* culture. Samples were rinsed twice in cold HBSS before being lysed in a commercial radioimmunoprecipitation assay (RIPA) buffer obtained from Thermo-Scientific (Rockford, IL) containing 3× protease inhibitors. Samples were lysed using a handheld sonicator wand while keeping samples on ice. Replicate lysates were pooled together and centrifuged at 15,000 RPM for 15 mins at 4 °C to pellet cell debris and the supernatant was collected and frozen at −20 °C until ready to be further assayed. Samples were thawed then denatured and reduced before running on a 4-20 % Ready Gel Tris-HCl gel (Bio-rad, Hercules, CA) using a Biorad Mini-Protean 3 electrophoresis unit. Proteins were transferred onto a Immobilon-P$^{SQ}$ PVDF membrane (EMD Millipore, Billerica, MA) using a wet tank transfer method for 2 hrs at 4 °C. Membranes were blocked in 5 % non-fat milk for 1 hour at room temp then rinsed three times for 5 min each. Blots were probed initially for alkaline phosphatase (ALP) using anti-alkaline phosphatase primary antibody (1:10,000, ab108337, Abcam, Cambridge, MA) overnight at 4 °C. Horseradish peroxidase conjugated goat anti-rabbit IgG H&L secondary antibody (1:20,000 Abcam ab6721) was used and membranes were developed using an enhanced chemiluminescence substrate solution (Thermo, Rockford, IL). Immunoblots were imaged using a Bio-rad Chemidoc XRS+ imager. (Hercules, CA). Immunoblots were subsequently stripped with Thermo Restore stripping buffer (Thermo, Rockford, IL) and

reprobed for osteocalcin (1:3000, Millipore ab10911), osteonectin (0.4 μg/ml, Abcam ab55847), osteopontin (0.1 μg/ml, Abcam ab11503), RANKL (1:5000, Abcam ab124797), and β-tubulin (1:500, Abcam ab6046) and developed. Blots were stripped and blocked in between probings.

### 2.3.11. Statistical analysis

Bioluminescence measurements on days 4, 7, 14, and 21 were normalized to their day 1 readings. Log-transformed normalized flux values were analyzed using a two-way repeated measures ANOVA. Comparisons between groups were performed using a Tukey-Kramer's post hoc test. $p < 0.05$ was considered significant. SAS Studio 3.2 was used for the analysis.

## 2.4. Results

### 2.4.1. Macroscopic analysis

Scanning electron micrographs revealed successful allograft diaphyseal surface coatings on the entire allograft with both the chitosan freeze-dried (FD) scaffold and the chitosan electrospun nanofiber (NF) scaffold, as seen in Figure 2.1. These scaffolds are stable with respect to further aqueous modification steps (neutralization with ammonium hydroxide and LbL deposition of seven alternating layers of TMC and heparin) with no gross morphological changes, as evidenced by the rightmost columns in Figure 2.1. Allografts directly coated with only PEMs of TMC and heparin exhibit minimal surface topographical changes. This is expected, as the PEMs should have a thickness of approximately 10-15 nm, which would be indistinguishable in the micrographs[37].

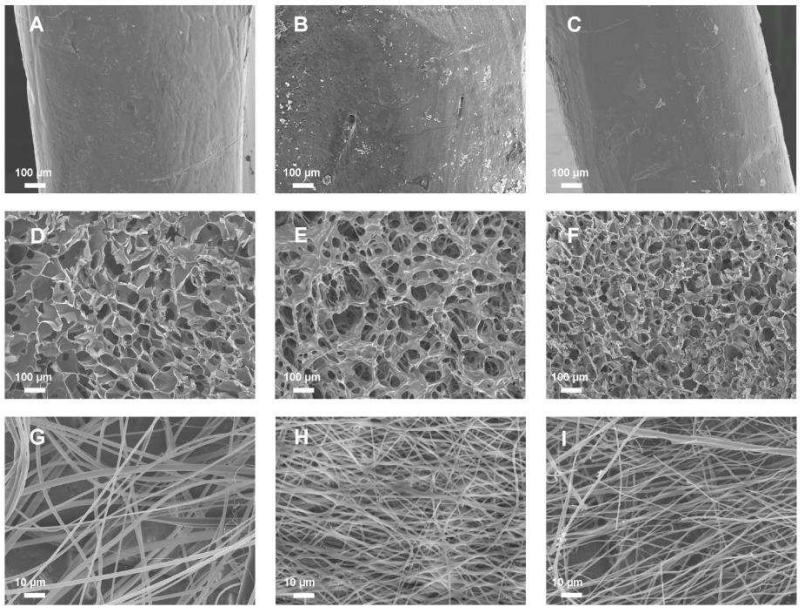


**Figure 2.1** Scanning electron micrographs of (top row) (A) cortical bone, (B) cortical bone coated with PUA, and (C) cortical bone coated with PUA and a TMC-heparin PEM; (middle row) (D) cortical bone coated with a chitosan freeze-dried (FD) scaffold, (E) the same FD scaffold after ammonium hydroxide neutralization, and (F) after TMC-heparin PEM deposition; (bottom row) (G) cortical bone coated with electrospun chitosan nanofibers (NF), (H) the NF after ammonium hydroxide neutralization, and (I) after TMC-heparin PEM deposition**.**

### 2.4.2. XPS analysis of surface modified allografts

The surface chemistry of PEM-modified bone and scaffolds was characterized using survey and high-resolution XPS spectra. High-resolution spectra confirm deposition of TMC and heparin on the allograft diaphyseal surface. Figure 2.2 shows complete attenuation of the Ca2p and P2p envelopes indicating complete surface coverage with PEMs. Figure 2.2 also shows the appearance of a sulfur S2p peak at 168.5 eV (sulfate), which confirms heparin deposition within the heparin-terminated PEMs.

In Figure 2.3, the attenuation of the amide peak at 400 eV and the appearance of an ammonium and amine peak in the N1s envelope at 402.8 eV and 399.2 eV, respectively,

confirms LbL deposition of the TMC-heparin PEM. Changes in the C1s and O1s envelopes of the XPS spectra are also characteristic of polysaccharide-based PEM deposition on bone.

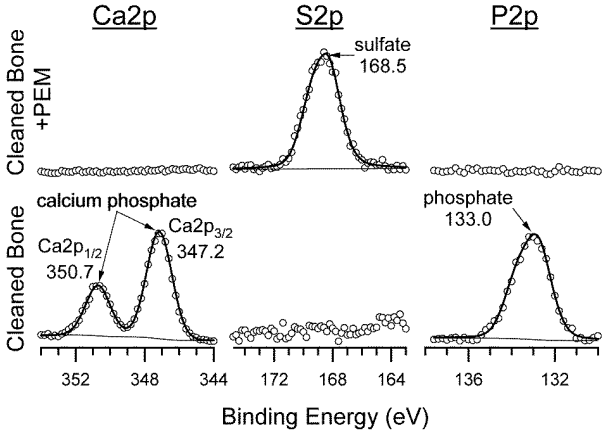


**Figure 2.2** High-resolution X-ray photoelectron spectra of the Ca2p, S2p, and P2p envelopes of cortical bone before and after TMC-heparin PEM deposition. Attenuation of calcium and phosphorus signals and appearance of sulfur (from sulfate in heparin) confirms PEM deposition.

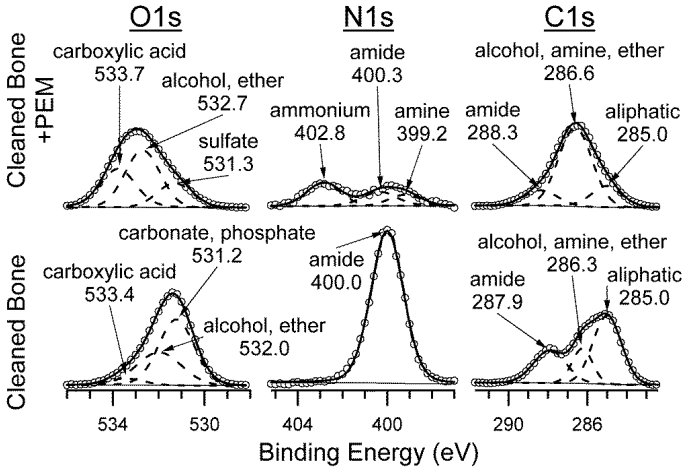


**Figure 2.3** High-resolution X-ray photoelectron spectra of the O1s, N1s and C1s envelopes of cortical bone before and after TMC-heparin PEM deposition. Differences in the spectra confirm deposition of TMC-heparin PEMs on cortical bone surface.

Figure 2.4 shows the N1s, C1s and S2p envelopes for the FD (left) and NF (right) modifications of bone. The bottom row is the neat scaffold immediately after freeze drying or

electrospinning. The middle row is the scaffold after ammonium hydroxide neutralization, and the top row is the PEM-modified scaffold. Notice that the neat NF scaffold has significant contributions from trifluoroacetate at 289.9 and 293.2 eV in the C1s envelope, indicating residual solvent from the electrospinning process. This must be in the form of a salt with the amine groups in the electrospun chitosan, since trifluoroacetate is detected under the high vacuum of the XPS chamber. As we have reported previously, neutralization with ammonium hydroxide completely removes the trifluoroacetate from the nanofibers [33]. LbL addition of heparin and TMC PEMs to the FD and NF scaffolds results in similar characteristics in the N1s, C1s and S2p envelopes, such as addition of sulfate and ammonium.

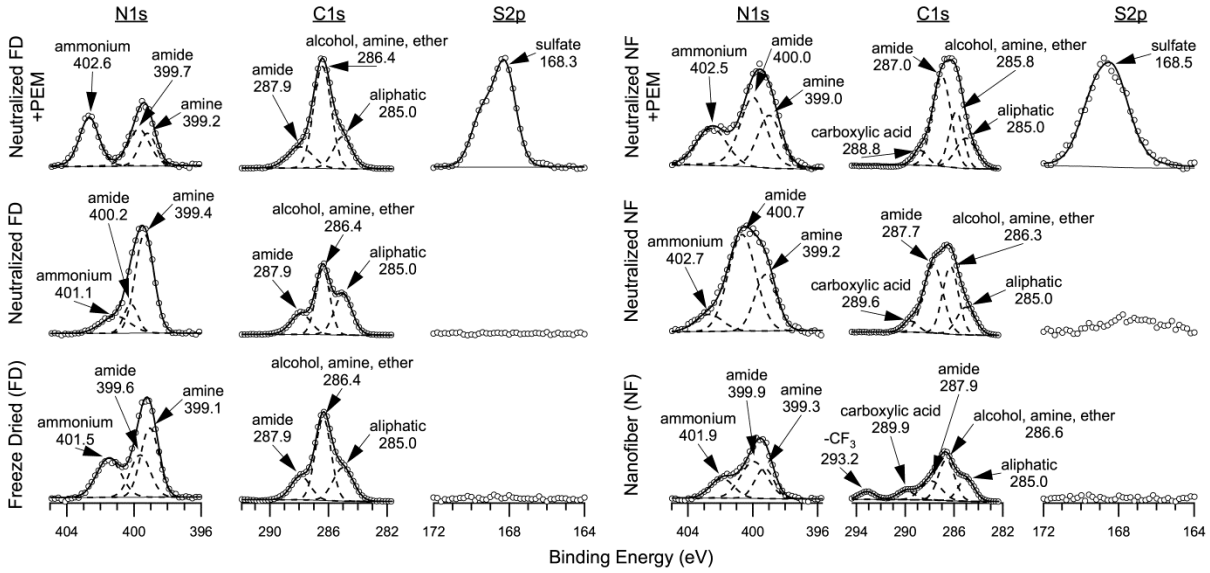


**Figure 2.4** High-resolution X-ray photoelectron spectra of the N1s, C1s, and S2p envelopes of cortical bone coated with chitosan FD scaffolds (left) and chitosan NF scaffolds (right). Bottom row shows neat FD and NF scaffolds; middle row shows scaffolds after ammonium hydroxide neutralization, and confirms removal of residual electrospinning solvent from NF scaffolds; top row shows PEM-modified scaffolds with features characteristic of TMC-heparin PEMs, such as ammonium and sulfate.

### 2.4.3. Cytocompatibility assay

Luc-ASCs were seeded onto each of the three tissue engineering scaffolds to discern whether these scaffolds might be used to support Luc-ASC transplantation. Figure 2.5 shows longitudinal tracking of Luc-ASCs on modified allografts over a 21 day period. Luc-ASCs seeded on NF-, PEM-modified, and uncoated allografts first showed an initial decrease in luminescence at day 4 and 7 but increased over time by day 21. FD-modified allografts demonstrated an initial decrease in luminescence with a limited increase in luminescence by day 21.

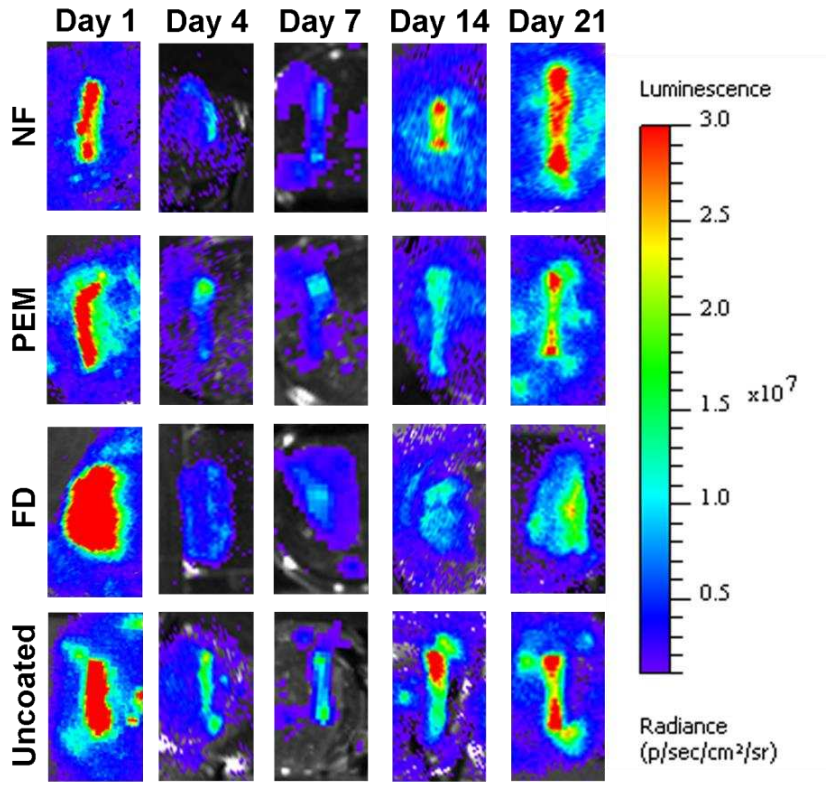


**Figure 2.5** Luc-ASCs seeded on modified allografts were longitudinally tracked in vitro for up to 21 days. Luc-ASCs were found to adhere, persist, and proliferate on modified allografts. Cell viability decreased at day 4 but cell numbers were rescued by day 21 on the uncoated and NF-modified allografts.

Figure 2.6 shows the normalized average photon flux after 21 days of *in vitro* culture. Values were normalized to the photon flux on day 1 for each sample to obviate concerns of heterogeneous initial cell seeding. Proliferation is observed for Luc-ASCs on uncoated, PEM-coated, and NF-coated allografts. The NF-coated allografts exhibit the largest increase in bioluminescent flux over time, indicating the greatest ASC proliferation. FD-coated allografts were the only scaffold to exhibit a significant difference in normalized average photon flux compared to all other treatments at each timepoint ($p < 0.05$). Figure 2.7 shows Luc-ASCs adopt a flat cellular morphology on PEM-coated and NF-coated allografts while Luc-ASCs on FD-coated allografts adopt a spherical morphology.

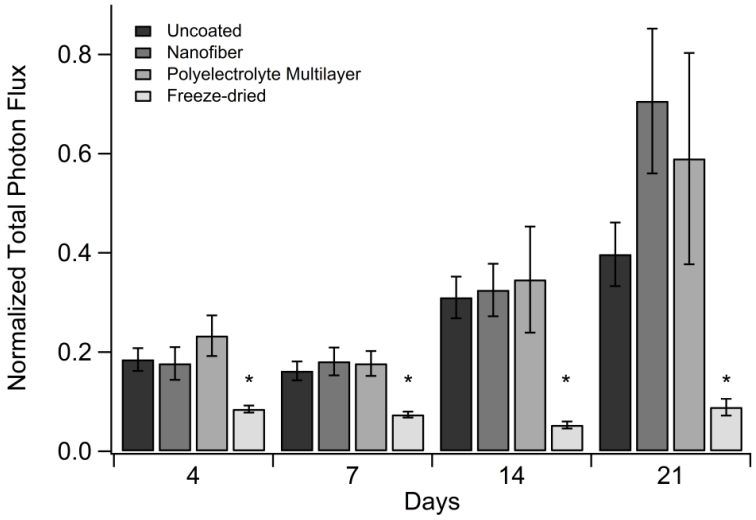


**Figure 2.6** Bioluminescence of Luc-ASCs seeded onto murine allografts modified with PEM, FD, or NF scaffolds (normalized to the day 1 value for each sample). Luc-ASCs proliferate on uncoated, NF- and PEM-modified allografts. Allografts modified with NF scaffolds and PEMs exhibit the highest luminescence after 21 days. Uncertainties are standard errors of the mean. * indicates statistically significant differences when compared to all other treatments on the same day ($p < 0.05$, $n = 4–10$).

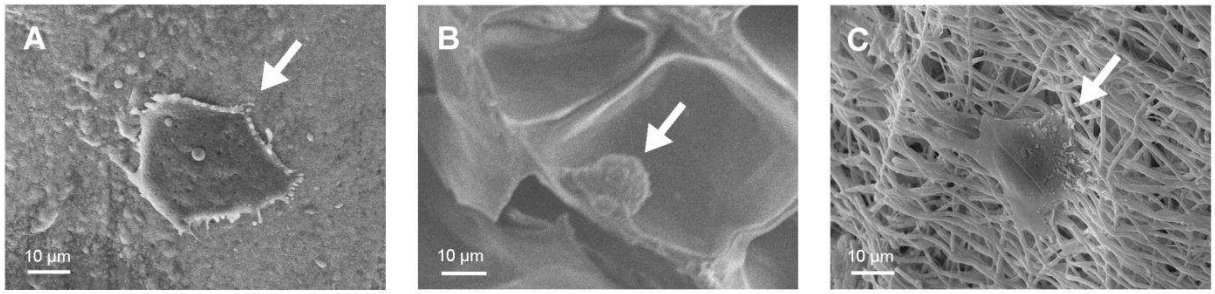


**Figure 2.7** Scanning electron micrographs show examples of Luc-ASCs cultured on (A) PEM-coated bone, (B) FD scaffolds on bone, and (C) NF scaffolds on bone. White arrows highlight Luc-ASCs.

### 2.4.4. Western blot results

Luc-ASCs osteogenic differentiation was evaluated by probing for osteogenic protein expression with Western blotting. Alkaline phosphatase (ALP) bands were observed at 75 kDa on days 7 and 21 for PEM, FD, and NF scaffolds as seen in Figure 2.8. Modified allografts displayed similar decreased ALP expression compared to an uncoated control on day 7. By day 21 modified allografts displayed increased ALP expression compared to an uncoated control with PEM-modified scaffolds having the highest ALP expression. Receptor activator of nuclear factor κ-B ligand (RANKL) bands were observed for NF- and PEM-modified allografts at 37 kDa on day 7 and day 21. RANKL bands of NF- and PEM-modified allografts had decreased expression by day 21 compared an uncoated control allograft. No RANKL expression was observed for FD-modified allografts at either days 7 or 21. No osteocalcin, osteopontin, or osteonectin expression was observed for any experimental group at either timepoint.

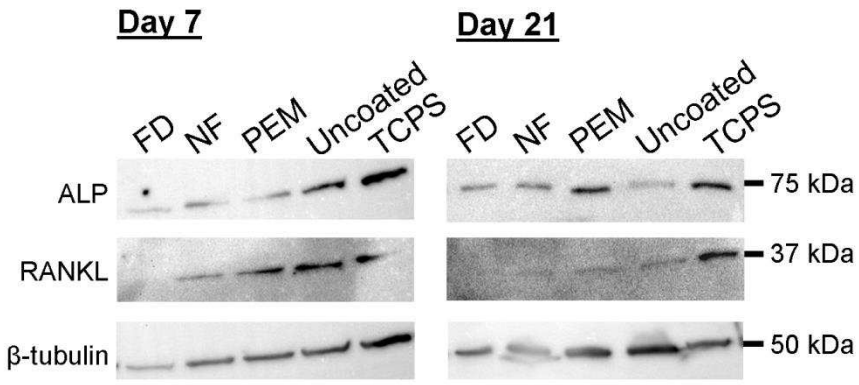


**Figure 2.8** Western Blotting demonstrated Luc-ASCs on NF- and PEM-modified allografts express ALP and RANKL at both days 7 and 21. FD-modified allografts expressed ALP on days 7 and 21. ALP and RANKL expression suggest Luc-ASCs maintain an osteoprogenitor phenotype.

## 2.5. Discussion

Novel composite scaffolds were created on cortical bone allografts by combining porous chitosan scaffolds with TMC and heparin thin films. TMC and heparin PEM deposition on cortical bone, FD-modified bone, and NF-modified bone produced a consistent multilayer structure across three diverse surfaces as confirmed with XPS analysis. Recent advances have been made to engineer biomimetic periosteal structures [38-41]. Our polysaccharide based scaffolds present an alternative approach to engineering a biomimetic periosteum using naturally derived materials. The free amino group in chitosan has a p$K_a$ of ~6.5, giving chitosan its cationic behavior, which can be used to incorporate anionic glycoaminoglycans such as heparin. Glycoaminoglycans are present in the extra cellular matrix of musculoskeletal tissues and serve as biological reservoirs to bind and stabilize growth factors. Growth factors such as FGF-2 and TGF-β1 are unstable in serum due to short plasma half-lives[42]. Our group has previously shown TMC and heparin PEMs can easily incorporate and stabilize growth factors that may be used to impart osteoinductive properties to these novel composite scaffolds[32].

To our knowledge, we report the first demonstration of electrospinning chitosan nanofibers directly onto a cortical bone surface creating an adherent ECM-mimetic scaffold directly on the cortical bone surface as confirmed by scanning electron micrographs. Scanning electron micrographs demonstrate minimal degradation of both FD and NF coatings on allografts throughout the various aqueous processing steps (Figure 2.1) and after a 13-day incubation in cell media (Figure 2.7). Neutralization of both FD and NF are necessary in order to make both FD and NF scaffolds survive the TMC and heparin PEM deposition process at neutral pH. Previous work in the literature has pointed out the importance of pH on TMC and heparin PEM fabrication and its effect on the antibacterial and heparin releasing properties of these multilayer films[43]. As our TMC had a DQ of 71%, we would expect a high bactericidal effect from these TMC coated scaffolds as observed by Follman et al and in line with observations made by Almodovar et al on TMC and heparin PEMs on cortical bone[10]. Such a high degree of quaternization would minimally release heparin at neutral pH due to strong electrostatic interactions between the heparin and TMC as observed by Follman and colleagues[43]. Both FD and NF scaffolds show a porous morphology that is important to tissue engineering applications in order to allow for cellular infiltration and mass transport of nutrients and metabolic wastes. Recent work by Lyu et al. have demonstrated that electrospinning fibers may be well suited for the creation of a periosteum-mimetic structure[44].

After the morphological and chemical characterization of the composite scaffolds, their cytocompatibility was evaluated. Luc-ASCs were shown to survive initial exposure to PEM-modified allograft coatings. Firefly luciferin uniquely requires ATP as a co-factor in order to actively bioluminesce[45]. The presence of ATP activity in Luc-ASCs demonstrates cellular metabolic activity and indicates viable cells. An initial decrease in bioluminescence signal was

observed at days 4 that may suggest initial cell toxicity. However, on the PEM- and NF-modified allografts, ASC proliferation was observed at later timepoints suggesting cell numbers could be rescued. FD-modified allografts were found to exhibit minimal proliferation over 21 days of *in vitro* culture which may be attributed to the scaffold surface topography that may not have been conducive for cell attachment as heparin has been found to mediate adipose-derived stem cell binding and proliferation[46,47]. NF-coated allograft showed the greatest ASC proliferation which could be explained by the scaffold's ECM-mimetic structure and porosity. Interestingly, ASCs persisted on the modified allografts for up to 21 days of *in vitro* culture without the incorporation of cell adhesion motifs as compared to the work by Hoffman et al[17]. ASC persistence up to 21 days *in vitro* suggests that PEM, FD, and NF scaffolds created from natural polysaccharide materials are cytocompatible and can be used for cell transplantation.

Adipose-derived stem cells are multipotent stem cells that can be harnessed for use in regenerative medicine applications, such as skeletal repair[48-50]. Consequently, evaluation of ASCs osteogenic response to our novel periosteum-mimetic scaffolds warranted investigation. Osteoblasts undergo a temporal specific sequence of gene and protein expression[51]. Noncollagenous proteins of bone such as osteocalcin, osteonectin, osteopontin, alkaline phosphatase, and RANKL can serve as phenotypic markers of osteoblastic cells. Western blotting was performed on Luc-ASC cell lysates to determine expression levels of these osteogenic protein markers. Osteocalcin, osteonectin, and osteopontin expression were not observed for Luc-ASCs cultured on modified allografts which suggest Luc-ASCs did not reach a full osteoblast phenotype. Previous studies have shown that topographical cues could drive stem cell differentiation but our results show modified allograft topography alone was insufficient to promote terminal Luc-ASC osteogenic differentiation.[52] However, ALP and RANKL expression

were observed on both days 7 and 21 of *in vitro* culture suggesting the periosteum-mimetic scaffolds containing heparin may still support an immature osteoprogenitor phenotype through mediating cell adhesion and proliferation. Heparin functionalized polyethylene glycol hydrogels have previously been found to promote human mesenchymal stem cell osteogenic differentiation as heparin can sequester growth factors important in bone cell regulation and differentiation[53,54]. It is important to note that ALP and RANKL are not specific markers to conclusively confirm osteogenic differentiation of Luc-ASCs. However, ALP has been implicated in the early mineralization phase of osteoprogenitors. RANKL is known to be involved in osteoclast activation which is important in the bone remodeling process[55]. RANKL expression by Luc-ASCs may assist in the initiation of bone resorption on cortical bone allografts which are known to undergo limited remodeling after allograft implantation[6].

### 2.6 Conclusion

In conclusion, we demonstrate here three potential new bone surface treatments that may be used to deliver osteoprogenitor cells. These three new composite scaffolds include heparin-TMC polyelectrolyte multilayers (PEMs) deposited on three surfaces directly onto cortical bone, onto freeze-dried (FD) porous chitosan scaffolds on cortical bone, and onto chitosan electrospun nanofibers (NF) on cortical bone. To our knowledge, this is the first demonstration of the direct modification of bone with these novel composite chitosan scaffolds that may be used to form a biomimetic periosteum. The PEM surface coatings resulted in consistent and conformal coatings across diverse surfaces. The combination of TMC and heparin thin films with porous chitosan scaffolds have created cytocompatible surface structures that can incorporate osteoprogenitor cells to create a periosteum-mimetic structure.

REFERENCES


1. Bucholz RW. Nonallograft osteoconductive bone graft substitutes. Clinical Orthopaedics and Related Research 2002(395):44-52.
2. Jahangir AA, Nunley RM, Mehta S, Sharan A. Bone-Graft Substitutes in Orthopaedic Surgery. AAOS *Now* Rockford, IL: American Academy of Orthopaedic Surgeons; 2008.
3. Colnot C, Zhang X, Knothe Tate ML. Current insights on the regenerative potential of the periosteum: molecular, cellular, and endogenous engineering approaches. Journal of Orthopaedic Research 2012;30(12):1869-1878.
4. Zhang X, Xie C, Lin ASP, Ito H, Awad H, Lieberman JR, Rubery PT, Schwarz EM, O'Keefe RJ, Guldberg RE. Periosteal progenitor cell fate in segmental cortical bone graft transplantations: implications for functional tissue engineering. Journal of Bone and Mineral Research 2005;20(12):2124-2137.
5. Bauer TW, Muschler GF. Bone graft materials. An overview of the basic science. Clinical Orthopaedics and Related Research 2000(371):10-27.
6. Koefoed M, Ito H, Gromov K, Reynolds DG, Awad HA, Rubery PT, Ulrich-Vinther M, Soballe K, Guldberg RE, Lin AS and others. Biological effects of rAAV-caAlk2 coating on structural allograft healing. Molelcular Therapy 2005;12(2):212-218.
7. Yazici C, Yanoso L, Xie C, Reynolds DG, Samulski RJ, Samulski J, Yannariello-Brown J, Gertzman AA, Zhang X, Awad HA and others. The effect of surface demineralization of cortical bone allograft on the properties of recombinant adeno-associated virus coatings. Biomaterials 2008;29(28):3882-3887.
8. Ogilvie CM, Crawford EA, Hosalkar HS, King JJ, Lackman RD. Long-term results for limb salvage with osteoarticular allograft reconstruction. Clinical Orthopaedics and Related Research 2009;467(10):2685-2690.
9. Zhang X, Awad HA, O'Keefe RJ, Guldberg RE, Schwarz EM. A perspective: engineering periosteum for structural bone graft healing. Clinical Orthopaedics and Related Research 2008;466(8):1777-1787.
10. Almodovar J, Mower J, Banerjee A, Sarkar AK, Ehrhart NP, Kipper MJ. Chitosan-heparin polyelectrolyte multilayers on cortical bone: Periosteum-mimetic, cytophilic, antibacterial coatings. Biotechnology and Bioengineering 2013;110(2):609-618.
11. Hoffman MD, Benoit DSW. Emerging Ideas: Engineering the Periosteum: Revitalizing Allografts by Mimicking Autograft Healing. Clinical Orthopaedics and Related Research 2013;471(3):721-726.
12. Ouyang HW, Cao T, Zou XH, Heng BC, Wang LL, Song XH, Huang HF. Mesenchymal stem cell sheets revitalize nonviable dense grafts: Implications for repair of large-bone and tendon defects. Transplantation 2006;82(2):170-174.
13. Xie C, Reynolds D, Awad H, Rubery PT, Pelled G, Gazit D, Guldberg RE, Schwarz EM, O'Keefe RJ, Zhang XP. Structural bone allograft combined with genetically engineered mesenchymal stem cells as a novel platform for bone tissue engineering. Tissue Engineering 2007;13(3):435-445.
14. Zhou Y, Chen F, Ho ST, Woodruff MA, Lim TM, Hutmacher DW. Combined marrow stromal cell-sheet techniques and high-strength biodegradable composite scaffolds for engineered functional bone grafts. Biomaterials 2007;28(5):814-824.

15. Ito H, Koefoed M, Tiyapatanaputi P, Gromov K, Goater JJ, Carmouche J, Zhang X, Rubery PT, Rabinowitz J, Samulski RJ and others. Remodeling of cortical bone allografts mediated by adherent rAAV-RANKL and VEGF gene therapy. Nature Medicine 2005;11(3):291-297.
16. Costa-Pinto AR, Reis RL, Neves NM. Scaffolds Based Bone Tissue Engineering: the Role of Chitosan. Tissue Engineering Part B: Reviews 2011;17(5):331-347.
17. Hoffman MD, Xie C, Zhang X, Benoit DSW. The effect of mesenchymal stem cells delivered via hydrogel-based tissue engineered periosteum on bone allograft healing. Biomaterials 2013;34(35):8887-8898.
18. Muzzarelli RAA. Chitins and chitosans for the repair of wounded skin, nerve, cartilage and bone. Carbohydrate Polymers 2009;76(2):167-182.
19. VandeVord PJ, Matthew HWT, DeSilva SP, Mayton L, Wu B, Wooley PH. Evaluation of the biocompatibility of a chitosan scaffold in mice. Journal of Biomedical Materials Research 2002;59(3):585-590.
20. Molinaro G, Leroux J-C, Damas J, Adam A. Biocompatibility of thermosensitive chitosan-based hydrogels: an in vivo experimental approach to injectable biomaterials. Biomaterials 2002;23(13):2717-2722.
21. Shin SY, Park HN, Kim KH, Lee MH, Choi YS, Park YJ, Lee YM, Ku Y, Rhyu IC, Han SB and others. Biological evaluation of chitosan nanofiber membrane for guided bone regeneration. Journal of Periodontology 2005;76(10):1778-1784.
22. Tomihata K, Ikada Y. In vitro and in vivo degradation of films of chitin and its deacetylated derivatives. Biomaterials 1997;18(7):567-575.
23. Nordtveit RJ, Vårum KM, Smidsrød O. Degradation of partially N-acetylated chitosans with hen egg white and human lysozyme. Carbohydrate Polymers 1996;29(2):163-167.
24. Vårum KM, Myhr MM, Hjerde RJN, Smidsrød O. In vitro degradation rates of partially N-acetylated chitosans in human serum. Carbohydrate Research 1997;299(1–2):99-101.
25. Jia Z, Shen D, Xu W. Synthesis and antibacterial activities of quaternary ammonium salt of chitosan. Carbohydrate Research 2001;333(1):1-6.
26. Loke WK, Lau SK, Yong LL, Khor E, Sum CK. Wound dressing with sustained anti-microbial capability. Journal of Biomedical Materials Research 2000;53(1):8-17.
27. Biagini G, Bertani A, Muzzarelli RAA, Damadei A, DiBenedetto G, Belligolli A, Ricotti G, Zucchini C, Rizzoli C. Wound management with N-carboxybutyl chitosan. Biomaterials 1991;12(3):281-286.
28. Ueno H, Yamada H, Tanaka I, Kaba N, Matsuura M, Okumura M, Kadosawa T, Fujinaga T. Accelerating effects of chitosan for healing at early phase of experimental open wound in dogs. Biomaterials 1999;20(15):1407-1414.
29. Azad AK, Sermsintham N, Chandrkrachang S, Stevens WF. Chitosan membrane as a wound-healing dressing: characterization and clinical application. Journal of Biomedical Materials Research Part B: Applied Biomaterials 2004;69(2):216-222.
30. Jiang T, Deng M, James R, Nair LS, Laurencin CT. Micro- and nanofabrication of chitosan structures for regenerative engineering. Acta Biomaterialia 2014;10(4):1632-1645.
31. Almodóvar J, Bacon S, Gogolski J, Kisiday JD, Kipper MJ. Polysaccharide-based polyelectrolyte multilayer surface coatings can enhance mesenchymal stem cell response to adsorbed growth factors. Biomacromolecules 2010;11:2629-2639.

32. Volpato FZ, Almodovar J, Erickson K, Popat KC, Migliaresi C, Kipper MJ. Preservation of FGF-2 bioactivity using heparin-based nanoparticles, and their delivery from electrospun chitosan fibers. Acta Biomaterialia 2012;8(4):1551-1559.
33. Almodóvar J, Kipper MJ. Coating Electrospun Chitosan Nanofibers with Polyelectrolyte Multilayers Using the Polysaccharides Heparin and N,N,N-Trimethyl Chitosan. Macromolecular Bioscience 2011;11(1):72-76.
34. Place LW, Kelly SM, Kipper MJ. Synthesis and Characterization of Proteoglycan-Mimetic Graft Copolymers with Tunable Glycosaminoglycan Density. Biomacromolecules 2014.
35. Place LW, Sekyi M, Kipper MJ. Aggrecan-mimetic, glycosaminoglycan-containing nanoparticles for growth factor stabilization and delivery. Biomacromolecules 2014;15(2):680-689.
36. de Britto D, Assis OBG. A novel method for obtaining a quaternary salt of chitosan. Carbohydrate Polymers 2007;69(2):305-310.
37. Almodóvar J, Place LW, Gogolski J, Erickson K, Kipper MJ. Layer-by-Layer Assembly of Polysaccharide-Based Polyelectrolyte Multilayers: A Spectroscopic Study of Hydrophilicity, Composition, and Ion Pairing. Biomacromolecules 2011;12(7):2755-2765.
38. Long T, Zhu Z, Awad HA, Schwarz EM, Hilton MJ, Dong Y. The effect of mesenchymal stem cell sheets on structural allograft healing of critical sized femoral defects in mice. Biomaterials 2014;35(9):2752-2759.
39. Kang YQ, Ren LL, Yang YZ. Engineering Vascularized Bone Grafts by Integrating a Biomimetic Periosteum and beta-TCP Scaffold. ACS Applied Materials & Interfaces 2014;6(12):9622-9633.
40. Hoffman MD, Van Hove AH, Benoit DS. Degradable hydrogels for spatiotemporal control of mesenchymal stem cells localized at decellularized bone allografts. Acta Biomaterialia 2014;10(8):3431-3441.
41. Shi X, Fujie T, Saito A, Takeoka S, Hou Y, Shu Y, Chen M, Wu H, Khademhosseini A. Periosteum-Mimetic Structures Made from Freestanding Microgrooved Nanosheets. Advanced Materials 2014;26(20):3290-3296.
42. Tessmar JK, Göpferich AM. Matrices and scaffolds for protein delivery in tissue engineering. Advanced Drug Delivery Reviews 2007;59(4):274-291.
43. Follmann HDM, Martins AF, Gerola AP, Burgo TAL, Nakamura CV, Rubira AF, Muniz EC. Antiadhesive and Antibacterial Multilayer Films via Layer-by-Layer Assembly of TMC/Heparin Complexes. Biomacromolecules 2012;13(11):3711-3722.
44. Lyu S, Huang C, Yang H, Zhang X. Electrospun fibers as a scaffolding platform for bone tissue repair. Journal of Orthopaedic Research 2013;31(9):1382-1389.
45. Hastings JW. Bioluminescence. In: Sperelakis N, editor. Cell Physiology Source Book: Essentials of Membrane Biophysics. Boston, MA: Academic Press; 2012. p 925-947.
46. Kim M, Kim YH, Tae G. Human mesenchymal stem cell culture on heparin-based hydrogels and the modulation of interactions by gel elasticity and heparin amount. Acta Biomaterialia 2013;9(8):7833–7844.
47. Park I-S, Han M, Rhie J-W, Kim SH, Jung Y, Kim IH, Kim S-H. The correlation between human adipose-derived stem cells differentiation and cell adhesion mechanism. Biomaterials 2009;30(36):6835–6843.

48. Xu Y, Malladi P, Wagner DR, Longaker MT. Adipose-derived mesenchymal cells as a potential cell source for skeletal regeneration. Current Opinion in Molecular Therapeutics 2005;7(4):300-305.
49. Zuk PA, Zhu M, Ashjian P, De Ugarte DA, Huang JI, Mizuno H, Alfonso ZC, Fraser JK, Benhaim P, Hedrick MH. Human Adipose Tissue Is a Source of Multipotent Stem Cells. Molecular Biology of the Cell 2002;13(12):4279-4295.
50. Zuk PA, Zhu M, Mizuno H, Huang J, Futrell JW, Katz AJ, Benhaim P, Lorenz HP, Hedrick MH. Multilineage cells from human adipose tissue: implications for cell-based therapies. Tissue Engineering 2001;7(2):211-228.
51. Aubin JE. Advances in the osteoblast lineage. Biochemistry and Cell Biology 1998;76(6):899-910.
52. Teo BK, Ankam S, Chan LY, Yim EK. Nanotopography/mechanical induction of stem-cell differentiation. Methods Cell Biol 2010;98:241-94.
53. Benoit DSW, Anseth KS. Heparin functionalized PEG gels that modulate protein adsorption for hMSC adhesion and differentiation. Acta Biomaterialia 2005;1(4):461–470.
54. Kang JM, Han M, Park IS, Jung Y, Kim SH, Kim S-H. Adhesion and differentiation of adipose-derived stem cells on a substrate with immobilized fibroblast growth factor. Acta Biomaterialia 2012;8(5):1759–1767.
55. Boyce BF, Xing L. Functions of RANKL/RANK/OPG in bone modeling and remodeling. Archives of Biochemistry and Biophysics 2008;473(2):139-146.

# CHAPTER 3: COMBINED DELIVERY OF FGF-2, TGF-B1, AND ADIPOSE-DERIVED STEM CELLS FROM AN ENGINEERED PERIOSTEUM TO A CRITICAL-SIZED MOUSE FEMUR DEFECT[2]

## 3.1. Summary

Critical-sized long bone defects suffer from complications including impaired healing and non-union due to substandard healing and integration of devitalized bone allograft. Removal of the periosteum contributes to the limited healing of bone allografts. Restoring a periosteum on bone allografts may provide improved allograft healing and integration. This article reports a polysaccharide-based tissue engineered periosteum that delivers basic fibroblast growth factor (FGF-2), transforming growth factor-β1 (TGF-β1), and adipose-derived mesenchymal stem cells (ASCs) to a critical-sized mouse femur defect. The tissue engineered periosteum was evaluated for improving bone allograft healing and incorporation by locally delivering FGF-2, TGF-β1 and supporting ASCs transplantation. ASCs were successfully delivered and longitudinally tracked at the defect site for at least 7 days post operation with delivered FGF-2 and TGF-β1 showing a mitogenic effect on the ASCs. At 6 weeks post implantation, data showed a non-significant increase in normalized bone callus volume. However, union ratio analysis showed a significant inhibition in allograft incorporation, confirmed by histological analysis, due to loosening of the nanofiber coating from the allograft surface. Ultimately, this investigation shows our tissue engineered periosteum can deliver FGF-2, TGF-β1, and ASCs to a mouse critical-sized femur defect and further optimization may yield improved bone allograft healing.

[2] Portions of this chapter appear in the following:
Romero, R., Travers, J.K., Asbury, E., Pennybaker, A., Chubb, L., Rose, R., Ehrhart, N.P., Kipper, M.J. "Combined delivery of FGF–2, TGF–β1, and adipose-derived stem cells from an engineered periosteum to a critical-sized mouse femur defect ". J Biomed Mater Res Part A. 2017. (105A). 900-911. Used with permission.

## 3.2. Introduction

Bone grafting procedures are on the rise in the US and world with over 2 million procedures performed annually worldwide and a half million procedures performed in the US.[1,2] Grafts are from an autogenic or allogenic source; autografts have superior clinical performance compared to allografts due to retention of native periosteal tissue and vascularization.[3] However, bone autografts are limited by potential complications such as donor site morbidity. Bone allografts provide an abundant source of replacement bone that can provide immediate structural support and can be used in challenging load-bearing orthopedic indications, such as large segmental defects. However, use of bone allografts can result in suboptimal healing, limited osteointegration compared to bone autografts, and possible disease transmission.[4] Bone allografts undergo rigorous processing which may include cleaning, freezing, and terminal sterilization to remove periosteal soft tissue and native cells to decrease the risk of infection and disease transmission.[5,6] Compromised allograft quality can lead to possible complications including fibrotic non–union, fracture, and ultimately premature failure of load-bearing allografts.[7,8] High failure rates of massive allografts have been reported after implantation, necessitating strategies to improve allograft healing.[9]

Restoring some functions of the native periosteum is a promising strategy for improving bone allograft healing.[10,11] Removal of the periosteum severely limits allograft healing because the periosteum is a vascularized tissue composed of an osteoconductive scaffold, osteoprogenitor cells, and osteoinductive factors which mediate fracture healing and bone autograft incorporation.[12-14] Proposed tissue engineered periosteums include those composed of synthetic polymers, ceramics and natural proteinaceous materials.[15-24] However, few attempts have been made to create a tissue engineered periosteum from purely polysaccharide materials

incorporating glycosaminoglycans (GAGs), which are key functional components of the natural periosteum.[25,26]

GAGs in the extracellular matrix (ECM), such as heparin, play critical roles in the structural and biochemical support of embedded cells. GAGs bind and present cytokines that regulate tissue maintenance and healing processes.[27] Many of these cytokines are growth factors with heparin-binding domains. The heparin-binding domains are closely clustered positively charged peptide residues that bind to polyanionic GAGs through electrostatic complementarity.[27,28] The polyanionic property of GAGs can also be exploited to complex heparin with the positively charged polysaccharide, chitosan. Chitosan has many advantages for engineering strategies for a variety of tissues, including bone, and is biodegradable, antimicrobial, and promotes wound healing.[29-34] Another strength of chitosan is its form factor versatility including nanoparticles, freeze-dried scaffolds and nanofibers.[35] Chitosan nanofibers mimic the periosteal ECM fibrous structure, and can be coated with heparin through electrostatic interactions.[36,37] Heparin-chitosan coatings on trabecular bone have been used to promote blood perfusion and reendothelialzation in a rabbit radial defect.[38] Therefore, a tissue engineered periosteum made from a combination of chitosan and heparin takes advantage of the inherent polysaccharide properties which other biomaterials do not naturally possess.

Including heparin in a tissue engineered periosteum also allows incorporation and delivery of heparin-binding growth factors. Use of osteoinductive growth factors for bone repair has generated high interest, but relatively limited examples of clinical translation.[39,40] Questions remain about the optimal dose, delivery profile, and growth factor combinations, which vary by animal model and clinical indication.[41] Basic fibroblast growth factor (FGF–2) and transforming growth factor-β1 (TGF–β1) have been minimally investigated for their potential to improve

healing in long bone segmental defects even though they are known to participate in skeletal development and maintenance.[42,43] FGF–2 has a mitogenic effect on mesenchymal stem cells and on cells committed to an osteogenic lineage.[44,45] Additionally, Fakhry et al. found that FGF–2 sensitized osteoprogenitors to other osteoinductive factors.[46] FGF–2 also promotes angiogenesis, which is intimately coupled with osteogenesis.[47,48] Similarly, TGF–β1 is involved in several processes important for successful fracture healing, including osteoprogenitor proliferation and differentiation, and has an osteoinductive effect.[43,49] Delivery of FGF-2 and TGF–β1 from a polysaccharide based tissue engineered periosteum may promote healing and improve allograft incorporation.

To mimic important features of the native periosteum, a tissue engineered periosteum should not only include an osteoconductive scaffold and osteoinductive cytokine signals, but also osteoprogenitor cells. Multipotent mesenchymal stem cells (MSCs) are isolated from adult tissues including bone marrow and adipose tissue and have shown promise in bone tissue engineering applications.[50,51] When adipose-derived stem cells (ASCs) are compared to bone marrow mesenchymal stem cells (BM-MSC), ASCs show advantages over BM-MSC including easier accessibility, higher yield of stem cells, and longer *in vitro* expansion periods before reaching senescence, which are all conducive for clinical translation.[52,53] ASCs derived from mice and humans promote healing in mouse critical-sized cranial defects when delivered via a PGLA scaffold, demonstrating their therapeutic potential in skeletal regeneration.[54,55] In addition, ASCs have immune evasive characteristics, allowing ASCs therapeutic effects to occur with a minimal host inflammatory response when used in an allogenic transplant application.[56] ASCs possess attractive qualities as an osteoprogenitor source to be incorporated into a tissue engineered periosteum.

To better understand non-healing bone injuries, animal models are used to investigate mechanisms of non-union and potential clinical interventions. Critical-sized bone defects are defined as bone defects unable to heal within an organism's lifespan.[57] In order to translate research developments from the bench to clinical applications, research and development is generally first attempted in small animal models to test their effectiveness and feasibility.[58] Mouse models are typically used due to their similar physiology to humans.[59] Low animal maintenance cost and rapid breeding allow for cost effective research for initial technology development. Yet, differences in mouse bone anatomy versus human bone limits results obtained when using mouse models as mice lack osteons in their bone structure whereas humans and larger mammals undergo Haversian type remodeling.[60] Mice also have accelerated bone healing when compared to humans and have continual bone growth throughout a mouse's life.[61] Researchers have recently created a critical-sized femoral segmental defect model in mice that can recapitulate aspects of bone graft healing and can screen biomaterial strategies to improve healing of large segmental defects.[62,63]

Previously, our group has demonstrated that heparin-chitosan complexes and coatings on tissue culture polystyrene, glass, and titanium can bind, stabilize, and deliver FGF-2. [37,44,64,65] We further developed similar nanostructured coatings for cortical bone, demonstrating support for mesenchymal stem cell adhesion, antimicrobial properties, cell proliferation, and sustaining ASCs in an osteoprogenitor phenotype.[66,67] Thus, we hypothesize that a polysaccharide-based tissue engineered periosteum composed of heparin-coated chitosan nanofibers would (1) provide sustained delivery of heparin-binding growth factors FGF-2 and TGF-β1, (2) support ASC delivery, and (3) improve allograft incorporation in a critical-sized mouse femoral defect.

### 3.3. Materials and methods

#### 3.3.1. Materials

Heparin sodium from porcine intestinal mucosa (14.4 kDa, 12.5% sulfur) was purchased from Celsus Laboratories (Cincinnati, OH). Chitosan (80 kDa, 9 % acetylated confirmed through $^{1}$H NMR) was acquired from Novamatrix (Sandvika, Norway). Chitosan was methylated to make *N*,*N*,*N*-trimethyl chitosan (TMC) following de Britto's and Asis' method and the degree of quaternization (DQ) of TMC was 71 %.[68] A detailed synthesis and characterization of TMC by $^{1}$H NMR was reported in the supplementary data in Romero et al 2014.[66] Heparin or TMC solutions were made by dissolving the polysaccharides in ultrapure water (18.2 MΩ·cm) at 0.01 M solutions (on a saccharide unit basis) then subsequently filtered with a 0.22 μm polyvinyldifluoride (PVDF) syringe filter (Fisher-Scientific, Pittsburgh, PA). L-Ascorbic acid-2-phosphate, β-glycerophosphate and sucrose were obtained from Sigma-Aldrich (St. Louis, MO). Sodium cacodylate trihydrate was purchased from Polysciences Inc. (Warrington, PA). Hexamethyldisilazane was purchased from Alfa Aesar (Ward Hill, MA). Dimethyl sulfoxide, dichloromethane (DCM) and trifluoroacetic acid (TFA) were purchased from Acros Organics (New Jersey, US). Dulbecco's Modification of Eagle's Medium-low glucose (DMEM), Hank's Balanced Salt Solution (HBSS), MEM vitamins, MEM nonessential amino acids, antibiotic-antimycotic solution, and 0.25% trypsin–EDTA were obtained from Corning (Manassas, VA). Fetal bovine serum (FBS) was obtained from Atlas Biologics (Fort Collins, CO). Recombinant human FGF–2 and TGF–β1 and Human Duoset ELISA Kits were obtained from R&D Systems. (Minneapolis, MN). Firefly D–luciferin was purchased from Gold Biotechnology (St. Louis, MO).

### 3.3.2. Mouse strains

Female 6–8 week donor BALB/c mice and recipient C57BL/6 mice were purchased from Harlan Laboratories, Inc. (Indianapolis, IN). Donor BALB/c allografts (4 mm) were harvested from freshly euthanized BALB/c mice. All experiments involving animal subjects were approved by Colorado State University's Institutional Animal Care and Use Committee (Protocol #11–2896A) and conducted in accordance with NIH guidelines for the care and use of laboratory animals (NIH Publication #85-23 Rev. 1985).

### 3.3.3. Allograft chitosan nanofiber coating with heparin and trimethyl chitosan polyelectrolyte multilayers

Immediately after harvesting BALB/c mid–diaphyseal femoral allografts, periosteal tissue was removed. The allografts were immersed in sterile 0.9% sodium chlorine solution then frozen at –80 °C for at least one week. Prior to modification with electrospun chitosan nanofibers, allografts were thawed, flushed with sterile ultrapure water to remove residual bone marrow and periosteal soft tissue removed. Allografts were sanitized by soaking in 70% ethanol for 15 minutes and then dried under vacuum. Allografts were then modified with electrospun chitosan nanofibers using our previously reported method.[66] Briefly, allografts were mounted onto a custom rotating collector positioned in front of the grounded collector electrode. A 7% (w/v) chitosan solution in 7:3 TFA:DCM solvent mixture, was electrospun onto the rotating bone. (Electrospinning parameters were as follows: flow rate = 1 ml $hr^{-1}$, voltage = 15 kV, tip–to–collector distance = 17.8 cm.) The allografts were rotated during nanofiber collection and coated for approximately 10 mins. Subsequently, the nanofibers were neutralized in 5 M $NH_4OH$ solution for 3 hours under gentle agitation.

Following neutralization, the allografts were rinsed well before deposition of trimethyl chitosan and heparin polyelectrolyte multilayers (PEM), according to our previously reported procedure.[66] Trimethyl chitosan and heparin polyelectrolyte multilayers were deposited onto chitosan nanofibers on the allografts by a layer–by–layer (LbL) fabrication technique. The chitosan nanofiber-coated allografts were immersed into alternating solutions of 0.01 M of trimethyl chitosan and heparin, starting with heparin as the first layer and an ultrapure water rinse between polysaccharide solutions. Seven alternating layers (4 heparin, 3 TMC) were deposited on the chitosan nanofibers, resulting in a terminal heparin layer. After PEM deposition, the allografts were sterilized by soaking in 70 % ethanol for 15 minutes then air dried prior to growth factor adsorption.

### 3.3.4. Growth factor adsorption and release

Recombinant human FGF–2 and TGF–β1were adsorbed onto heparin-terminated PEMs on chitosan nanofiber-coated allografts from a 1000 ng/ml and 100 ng/ml solution. Allografts were immersed in a growth factor-containing solution for one hour at room temperature under gentle agitation. FGF–2 and TGF–β1 *in vitro* release was tested via ELISA. PEM-modified chitosan nanofiber allografts (n=3 per solution concentration) coated with growth factor were immersed in 500 µl of PBS in a 48-well plate then incubated at 37 °C, and 450 µl of PBS were removed at pre–determined time points and the removed PBS replenished. Growth factor-containing aliquots were frozen at –20 °C until analyzed. FGF–2 and TGF–β1 aliquots were assayed with their respective human Duoset ELISA kit following the manufacturer's kit instructions. To assess the amount of FGF–2 and TGF–β1 adsorbed onto implanted nanofiber allografts, a subtraction method was used. A mixed solution of FGF–2 and TGF–β1 (both at

1000 ng/ml) was made in PBS and allografts were immersed for an hour. An aliquot of the original growth factor solution was kept and a growth factor post adsorption aliquot was stored. The difference of these solutions measured the amount of FGF–2 and TGF–β1 adsorbed on the nanofiber allografts.

### 3.3.5. Luciferase–expressing adipose derived stem cells isolation, culture expansion, and allograft cell seeding

Luc–ASCs were isolated from abdominal adipose tissue of (FVB/NTsv-Tg(svyb-luc)-Xen) mice from Taconic (Hudson, NY). Briefly, abdominal adipose tissue was minced and collagenase treated for 30 minutes at 37 °C in DMEM low glucose with antibiotic/antimycotic. The cell suspension was centrifuged, re-suspended, centrifuged again, before the supernatant was aspirated. The resulting cell pellet was plated onto tissue culture flasks and incubated for 4 days before an initial media change with ASC growth media. Luc–ASCs growth media consisted of DMEM low glucose, 15% FBS, 1% antibiotic/antimycotic and supplemented with 1X MEM vitamins and 1X MEM non–essential vitamins. Plastic adherent Luc–ASCs were selected by removing non–adherent cells. The Luc–ASCs were grown until approximately 80% confluent then trypsinized and cryopreserved until needed. We confirmed that these cells have potential to differentiate along both osteogenic and adipogenic lineages, as described in the supporting information, and shown in Figure A2.1.

Passage 1 Luc-ASCs were thawed and culture expanded in a humidified incubator at 37 °C, 5 % $CO_2$ in ASC growth media. Luc–ASCs were split with 0.25% trypsin when about 80% confluent. Passage 3 Luc–ASCs were used in all experiments. After FGF–2 and TGF–β1 adsorption onto nanofiber allografts, allografts were transferred to new wells then seeded with a

highly concentrated Luc–ASCs solution (500,000 cells in 30 µl). The Luc–ASCs were allowed to attach for 1 hour in a humidified incubator at 37 °C, 5 % $CO_2$ before being moved to new wells and immersed in Luc–ASCs growth media. The Luc–ASCs seeding occurred the evening before *in vivo* implantation.

### 3.3.6. Allograft implantation into critical-sized mouse femoral defect model

C57BL/6 female mice (6–8 weeks old) were allografts recipients. The left hindlimb was shaved and aseptically prepared for surgery. The recipient mice were anesthetized via inhaled isoflurane (3 %), injected with slow release buprenorphine (0.6 mg/kg) as an analgesic, and kept on a warming pad throughout the surgical procedure. A 7–8 mm incision was made to laterally approach the femur to create a critical–sized 4-mm mid–diaphyseal femoral defect using a diamond-tip bone saw. A 23-gauge intramedullary pin was inserted through the trochanteric fossa, through the medullary cavity of the modified allograft, and seated into the metaphysis of the distal femur to stabilize the construct. Sutures were used to close soft tissues and skin staples were used to protect the incision. Mice were placed in a recovery cage and observed until awake and ambulatory.

Prior to surgery, each mouse was randomly assigned to one of 4 treatment groups. Animals received either untreated allografts, allografts seeded with ASCs (+ASCs), allografts modified with nanofibers (+NF), or allografts modified with nanofibers and ASCs (+NF+ ASCs), with n=13 in each experimental group. Mice were observed daily for the first week and weekly thereafter and scores of weight, activity, appearance, and ambulation were recorded. Six weeks post-surgery, mice were euthanized by cervical dislocation under deep anesthesia via inhaled isoflurane. Grafted femurs were harvested and dissected of non–adherent musculature

and formalin fixed in neutral buffered formalin for 24 hours. After 24 hours, the intramedullary pin was removed for subsequent micro–computed tomography and histological analysis.

### 3.3.7. Longitudinal luciferase expressing adipose-derived stem cells in vivo tracking

Implanted Luc–ASCs on allografts were longitudinally tracked via bioluminescent imaging. An IVIS-100 *in vivo* imaging system from PerkinElmer (Waltham, MA) with a humidified chamber was used to acquire bioluminescence on post–operative days 1, 4, 7, 11, 14, and weekly thereafter. Recipient mice were injected subcutaneously along the dorsum with 100 µl of 30 mg/mL firefly D–luciferin. After 5 minutes, mice were anesthetized under inhaled isoflurane (3%) then immediately imaged under anesthesia to record their bioluminescence signal. After imaging, mice were moved to a recovery cage and monitored until recovered.

### 3.3.8. Micro–computed tomography analysis

A Scanco µCT 80 (Scanco Medical; Bruttisellen, Switzerland) was used to obtain 3-D reconstructions of grafted femurs. Excised femurs were formalin fixed and imaged in the sample holder containing 10% neutral buffered formalin. Samples were imaged with the following parameters: 10 µm voxel size, 70 kVp, 114 µAs, 500 ms integration time. The allografts were imaged to record the allograft defect site along with at least 1 mm of host tissue in the proximal and distal direction. New bone volume was calculated as reported by Koefoed et al. and Reynolds et al.[69,70] Briefly, the total bone volume ($BV_{Total}$) of the allograft and new bone was calculated by segmenting the 2-D cross sectional images. Another calculation was performed segmenting out the new bone volume, leaving only the allograft ($BV_{Graft}$). Subtracting $BV_{Graft}$ from $BV_{Total}$ led to new bone volume ($BV_{New}$). New bone volume was normalized to the allograft

length as determined by microCT. The polar moment of inertia was also calculated for each 2-D cross section and averaged over the volume of analysis. Longitudinal cross sections of 3-D reconstructions were made to qualitatively assess allograft remodeling and incorporation.

### 3.3.9. Union ratio analysis

The allografts' union ratios were calculated using the method reported by Reynolds et al. using MATLAB R2008b (The Mathworks, Natick, MA).[71] Briefly, transverse μCT cross sections were contoured to identify adjacent bone to endosteal and periosteal surfaces. The union ratio algorithm calculates the allograft surface area contacting new bone divided by the total surface area of the allograft. The algorithm separately evaluates the proximal and distal halves of the allograft and calculates a union ratio for each allograft half. The minimum value is taken as the union ratio.

### 3.3.10. Blinded histological analysis

After finishing the μCT imaging and analysis, the excised femurs were rinsed of formalin and decalcified using Immunocal (StatLab Medical Products, McKinney, TX) for 24 hours. The samples were then dehydrated using an ethanol series and final xylene step and subsequently paraffin embedded. Five-μm slices were obtained and stained with hematoxylin and eosin (H&E) stains. H&E slides were blindly evaluated by a board certified veterinary pathologist (Kampath Diagnostics, Fort Collins, CO). The slides were scored with a value of 0, 1, 2, or 3 corresponding to none, mild, moderate, marked, respectively, for each parameter evaluated. The following parameters associated with graft incorporation and remodeling were evaluated: overall graft incorporation, host-graft bridging callus, inflammation, fibroplasia (periosteal, endosteal,

proximal and distal graft ends), graft associated cutting cones, graft resorption, graft associated marrow, and graft associated trabecular bone. Images of the femur defect region and allograft proximal and distal ends were acquired via light microscopy.

### 3.3.11. Statistical analysis

A two–way ANOVA with Tukey's post-hoc test ($\alpha$=0.05) was performed on log-transformed normalized new bone volume, union ratio, and histological data. A log transformation was used to ensure data were normally distributed. Statistical analysis was performed using SAS Studio 3.2.

## 3.4. Results

### 3.4.1. Chitosan nanofiber coating of bone allografts

Chitosan nanofibers were successfully electrospun onto BALB/c mouse femoral allografts and shown to homogenously cover the entire allograft as seen in Figure 3.1. The coating method resulted in some circumferential alignment of nanofibers. Higher magnification images showed the nanofibers have an approximate diameter less than 1 μm.

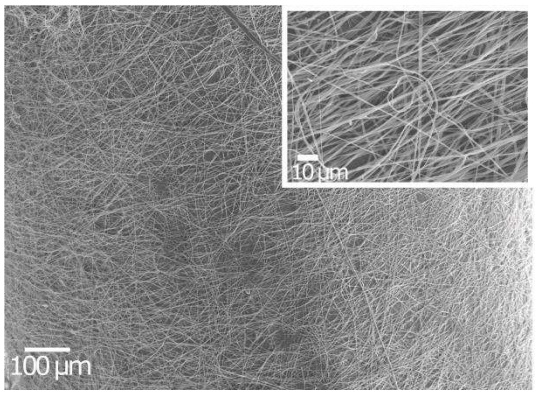


**Figure 3.1** Representative scanning electron micrograph of chitosan nanofibers conformally coating allografts. (Inset) Magnified micrograph of chitosan nanofibers showing a fiber diameter less than 1 μm.

### 3.4.2. Growth factor *in vitro* release characterization

The average (± standard error) amount of FGF–2 and TGF–β1 loaded onto nanofiber allografts was 127 ± 14 ng and 322 ± 32 ng, respectively, from the 1000 ng/mL solutions. When normalized to the average initial weight of the recipient mice, this resulted in growth factor doses of 6.79 ng /g of FGF–2 and 17.22 ng /g of TGF–β1. Figure 3.2 shows the *in vitro* release profiles of FGF–2 and TGF–β1 from nanofiber-coated mouse femoral allografts modified with TMC and heparin PEMs measured by ELISA over 7 days.

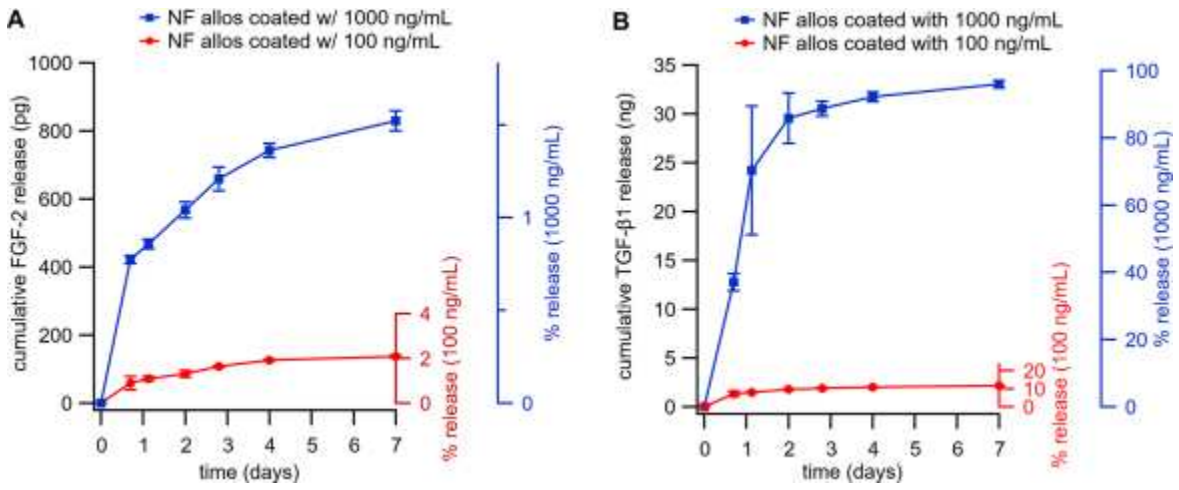


**Figure 3.2** Cumulative (A) FGF–2 and (B) TGF–β1 *in vitro* release profiles from nanofiber allografts (average ± SE). Right-hand axes show the percent of the adsorbed growth factor that is represented by the corresponding cumulative release on the left-hand axis for each condition.

FGF–2 and TGF–β1 both exhibit a burst release over the first day, followed by extended release over one week. The rate of growth factor release over the first week from the nanofiber-coated allografts was modulated by adjusting the initial FGF–2 and TGF–β1 solution concentrations from which the growth factor was adsorbed (100 ng $mL^{-1}$ or 1000 ng $mL^{-1}$). The complete 20-day release data are shown in the supporting information, Figure A2.2. Only about 1.5 % to 2.5 % of the adsorbed FGF–2 is released, and detectable in solution, whereas 95% of the total TGF–β1 adsorbed is released by day 6.

### 3.4.3. Chitosan nanofiber mediated luciferase expressing adipose-derived stem cells transplantation and persistence

Efficient and uniform seeding of Luc-ASCs on nanofiber scaffolds is required for these to be used for cell delivery. We used epifluorescence microscopy to confirm that the method reported here results in essentially complete coverage of the nanofiber scaffolds with Luc-ASCs. An example micrograph is shown in the supporting information, Figure A2.3. Bioluminescence imaging confirmed Luc-ASCs seeded onto nanofiber allografts were successfully delivered to the femoral defect site as seen in Figure 3.3.

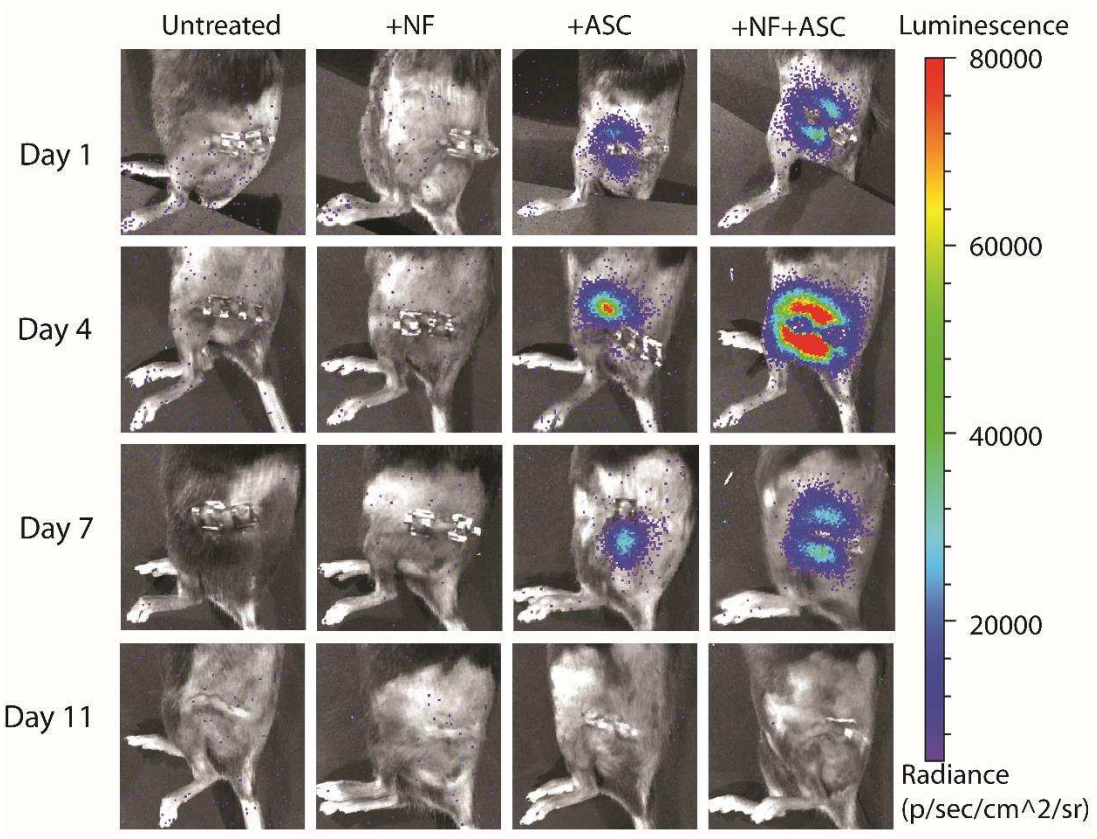


**Figure 3.3** Longitudinal bioluminescence imaging in mice observed that Luc–ASCs persist in the femur defect site for at least 7 days. An increase in bioluminescence is observed at day 4 suggesting Luc–ASCs respond to local bioactive growth factor released from chitosan nanofibers (NF). No bioluminescence can be seen groups without ASCs.

No background bioluminesence was observed in mice that did not receive transplanted ASCs as the left two columns of Figure 3.3. The Luc-ASCs were longitudinally tracked *in vivo* and found to persist at the defect site for at least 7 days. By day 11, no bioluminescent signal was detectable. In the treatment groups containing Luc-ASCs, bioluminescence increased on Day 4 compared to Day 1 and subsequently decreased on day 7, however not to day 1 levels. The greatest bioluminescence was observed in the treatment group containing both Luc-ASCs and nanofibers with dual growth factor delivery.

### 3.4.4. Engineered periosteum bone callus formation

The μCT 3-D reconstructions in Figure 3.4A show good host–graft apposition in all groups. Some bridging bone callus concentrated at the proximal and distal host–graft junctions was observed post–operative 6 weeks. Vertical cross sections revealed allograft remodeling and minimal graft incorporation at the host–graft junctions. New bone volume, normalized to the region of interest, was calculated and is plotted in Figure 3.4B. While no statistical differences are observed among treatment groups, a general trend of increased new bone volume is observed in experimental groups treated with Luc–ASCs compared to their respective cell-free controls. Allografts treated with only Luc–ASCs have an increase of 31.8% normalized new bone volume compared to the untreated allografts, while allografts treated with both Luc–ASCs and nanofiber coating have an increase of 19.5% over the allografts treated with only nanofibers. The nanofiber coating resulted in a minimal increase of normalized new bone volume (4.1%) compared to untreated allografts. Despite these differences in new bone volume, no statistical differences between any groups are observed for normalized new bone volume and average polar moment of inertia.

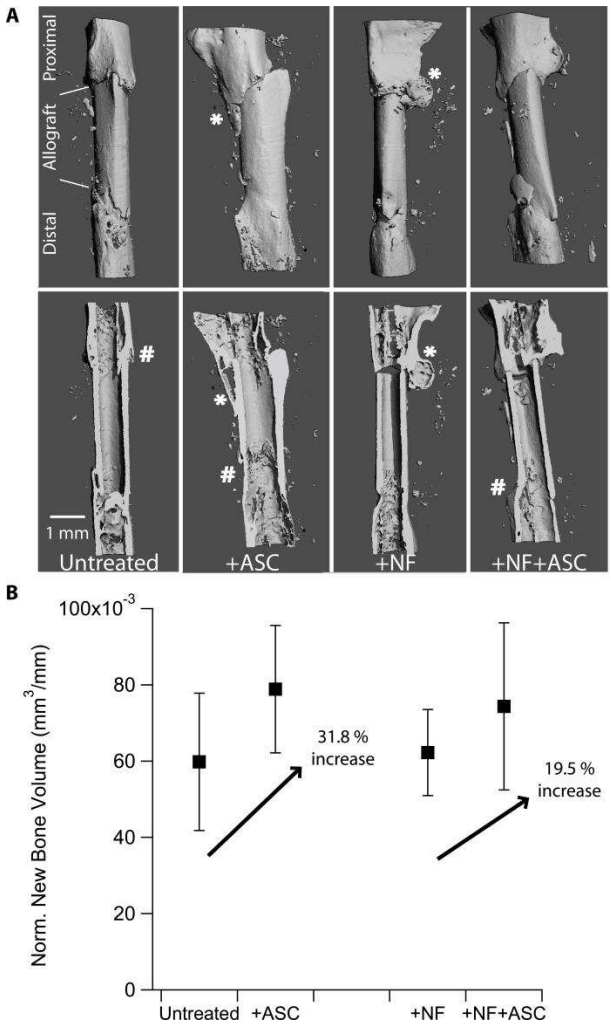


**Figure 3.4** (A) Representative μCT 3D reconstructions. (Top row) 3D reconstructions of the region of interest showing the femur defect, proximal, and distal host tissue and bone callus (*) (Bottom row) Longitudinal cross sections reveal graft incorporation at certain host-graft junctions (#). (B) μCT data analysis (average± SE) shows Luc–ASCs treated allografts generally increased new bone volume formation. ASC treated allografts increased new bone volume by 31.8% compared to untreated allografts while nanofiber+ASC allografts only increased new bone volume by 19.5% compared to nanofiber allografts. However, these increases were not statistically significant.

### 3.4.5. Allograft incorporation via histological and union ratio analyses

Histological sections of the implanted allografts were evaluated by a blinded veterinary pathologist to assess their degree of incorporation into the femur defect. Values for criteria used to assess allograft incorporation are found in Table 3.1.

Table 3.1 Average Scores of Blinded Histological Analysis[a]

| Category | Uncoated Control | Allograft + ASCs | Nanofibers | Nanofibers +ASC |
|---|---|---|---|---|
| Endosteal fibroplasia | 2.4 ± 0.7 | 2.3 ± 0.7 | 2.7 ± 0.5 | 1.8 ± 0.7 |
| Bridging callus | 1.1 ± 0.8 | 1.1 ± 0.8 | 0.7 ± 0.5 | 0.6 ± 0.5 |
| Graft resorption | 1.1 ± 0.3 | 1.1 ± 0.4 | 1.0 ± 0.0 | 1.1 ± 0.3 |
| Graft-associated marrow | 1.6 ± 0.5 | 1.4 ± 0.5 | 0.7 ± 0.7 | 0.4 ± 0.5 |
| Graft-associated trabecular bone | 1.0 ± 1.0 | 1.1 ± 0.8 | 0.3 ± 0.7 | 0.4 ± 0.7 |
| Overall graft incorporation | 1.6 ± 0.7 | 1.8 ± 0.6 | 1.1 ± 0.9 | 1.2 ± 0.9 |
| Inflammation | 1.0 ± 0.7 | 1.1 ± 0.4 | 1.4 ± 0.5 | 0.9 ± 0.3 |

[a]In each category, 0 = “none”, 1 = “mild”, 2 = “moderate”, 3 = “marked”

In some regions, the nanofibers persisted around the allografts for six weeks, however the nanofiber coating is not uniform in the histological sections. An example of the nanofiber coating (dark purple) apparently inhibiting allograft incorporation is seen in Figure 3.5A. This may be attributed to loosening of the nanofiber coating over time *in vivo* confirmed through histology. This phenomenon may contribute to the lower level of bridging callus being formed at the host-graft junction as seen in the blinded histological evaluation. Specifically, the overall graft incorporation score, proximal graft end fibroplasia and distal graft end fibroplasia ($p= 0.0117, 0.024, 0.0004$ respectively) are significantly decreased in nanofiber treated allografts compared to allografts with no nanofiber coating. Similarly, the amount of host-graft bridging callus formed was lower in nanofiber treated allografts compared to allografts without nanofibers.

The histological results of inhibited allograft incorporation are consistent with our observed union ratio results, which quantifies host-graft connectivity using μCT data. The average union ratio for each group can be seen in Figure 3.5B.

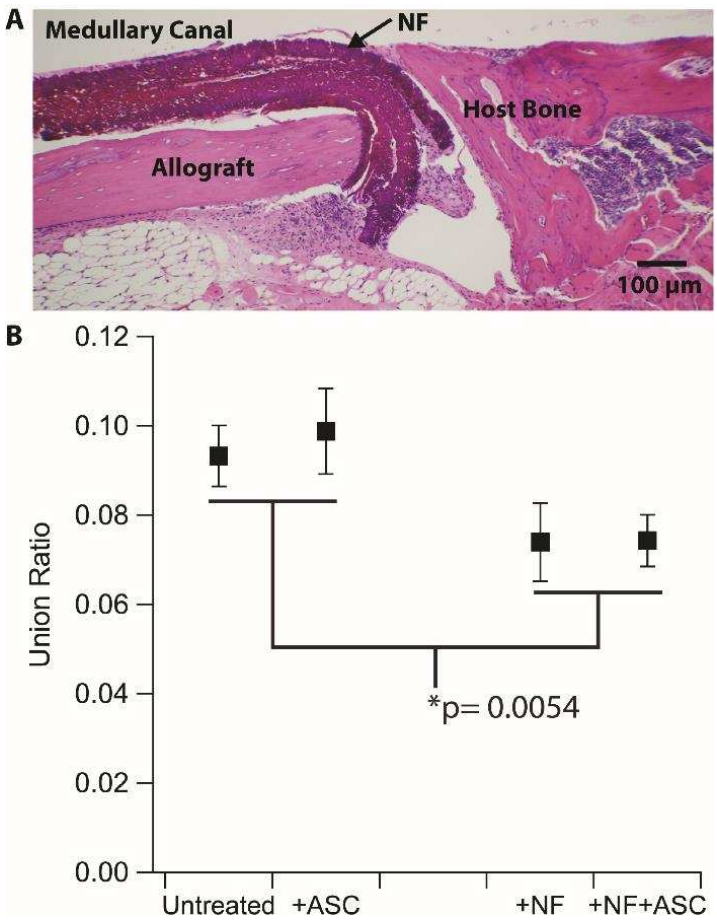


**Figure 3.5** (A) H&E stained section of a graft-host junction showing inhibited allograft incorporation due to loosen nanofiber coating. (B) Union ratio analysis (average ± SE) confirms significantly decreased allograft incorporation by nanofiber treated allografts compared to groups without nanofiber treatment ($p = 0.0054$).

A significant decrease in union ratio was observed between treatment groups including the nanofiber coating compared to allografts with no nanofiber coating ($p = 0.0054$). This resulted in an average union ratio decrease of 20.5% in nanofiber treated allografts compared to untreated allografts at post-operative week 6. Union ratio results reinforced our histological observations that lower graft-host connectivity occurred in nanofiber treated allografts and may be attributed to nanofiber movement and to non-uniform nanofiber degradation.

### 3.4.6. Additional histological outcomes—allograft maturity, inflammation, graft remodeling

Surprisingly, the nanofiber coating delayed maturity of the implanted allograft evidenced by the decreased graft associated marrow and trabecular bone scores compared to the groups with no nanofiber coating (Table 3.1). While no chronic inflammation was observed, the nanofiber coating seems to slightly elevate inflammation scores. However, implanted ASCs mediate this inflammatory response, reducing inflammation back to control levels. No significant differences were found in the following parameters: periosteal fibroplasia, host-graft bridging callus, graft associated cutting cones, graft resorption, and inflammation. The nanofiber coating stained a dark purple and was found on both periosteal and endosteal surfaces, confirming its presence at post-operative week 6, not having been completely degraded or cleared.

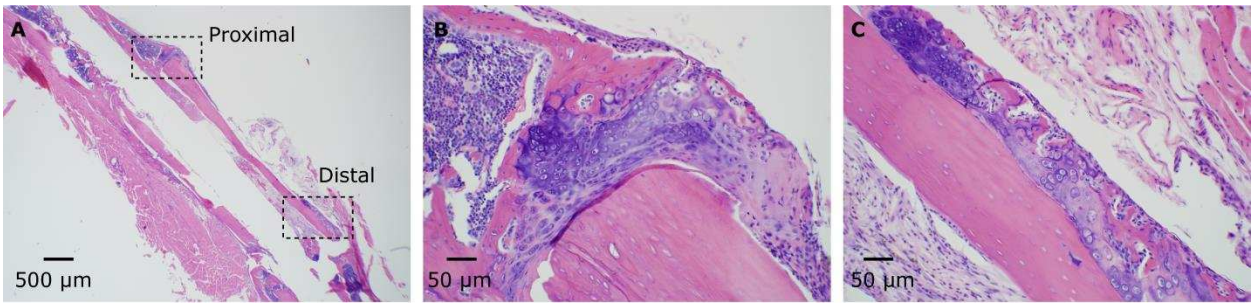


**Figure 3.6** (A) H&E stained section of rare observation of new periosteal cartilage and bone. (B) Higher magnification image of the cartilage present at one proximal host-graft junction. Chondrocytes in cartilage lacunae are visible. (C) Distal host-graft junction shows live new periosteal bone as well as hypertrophic cartilage.

### 3.4.7. Observation of periosteal cartilage and bone

Periosteal cartilage and bone are observed in 2 cases (out of n=18) of samples that included FGF–2 and TGF–β1 delivered from a nanofiber scaffold (w/ or w/o ASCs). Figure 3.6 shows the femur defect site along with higher magnification images showing cartilage tissue and

periosteal bone formation. Atrophic regions in the new periosteal cartilage are seen at the proximal and distal host-graft junctions. Nucleated live bone adjacent to non-nucleated allograft is seen at the distal periosteal surface.

### 3.5. Discussion

#### 3.5.1. Engineered periosteum simultaneously delivers fibroblast growth factor-2 and transforming growth factor-β1 to femur defect

The periosteum is composed of a fibrous tissue layer containing osteoinductive factors and osteoprogenitor cells.[13,72] ECM-mimetic chitosan nanofibers were deposited on the allograft surface to create a fibrous porous coating. Further nanofiber modification via layer-by-layer deposition of TMC and heparin allowed adsorption of heparin binding growth factors, FGF–2 and TGF–β1.[43,73] An advantage of our tissue engineered periosteum is the incorporation of heparin, which stabilizes FGF–2.[64] Heparin binding dramatically extends the half-life of FGF-2 and may also improve TGF–β1 signaling.[44,64,74,75] Previous animal studies have relied on supraphysiologal doses of single growth factors at the fracture site.[49,76-78] Larger doses were needed to achieve a therapeutic dose high enough to overcome the short half–life of FGF–2 and TGF–β1, which is on the order of minutes or hours.[79] Our engineered periosteum locally delivered *in vivo* hundreds of ng of FGF–2 and TGF–β1, which are more physiologically relevant doses than previous studies have achieved. *In vitro* release results demonstrate that different biologically relevant amounts of FGF–2 and TGF–β1 can be delivered from our engineered periosteum by changing the growth factor concentration in the solution used to adsorb FGF–2 and TGF–β1. The ability to modulate the amount of released growth factors from our engineered periosteum is important, as osteoprogenitors exhibit a biphasic response to both FGF–2 and TGF–β1.[42,44,45,80,81]

As bone fracture healing is a complex cascade of signaling cytokines, single growth factor delivery systems may provide insufficient stimuli for new bone formation, let alone vascularization. Delivery strategies releasing multiple growth factors, either simultaneously or sequentially, are ripe for investigation.[39,82] This paper uniquely investigates FGF–2 and TGF–β1 simultaneous delivery to a mouse critical-sized femoral defect. This specific combination of FGF–2 and TGF–β1 delivery was hypothesized to increase allograft healing and incorporation based on previously reported examples of FGF–2 and TGF–β1 to positively affecting bone healing.[49,83] Simultaneous delivery of bioactive FGF–2 and TGF–β1 showed a mitogenic effect on co-delivered osteoprogenitor ASCs, supported by the increased bioluminescent signal in NF+ASC allografts compared to ASC only allografts. However, this study found that simultaneous delivery of FGF–2 and TGF–β1 to a critical-sized mouse femur defect did not significantly improve allograft healing and incorporation outcomes measured at six weeks after implantation. This unexpected result may be attributed to the nanofiber coating acting as a barrier to allograft incorporation as seen in the histological results, the non-optimal therapeutic dose of FGF–2 and TGF–β1 for bone regeneration, and release kinetics of delivered growth factors. FGF–2 has conflicting support in the literature with some studies observing increased bone formation while others groups see no improvement in fracture healing with FGF–2 delivery.[76,84-86] This may have to do with the dosage used in each study and the animal model used. Similarly, TGF–β1 delivery was found not to be osteoinductive which was previously observed when TGF–β1 was delivered from a collagen sponge to a critical-sized rabbit tibial defect.[49] This suggests differences in physiological response to TGF–β1 between mice and rabbits. While FGF-2 and TGF–β1 did not synergistically promote new bone formation, other growth factors could be easily investigated due to the incorporation of heparin into our scaffold

material. Alternative heparin-binding growth factors could be delivered and investigated with our engineered periosteum. Further investigation is needed to determine optimized spatiotemporal delivery of combined and/or sequential FGF–2 and TGF–β1 delivery or of other growth factors which may improve bone allograft healing and incorporation in a long bone fracture healing environment.

### 3.5.2. Engineered periosteum delivers Luc–ASCs to defect site

Prior work suggests that mesenchymal stem cell transplantation may positively affect bone healing.[55,87-89] Herein, it was hypothesized that nanofiber scaffolds that deliver FGF-2 and TGF–β1 with ASCs could improve cortical bone allograft healing in a mouse critical sized femoral defect. Thus Luc–ASCs, along with FGF-2 and TGF-β1, were delivered to a mouse femur defect via an engineered periosteum. Our study used Luc–ASCs in this animal model to simultaneously and longitudinally track ASC viability and localization as firefly luciferin requires ATP as a co-factor for bioluminescence whereas other markers, like green fluorescent protein, may still provide fluorescent signal after cells have died due to its high stability.[90,91] Subcutaneous dorsal injection of luciferin in the lower back of the mouse was adequate to deliver luciferin to Luc–ASCs and confirm their localization at the femur defect site. Bioluminescence imaging demonstrated successful localization of Luc–ASCs at the femoral defect and persistence for at least 7 days, in line with observations from similar studies.[92] Increased bioluminescent signal in ASCs exposed to growth factors at days 1, 4, and 7 compared to ASCs delivered alone support that ASCs responded to bioactive growth factor delivery indicating successful co-localization of the ASCs and growth factors at the femur defect site and resulting in ASC proliferation.

Over time, ASCs bioluminescence decreased below levels of detection of the bioluminescence imager even after direct injection of luciferin at the femur defect site. Previous reports of motile cell delivery to a mouse femur defect attribute reduced fluorescence to their ability to migrate into surrounding soft tissues, dissipating the surviving ASCs' fluorescent signal.[92] An alternative explanation for the loss of Luc-ASC bioluminescence may be mismatched H-2 major histocompatibility haplotypes between FVB/N-sourced Luc-ASC and C57BL/6 recipient mice. ASC express major histocompatibility complex class I markers but lack major histocompatibility complex class II markers.[93] However, undifferentiated ASC, like those used in this study, have been shown to possess immune evasive characteristics as well as immunosuppressive properties.[94-96] Thus, a combination of a slight immune response and compromised nutrient and oxygen transport in the femur defect may have contributed to decreased Luc-ASC bioluminescence over time.

Overall, μCT analysis of new bone volume showed that allograft treatments with ASCs had a trend of increased bone formation compared to their respective cell-free controls, in line with observations in the literature showing ASCs having a therapeutic effect on bone formation.[54] However, a statistically significant increase in bone was not found in ASC-treated allografts suggesting ASC delivery alone or with co-delivered FGF-2 and TGF-β1 was insufficient for robust new bone formation. It has been previously reported that ASCs may have less of an osteogenic potential than similar mesenchymal stem cells derived from bone marrow cells and require osteogenic pre-induction before implantation for robust bone formation.[97] The ASCs used in this experiment were not osteogenically induced prior to implantation. By not osteogenically inducing our ASCs before implantation, we could better investigate the effect of the engineered periosteum scaffold on the implanted ASCs. While it appears the ASCs were not

osteogenicallly induced *in vivo* by the engineered periosteum to produce new bone formation, more new bone formation was observed in ASC seeded allografts compared to their respective cell free controls and supports that the ASCs may have acted therapeutically through trophic secretion rather than direct engraftment as suggested by Prockop.[98] 3D reconstructions of μCT data show bone callus is concentrated at the proximal and distal host-graft junctions. Surprisingly, little to no callus was observed along the mid-diaphyseal surface, with any bone callus typically extending from the proximal or distal host tissue. This is in line with reports that allografts undergoing a creeping substitution remodeling process.[99] With new bone formation concentrated on the host-graft junctions, our data supports previous observations that ASCs alone minimally enhance bone formation in a mouse critical-sized femur defect and require osteogenic pre-induction or genetic modification to express more potent osteoinductive growth factors such as bone morphogenetic protein 2.[89,100]

### 3.5.3. Design considerations of a tissue engineered periosteum

It is hypothesized that a periosteum mimic able to combine an osteocondutive scaffold, osteoinductive factors, and osteogenic cells would enhance long bone allograft incorporation.[10,11] Previous work in this area delivered green fluorescent protein-positive BM-MSCs via a degradable polyethylene glycol hydrogel and have found therapeutic effects such as increased allograft incorporation and vascularization.[15,92,101] Other approaches to locally deliver MSCs in a mouse femur defect include a cell sheet technology that is promising yet potentially time consuming process to prepare samples.[102] In contrast, our engineered periosteum is made of a naturally occurring and compatible chitosan as well as the glycosaminoglycan, heparin, which allowed successful delivery of ASCs along with FGF-2 and TGF-B1 without the added need of a

cell adhesion motif. The increased bone formation observed with our engineered periosteum did not span the entire allograft. This could be because our chitosan nanofiber scaffold does not completely degrade within the allograft healing time frame. Studies have shown that chitosan's degradation rate can be tuned by modifying chitosan's average molecular weight or its degree of deacetylation offering an opportunity for further optimization for specific applications.[103]

The periosteum's native anchoring structure consists of Sharpey fibers inserted into the cortical bone.[104] Our histological results suggest that by week 6, our nanofiber scaffolds detached from the periosteal surface of the allograft, translated, and acted as a barrier in some cases at the host-graft junction. This is most likely due the nanofibers experiencing shear forces from the surrounding soft tissues, as the mice were ambulatory upon waking from anesthesia after allograft implantation. However, it was observed in limited instances of allografts with nanofiber scaffold delivering FGF-2 and TGF-β1 that periosteal hypertrophic cartilage and live bone formed. This result gives evidence of possible osteoinductive qualities of the delivered FGF-2 and TGF-β1. Unfortunately, no approach using a tissue engineering periosteum to improve bone allograft healing to the level of the clinical gold standard of bone autografts exists as many technical hurdles remain. Obstacles such as a simple, efficient, and homogenous cell seeding process on a tissue engineered periosteum, the lack of vascularization in bone allografts and the optimal spatiotemporal delivery of growth factors to recapitulate the native healing cascade have prevented immediate improvement of bone allograft healing and incorporation but nevertheless do not present insurmountable challenges.

### 3.6. Conclusion

This study reports a new type of tissue engineered periosteum derived from naturally occurring polysaccharides chitosan and heparin that successfully combined ASCs, FGF-2 and TGF-β1 delivery to a critical-sized mouse femur defect. Implanted ASCs responded to bioactive engineered periosteum, resulting in ASC proliferation in the femur defect region and ASC persistence at the defect site for at least 7 days. Increased bone callus formation, concentrated at the host-graft junctions, was observed in ASC-treated allografts compared to their cell-free controls. However, this increase was not statistically significant. Unexpectedly, the nanofiber scaffold detached *in vivo* from the allograft periosteal surface and may have acted as a barrier to allograft incorporation in certain cases, as confirmed by a blinded histological and μCT union ratio analysis. In limited cases in our histological analysis, periosteal cartilage and new bone formation was observed in allografts delivering FGF-2 and TGF-β1. Our results show that engineering a periosteum on bone allografts can improve the delivery of exogenous cells to the defect site without causing chronic inflammation, and that additional work is necessary to ensure that the engineered periosteum does not interfere with the host-graft junction.

# REFERENCES


1. Greenwald AS, Boden SD, Goldberg VM, Khan Y, Laurencin CT, Rosier RN. Bone-Graft Substitutes: Facts, Fictions, and Applications. The Journal of Bone and Joint Surgery 2001;83(3):S98-103.
2. Jahangir AA, Nunley RM, Mehta S, Sharan A. Bone-Graft Substitutes in Orthopaedic Surgery. AAOS *Now* Rockford, IL: American Academy of Orthopaedic Surgeons; 2008.
3. Khan SN, Cammisa FP, Jr., Sandhu HS, Diwan AD, Girardi FP, Lane JM. The biology of bone grafting. J Am Acad Orthop Surg 2005;13(1):77-86.
4. Blokhuis TJ, Arts JJ. Bioactive and osteoinductive bone graft substitutes: definitions, facts and myths. Injury 2011;42(Suppl 2):S26-9.
5. Boyce T, Edwards J, Scarborough N. Allograft bone. The influence of processing on safety and performance. Orthop Clin North Am 1999;30(4):571-81.
6. McAllister DR, Joyce MJ, Mann BJ, C. Thomas Vangsness J. Allograft Update: The Current Status of Tissue Regulation, Procurement, Processing, and Sterilization. The American Journal of Sports Medicine 2007;35(12):2148-2158.
7. Dion N, Sim FH. The Use of Allografts in Orthopaedic Surgery - Part I: The Use of Allografts in Musculoskeletal Oncology. The Journal of Bone and Joint Surgery 2002;84(4):644-654.
8. Berrey BH, Lord CF, Gebhardt MC, Mankin HJ. Fractures of allografts. Frequency, treatment, and end-results. J Bone Joint Surg Am 1990;72(6):825-33.
9. Wheeler DL, Enneking WF. Allograft bone decreases in strength in vivo over time. Clin Orthop Relat Res. United States; 2005. p 36-42.
10. Zhang X, Awad HA, O'Keefe RJ, Guldberg RE, Schwarz EM. A perspective: Engineering periosteum for structural bone graft healing. Clinical Orthopaedics and Related Research 2008;466(8):1777-1787.
11. Hoffman MD, Benoit DSW. Emerging Ideas: Engineering the Periosteum: Revitalizing Allografts by Mimicking Autograft Healing. Clinical Orthopaedics and Related Research 2013;471(3):721-726.
12. Allen MR, Hock JM, Burr DB. Periosteum: biology, regulation, and response to osteoporosis therapies. Bone 2004;35(5):1003-12.
13. Dwek JR. The periosteum: what is it, where is it, and what mimics it in its absence? Skeletal Radiol 2010;39(4):319-23.
14. Zhang X, Xie C, Lin ASP, Ito H, Awad H, Lieberman JR, Rubery PT, Schwarz EM, O'Keefe RJ, Guldberg RE. Periosteal progenitor cell fate in segmental cortical bone graft transplantations: implications for functional tissue engineering. Journal of Bone and Mineral Research 2005;20(12):2124-2137.
15. Hoffman MD, Xie C, Zhang X, Benoit DSW. The effect of mesenchymal stem cells delivered via hydrogel-based tissue engineered periosteum on bone allograft healing. Biomaterials 2013;34(35):8887-8898.
16. Ito H, Koefoed M, Tiyapatanaputi P, Gromov K, Goater JJ, Carmouche J, Zhang X, Rubery PT, Rabinowitz J, Samulski RJ and others. Remodeling of cortical bone allografts mediated by adherent rAAV-RANKL and VEGF gene therapy. Nature Medicine 2005;11(3):291-297.

17. Shi XT, Chen S, Zhao YH, Lai C, Wu HK. Enhanced Osteogenesis by a Biomimic Pseudo-Periosteum-Involved Tissue Engineering Strategy. Advanced Healthcare Materials 2013;2(9):1229-1235.
18. Kang YQ, Ren LL, Yang YZ. Engineering Vascularized Bone Grafts by Integrating a Biomimetic Periosteum and beta-TCP Scaffold. ACS Applied Materials & Interfaces 2014;6(12):9622-9633.
19. Kim S, Bedigrew K, Guda T, Maloney WJ, Park S, Wenke JC, Yang YP. Novel osteoinductive photo-cross-linkable chitosan-lactide-fibrinogen hydrogels enhance bone regeneration in critical size segmental bone defects. Acta Biomaterialia 2014;10(12):5021–5033.
20. Chou Y-C, Cheng Y-S, Hsu Y-H, Yu Y-H, Liu S-J. A bio-artificial poly( D,L -lactide-co-glycolide) drug-eluting nanofibrous periosteum for segmental long bone open fractures with significant periosteal stripping injuries. International Journal of Nanomedicine 2016;11:941-953.
21. Chun YY, Wang JK, Tan NS, Chan PPY, Tan TTY, Choong C. A Periosteum-Inspired 3D Hydrogel-Bioceramic Composite for Enhanced Bone Regeneration. Macromolecular Bioscience 2016;16(2):276-287.
22. Ding X, Wu C, Ha T, Wang L, Huang Y, Kang H, Zhang Y, Liu H, Fan Y. Hydroxyapatite-containing silk fibroin nanofibrous scaffolds for tissue-engineered periosteum. Rsc Advances 2016;6(23):19463-19474.
23. Zhao L, Zhao J, Yu J, Zhao X, Chen Q, Huang Y. In vitro study of bioactivity of homemade tissue-engineered periosteum. Mater Sci Eng C Mater Biol Appl 2016;58:1170-6.
24. Chen K, Lin X, Zhang Q, Ni J, Li J, Xiao J, Wang Y, Ye Y, Chen L, Jin K and others. Decellularized periosteum as a potential biologic scaffold for bone tissue engineering. Acta Biomaterialia 2015;19:46-55.
25. Almodóvar J, Mower J, Banerjee A, Sarkar AK, Ehrhart NP, Kipper MJ. Chitosan-heparin polyelectrolyte multilayers on cortical bone: Periosteum-mimetic, cytophilic, antibacterial coatings. Biotechnology and Bioengineering 2013;110(2):609-618.
26. Caridade SG, Monge C, Almodovar J, Guillot R, Lavaud J, Josserand V, Coll J-L, Mano JF, Picart C. Myoconductive and osteoinductive free-standing polysaccharide membranes. Acta Biomaterialia 2015;15:139-149.
27. Mulloy B, Rider CC. Cytokines and proteoglycans: an introductory overview. Biochem Soc Trans 2006;34(Pt 3):409-13.
28. Harmer NJ, Ilag LL, Mulloy B, Pellegrini L, Robinson CV, Blundell TL. Towards a resolution of the stoichiometry of the fibroblast growth factor (FGF)–FGF receptor–heparin complex. Journal of Molecular Biology 2004;339(4):821-834.
29. Tomihata K, Ikada Y. In vitro and in vivo degradation of films of chitin and its deacetylated derivatives. Biomaterials 1997;18(7):567-575.
30. VandeVord PJ, Matthew HWT, DeSilva SP, Mayton L, Wu B, Wooley PH. Evaluation of the biocompatibility of a chitosan scaffold in mice. Journal of Biomedical Materials Research 2002;59(3):585-590.
31. Jia Z, Shen D, Xu W. Synthesis and antibacterial activities of quaternary ammonium salt of chitosan. Carbohydrate Research 2001;333(1):1-6.

32. Azad AK, Sermsintham N, Chandrkrachang S, Stevens WF. Chitosan membrane as a wound-healing dressing: characterization and clinical application. Journal of Biomedical Materials Research Part B: Applied Biomaterials 2004;69(2):216-222.
33. Kim I-Y, Seo S-J, Moon H-S, Yoo M-K, Park I-Y, Kim B-C, Cho C-S. Chitosan and its derivatives for tissue engineering applications. Biotechnology Advances 2008;26(1):1–21.
34. Costa-Pinto AR, Reis RL, Neves NM. Scaffolds Based Bone Tissue Engineering: the Role of Chitosan. Tissue Engineering Part B: Reviews 2011;17(5):331-347.
35. Jiang T, Deng M, James R, Nair LS, Laurencin CT. Micro- and nanofabrication of chitosan structures for regenerative engineering. Acta Biomaterialia 2014;10(4):1632-1645.
36. Frohbergh ME, Katsman A, Botta GP, Lazarovici P, Schauer CL, Wegst UG, Lelkes PI. Electrospun hydroxyapatite-containing chitosan nanofibers crosslinked with genipin for bone tissue engineering. Biomaterials 2012;33(36):9167-78.
37. Almodóvar J, Kipper MJ. Coating electrospun chitosan nanofibers with polyelectrolyte multilayers using the polysaccharides heparin and N,N,N-trimethyl chitosan. Macromolecular bioscience 2011;11(1):72-6.
38. Sun XJ, Peng W, Yang ZL, Ren ML, Zhang SC, Zhang WG, Zhang LY, Xiao K, Wang ZG, Zhang B and others. Heparin-chitosan-coated acellular bone matrix enhances perfusion of blood and vascularization in bone tissue engineering scaffolds. Tissue Eng Part A 2011;17(19-20):2369-78.
39. Mehta M, Schmidt-Bleek K, Duda GN, Mooney DJ. Biomaterial delivery of morphogens to mimic the natural healing cascade in bone. Advanced Drug Delivery Reviews 2012;64(12):1257-1276.
40. Willie BM, Petersen A, Schmidt-Bleek K, Cipitria A, Mehta M, Strube P, Lienau J, Wildemann B, Fratzl P, Duda G. Designing biomimetic scaffolds for bone regeneration: why aim for a copy of mature tissue properties if nature uses a different approach? Soft Matter 2010;6(20):4976-4987.
41. Santo VE, Gomes ME, Mano JF, Reis RL. Controlled Release Strategies for Bone, Cartilage, and Osteochondral Engineering-Part II: Challenges on the Evolution from Single to Multiple Bioactive Factor Delivery. Tissue Engineering Part B-Reviews 2013;19(4):327-352.
42. Du XL, Xie YL, Xian CJ, Chen L. Role of FGFs/FGFRs in skeletal development and bone regeneration. Journal of Cellular Physiology 2012;227(12):3731-3743.
43. Janssens K, ten Dijke P, Janssens S, Van Hul W. Transforming growth factor-beta 1 to the bone. Endocrine Reviews 2005;26(6):743-774.
44. Almodóvar J, Bacon S, Gogolski J, Kisiday JD, Kipper MJ. Polysaccharide-based polyelectrolyte multilayer surface coatings can enhance mesenchymal stem cell response to adsorbed growth factors. Biomacromolecules 2010;11(10):2629-39.
45. Zellin G, Linde A. Effects of recombinant human fibroblast growth factor-2 on osteogenic cell populations during orthopic osteogenesis in vivo. Bone 2000;26(2):161-8.
46. Fakhry A, Ratisoontorn C, Vedhachalam C, Salhab I, Koyama E, Leboy P, Pacifici M, Kirschner RE, Nah HD. Effects of FGF-2/-9 in calvarial bone cell cultures: differentiation stage-dependent mitogenic effect, inverse regulation of BMP-2 and noggin, and enhancement of osteogenic potential. Bone 2005;36(2):254-66.

47. Cross MJ, Claesson-Welsh L. FGF and VEGF function in angiogenesis: signalling pathways, biological responses and therapeutic inhibition. Trends in Pharmacological Sciences 2001;22(4):201-207.
48. Kanczler JM, Oreffo ROC. Osteogenesis and angiogenesis: The potential for engineering bone. European Cells & Materials 2008;15:100-114.
49. Ehrhart NP, Hong L, Morgan AL, Eurell JA, Jamison RD. Effect of transforming growth factor-beta 1 on bone regeneration in critical-sized bone defects after irradiation of host tissues. American Journal of Veterinary Research 2005;66(6):1039-1045.
50. Jones E. Mesenchymal stem cells and bone regeneration: Current status. 2011;42(6):562–568.
51. Steinert AF, Rackwitz L, Gilbert F, Noth U, Tuan RS. Concise review: the clinical application of mesenchymal stem cells for musculoskeletal regeneration: current status and perspectives. Stem Cells Transl Med 2012;1(3):237-47.
52. Kern S, Eichler H, Stoeve J, Klüter H, Bieback K. Comparative analysis of mesenchymal stem cells from bone marrow, umbilical cord blood, or adipose tissue. Stem Cells 2006;24(5):1294-301.
53. Dmitrieva RI, Minullina IR, Bilibina AA, Tarasova OV, Anisimov SV, Zaritskey AY. Bone marrow- and subcutaneous adipose tissue-derived mesenchymal stem cells: differences and similarities. Cell Cycle 2012;11(2):377-83.
54. Cowan CM, Shi YY, Aalami OO, Chou YF, Mari C, Thomas R, Quarto N, Contag CH, Wu B, Longaker MT. Adipose-derived adult stromal cells heal critical-size mouse calvarial defects. Nat Biotechnol 2004;22(5):560-7.
55. Levi B, James AW, Nelson ER, Vistnes D, Wu B, Lee M, Gupta A, Longaker MT. Human adipose derived stromal cells heal critical size mouse calvarial defects. PLoS One 2010;5(6):e11177.
56. Ankrum JA, Ong JF, Karp JM. Mesenchymal stem cells: immune evasive, not immune privileged. Nature Biotechnology 2014;32:252-260.
57. Schmitz JP, Hollinger JO. The critical size defect as an experimental model for craniomandibulofacial nonunions. Clin Orthop Relat Res 1986(205):299-308.
58. Muschler GF, Raut VP, Patterson TE, Wenke JC, Hollinger JO. The Design and Use of Animal Models for Translational Research in Bone Tissue Engineering and Regenerative Medicine. Tissue Engineering Part B-Reviews 2010;16(1):123-145.
59. Harris JS, Bemenderfer T, B., Wessel AR, Kacena MA. A review of mouse critical size defect models in weight bearing bones. Bone 2013;55(1):241–247.
60. Treuting PM, Dintzis SM, editors. Comparative Anatomy and Histology: A Mouse and Human Atlas 1ed: Academic Press; 2011. 474 p.
61. Petite H, Quarto R, editors. Engineered Bone. 1 ed: Landes Bioscience; 2005. 225 p.
62. Tiyapatanaputi P, Rubery PT, Carmouche J, Schwarz EM, O'keefe RJ, Zhang X. A novel murine segmental femoral graft model. J Orthop Res 2004;22(6):1254-60.
63. Xie C, Reynolds D, Awad H, Rubery PT, Pelled G, Gazit D, Guldberg RE, Schwarz EM, O'Keefe RJ, Zhang X. Structural bone allograft combined with genetically engineered mesenchymal stem cells as a novel platform for bone tissue engineering. Tissue Eng 2007;13(3):435-45.
64. Volpato FZ, Almodóvar J, Erickson K, Popat KC, Migliaresi C, Kipper MJ. Preservation of FGF-2 bioactivity using heparin-based nanoparticles, and their delivery from electrospun chitosan fibers. Acta biomaterialia 2012;8(4):1551-1559.

65. Place LW, Sekyi M, Kipper MJ. Aggrecan-mimetic, glycosaminoglycan-containing nanoparticles for growth factor stabilization and delivery. Biomacromolecules 2014;15(2):680-689.
66. Romero R, Chubb L, Travers JK, Gonzales TR, Ehrhart NP, Kipper MJ. Coating cortical bone allografts with periosteum-mimetic scaffolds made of chitosan, trimethyl chitosan, and heparin. Carbohydr Polym 2015;122:144-51.
67. Almodovar J, Mower J, Banerjee A, Sarkar AK, Ehrhart NP, Kipper MJ. Chitosan-heparin polyelectrolyte multilayers on cortical bone: Periosteum-mimetic, cytophilic, antibacterial coatings. Biotechnology and Bioengineering 2013;110(2):609-618.
68. de Britto D, Assis OBG. A novel method for obtaining a quaternary salt of chitosan. Carbohydrate Polymers 2007;69(2):305-310.
69. Reynolds DG, Hock C, Shaikh S, Jacobson J, Zhang X, Rubery PT, Beck CA, O'keefe RJ, Lerner AL, Schwarz EM and others. Micro-computed tomography prediction of biomechanical strength in murine structural bone grafts. J Biomech 2007;40(14):3178-86.
70. Koefoed M, Ito H, Gromov K, Reynolds DG, Awad HA, Rubery PT, Ulrich-Vinther M, Soballe K, Guldberg RE, Lin AS and others. Biological effects of rAAV-caAlk2 coating on structural allograft healing. Molelcular Therapy 2005;12(2):212-218.
71. Reynolds DG, Shaikh S, Papuga MO, Lerner AL, O'Keefe RJ, Schwarz EM, Awad HA. muCT-based measurement of cortical bone graft-to-host union. J Bone Miner Res 2009;24(5):899-907.
72. Colnot C, Zhang X, Knothe Tate ML. Current insights on the regenerative potential of the periosteum: molecular, cellular, and endogenous engineering approaches. Journal of Orthopaedic Research 2012;30(12):1869-1878.
73. Beenken A, Mohammadi M. The FGF family: biology, pathophysiology and therapy. Nature Reviews Drug Discovery 2009;8(3):235-253.
74. McCaffrey TA, Falcone DJ, Du B. Transforming growth factor-beta 1 is a heparin-binding protein: identification of putative heparin-binding regions and isolation of heparins with varying affinity for TGF-beta 1. J Cell Physiol 1992;152(2):430-40.
75. Lyon M, Rushton G, Gallagher JT. The interaction of the transforming growth factor-betas with heparin/heparan sulfate is isoform-specific. J Biol Chem 1997;272(29):18000-6.
76. Nakajima F, Ogasawara A, Goto K, Moriya H, Ninomiya Y, Einhorn TA, Yamazaki M. Spatial and temporal gene expression in chondrogenesis during fracture healing and the effects of basic fibroblast growth factor. J Orthop Res 2001;19(5):935-44.
77. Komaki H, Tanaka T, Chazono M, Kikuchi T. Repair of segmental bone defects in rabbit tibiae using a complex of beta-tricalcium phosphate, type I collagen, and fibroblast growth factor-2. Biomaterials 2006;27(29):5118-26.
78. Joyce ME, Roberts AB, Sporn MB, Bolander ME. Transforming growth factor-beta and the initiation of chondrogenesis and osteogenesis in the rat femur. J Cell Biol 1990;110(6):2195-207.
79. Tessmar JK, Göpferich AM. Matrices and scaffolds for protein delivery in tissue engineering. Advanced Drug Delivery Reviews 2007;59(4):274-291.
80. Zellin G, Beck S, Hardwick R, Linde A. Opposite effects of recombinant human transforming growth factor-beta 1 on bone regeneration in vivo: Effects of exclusion of periosteal cells by microporous membrane. Bone 1998;22(6):613-620.

81. Centrella M, McCarthy TL, Canalis E. Transforming growth factor beta is a bifunctional regulator of replication and collagen synthesis in osteoblast-enriched cell cultures from fetal rat bone. J Biol Chem 1987;262(6):2869-74.
82. Richardson TP, Peters MC, Ennett AB, Mooney DJ. Polymeric system for dual growth factor delivery. Nature Biotechnology 2001;19(11):1029-1034.
83. Kwan MD, Sellmyer MA, Quarto N, Ho AM, Wandless TJ, Longaker MT. Chemical Control of FGF-2 Release for Promoting Calvarial Healing with Adipose Stem Cells. Journal of Biological Chemistry 2011;286(13):11307-11313.
84. Takechi M, Tatehara S, Satomura K, Fujisawa K, Nagayama M. Effect of FGF-2 and melatonin on implant bone healing: a histomorphometric study. J Mater Sci Mater Med 2008;19(8):2949-52.
85. Kawaguchi H, Oka H, Jingushi S, Izumi T, Fukunaga M, Sato K, Matsushita T, Nakamura K. A local application of recombinant human fibroblast growth factor 2 for tibial shaft fractures: A randomized, placebo-controlled trial. J Bone Miner Res 2010;25(12):2735-43.
86. Nakajima F, Nakajima A, Ogasawara A, Moriya H, Yamazaki M. Effects of a single percutaneous injection of basic fibroblast growth factor on the healing of a closed femoral shaft fracture in the rat. Calcif Tissue Int 2007;81(2):132-8.
87. Xu Y, Malladi P, Wagner DR, Longaker MT. Adipose-derived mesenchymal cells as a potential cell source for skeletal regeneration. Current Opinion in Molecular Therapeutics 2005;7(4):300-305.
88. Peterson B, Zhang J, Iglesias R, Kabo M, Hedrick M, Benhaim P, Lieberman JR. Healing of critically sized femoral defects, using genetically modified mesenchymal stem cells from human adipose tissue. Tissue Eng 2005;11(1-2):120-9.
89. Tseng SS, Lee MA, Reddi AH. Nonunions and the potential of stem cells in fracture-healing. J Bone Joint Surg Am 2008;90 Suppl 1:92-8.
90. Hastings JW. Bioluminescence. In: Sperelakis N, editor. Cell Physiology Source Book: Essentials of Membrane Biophysics. Boston, MA: Academic Press; 2012. p 925-947.
91. Corish P, Tyler-Smith C. Attenuation of green fluorescent protein half-life in mammalian cells. Protein Eng 1999;12(12):1035-40.
92. Hoffman MD, Van Hove AH, Benoit DS. Degradable hydrogels for spatiotemporal control of mesenchymal stem cells localized at decellularized bone allografts. Acta Biomaterialia 2014;10(8):3431-3441.
93. Lohan P, Coleman CM, Murphy JM, Griffin MD, Ritter T, Ryan AE. Changes in immunological profile of allogeneic mesenchymal stem cells after differentiation: should we be concerned? Stem Cell Res Ther 2014;5(4).
94. Kim I, Bang SI, Lee SK, Park SY, Kim M, Ha H. Clinical Implication of Allogenic Implantation of Adipogenic Differentiated Adipose-Derived Stem Cells. Stem Cells Translational Medicine 2014;3(11):1312-1321.
95. Ribeiro A, Laranjeira P, Mendes S, Velada I, Leite C, Andrade P, Santos F, Henriques A, Grãos M, Cardoso CMP and others. Mesenchymal stem cells from umbilical cord matrix, adipose tissue and bone marrow exhibit different capability to suppress peripheral blood B, natural killer and T cells. Stem Cell Res Ther 2013;4(5):125.
96. Niemeyer P, Kornacker M, Mehlhorn A, Seckinger A, Vohrer J, Schmal H, Kasten P, Eckstein V, Sudkamp NP, Krause U. Comparison of immunological properties of bone

marrow stromal cells and adipose tissue-derived stem cells before and after osteogenic differentiation in vitro. Tissue Eng 2007;13(1):111-21.
97. Ruetze M, Richter W. Adipose-derived stromal cells for osteoarticular repair: trophic function versus stem cell activity. Expert Rev Mol Med; 2014.
98. Prockop DJ. Repair of tissues by adult stem/progenitor cells (MSCs): controversies, myths, and changing paradigms. Mol Ther 2009;17(6):939-46.
99. Koefoed M, Ito H, Gromov K, Reynolds DG, Awad HA, Rubery PT, Ulrich-Vinther M, Soballe K, Guldberg RE, Lin ASP and others. Biological effects of rAAV-caAlk2 coating on structural allograft healing. Molecular Therapy 2005;12(2):212-218.
100. Lin CY, Chang YH, Sung LY, Chen CL, Lin SY, Li KC, Yen TC, Lin KJ, Hu YC. Long-term tracking of segmental bone healing mediated by genetically engineered adipose-derived stem cells: focuses on bone remodeling and potential side effects. Tissue Eng Part A 2014;20(9-10):1392-402.
101. Hoffman MD, Benoit DSW. Emulating native periosteum cell population and subsequent paracrine factor production to promote tissue engineered periosteum-mediated allograft healing. Biomaterials 2015;52:426-440.
102. Long T, Zhu Z, Awad HA, Schwarz EM, Hilton MJ, Dong Y. The effect of mesenchymal stem cell sheets on structural allograft healing of critical sized femoral defects in mice. Biomaterials 2014;35(9):2752-2759.
103. Dash M, Chiellini F, Ottenbrite RM, Chiellini E. Chitosan-A versatile semi-synthetic polymer in biomedical applications. Progress in Polymer Science 2011;36(8):981-1014.
104. Chang H, Tate MLK. Concise Review: The Periosteum: Tapping into a Reservoir of Clinically Useful Progenitor Cells. Stem Cells Translational Medicine 2012;1(6):480-491.

# CHAPTER 4: IN-VITRO DELIVERY OF FGF-2 AND TGF-B1 FROM AN ENGINEERED PERIOSTEUM SYNERGISTICALLY PROMOTES PROLIFERATION AND INHIBITS DIFFERENTIATION OF MOUSE ADIPOSE-DERIVED STEM CELLS

## 4.1. Summary

Critical-sized bone defects require clinical intervention including bone graft transplantation to heal the injury. Unfortunately, approximately 5-10% of cases can result in complications such as delayed union or non-union of the bone graft. Recently, periosteum-inspired strategies to improve bone allograft healing and osseointegration have been proposed and investigated. In this work, three different engineered periostea made from chitosan, trimethyl chitosan, and heparin on mouse bone allografts were investigated to determine fibroblast growth factor-2 (FGF-2) and transforming growth factor-β1 (TGF-β1) *in vitro* release kinetics from engineered periostea. Mouse adipose-derived stem cells (Luc-ASC) were cultured on the engineered periostea for 21 days and their proliferation and differentiation response to released bioactive growth factors from the engineered periostea were evaluated using bioluminescence imaging and Western blot analysis. Alkaline phosphatase and receptor activator of nuclear factor kappa-B ligand protein expression were not inhibited in Luc-ASC by co-delivery of FGF-2 and TGF-β1 from engineered periosteum while osteocalcin, osteopontin, and osteonectin proteins were undetected suggesting Luc-ASC maintained an osteoprogenitor phenotype as Luc-ASC did not osteogenically differentiate. Relative gene expression studies of Luc-ASC cultured on periosteum-like chitosan nanofibers delivering FGF-2 and TGF-β1 further confirmed Luc-ASC did not differentiate down osteogenic, adipogenic, or chondrogenic lineages. Overall, this work supports a polysaccharide-based engineered periosteum to delivery multiple growth factors and a multipotent cell population to modulate bone allograft healing.

## 4.2. Introduction

Bone fractures place a substantial health and economic burden on the US and global populations.[1-5] Thus research into therapeutic interventions for bone fractures are necessary, especially for clinically challenging indications such as large bone fractures due to traumatic injury or osteosarcoma resection. Critical-sized bone defects require clinical intervention either through bone autograft or bone allograft implantation to stabilize and eventually integrate with native bone tissue. Bone autografts are the current clinical gold standard evidenced by their high success rate of integration and remodeling due to retention of native bone tissue architecture.[6,7] However, bone autografts have limits on the autograft size and complications such as donor site morbidity. On the other hand, bone allografts are another clinical option that obviate these limitations and complications, as bone allografts are sourced from cadaveric tissue donors. This source allows for larger bone graft sizes compared to bone autografts without causing donor site morbidity. While there are inherent risks to using bone allografts, these risks can be mitigated through proper donor screening, bone allograft cleaning, and sterilization. However, bone allograft processing compromises the regenerative capacity of bone allografts by removing important biological material, such as the periosteum, which is key to mediating bone fracture healing.[8] Consequently, allografts suffer from a different set of complications such as delayed union or non-union and secondary fractures are possible. Limited healing also increases the risk of infections due to subsequent secondary surgical intervention. It is generally accepted that bone healing problems, such as delayed union or nonunion, occur in 5 to 10% of bone fractures.[9] Since the periosteum is integral to bone fracture healing, there is interest in developing periosteum-mimetic strategies to improve bone allograft healing.

The periosteum, a thin tissue layer present on the non-articulating surfaces of bone, can serve as a model tissue architecture to emulate in order to enhance bone allograft healing and integration.[10,11] The periosteum's structure is osteoconductive, contains osteoinductive proteins, and osteoprogenitor cells and contributes to the periosteum's role as a regenerative reservoir in bone fracture healing.[12] Many approaches have been attempted to emulate the native periosteum architecture using proteins, synthetic polymers, ceramics, and polysaccharides to improve bone graft healing.[13-25] However, polysaccharide-based materials that incorporate glycosaminoglycans (GAGs) have not been thoroughly investigated as a periosteum substitute.

GAGs are naturally present in the mammalian extracellular matrix (ECM) and possess biochemical function by sequestering cytokines, including growth factors, from the extracellular milieu.[26] GAGs, such as heparan sulfate or heparin, release growth factors when needed through ECM enzyme-mediated degradation during tissue remodeling.[27,28] In bone fracture healing, multiple growth factors and cytokines are involved including members of the fibroblast growth factor (FGF) family and transforming growth factor (TGF) superfamily.[29,30] Research studies have previously focused on single growth factor delivery for improving bone fracture healing but investigating multiple growth factor delivery is important to mimic the native tissue response.[31] However, one difficulty of using growth factors, such as FGF-2 and TGF-β1, is their very short *in vivo* plasma half-lives, which are on the order of minutes or hours.[32] Heparin has been shown to bind and modulate FGF-2 and TGF-β1 signaling.[33,34] Heparin incorporation into an engineered periosteum provides a direct avenue to locally deliver growth factors to a bone fracture healing environment and the cells present within.

During initial fracture callus formation, the periosteum has been shown to contribute a significant amount of progenitor cells that are responsible for callus mineralization.[35] This result

supports using an engineered periosteum to deliver an osteoprogenitor cell population to modulate fracture healing. Various sources of multipotent stem cells, such as bone marrow mesenchymal stem cells, periosteum-derived stem cells, and adipose-derived stem cells have been investigated to improve bone fracture healing.[36-38] However, adipose-derived stem cells possess many advantages over bone marrow mesenchymal stem cells and periosteum-derived stem cells including, ease of harvest, increased number of stem cells compared to bone marrow derived cells, established immunomodulatory effects, and secretion of cell-signaling cytokines.[38-40] Previous reports have shown adipose-derived stem cells have promising therapeutic effects on fracture healing and motivate the use of adipose-derived stem cells to improve bone graft osseointegration.[41-43]

Previously, our lab confirmed the cytophilic and antimicrobial properties of an engineered periosteum containing trimethyl chitosan *in vitro* as well as its ability to delivery FGF-2, TGF-β1 and adipose-derived stem cells to a mouse critical-sized femur defect.[22,44,45] Despite the promising properties of this engineered periosteum, we found bone allograft healing outcomes were not substantially improved, 6 weeks post implantation.[44] To better understand how the features of engineered periostea should be tailored to improve cell responses, the aims of this work are to 1) characterize our engineered periostea's FGF-2 and TGF-β1 *in vitro* release kinetics via ELISA and 2) characterize the *in vitro* response of mouse luciferase-expressing adipose-derived stem cells (Luc-ASC) cultured on our engineered periostea delivering FGF-2 and TGF-β1. We used bioluminescence imaging to longitudinally track cell viability and proliferation, Western Blot to detect Luc-ASC osteogenic protein expression, and relative gene expression studies to assess FGF-2 and TGF-β1 effect on Luc-ASC differentiation.

## 4.3. Materials and methods

### 4.3.1. Materials

Heparin sodium from porcine intestinal mucosa (14.4 kDa, 12.5% sulfur) was purchased from Celsus Laboratories (Cincinnati, OH). Chitosan (80 kDa, 9 % acetylated confirmed through $^1$H NMR) was acquired from Novamatrix (Sandvika, Norway). Chitosan was methylated to make *N*,*N*,*N*-trimethyl chitosan (TMC) following de Britto's and Asis' method and the degree of quaternization (DQ) of TMC was 71 %.[46] A detailed synthesis and characterization of TMC by $^1$H NMR was reported in the supplementary data in Romero et al 2014.[45] Heparin or TMC solutions were made by dissolving the polysaccharides in ultrapure water (18.2 MΩ·cm) at 0.01 M solutions (on a saccharide unit basis) then subsequently filtered with a 0.22 μm polyvinyldifluoride (PVDF) syringe filter (Fisher-Scientific, Pittsburgh, PA). L-ascorbic acid-2-phosphate, β-glycerophosphate, sucrose, human plasma fibronectin, cetyltrimethylammonium bromide (CTAB), and polyvinylpyrrolidone (PVP-40, $M_w$ = 40,000) were obtained from Sigma-Aldrich (St. Louis, MO). Sodium cacodylate trihydrate was purchased from Polysciences Inc. (Warrington, PA). Hexamethyldisilazane was purchased from Alfa Aesar (Ward Hill, MA). Dimethyl sulfoxide, dichloromethane (DCM), trifluoroacetic acid (TFA), and chloroform:isoamyl alcohol (24:1) were purchased from Acros Organics (New Jersey, US). Dulbecco's Modification of Eagle's Medium-low glucose (DMEM), Hank's Balanced Salt Solution (HBSS), 100X Minimum Essential Medium (MEM) vitamins, 100X MEM non-essential amino acids, antibiotic-antimycotic solution, and 0.25% trypsin–EDTA were obtained from Corning (Manassas, VA). Fetal bovine serum was obtained from Atlas Biologics (Fort Collins, CO). Recombinant human FGF–2 and TGF–β1 and Human Duoset ELISA Kits were

obtained from R&D Systems. (Minneapolis, MN). Firefly D–luciferin was purchased from Gold Biotechnology (St. Louis, MO).

### 4.3.2. Murine bone allograft harvest and cleaning

Murine femurs and humeri allografts (4 mm) were harvested from C3H mice (Age 7-9 weeks) sacrificed for another study. All mice used in this study were cared for under Colorado State University's Institutional Animal Care Review Board protocol. Immediately after harvesting C3H mid–diaphyseal femoral allografts, periosteal tissue was removed. The allografts were immersed in sterile 0.9% sodium chlorine solution then frozen at –80 °C for at least two weeks.

### 4.3.3. Chitosan-based engineered periostea on mouse cortical bone allografts

Harvested cortical bone allografts' diaphyseal surfaces were coated with one of three engineered periosteums—polyelectrolyte multilayers (PEM), freeze dried chitosan (FD), and electrospun chitosan nanofibers (NF) as previously described.[45] Briefly, to prepare PEM-modified bone allografts, cleaned allografts were first immersed overnight in a 10 mM solution of phosphonoundecanoic acid (PUA) in dimethyl sulfoxide. PUA-modified bone allografts were rinsed thoroughly and then subjected to layer-by-layer (LbL) deposition of alternating filtered TMC and heparin solutions with TMC being the first layer deposited. Five minute adsorption steps were used for each polyelectrolyte solution with a 5-minute ultrapure water rinse step between PEM adsorption steps, with all steps performed under gentle agitation. Heparin-terminated six-layer PEMs were deposited onto the allograft surface.

Bone allografts modified with freeze-dried porous chitosan scaffold were prepared by immersing cleaned bone allografts in a custom cylindrical mold with a 6 % (w/v) chitosan in 0.34 M acetic acid solution and frozen at −20 °C for 24 hours. The custom mold assembly was then subsequently lyophilized for 48 hours, after which the chitosan scaffold on the allograft was mechanically shaved with a razor and neutralized with a 5 M $NH_4OH$ solution for 6 hours. We refer to this as the "FD" (freeze-dried) scaffold. After neutralization, the FD chitosan scaffold was ready for surface modification with TMC and heparin PEMs.

Bone allografts modified with chitosan nanofiber scaffolds were prepared by directly electrospinning onto the bone diaphyseal surface using a custom rotating collector apparatus. A rotating shaft with a custom allograft holder was placed in front of 1/16-inch copper plate covered with grounded aluminum foil which served as the grounded collector. A horizontal electrospinning setup was used consisting of a syringe pump (Kent Scientific Genie Plus syringe pump, Torrington, CT) containing a glass syringe and 18-gauge blunt-tip needle attached to the positive lead. Electrospinning parameters consisted as follows: needle tip–to–collector distance = 7 inches, volumetric flow rate = 1 $ml \cdot hr^{-1}$, V = 18 kV. Chitosan was dissolved in a 7 % (w/v) solution in a 7:3 TFA:DCM ratio for 24 hours before electrospinning. The nanofiber scaffold was stabilized by a 5 M $NH_4OH$ treatment step for 6 hours, as we have previously reported.[47] We refer to this as the "NF" (nanofiber) scaffold. After neutralization, both FD- and NF-modified scaffolds were ready for subsequent surface modification with TMC and heparin PEMs as described above. Since the FD and NF scaffolds were made of chitosan, subsequent LbL surface modification always used heparin as the initial layer. Seven total layers were deposited to achieve a terminal heparin layer.

### 4.3.4. Engineered periostea morphological and surface chemistry characterization

Scanning electron microscopy (SEM) was used to characterize the morphology of cleaned allografts, PEM, FD, and NF-modified allografts. Untreated allografts, PEM-modified, and NF-modified allografts were coated with 10 nm of gold and FD-modified allografts were coated with 20 nm of gold before imaging with a scanning electron microscope (JEOL JSM-6500F, Tokyo, Japan). Micrographs were taken at several magnifications and allografts were rotated within the imaging chamber to confirm conformal scaffold allograft coverage.

X-ray photoelection spectroscopy (XPS) was used investigate the surface chemistry of unmodified cleaned allografts, PEM-, FD-, and NF-modified allografts. Spectra were obtained using a Phi Electronics 5800 Spectrometer (Chanhassen, MN) equipped with a monochromatic Al Kα x-ray source ($h\nu$ = 1486.6 eV), a hemispherical analyzer, and multichannel detector. High resolution spectra of O1s, N1s, C1s, S2p, Ca2p, P2p envelopes were obtained using a 23.5 eV analyzer pass energy with 0.1 eV steps and an X-ray spot of 800 μm. All spectra were obtained with a photoelectron takeoff angle of 45°. A low energy electron gun was used for charge neutralization. Spectra curve fitting was done using Phi Electronics Multipak version 9.3 (Chanhassen, MN). Curve fitting of all spectra used a Shirley background. Gaussian peaks were fit according to expected functional groups. The height of each peak was fit first while keeping each peak's position, full width half max (fwhm), and percent Gaussian fixed. Then the fwhm, percent Gaussian, and finally position were fit while minimizing the chi squared value. [48] Spectra were aligned to the aliphatic carbon peak at 284.7 eV in the C1s envelope.

### 4.3.5. Growth factor adsorption and release from engineered periosteums

Recombinant human FGF–2 and TGF–β1 were adsorbed onto heparin-terminated PEM-, FD-, and NF-modified bone allografts from 1000 $ng \cdot ml^{-1}$ solutions. Allografts were immersed in the appropriate growth factor-containing solution for one hour at room temperature under gentle agitation. To measure growth factor release, modified allografts (n=3 for each type) with adsorbed growth factor were immersed in 500 µl of PBS in a 48-well plate then incubated at 37 °C. PBS supernatant (450 µl) was removed at pre–determined time points and removed PBS replenished. Growth factor-containing supernatant aliquots were frozen at –20 °C until analyzed. Supernatant aliquots were assayed with the respective human Duoset ELISA kit (R&D Systems, Inc, Minneapolis, MN) following the manufacturer's kit instructions. Absorbance values were measured at 450 and 540 nm using a BioTek Synergy H1 plate reader (Winooski, VT). The amount of initial FGF–2 and TGF–β1 adsorbed to the modified allografts was determined via the difference of the complete and post-adsorption growth factor solutions. Cumulative release of FGF–2 and TGF–β1 from modified allografts was calculated from the concentrations in the supernatant aliquots.

### 4.3.6. Luciferase–expressing adipose-derived stem cells isolation, culture expansion, and cell seeding on engineered allografts

Luciferase–expressing adipose derived stem cells (Luc–ASC) were isolated from abdominal adipose tissue of (FVB/NTsv-Tg(svyb-luc)-Xen) mice from Taconic (Hudson, NY). Briefly, abdominal adipose tissue was minced and collagenase treated for 30 minutes at 37 °C in low-glucose DMEM with antibiotic/antimycotic. The cell suspension was centrifuged, re-suspended, centrifuged again, before the supernatant was aspirated. The resulting cell pellet was

plated onto tissue culture flasks and incubated for 4 days before an initial media change with ASC growth media. Luc–ASC growth media consisted of low-glucose DMEM, 15% FBS, 1% antibiotic/antimycotic and supplemented with 1X MEM vitamins and MEM non–essential vitamins. Plastic adherent Luc–ASC were selected by removing non–adherent cells. The Luc–ASC were grown until approximately 80% confluent then trypsinized and cryopreserved until needed. Luc-ASC bipotential osteogenic and adipogenic differention was confirmed using Alizarin and Oil Red O stains as previously reported.[49]

Passage 1 Luc–ASC were thawed and culture expanded in a humidified incubator at 37 °C, 5 % $CO_2$, in ASC growth media. Luc–ASC were split with 0.25% trypsin when about 80% confluent. Passage 4 and 5 Luc–ASC were used in all experiments. Engineered allografts were placed in 48-well microtiter plates with non-adherent well coatings and seeded with a highly concentrated Luc–ASC solution (500,000 cells in 30 µl). The Luc–ASC were allowed to attach for 1 hour in a humidified incubator at 37 °C, 5 % $CO_2$ before being moved to new wells. Luc-ASC-seeded engineered allografts were cultured at 37 °C and 5 % $CO_2$ in a humidified incubator for 21 days with media changes every 2-3 days in osteogenic supplemented media (OSM), defined as ASC growth media plus 20 mM β-glycerophosphate and 50 µM ascorbic acid-2-phosphate with no induction hormone.

### 4.3.7. Luciferase expressing adipose-derived stem cells bioluminescence proliferation assay

For Luc–ASC bioluminescence proliferation experiments on each type of engineered periosteum, four experimental groups were investigated: untreated bone allografts, growth factor-free engineered allografts, TGF–β1 coated, or FGF–2 and TGF–β1 coated engineered allografts (n = 10 per group). Luc-ASC were cultured on modified allografts for 21 days. At days

1, 4, 7, 14, and 21, fresh media containing 0.6 mg $mL^{-1}$ firefly luciferin substrate was added to each well and incubated for approximately 5 minutes at room temperature. Bioluminescence readings were taken on an IVIS-100 in vivo imaging system from PerkinElmer (Waltham, MA) using a humidified chamber. A threshold for bioluminescence was applied to acquired images and the total photon flux was calculated for each allograft. The average total photon flux of each allograft was calculated and then normalized to each allografts' day 1 reading to account for heterogenous cell seeding. Cell-free untreated allografts in media containing firefly luciferin substrate served as negative controls and as expected, showed no bioluminescence.

### 4.3.8. Luciferase expressing adipose-derived stem cells osteogenic protein expression evaluation by Western Blot

Western blots of Luc-ASC cultured on growth factor-free engineered allografts, TGF–β1 coated, and FGF–2 and TGF–β1 coated engineered allografts were evaluated for osteogenic protein expression after 7 and 21 days of in-vitro culture. Samples were rinsed twice in cold HBSS before being lysed in a commercial radioimmunoprecipitation assay (RIPA) buffer obtained from Thermo-Scientific (Rockford, IL) containing 3× protease inhibitors. Samples were lysed using a handheld sonicator wand while keeping samples on ice. Replicate lysates were pooled together and centrifuged at 15,000 RPM for 15 min at 4 °C to pellet cell debris and the supernatant was collected and frozen at −20 °C until ready to be further assayed. Samples were thawed then denatured and reduced before running on a 4-20 % Ready Gel Tris-HCl gel (Bio-rad, Hercules, CA) using a Biorad Mini-Protean 3 electrophoresis unit. Proteins were transferred onto a Immobilon-PSQ PVDF membrane (EMD Millipore, Billerica, MA) using a wet tank transfer method for 2 hrs at 4 °C.

Membranes were blocked in 5 % non-fat milk for 1 hour at room temp then rinsed three times for 5 min each. Blots were probed initially for alkaline phosphatase (ALP) using anti-alkaline phosphatase primary antibody (1:10,000, ab108337, Abcam, Cambridge, MA) overnight at 4 °C. Horseradish peroxidase conjugated goat anti-rabbit IgG H&L secondary antibody (1:20,000 Abcam ab6721) was used and membranes were developed using an enhanced chemiluminescence substrate solution (Thermo, Rockford, IL). Immunoblots were imaged using a Bio-Rad Chemidoc XRS+ imager. (Hercules, CA). Immunoblots were subsequently stripped with Thermo Restore stripping buffer (Thermo, Rockford, IL) and reprobed for osteocalcin (1:3000, Millipore ab10911), osteonectin (0.4 $\mu g \cdot ml^{-1}$, Abcam ab55847), osteopontin (0.1 $\mu g \cdot ml^{-1}$, Abcam ab11503), receptor activator of nuclear factor kappa-B ligand (RANKL,1:5000, Abcam ab124797), and β-tubulin (1:500, Abcam ab6046),with immunoblots stripped and blocked between probings. β-tubulin was used as a loading control to evaluate protein loading in each lane.

### 4.3.9. Screening reference gene stability for quantitative real-time polymerase chain reaction

Multiple reference genes were screened before conducting quantitative real-time PCR gene expression experiments in mouse luciferase-expressing mouse adipose-derived stem cells. Passage 5 Luc-ASC were cultured on chitosan NF coated with either 1000 ng/ml of FGF-2 or TGF-β1 for 7 and 21 days. RNA was isolated using the methods described in methods section 2.9. Pre-designed primers for *Mus musculus* glyceraldehyde-3-phosphate dehydrogenase (*Gapdh*), ubiquitin C (*Ubc*), succinate dehydrogenase complex, subunit A (*Sdha*), and phospholipase A2 (*Ywhaz*) hydrolysis probes from geNorm reference gene selection kits

(Primerdesign Ltd, United Kingdom) were used to compare reference gene stability in Luc-ASC when exposed to chitosan NF coated with either FGF-2 or TGF-β1. Using the qbase+ software version 3.0 (Biogazelle, Ghent, Belgium), qbase+ algorithms determined that *Ywhaz* was the most stable reference gene of the genes tested.[50]

### 4.3.10. Luciferase expressing adipose-derived stem cells multipotent gene expression by quantitative real-time polymerase chain reaction

PEM-modified NF mats were manufactured as previously reported, adhered onto the well bottoms of 48-well microtiter plates, and 275 µl of 25 µg $ml^{-1}$ fibronectin solution was dispensed onto the NF mats.[51] The fibronectin solution was allowed to adhere onto NF mats for 1 hour at room temperature. FGF-2, TGF-β1, or both (175 µl of 1000 ng·$ml^{-1}$) were subsequently adsorbed onto fibronectin coated NF mats. Luc-ASC were seeded ($5x10^6$ cells in 30 µl) onto NF mats and allowed to attach for 1 hour at room temperature before being moved into new wells and 500 µl OSM was added. Luc-ASC were cultured for 7 and 21 days in OSM without any induction hormone.

RNA from Luc-ASC was isolated adapting procedures from Wang and Stegemann and Yu et al.[52,53] Briefly, culture media was aspirated, cells were rinsed with PBS, and Luc-ASC were incubated for 10 minutes in a CTAB extraction buffer (pH=8.0, 65 °C, 2% CTAB, 2 M NaCl, 20 mM EDTA, 100 mM Tris-HCl, 2% PVP-40, 1% β-mercaptoethanol). The cell lysate was moved to microcentrifuge tubes and chloroform-isoamyl alcohol (24:1) was added at a 1:1 ratio to CTAB lysis buffer. Samples were vortexed and then centrifuged at 15,000 g for 5 minutes at room temperature. The upper clear aqueous supernatant was transferred to a new microcentrifuge tube and fresh chloroform-isoamyl alcohol (24:1) was added at a 1:1 ratio,

thoroughly vortexed, and centrifuged once again. The supernatant was again moved to a new microcentrifuge tube and chilled ammounium acetate was added to the tube for a final concentration of 0.5 M ammonium acetate. Two µl of Glycoblue™ Coprecipitant (Applied Biosystems, Foster City, CA) was added to the samples, vortexed, and chilled isopropanol was added at a 1:1 ratio then vortexed again. Samples were then stored at -20 °C for 15 mins. Samples were centrifuged at 15,000 g for 15 mins to pellet RNA. The supernatant was then decanted and the RNA pellet was washed with 1 ml of 75% ethanol, centrifuged, decanted and air dried. The RNA pellet was resuspended in 50 µl of RNase-free water and quantified using a Nanodrop 2000 (Thermo Fisher Scientific, Waltham, MA). A 260/280 ratio ≥1.9 was observed in all samples and RNA purity was sufficient for downstream analysis.

RNA was then DNAse-treated to remove contaminating gDNA using Thermo Fisher Scientific's DNA-free™ DNA Removal kit (Waltham, MA) according to kit instructions. DNase-treated RNA (150-175 ng) was then reverse transcribed using Applied Biosystems High-Capacity RNA-to-cDNA™ Kit (Foster City, CA) in 20 µl reaction volumes following manufacturer's kit instructions using a Bio-Rad thermocycler S1000 (Hercules, CA). Synthesized cDNA was then frozen at -20 °C until analyzed. Quantitative real-time PCR (qPCR) was used to evaluate relative gene expression on Days 7 and 21 using thawed cDNA with appropriate negative reverse transcription controls for each sample and no template controls for each gene analyzed. Pre-designed primers and FAM labeled hydrolysis probes were used for the following genes: *Alpl, Bglap, Col1a1, Col2a1, Pparg, Runx2, Sox9, Tnfsf11,* and *Vegfa* (Integrated DNA Technologies, Inc., Coralville, IA). *Ywhaz* was used as the reference gene. Methods describing experiments to determine reference gene stability are described in supplementary information. Primer and probe sequences can be found in Appendix Table A3.1.

Duplicate 20 µl reaction volumes were run using an Applied Biosystems 7300 Real-Time PCR System, white VersiPlate 96-well PCR plates covered with Versicap ultra clear caps (Thermo Fisher Scientific, Waltham, MA), Taqman Gene Expression Master Mix (Applied Biosystems, Foster City, CA) and RNAse-free water (Sigma-Aldrich, St. Louis, MO). The following cDNA amplification program was used: an initial 2 min step at 50 °C followed by a 10 min step at 95 °C, followed by 40 cycles of 15 seconds at 95 °C and data acquisition step of 1 min at 60 °C. Relative gene expression was normalized to Luc-ASC cultured on PEM-modified NF at D1 according to the comparative CT method.[54,55] Quantification cycle ($C_q$) values were extracted from qPCR data using Sequence Detection Software version 1.4 and RQ Study Application (Applied Biosystems Foster City, CA) using a manual baseline and setting a $C_q$ threshold above background noise within the linear amplification phase.

### 4.3.11. Confirmation of luciferase expressing adipose-derived stem cells osteogenic gene expression

An experiment was conducted to confirm Luc-ASC could express the genes listed in Table A3.1. Passage 3 Luc-ASC were cultured in a 48 well TCPS plate. Luc-ASC were seeded subconfluent at a density of 5000 cells $cm^{-2}$ and allowed to attach overnight in Luc-ASC growth media. Luc-ASC were cultured in either Luc-ASC growth media (GM, DMEM low glucose, 15 % FBS, 1% anti/anti, 1X MEM vitamins, 1X MEM non-essential amino acids), osteogenically supplement media (OSM, GM+ 50 µM ascorbic-2-phosphate, 20 mM β-glycerophosphate), OSM+ 10 nM dexamethasone (Sigma Aldrich), or OSM+ 5 µM retinoic acid (Sigma) for up to 21 days in a humidified incubator with media changes occurring every 2-3 days. RNA was

isolated at day 1, 7, 21, reverse transcribed to cDNA, and relative gene expression was evaluated using quantitative real-time PCR using the methods described in subsection 4.3.10.

### 4.3.10. Statistical analysis

A repeated measures two-factor ANOVA and two-factor ANOVA ($\alpha$=0.05) were used to conduct statistical analysis of longitudinal log transformed normalized bioluminescence measurement and $\Delta\Delta$Cq values data, respectively. A post hoc Tukey-Kramer's adjustment was used in each analysis. SAS Studio 3.6 was used to conduct the analysis.

## 4.4. Results

### 4.4.1. Scanning electron microscopy and x-ray photoelectron spectroscopy characterization of engineered periosta on bone allografts

Figure 4.1A shows SEM micrographs and confirms chitosan FD and NF scaffolds completely cover bone allografts as well as retain their morphology after TMC and heparin deposition. As expected, SEM does not resolve features of the ultra-thin PEM modification on allograft bone or FD and NF scaffolds. However, XPS high resolution spectra, as seen in Figure 4.1B, confirm characteristic changes in the N1s and S2p envelopes consistent with heparin, chitosan, and TMC chemical structures, supporting LbL deposition of TMC and heparin as PEM on allograft bone as well as chitosan FD and NF scaffolds as previously reported.[45] Table 4.1 lists atomic percentages of N1s and S2p envelopes and the nitrogen to sulfur ratio. Table A3.2 contains atomic percentages of C1s, O1s, Ca2p and P2p and carbon to oxygen ratio. Similar ratios of nitrogen to sulfur and carbon to oxygen on the PEM, FD, and NF-modified allograft

bone indicate that similar surface chemistries are present on the three- different engineered periostea. As expected, attenuated Ca and P signals in PEM, FD, and NF-modified allografts support surface chemistry modification compared to untreated allograft bone.

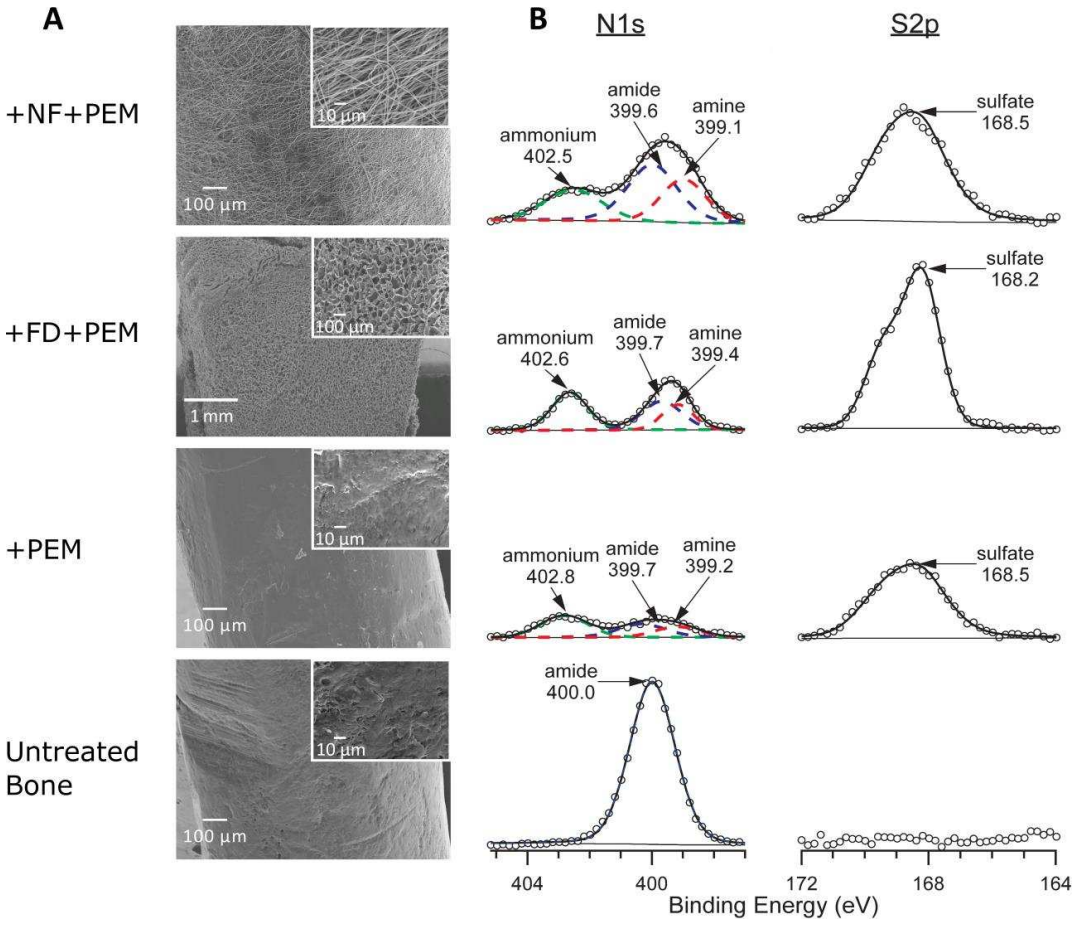


**Figure 4.1** SEM and XPS characterization of engineered allografts. (A) SEM micrographs of untreated bone with engineered periosteums. Inset shows higher magnification images. Diverse surface morphologies are observed as well as complete coverage of bone allograft periosteal surface. (B) High resolution spectra of N1s and S2p envelopes. Appearance of ammonium and amine in the N1s envelope of PEM, FD, and NF scaffolds compared to untreated bone confirm similar surface chemistry modifications across 3 types of engineered periosteums. Appearance of a sulfate peak in S2p envelopes of PEM, FD, and NF scaffolds confirm heparin incorporation into engineered periosteums.

Table 4.1. Average % atomic concentration of N and S from engineered periosteums on bone allografts[a]

| | N1s | S2p | N/S |
|---|---|---|---|
| Untreated Bone | 12.0 ± 0.4 | 0.4 ± 0.0 | 32.9 ± 2.5 |
| +PEM | 5.7 ± 1.3 | 2.1 ± 0.1 | 2.8 ± 0.6 |
| FD | 7.3 ± 0.0 | n.d. | n.c. |
| FD+PEM | 4.6 ± 0.1 | 2.3 ± 0.0 | 2.0 ± 0.0 |
| NF | 6.0 ± 0.0 | n.d. | n.c. |
| NF+PEM | 5.9 ± 0.1 | 1.3 ± 0.1 | 4.7 ± 0.6 |

[a]Values are average ± range. Data are from XPS high resolution

### 4.4.2. Fibroblast growth factor-2 and transforming growth factor-β1 *in vitro* adsorption and release from engineered periostea

Heparin incorporation on PEM-modified allograft bone, FD, or NF scaffolds led to heparin mediated FGF-2 and TGF-β1 adsorption on all engineered periosteums. Released FGF-2 and TGF-β1 from engineered periosteums were evaluated using ELISA. *In vitro* release profiles are shown in Figure 4.2**.** Insets in both Figure 4.2A and 4.2B show cumulative FGF-2 and TGF-β1 release, respectively, from PEM-modified allografts over 3 days. Both FGF-2 and TGF-β1 release from engineered periosteums exhibit burst release kinetics within the first 3 days. However, FGF-2 release up to 14 days is observed in engineered periosteums. FD-modified allografts release the highest amounts of FGF-2 and TGF-β1 compared to PEM or NF-modified allografts. The cumulative percent retention of FGF-2 and TGF-β1 on engineered periosteums (Table 4.2) confirms that most of the FGF-2 and TGF-β1 is retained at day 14 and 7, respectively on engineered periosteums except for TGF-β1 coated NF-modified allografts.

Table 4.2: Average Percent Cumulative Retention of FGF-2 and TGF-β1 on engineered periosteums

| | Percent Growth Factor Retained[a] | |
|---|---|---|
| Engineered Periosteum | FGF-2 Day 14 | TGF-β1 Day 7 |
| PEM | 98.9 ± 0.6 | 99.7 ± 0.5 |
| FD | 99.6 ± 0.2 | 92.9 ± 0.9 |
| NF | 98.4 ± 1.7 | 4.0 ± 0.6 |

[a]Average ± SEM

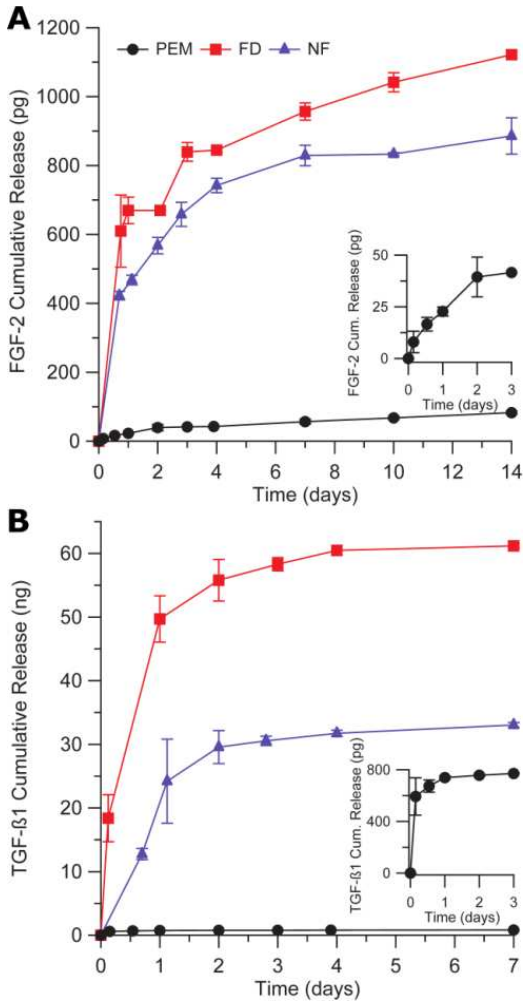


**Figure 4.2** FGF–2 and TGF–β1 *in vitro* release profiles from PEM, FD, and NF engineered periosteums. (average ± SEM). (A) FGF–2 and (B) TGF–β1 release was measured over 14 and 7 days respectively from 1000 ng/ml growth factor containing solutions. Release profiles show that FD scaffolds release the greatest amount of growth factor followed by NF and then PEM scaffolds. Insets show magnified FGF-2 and TGF–β1 release kinetics from PEM scaffolds over 3 days

### 4.4.3. Luciferase expressing adipose-derived stem cells response to growth factors delivered from engineered periosteums

Figure 4.3A shows longitudinal bioluminescence tracking of Luc-ASC cultured on untreated allografts and engineered periosteums delivering either no growth factor, TGF-β1 alone, or both FGF-2 and TGF-β1. Luc-ASC display divergent responses to the engineered

periosteums. The FD scaffold significantly lowers the bioluminescence in Luc-ASC at each timepoint compared to the untreated allografts whereas PEM and NF-modified allografts show statistically similar bioluminescence compared to untreated allografts at each time point. When TGF-β1 alone is delivered from the engineered periosteums to Luc-ASC, no statistically significant effect on Luc-ASC bioluminescence is observed compared to the corresponding growth-factor free conditions, except in the case of the FD scaffold on day 4, where TGF-β1 coated FD-modified allografts show a significant decrease in bioluminescence compared to FD-modified allografts. At days 4 and 7, co-delivery of TGF-β1 and FGF-2 from PEM and NF-modified allografts are statistically similar with other PEM or NF experimental groups, respectively, at the same timepoint.

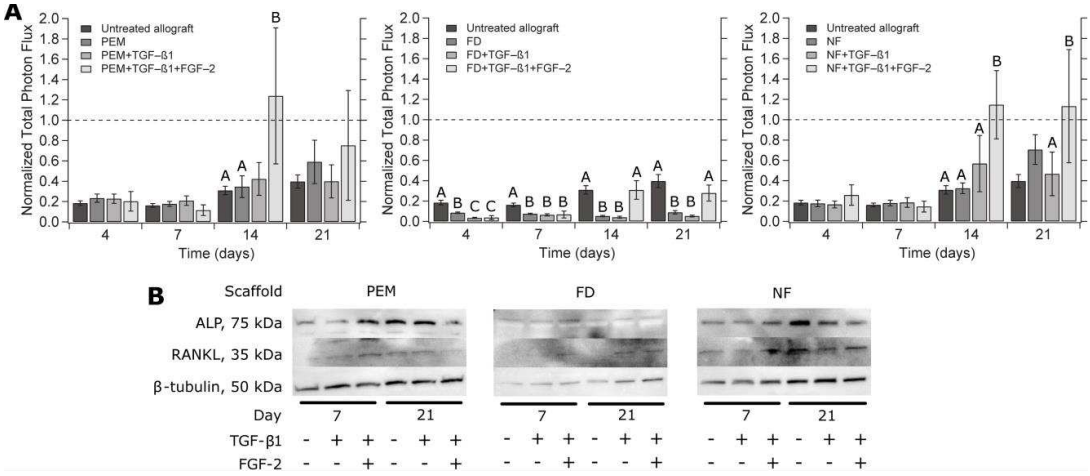


**Figure 4.3** Bioluminescence imaging and Western Blot analysis of Luc-ASC response to engineered periosteums. (A). Normalized bioluminescence (average ± SEM) from Luc-ASC cultured on engineered periosteums (PEM, left, FD, center, NF, right) delivering TGF-β1 only or both TGF-β1 and FGF-2. Significantly higher bioluminescence is observed in treatments groups delivering TGF-β1 and FGF-2 compared to growth factor free groups or TGF-β1 only on day 14 for PEM and NF scaffolds or for NF on day 21. Letters designate statistically significant different groups ($p < 0.05$) at the same time point. Unlabeled groups are statistically similar to all other groups at the same timepoint. (B) Western blots of Luc-ASC response to engineered periosteums without any growth factor, TGF-β1 only or both TGF-β1 and FGF-2 delivery. ALP and RANKL expression are detected and not inhibited on PEM and NF scaffolds at both day 7 and day 21. Limited ALP expression on FD scaffolds is seen on days 7 and 21. RANKL expression on FD scaffolds is generally only seen on day 7 and 21 when both TGF-β1 and FGF-2 are delivered.

Interestingly, at day 14 co-delivery of TGF-β1 and FGF-2 from PEM and NF-modified allografts leads to a statistically higher bioluminescence compared to untreated allografts, growth factor-free PEM and NF-modified allografts, and TGF-β1 coated NF-modified allografts. At day 21, TGF-β1 and FGF-2 coated NF-modified allografts still display statistically increased bioluminescence compared to TGF-β1 only and to growth factor-free NF-modified allografts, whereas TGF-β1 and FGF-2 coated PEM-modified allografts show statistically similar bioluminescence to all other PEM experimental groups. At day 14 and 21, co-delivery of TGF-β1 and FGF-2 from FD-modified allografts show recovery of bioluminescence levels statistically similar with untreated allograft control group, whereas FD-modified and TGF-β1 coated FD-modified allografts show significantly decreased bioluminescence compared to untreated allografts controls and TGF-β1 and FGF-2 coated FD-modified allografts. In sum, the FD-scaffold tends to reduce cell proliferation compared to untreated bone. TGF-β1 does not promote cell proliferation, but FGF-2 in combination with TGF-β1 does promote cell proliferation.

### 4.4.4. Growth factor effect on luciferase expressing adipose-derived stem cells osteogenic protein expression

Osteogenic protein expression from Luc-ASC cultured on engineered periosteums was evaluated by Western blot. Luc-ASC were cultured on untreated allografts and engineered periosteums delivering either no growth factor, TGF-β1 alone, or both FGF-2 and TGF-β1 for 7 and 21 days. Figure 4.3B shows chemiluminescence images of immunoblots. ALP and RANKL expression is observed in Luc-ASC cultured on PEM and NF-modified allografts on days 7 and 21. Slight ALP expression is observed in Luc-ASC cultured on FD-modified allografts on days 7 and 21 while no RANKL expression is observed. TGF-β1 only or TGF-β1 and FGF-2 delivery

from engineered periosteums did not inhibit ALP and RANKL expression in Luc-ASC on days 7 and 21. No RANKL expression is observed in Luc-ASC from TGF-β1 coated FD-modified allografts at day 7, yet expression is observed at 21. Luc-ASC cultured on TGF-β1 and FGF-2 coated FD-modified allografts show RANKL expression at days 7 and 21. No detectable signal was observed for osteocalcin, osteonectin, or osteopontin in any group or timepoint, similar to previous reports.[45]

### 4.4.5. Luciferase expressing adipose-derived stem cells relative gene expression via quantitative real-time polymerase chain reaction

From the results described in previous sections, we observed that 1) NF scaffolds deliver greater FGF-2 and TGF-β1 amounts compared to PEM scaffolds (Figure 4.2), and 2) Luc-ASC viability on FD scaffolds is reduced compared to the NF scaffolds (Figure 4.3). Based on these observations, the NF scaffolds were selected for further gene expression analysis. Relative gene expression studies were conducted to determine how Luc-ASC responded to the delivery of FGF-2 only, TGF-β1 only, or both FGF-2 and TGF-β1 from PEM-modified NF scaffolds. As Luc-ASC are known to possess multipotent differentiation capacities, the following genes were evaluated: osteogenic genes *Alpl, Bglap, Col1a1, Runx2, Tnfsf11, Vegfa*; early adipogenic transcription factor, *Pparg*; and chondrogenic genes *Sox9* and *Col2a1*. *Pparg* and *Runx2* $\log_2$ mean fold changes are shown Figure 4.4A, and *Alpl, Col1a1,* and *Vegfa* $\log_2$ mean fold changes are shown in Figure 4.4B. Significant *Pparg* downregulation occurs in TGF-β1 containing treatment groups at day 7 with synergistic downregulation in FGF-2 and TGF-β1 treated Luc-ASC compared to growth factor-free NF at the same timepoint and relative to Luc-ASC on NF at day 1. No significant differences are observed in *Pparg* expression among experimental groups

at day 21. *Runx2* expression is generally downregulated at days 7 and day 21 relative to ASC on NF at day 1, with a significant downregulation of approximately 60% occurring in NF co-delivering FGF-2 and TGF-β1 to Luc-ASC at day 7 compared to all other treatment groups at the same timepoint. *Alpl* expression relative to Luc-ASC on NF on day 1 is significantly inhibited by FGF-2, TGF-β1, and FGF-2 and TGF-β1 delivery to Luc-ASC at day 7 compared to growth factor-free Luc-ASC on NF. At day 21, significant inhibition of *Alpl* is observed in Luc-ASC cultured on FGF-2 and TGF-β1 coated NF compared to growth factor-free NF at the same timepoint, whereas slight downregulation, but not statistically different expression to growth factor-free NF, is observed in Luc-ASC cultured on FGF-2 or TGF-β1 coated NF at day 21.

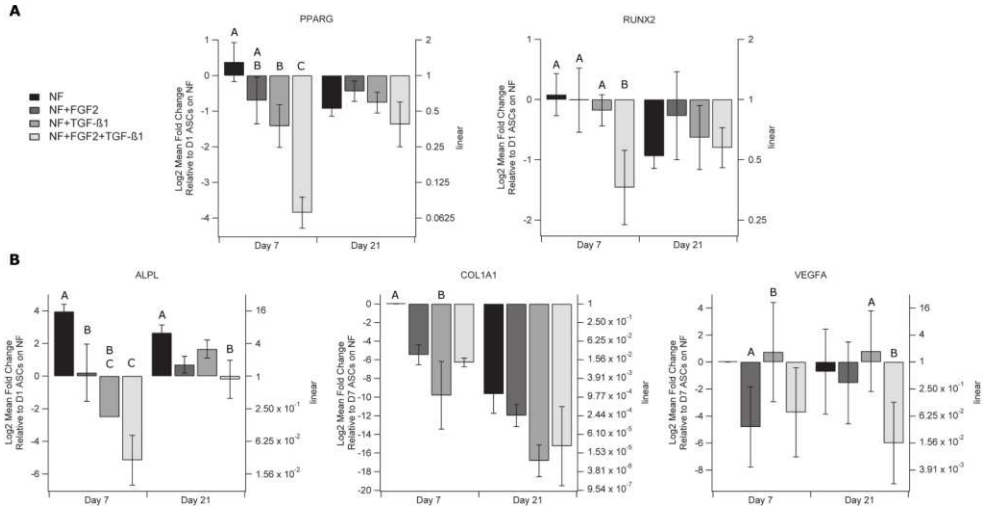


**Figure 4.4** Relative gene expression of Luc-ASC on PEM-modified NF mats delivering FGF-2, TGF-β1, or both TGF-β1 and FGF-2 at days 7 and day 21. Data are presented as log2 mean fold changes on the left axis with corresponding linear values on the right axis. Letters designate statistically significant different groups ($p < 0.05$) at the same time point. Unlabeled groups are statistically similar to all other groups at the same time point. (A, top row) Luc-ASC *Pparg* and *Runx2* expression was downregulated at day 7 and 21 when exposed to FGF-2, TGF-β1 or both when delivered from PEM-modified NFs relative to Luc-ASC cultured on NF at day 1. (B, bottom row) *Alpl*, *Col1a1*, and *Vegfa* expression at day 7 and 21. *Alpl* expression was inhibited in growth factor containing treatments at day 7 and day 21compared to growth factor-free control at the same time point. Luc-ASC *Col1a1* expression was downregulated at day 7 and 21 in growth factor containing groups. *Vegfa* expression was downregulated at day 7 and 21in FGF-2 containing groups compared to growth factor-free control group at day 7. TGF-β1 was significantly increased compared to FGF-2 coated NFs and FGF-2+TGF-β1 coated NFs on day 7 and 21, respectively.

As no detectable *Col1a1*, *Vegfa*, *Tnfsf11,* and *Sox9* expression was observed in ASC cultured on NF at day 1, *Col1a1*, *Vegfa*, *Tnfsf11,* and *Sox9* gene expression was normalized to day 7 Luc-ASC on NF. *Col1a1* expression is downregulated at day 7 in Luc-ASC cultured on FGF-2, TGF-β1, and FGF-2 and TGF-β1 coated NF generally resulting in downregulation of at least 16-fold relative to Luc-ASC on growth factor-free NF at day 7. *Col1a1* downregulation continues at day 21 in Luc-ASC cultured on FGF-2, TGF-β1, and FGF-2 and TGF-β1 coated NF. *Vegfa* gene expression in Luc-ASC is downregulated by FGF-2 only and FGF-2 and TGF-β1 coated NF at day 7 and 21 relative to day 7 Luc-ASC on NF. *Vegfa* expression in Luc-ASC is minimally upregulated by TGF-β1 coated NF at day 7 and 21 and is statistically different from FGF-2 coated NF at day 7 and FGF-2 and TGF-β1 coated NF at day 21. At day 7, *Tnfsf11,* and *Sox9* expression is only observed in Luc-ASC cultured on growth factor-free NF whereas experimental groups delivering FGF-2, TGF-β1, or both from NF show no detectable *Tnfsf11* and *Sox9* expression (not shown). However, at day 21, approximately 92, 60, and 80 % *Tnfsf11* downregulation occurs in Luc-ASC cultured on NF delivering FGF-2, TGF-β1, or both, respectively, relative to day 7 Luc-ASC on NF. Luc-ASC cultured on FGF-2 and TGF-β1 coated NF at day 21 show a 45 % *Sox9* downregulation relative to Luc-ASC on NF at day 7 (not shown). No detectable *Bglap* expression was observed in any samples at any timepoint.

In a separate experiment, Luc-ASC were cultured on TCPS in osteogenic supplemented media containing osteogenic induction hormones, dexamethasone or retinoic acid, to confirm Luc-ASC could express genes listed in Table A3.1. Relative gene expression of *Runx2, Pparg, Alpl, Bmp2*, and *Vegfa* are shown in Figure 4.5. Unexpectedly, *Runx2*, an early ostegenic transcription factor, is not significantly upregulated when Luc-ASC were cultured with osteogenic induction hormones dexamethasone and retinoic acid. *Pparg* expression, an early

adipogenic transcription factor, is significantly upregulated on day 1 in treatments containing osteogenic supplements L-ascorbic-2-phosphate and β-glycerophosphate and generally down regulated on days 7 and 21. *Alpl* expression is significantly increased in on days 1, 7, and 21 in Luc-ASC treated with retinoic acid compared to all other treatment groups at each timepoint. *Bmp2* expression is generally downregulated at day 1 and 7 with *Bmp2* expression significantly upregulated at day 21 in OSM- and retinoic acid-treated Luc-ASC. *Vegfa* expression is downregulated on days 1 and 7 for all treatment groups. On day 21, *Vegfa* expression is upregulated in all treatment groups.

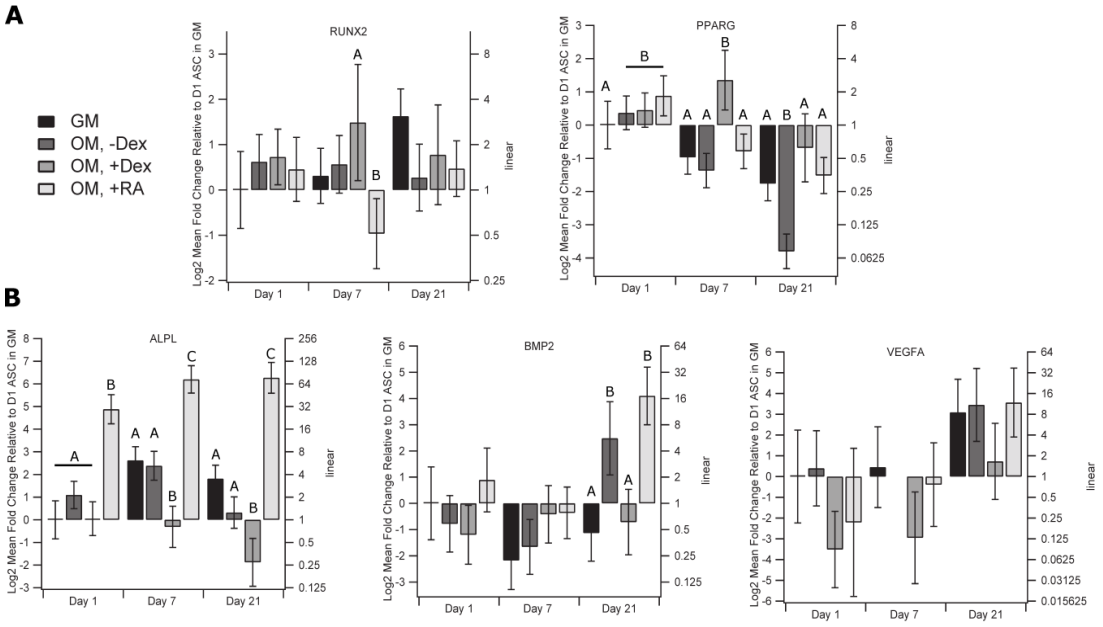


**Figure 4.5** Relative gene expression of Luc-ASC cultured with osteogenic supplemented media containing dexamethasone or retinoic acid. Studies confirmed Luc-ASC expressed *Runx2*, *Pparg*, *Alpl*, *Bmp2*, *Vegf*. Luc-ASC cultured in OSM+retinoic acid show evidence of Luc-ASC osteogenic commitment by upregulated *Alpl* expression at days 1, 7, 21 and *Bmp2* expression at day 21 compared to all other treatment groups at the same timepoint.

*Col1a1* and *Sox9* expression was only detected on days 1 and 21 and is shown in Figure 4.6. *Col1a1* expression on day 1 increased two-fold in retinoic acid-treated Luc-ASC and is downregulated at least 25% in other treatment groups. On day 21, *Col1a1* expression is

downregulated 40% in GM-treated Luc-ASC and at least 87.5% in all OSM-treated Luc-ASC groups. Day 1 Luc-ASC *Sox9* expression is upregulated in dexamethasone-free OSM while addition of dexamethasone downregulates *Sox9* expression. By day 21, *Sox9* expression was upregulated at least 4 fold in all treatment groups.

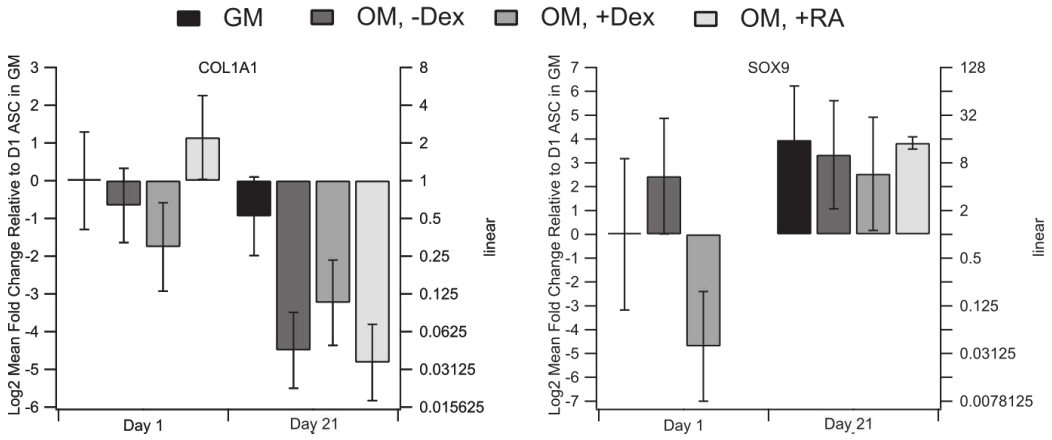


**Figure 4.6** Luc-ASC *Col1a1* and *Sox9* relative gene expression is only observed on day 1 and 21.

Luc-ASC *Col2a1,* and *Tnfsf11* expression was not detected in any treatment or timepoint. Luc-ASC *Bglap* expression was not reliable as amplification was seen in corresponding negative reverse transcription controls.

## 4.5. Discussion

### 4.5.1. Growth factor retention and release from engineered allografts

As an extension of our previous work, studies were conducted to determine if growth factor delivery from our engineered periosteums was possible.[45] Immunoassays were used to characterize the release profiles of FGF-2 and TGF-β1 from engineered allografts. FGF-2 and TGF-β1 have been studied previously and shown to be involved in bone fracture healing as well

as bone tissue morphogenesis.[56-60] While the three different allografts exhibit very different surface morphologies in SEM micrographs, similar release profiles for FGF-2 and TGF-β1 are observed among the engineered allografts. FGF-2 release kinetics show that a burst release occurs within the first 4 days, regardless of scaffold type. Interestingly, the percent release of FGF-2 at day 14 from these samples were less than 2% of the total amount of FGF-2 adsorbed onto the scaffolds, which suggests much of the FGF-2 is retained on the heparin containing engineered periosteums. This may be beneficial as heparin is known to modulate FGF-2 and FGF-receptor signaling. Physiologically relevant amounts of FGF-2 were released from the engineered periosteums cumulatively releasing 10s to 100s of picograms of FGF-2, with the PEM-, FD-, and NF-modified allografts approximately retaining 7.4, 311, and 54.7 ng of FGF-2, respectively. Intuitively, the FD- and NF-modified allografts' increased surface area showed higher growth factor loading capacity compared to PEM-modified allografts.

Similar to released FGF-2, TGF-β1 release was confirmed from all three engineered periosteums, with a burst of TGF-β1 release occurring within the first 2 days. Minimal detectable TGF-β1 release was observed beyond the day 2 timepoint. As expected, the FD- and NF-modified allografts displayed increased loading capacity compared to the PEM-modified allografts. The measured amounts of TGF-β1 released from the engineered periosteum were in line with physiologically relevant doses previously reported in the literature when soluble TGF-β1 was delivered to mouse ASC that inhibited mouse ASC proliferation or stimulated cytokine release in human ASC.[61,62] Previous studies relied on supraphysiological doses of FGF-2 and TGF-β1 for therapeutic purposes to overcome FGF-2 and TGF-β1's short *in-vivo* plasma half-life.[32,57,59,63,64] Ultimately, the different engineered periosteums provided flexibility in scaffold

design as well confirming *in vitro* retention and release of physiologically relevant FGF-2 and TGF-β1 doses.

### 4.5.2. Luciferase expressing adipose-derived stem cells response to growth factors delivered from engineered periostea

Following confirmation of *in-vitro* FGF-2 and TGF-β1 retention and release on engineered periostea, longitudinal bioluminescent imaging studies were conducted to characterize Luc-ASC viability and proliferation in response to FGF-2 and TGF-β1 delivered from the engineered periostea. Firefly luciferase requires ATP and $O_2$ as co-factors with luciferin for bioluminescence, suggesting metabolically active Luc-ASC are present with detection of bioluminescence.[65] We observed bioluminescence on all engineered allografts at each timepoint confirming the presence of viable Luc-ASC. Unexpectedly, delivered TGF-β1 was observed to have no statistically significant effect on Luc-ASC bioluminescence at any timepoint compared to TGF-β1 free control groups except on day 4 where a significant inhibition of bioluminescence was observed in TGF-β1 coated FD-modified allograft compared to TGF-β1 free samples. Levi and co-authors previously found mouse ASC proliferation to be significantly inhibited when culture media was supplemented with 2.5-10 ng/ml of TGF-β1 compared to TGF-β1 free media.[61] In the previous study, TGF-β1 media supplementation most likely occurred with each media change resulting in a more constant TGF-β1 dose to the mouse ASC, while TGF-β1 released from our engineered periosteums would have been released within the first 48 hours of Luc-ASC contact with engineered periosteums. This suggests that a constant TGF-β1 supplementation may be required for a sustained inhibition of mouse ASC proliferation. TGF-β1

delivery to pre-osteoblastic mouse MC3T3-E1 cells also previously showed signs of inhibiting MC3T3-E1 cell proliferation.[66]

We did observe increased Luc-ASC bioluminescence in FGF-2 and TGF-β1 coated PEM- and NF-modified allografts at days 14 and 21 compared to FGF-2-free control groups (at the same timepoint) confirming bioactive FGF-2 delivery. At days 14 and 21, FGF-2 and TGF-β1 coated FD-modified allografts bioluminescence recovered to untreated allograft levels at the same timepoint suggesting proliferative rescue of Luc-ASC by FGF-2. These observations are in line with FGF-2's well known mitogenic effect on mammalian cell populations including FGF-2 delivery from heparin containing PEM-modified TCPS to ovine bone marrow derived mesenchymal stem cells as well as a FGF-2 proliferative effect on mouse ASC.[33,67] Comparing combined delivery of FGF-2 and TGF-β1 to TGF-β1 only delivery to Luc-ASC, we infer that FGF-2 was the dominant growth factor driving the Luc-ASC increased bioluminescence; FGF-2's mitogenic effect was not abolished with co-delivered TGF-β1 to mouse Luc-ASC.

We hypothesized that co-delivery of FGF-2 and TGF-β1 to Luc-ASC may have effects on Luc-ASC conducive for bone tissue engineering applications such as ASC osteogenic differentiation. However, Western blot and gene expression results suggest the opposite effect leading to a proliferative osteoprogenitor phenotype in mouse Luc-ASC. Mesenchymal stem cell osteogenic differentiation follows a well-defined sequence of gene and protein expression.[38,68] No detection of common osteoblastic markers of osteocalcin, osteonectin, or osteopontin suggest Luc-ASC cultured on engineered allografts did not terminally differentiate by day 7 or 21 in line with previous observations in the literature confirming FGF-2 and TGF-β1 inhibits osteogenic differentiation in mouse ASC.[61,69,70] However, FGF-2 or TGF-β1 did not inhibit ALP expression at day 7 or day 21, suggesting maintenance of an immature osteoprogenitor phenotype. We also

observe RANKL expression in Luc-ASC cultured on all PEM- and NF-modified allografts and FGF-2 and TGF-β1coated FD-modified allografts at day 7 and 21 suggesting FGF-2 and TGF-β1 do not inhibit RANKL expression. Cortical bone allografts are known to experience limited remodeling.[71] RANKL is linked to activing osteoclastic bone resorption, suggesting FGF-2 and TGF-β1 delivery to Luc-ASC from our engineered periosteum would be an additional source of RANKL to promote bone remodeling.

Luc-ASC gene expression studies were conducted to verify Western blot results and further investigate FGF-2 and TGF-β1 effects on Luc-ASC differentiation. FGF-2 and TGF-β1 are well known to be involved in bone fracture healing and participate in mesenchymal stem cell differentiation.[56,57,72,73] Gene expression studies revealed Luc-ASC cultured on FGF-2 and TGF-β1 coated PEM-modified NF have significantly downregulated *Pparg* and *Runx2* expression compared to growth factor-free PEM-modified NF at day 7 suggesting FGF-2 and TGF-β1 synergistically inhibit Luc-ASC differentiation down adipogenic and osteogenic lineages similar to previous gene expression studies of mouse ASC when cultured in the presence of FGF-2 or TGF-β1.[61,69] By day 21, Luc-ASC cultured on PEM-modified NF display continued downregulation of *Pparg* and *Runx2* although no significant differences among experimental groups are observed. Downregulated *Sox9* expression in FGF-2 and TGF-β1 coated PEM-modified NF at day 21 along with no *Col2a1* gene expression at either day 7 or day 21 also confirms that Luc-ASC do not differentiate down a chondrogenic lineage.

To further confirm inhibition of osteogenic differentiation in Luc-ASC, common osteogenic genes such as *Alpl, Col1a1, Bglap*, and *Tnfsf11* were also evaluated. Generally, Luc-ASC cultured on FGF-2 and TGF-β1 coated NF inhibited *Alpl* and *Col1a1* expression compared to their respective growth factor-free NF at both day 7 and 21 again supporting that Luc-ASC

were not terminally differentiated down an osteogenic lineage. This was further supported by no detectable Luc-ASC *Bglap* expression either time point. Luc-ASC cultured on FGF-2 and TGF-β1 coated NF result in downregulation of *Tnfsf11* expression at day 21 suggesting FGF-2 and TGF-β1 delivery can modulate *Tnfsf11* expression, which presents an avenue for influencing the bone remodeling process. While FGF-2 and TGF-β1 inhibited mouse ASC osteogenic differentiation, it should be noted that divergent ASC differentiation potential occurs depending on the species of ASC derivation, especially when ASC are exposed to FGF-2 or TGF-β1.[61,67,74,75] FGF-2 and TGF-β1 signaling are highly context dependent and careful experimental design is necessary to achieve results with the greatest clinical revelance.[41,57,76] Overall, dual FGF-2 and TGF-β1 delivery from PEM-modified NF and engineered periosteums synergistically retain Luc-ASC stemness and provide the ability to deliver bioactive heparin-binding growth factors and Luc-ASC for potential therapeutic uses in bone tissue engineering.

### 4.5.3. Luciferase expressing adipose-derived stem cells response to osteogenic induction hormones

To confirm Luc-ASC could express osteogenic genes, a separate gene expression study was conducted on Luc-ASC cultured on tissue culture polystyrene in GM, OSM, OSM+dexamethasone, and OSM+retinoic acid for 21 days. The addition of induction hormones dexamethasone or retinoic acid was expected to provide an osteoinductive stimuli to ASC as previously reported.[77] Surprisingly, terminal Luc-ASC osteogenic differentiation was not confirmed as osteoblast specific *Col1a1* and *Bglap* expression was not detected. However, Luc-ASC cultured in OSM+retinoic acid induced a significantly upregulated *Alpl* expression at days 1, 7, and 21 and *Bmp2* expression at day 21 suggesting commitment to an osteogenic lineage in

line with previous reports of retinoic acid osteoinductivity.[78,79] This is further supported by the inhibition of early adipogenic transcription factor *Pparg* expression by day 21 in OSM+retinoic acid treated Luc-ASC.

### 4.6. Conclusion

In summary, our engineered periosteums were confirmed to co-deliver bioactive FGF-2 and TGF-β1 to mouse Luc-ASC which inhibited differentiation in Luc-ASC and had a proliferative effect on Luc-ASC. This work expands the materials used in periosteum tissue engineering and showcases the ability of using a polysaccharide-based approach to engineer periosteums. The versatility of the different periosteums allow for further investigation using alternate heparin-binding growth factors as well different mesenchymal cell sources to further optimize the therapeutic response of engineered periosteum for bone regeneration applications.

# REFERENCES


1. (US) OotSG. Bone Health and Osteoporosis: A Report of the Surgeon General. Volume 4, The Frequency of Bone Disease: Rockville (MD): Office of the Surgeon General (US); 2004.
2. (US) OotSG. Bone Health and Osteoporosis: A Report of the Surgeon General. Volume 5, The Burden of Bone Disease. Rockville (MD): Office of the Surgeon General (US): Office of the Surgeon General (US); 2004.
3. Mathew G, Hanson BP. Global burden of trauma: Need for effective fracture therapies. Indian J Orthop; 2009. p 111-6.
4. Meling T, Harboe K, Soreide K. Incidence of traumatic long-bone fractures requiring in-hospital management: a prospective age- and gender-specific analysis of 4890 fractures. Injury 2009;40(11):1212-9.
5. Hak DJ, Fitzpatrick D, Bishop JA, Marsh JL, Tilp S, Schnettler R, Simpson H, Alt V. Delayed union and nonunions: epidemiology, clinical issues, and financial aspects. Injury 2014;45 Suppl 2:S3-7.
6. Sen MK, Miclau T. Autologous iliac crest bone graft: should it still be the gold standard for treating nonunions? Injury 2007;38 Suppl 1:S75-80.
7. Blokhuis TJ, Arts JJ. Bioactive and osteoinductive bone graft substitutes: definitions, facts and myths. Injury 2011;42(Suppl 2):S26-9.
8. Roberts SJ, van Gastel N, Carmeliet G, Luyten FP. Uncovering the periosteum for skeletal regeneration: The stem cell that lies beneath. Bone 2015;70:10-18.
9. Gomez-Barrena E, Rosset P, Lozano D, Stanovici J, Ermthaller C, Gerbhard F. Bone fracture healing: cell therapy in delayed unions and nonunions. Bone 2015;70:93-101.
10. Zhang X, Awad HA, O'Keefe RJ, Guldberg RE, Schwarz EM. A perspective: Engineering periosteum for structural bone graft healing. Clinical Orthopaedics and Related Research 2008;466(8):1777-1787.
11. Vas WJ, Shah M, Al Hosni R, Owen HC, Roberts SJ. Biomimetic strategies for fracture repair: Engineering the cell microenvironment for directed tissue formation. J Tissue Eng 2017;8:2041731417704791.
12. Colnot C, Zhang X, Knothe Tate ML. Current insights on the regenerative potential of the periosteum: molecular, cellular, and endogenous engineering approaches. Journal of Orthopaedic Research 2012;30(12):1869-1878.
13. Hoffman MD, Benoit DSW. Emulating native periosteum cell population and subsequent paracrine factor production to promote tissue engineered periosteum-mediated allograft healing. Biomaterials 2015;52:426-440.
14. Hoffman MD, Xie C, Zhang X, Benoit DSW. The effect of mesenchymal stem cells delivered via hydrogel-based tissue engineered periosteum on bone allograft healing. Biomaterials 2013;34(35):8887-8898.
15. Shi X, Fujie T, Saito A, Takeoka S, Hou Y, Shu Y, Chen M, Wu H, Khademhosseini A. Periosteum-Mimetic Structures Made from Freestanding Microgrooved Nanosheets. Advanced Materials 2014;26(20):3290-3296.

16. Shi XT, Chen S, Zhao YH, Lai C, Wu HK. Enhanced Osteogenesis by a Biomimic Pseudo-Periosteum-Involved Tissue Engineering Strategy. Advanced Healthcare Materials 2013;2(9):1229-1235.
17. Kang YQ, Ren LL, Yang YZ. Engineering Vascularized Bone Grafts by Integrating a Biomimetic Periosteum and beta-TCP Scaffold. ACS Applied Materials & Interfaces 2014;6(12):9622-9633.
18. Chou Y-C, Cheng Y-S, Hsu Y-H, Yu Y-H, Liu S-J. A bio-artificial poly( D,L -lactide-co-glycolide) drug-eluting nanofibrous periosteum for segmental long bone open fractures with significant periosteal stripping injuries. International Journal of Nanomedicine 2016;11:941-953.
19. Ding X, Wu C, Ha T, Wang L, Huang Y, Kang H, Zhang Y, Liu H, Fan Y. Hydroxyapatite-containing silk fibroin nanofibrous scaffolds for tissue-engineered periosteum. Rsc Advances 2016;6(23):19463-19474.
20. Zhao L, Zhao J, Yu J, Zhao X, Chen Q, Huang Y. In vitro study of bioactivity of homemade tissue-engineered periosteum. Mater Sci Eng C Mater Biol Appl 2016;58:1170-6.
21. Chen K, Lin X, Zhang Q, Ni J, Li J, Xiao J, Wang Y, Ye Y, Chen L, Jin K and others. Decellularized periosteum as a potential biologic scaffold for bone tissue engineering. Acta Biomaterialia 2015;19:46-55.
22. Almodovar J, Mower J, Banerjee A, Sarkar AK, Ehrhart NP, Kipper MJ. Chitosan-heparin polyelectrolyte multilayers on cortical bone: Periosteum-mimetic, cytophilic, antibacterial coatings. Biotechnology and Bioengineering 2013;110(2):609-618.
23. Caridade SG, Monge C, Almodovar J, Guillot R, Lavaud J, Josserand V, Coll J-L, Mano JF, Picart C. Myoconductive and osteoinductive free-standing polysaccharide membranes. Acta Biomaterialia 2015;15:139-149.
24. Li N, Song J, Zhu G, Li X, Liu L, Shi X, Wang Y. Periosteum tissue engineering-a review. Biomaterials Science 2016;4(11):1554-1561.
25. Wang Q, Xu J, Jin H, Zheng W, Zhang X, Huang Y, Quian Z. Artificial periosteum in bone defect repair—A review. Chinese Chemical Letters 2017.
26. Mulloy B, Rider CC. Cytokines and proteoglycans: an introductory overview. Biochem Soc Trans 2006;34(Pt 3):409-13.
27. Rosen SD, Lemjabbar-Alaoui H. Sulf-2: an extracellular modulator of cell signaling and a cancer target candidate. Expert Opin Ther Targets 2010;14(9):935-49.
28. Lu P, Takai K, Weaver VM, Werb Z. Extracellular Matrix Degradation and Remodeling in Development and Disease. Cold Spring Harb Perspect Biol; 2011.
29. Einhorn TA, Gerstenfeld LC. Fracture healing: mechanisms and interventions. Nature Reviews Rheumatology 2015;11(1):45-54.
30. Marsell R, Einhorn TA. The biology of fracture healing. Injury 2011;42(6):551-5.
31. Richardson TP, Peters MC, Ennett AB, Mooney DJ. Polymeric system for dual growth factor delivery. Nature Biotechnology 2001;19(11):1029-1034.
32. Tessmar JK, Gopferich AM. Matrices and scaffolds for protein delivery in tissue engineering. Advanced Drug Delivery 2007;59(4-5):274-291.
33. Almodóvar J, Bacon S, Gogolski J, Kisiday JD, Kipper MJ. Polysaccharide-based polyelectrolyte multilayer surface coatings can enhance mesenchymal stem cell response to adsorbed growth factors. Biomacromolecules 2010;11(10):2629-39.

34. Lyon M, Rushton G, Gallagher JT. The interaction of the transforming growth factor-betas with heparin/heparan sulfate is isoform-specific. J Biol Chem 1997;272(29):18000-6.
35. Zhang XP, Xie C, Lin ASP, Ito H, Awad H, Lieberman JR, Rubery PT, Schwarz EM, O'Keefe RJ, Guldberg RE. Periosteal progenitor cell fate in segmental cortical bone graft transplantations: Implications for functional tissue engineering. Journal of Bone and Mineral Research 2005;20(12):2124-2137.
36. Chang H, Tate MLK. Concise Review : The Periosteum : Tapping into a Reservoir of Clinically Useful Progenitor Cells. Stem Cells Translational Medicine 2012;1:480-491.
37. Caplan AI. Adult mesenchymal stem cells for tissue engineering versus regenerative medicine. J Cell Physiol 2007;213(2):341-7.
38. Levi B, Longaker MT. Concise review: adipose-derived stromal cells for skeletal regenerative medicine. Stem Cells 2011;29(4):576-82.
39. Orbay H, Tobita M, Mizuno H. Mesenchymal Stem Cells Isolated from Adipose and Other Tissues: Basic Biological Properties and Clinical Applications. Stem Cells International 2012.
40. Barba M, Taranto GD, Lattanzi W. Adipose-derived stem cell therapies for bone regeneration. Expert Opinion on Biological Therapy 2017;17(6):677-689.
41. Senarath-Yapa K, McArdle A, Renda A, Longaker MT, Quarto N. Adipose-Derived Stem Cells: A Review of Signaling Networks Governing Cell Fate and Regenerative Potential in the Context of Craniofacial and Long Bone Skeletal Repair. International Journal of Molecular Sciences 2014;15(6):9314-9330.
42. Kwan MD, Sellmyer MA, Quarto N, Ho AM, Wandless TJ, Longaker MT. Chemical Control of FGF-2 Release for Promoting Calvarial Healing with Adipose Stem Cells. Journal of Biological Chemistry 2011;286(13):11307-11313.
43. Cowan CM, Shi YY, Aalami OO, Chou YF, Mari C, Thomas R, Quarto N, Contag CH, Wu B, Longaker MT. Adipose-derived adult stromal cells heal critical-size mouse calvarial defects. Nat Biotechnol 2004;22(5):560-7.
44. Romero R, Travers JK, Asbury E, Pennybaker A, Chubb L, Rose R, Ehrhart NP, Kipper MJ. Combined delivery of FGF-2, TGF-beta 1, and adipose-derived stem cells from an engineered periosteum to a critical-sized mouse femur defect. Journal of Biomedical Materials Research Part A 2017;105(3):900-911.
45. Romero R, Chubb L, Travers JK, Gonzales TR, Ehrhart NP, Kipper MJ. Coating cortical bone allografts with periosteum-mimetic scaffolds made of chitosan, trimethyl chitosan, and heparin. Carbohydr Polym 2015;122:144-51.
46. de Britto D, Assis OBG. A novel method for obtaining a quaternary salt of chitosan. Carbohydrate Polymers 2007;69(2):305-310.
47. Almodóvar J, Kipper MJ. Coating Electrospun Chitosan Nanofibers with Polyelectrolyte Multilayers Using the Polysaccharides Heparin and N,N,N-Trimethyl Chitosan. Macromolecular Bioscience 2011;11(1):72-76.
48. Almodóvar J, Place LW, Gogolski J, Erickson K, Kipper MJ. Layer-by-Layer Assembly of Polysaccharide-Based Polyelectrolyte Multilayers: A Spectroscopic Study of Hydrophilicity, Composition, and Ion Pairing. Biomacromolecules 2011;12(7):2755-2765.
49. Romero R, Travers JK, Asbury E, Pennybaker A, Chubb L, Rose R, Ehrhart NP, Kipper MJ. Combined delivery of FGF-2, TGF-beta1, and adipose-derived stem cells from an

engineered periosteum to a critical-sized mouse femur defect. J Biomed Mater Res A 2017;105(3):900-911.
50. Hellemans J, Mortier G, De Paepe A, Speleman F, Vandesompele J. qBase relative quantification framework and software for management and automated analysis of real-time quantitative PCR data. Genome Biology 2007;8(2).
51. Almodóvar J, Kipper MJ. Coating electrospun chitosan nanofibers with polyelectrolyte multilayers using the polysaccharides heparin and N,N,N-trimethyl chitosan. Macromolecular bioscience 2011;11(1):72-6.
52. Wang L, Stegemann JP. Extraction of High Quality RNA from Polysaccharide Matrices using Cetlytrimethylammonium Bromide. Biomaterials 2010;31(7):1612.
53. Yu C, Young S, Russo V, Amsden BG, Flynn LE. Techniques for the isolation of high-quality RNA from cells encapsulated in chitosan hydrogels. Tissue Eng Part C Methods 2013;19(11):829-38.
54. Schmittgen TD, Livak KJ. Analyzing real-time PCR data by the comparative C(T) method. Nat Protoc 2008;3(6):1101-8.
55. Livak KJ, Schmittgen TD. Analysis of relative gene expression data using real-time quantitative PCR and the 2(-Delta Delta C(T)) Method. Methods 2001;25(4):402-8.
56. Schmid GJ, Kobayashi C, Sandell LJ, Ornitz DM. Fibroblast growth factor expression during skeletal fracture healing in mice. Dev Dyn 2009;238(3):766-74.
57. Du XL, Xie YL, Xian CJ, Chen L. Role of FGFs/FGFRs in skeletal development and bone regeneration. Journal of Cellular Physiology 2012;227(12):3731-3743.
58. Lieberman JR, Daluiski A, Einhorn TA. The Role of Growth Factors in the Repair of Bone. The Journal of Bone and Joint Surgery 2002;84(6):1032-1044.
59. Janssens K, ten Dijke P, Janssens S, Van Hul W. Transforming growth factor-beta 1 to the bone. Endocrine Reviews 2005;26(6):743-774.
60. Wu M, Chen G, Li YP. TGF-beta and BMP signaling in osteoblast, skeletal development, and bone formation, homeostasis and disease. Bone Res 2016;4:16009.
61. Levi B, James AW, Xu Y, Commons GW, Longaker MT. Divergent Modulation of Adipose-Derived Stromal Cell Differentiation by TGF-beta 1 Based on Species of Derivation. Plastic and Reconstructive Surgery 2010;126(2):412-425.
62. Rodriguez TM, Saldias A, Irigo M, Zamora JV, Perone MJ, Dewey RA. Effect of TGF-beta1 Stimulation on the Secretome of Human Adipose-Derived Mesenchymal Stromal Cells. Stem Cells Transl Med 2015;4(8):894-8.
63. Ehrhart NP, Hong L, Morgan AL, Eurell JA, Jamison RD. Effect of transforming growth factor-beta 1 on bone regeneration in critical-sized bone defects after irradiation of host tissues. American Journal of Veterinary Research 2005;66(6):1039-1045.
64. Saltzman WM. Growth-Factor Delivery in Tissue Engineering. MRS Bulletin 1996;21(11):62-65.
65. Hastings JW. Bioluminescence. In: Sperelakis N, editor. Cell Physiology Source Book: Essentials of Membrane Biophysics. Boston, MA: Academic Press; 2012. p 925-947.
66. Noda M, Rodan GA. Type-beta transforming growth factor inhibits proliferation and expression of alkaline phosphatase in murine osteoblast-like cells. Biochem Biophys Res Commun 1986;140(1):56-65.
67. Quarto N, Longaker MT. FGF-2 Inhibits Osteogenesis in Mouse Adipose Tissue-Derived Stromal Cells and Sustains their Proliferative and Osteogenic Potential State. Tissue Engineering 2006;12(6):1405-1418.

68. Long F. Building strong bones: molecular regulation of the osteoblast lineage. Nat Rev Mol Cell Biol 2011;13(1):27-38.
69. Quarto N, Longaker MT. FGF-2 inhibits osteogenesis in mouse adipose tissue-derived stromal cells and sustains their proliferative and osteogenic potential state. Tissue Eng 2006;12(6):1405-18.
70. Quarto N, Wan DC, Longaker MT. Molecular mechanisms of FGF-2 inhibitory activity in the osteogenic context of mouse adipose-derived stem cells (mASCs). Bone 2008;42(6):1040-52.
71. Koefoed M, Ito H, Gromov K, Reynolds DG, Awad HA, Rubery PT, Ulrich-Vinther M, Soballe K, Guldberg RE, Lin ASP and others. Biological effects of rAAV-caAlk2 coating on structural allograft healing. Molecular Therapy 2005;12(2):212-218.
72. Cho TJ, Gerstenfeld LC, Einhorn TA. Differential temporal expression of members of the transforming growth factor beta superfamily during murine fracture healing. J Bone Miner Res 2002;17(3):513-20.
73. Grafe I, Alexander S, Peterson JR, Snider TN, Levi B, Lee B, Mishina Y. TGF-β Family Signaling in Mesenchymal Differentiation. Cold Spring Harb Perspect Biol 2017.
74. Levi B, James AW, Glotzbach JP, Wan DC, Commons GW, Longaker MT. Depot-Specific Variation in the Osteogenic and Adipogenic Potential of Human Adipose-Derived Stromal Cells. Plastic and Reconstructive Surgery 2010;126(3):822-834.
75. Levi B, Nelson ER, Brown K, James AW, Xu D, Dunlevie R, Wu JC, Lee M, Wu B, Commons GW and others. Differences in Osteogenic Differentiation of Adipose-Derived Stromal Cells from Murine, Canine, and Human Sources In Vitro and In Vivo. Plastic and Reconstructive Surgery 2011;128(2):373-386.
76. Morikawa M, Derynck R, Miyazono K. TGF-β and the TGF-β Family: Context-Dependent Roles in Cell and Tissue Physiology. Cold Spring Harbor Perspectives in Biology 2016;8:a021873.
77. Grottkau BE, Lin Y. Osteogenesis of Adipose-Derived Stem Cells. Bone Res 2013;1(2):133-45.
78. Malladi P, Xu Y, Yang GP, Longaker MT. Functions of vitamin D, retinoic acid, and dexamethasone in mouse adipose-derived mesenchymal cells. Tissue Engineering 2006;12(7):2031-2040.
79. Wan DC, Shi YY, Nacamuli RP, Quarto N, Lyons KM, Longaker MT. Osteogenic differentiation of mouse adipose-derived adult stromal cells requires retinoic acid and bone morphogenetic protein receptor type IB signaling. Proc Natl Acad Sci U S A 2006;103(33):12335-40.

# CHAPTER 5: CONCLUSIONS AND FUTURE DIRECTIONS

## 5.1. Conclusions

This dissertation investigated the *in vitro* and *in vivo* performance of polysaccharide-based engineered periostea on mouse cortical bone allografts delivering fibroblast growth factor-2 (FGF-2) and transforming growth factor (TGF-β1) to mouse adipose-derived stem cells (Luc-ASC). Chitosan-based periostea were first engineered on the periosteal surface cortical bone and the engineered periostea' macroscopic and surface chemistry composition was characterized via scanning electron microscopy and x-ray photoelectron spectroscopy, respectively. After confirmation of heparin incorporation in engineered periostea, FGF-2 and TGF-β1 *in vitro* release was characterized with ELISA. *In vitro* cytocompatibility and Luc-ASC response to FGF-2 and TGF-β1 delivered from engineer periostea was evaluated using bioluminescence imaging and Western Blot, respectively.

Nanofiber (NF) engineered periosteum delivering FGF-2, TGF-β1, and Luc-ASC to a critical-sized mouse femur defect to was assessed using bioluminescence imaging, microcomputed tomography, union ratio analysis, and blinded histological analysis. Relative gene expression studies of Luc-ASC cultured on FGF-2- and TGF-β1-coated chitosan NF (modified with heparin and trimethyl chitosan polyelectrolyte multilayers) to determine whether Luc-ASC differentiated in response to delivered FGF-2- and TGF-β1.

The objectives of this work were achieved as described below:

**Objective 1:** Engineer periostea on mouse cortical bone allografts.

Objective 1 is addressed in chapter 2. Polysaccharide-based periostea were engineered on mouse cortical bone. Engineered periostea microscopic structure was characterized with

scanning election microscopy and diverse surface topographies were observed among the three engineered periostea. Porous freeze-dried and nanofiber structures were retained after several aqueous processing steps allowing heparin incorporation. X-ray photoelectron spectroscopy confirmed polyelectrolyte multilayers (PEM) of trimethyl chitosan and heparin were deposited on cortical bone surface and freeze-dried and nanofiber engineered periostea resulting in similar surface chemistries among the engineered periostea with divergent microscopic structure. Bioluminescence imaging confirmed luciferase-expressing mouse adipose-derived stem cells (Luc-ASC) could be cultured on engineered periostea and maintained an osteoprogenitor phenotype. Successful manufacture of engineered periostea structures on cortical bone may be used as a novel tissue engineering scaffolds for *in vitro* and *in vivo* investigations in tissue regeneration.

**Objective 2:** Determine *in vitro* effects of engineered periosteum on murine adipose-derived stem cells.

Objective 2 is addressed in chapter 4. Heparin incorporation into engineered periostea allowed electrostatic binding of FGF-2 and TGF-β1. FGF-2 and TGF-β1 measurable release was detected with ELISA and showed FGF-2 and TGF-β1 burst release kinetics. The majority of FGF-2 released within 4 days with detectable release up to 14 days. The majority of TGF-β1 released within 2 days with minimal detectable release up to 4 days. When compared to each other, freeze-dried scaffolds released the largest amounts of FGF-2 and TGF-β1, followed by nanofiber scaffolds, with PEM scaffolds releasing the least amounts of FGF-2 and TGF-β1, intuitively correlating with scaffold surface area. Longitudinal bioluminescence imaging of luciferase-expressing Luc-ASC demonstrated all three engineered could supported viable cells

and Luc-ASC adhesion without additional cell adhesion motifs. While bioluminescence was inhibited compared to each samples' day 1 bioluminescence signal at days 4 and 7 regardless of treatment, FGF-2 and TGF-β1 released from PEM and NF engineered periosteum caused recovery of bioluminescence by day 14 for both scaffolds and continued elevated bioluminescence at day 21 on NF engineered periosteum. Alkaline phosphatase (ALP) and receptor activator of nuclear factor-kappaB ligand (RANKL) protein expression was observed in Luc-ASC cultured on PEM and NF engineered periosteum delivering FGF-2 and TGF-β1 at days 7 and 21 suggesting FGF-2 and TGF-β1 did not inhibit ALP and RANKL expression. This result suggested the Luc-ASC retain an osteoprogenitor phenotype on our engineered periosteum. Further gene expression studies of Luc-ASC cultured on NF engineered periosteum delivering FGF-2 and TGF-β1 showed inhibited osteogenic, chondrogenic, and adipogenic differentiation confirming Western blot results. These results confirmed that biological augmentation of engineered periostea can occur with adsorbed heparin binding growth factors and a progenitor cell source and may be a viable option to augment bone allograft healing.

**Objective 3:** Determine *in vivo* effects of engineered periosteum in a murine femoral defect model.

Objective 3 is addressed in chapter 3. Observing that NF engineered periosteum released higher amounts of FGF-2 and TGF-β1 compared to PEM engineered periosteum and supported increased Luc-ASC viability compared to FD engineered periosteum, NF engineered periosteum was selected to investigate *in vivo* in a mouse critical-sized femur defect. Successful Luc-ASC localization and persistence in femur defect for at least 7 days was confirmed with longitudinal bioluminescence imaging. Bioactive FGF-2 and TGF-β1 delivery was confirmed by observation

of increased bioluminescence in implanted Luc-ASC with FGF-2 and TGF-β1 at day 4 compared growth factor-free treated Luc-ASC. Microcomputed tomography analysis of excised mouse femurs at week 6 revealed increased bone volume in Luc-ASC-treated groups compared to their respective cell-free control. However, this increase was not statistically significant. Histological analysis showed persistence of NF in femur defect site inhibiting allograft incorporation with host bone tissue. Union ration analysis confirmed this observation with a significant decrease in union ratio in NF-treated groups compared to non-NF treated groups. Interestingly, rare observation of periosteal bone and cartilage was observed in a 10% of cases receiving NF engineered periosteum delivering FGF-2 and TGF-β1 to the femur defect. These results demonstrate that the NF engineered periosteum can successfully co-deliver FGF-2, TGF-β1, and Luc-ASC to a mouse femur defect. While minimal therapeutic effect on bone allograft healing and integration was observed with our engineered periosteum, this work represents a proof-of-concept study and further optimization of the engineered periosteum may result in more robust bone allograft healing.

### 5.2. Future directions

The field of periosteum tissue engineering is young and this work contributes significantly in the area of polysaccharide-based periosteum substitutes. However, there are limitations to this work that should be addressed in future studies. The periosteum structure is highly vascularized and innervated. A true periosteum mimic would contain these important structures to fully translate the periosteum's regenerative power. Vascularized bone tissue engineering is the next frontier in the field of bone tissue engineering with the ultimate goal of creating clinically relevant amounts of bone tissue. Effective incorporation of an endothelial cell

population within the periosteum substitute structure may improve allograft healing due to proangiogenic and osteogenic effects. Co-transplanted progenitor cells and endothelial cells may lead to enhanced cell engraftment by increasing the probability of revascularization occurring in the bone defect site and anastomosis with host vasculature providing crucial oxygen and nutrient transport. With the advent of additive manufacturing techniques and the advancement of biomaterial technology, patterned vasculature structures within a periosteum substitute could be possible. Periosteum tissue engineering has the potential to revitalize bone allografts to eventually reach clinical equivalence with bone autograft healing.

The limited effect of our engineered periosteum on bone allograft healing and incorporation in a mouse femur defect demonstrates suboptimal design of our engineered periosteum. Large variability within our experimental replicates in our *in vivo* study suggests more attention should be paid to in previous steps to eliminate sample heterogeneity at each step of production (engineered periosteum manufacturing, growth factor loading, and cell seeding). The degradation rate of our engineered periosteum should be tuned to match the native tissue mineralization rate. Our engineered periosteum shifted once implanted due to shear forces of the surrounding musculature. A more robust anchoring system for our engineered periosteum to the periosteal bone surface analogous to Sharpey's fibers would allow our engineered periosteum to more accurately deliver growth factors or cells to the intended location. Possible strategies to improve engineered periostea anchoring include incorporating a calcium binding motif such as citrate or a bioahesive motif modeled after mussel foot proteins on the engineered periosteum's periosteal surface. Inspiration could also be taken from the engineering of osteochondral structures such as tendon insertion points.

For engineering a periosteum substitute on bone allografts for improved bone allograft incorporation, previous research has generally focused on increasing mineralization around the bone allograft through delivery of a potent osteoinductive factor such as BMP-2 or mesenchymal stem cell transplantation to a bone defect. While progenitor cell implantation or osteoinductive signaling has shown some therapeutic effects such as enhanced bone allograft biomechanical and graft incorporation, these techniques have not been clinically translated in the repair of large segmental bone defects suggesting the optimal combination of growth factor(s), and progenitor cell(s) has yet to be discovered to best improve bone allograft healing. The combination of FGF-2 and TGF-β1 with mouse Luc-ASC was shown to promote Luc-ASC proliferation and inhibit osteogenic differentiation. Counterintuitively, maintaining stemness in allogeneically transplanted Luc-ASC may prolong Luc-ASC immune evasive properties allowing Luc-ASC therapeutic trophic effects to persist longer in the bone defect. Maintaining Luc-ASC stemness *in vivo* may also allow Luc-ASC to differentiate down alternative lineages such as chondrogenic or myogenic first before eventually committing to an osteogenic phenotype. Exploring strategies to help progenitor cells persist after *in vivo* implantation is one of the greatest hurdles keeping cell-based therapeutics from being translated to the clinic.

Growth factors and their combinations outside of the popular BMP-2 and VEGF still need to be investigated to improve bone allograft healing. Challenges facing these future experiments include selecting the optimal growth factor dose, temporal delivery schedule (simultaneous vs. subsequent), and proper combination. More studies need to be performed to elucidate the growth factor signaling that occurs in the bone callus during fracture repair. Consequently, *in vitro* screening of other growth factors and their effect on endogenous cells as well as co-transplanted progenitor cells need to be rigorously studied to tailor the therapeutic

response. Alternate future strategies may include only using the active growth factor signaling peptide sequence to elicit a therapeutic response in exposed cells as well as delivering other potent signaling molecules such as miRNA.

Tissue engineered periosteum is one application for the work presented in this dissertation. Eventually, with an optimized periosteum design, a platform for investigating bone graft healing can be achieved. Ideally, insights from this platform could be extended to regenerate other tissues in determining optimal growth factor delivery regimes and therapeutic progenitor cell incorporation.

# APPENDIX

## A1. Supplementary information for coating cortical bone allografts with periosteum-mimetic scaffolds made of chitosan, trimethyl chitosan and heparin

### A1.1. Synthesis of *N,N,N*–trimethyl chitosan

TMC was synthesized following de Britto and Assis's synthesis .[1] Chitosan (0.5 g) was reacted with 10 mL of dimethyl sulfate with 2 mL of ultrapure water, 0.4 g NaOH, and 0.6 g of NaCl at room temperature and vigorously shaken for 6 hours. The reaction product was purified by dialysis (Fisher-Scientific; Pittsburgh, PA; 12,000 to 14,000 MWCO) with buffers of decreasing salt concentration (0.5 M, 0.25 M, 0.10 M NaCl/NaOH) for 3 days with buffer changes occurring approximately every 12 hours. TMC was then precipitated with acetone, dried, and stored at 4 °C for long term storage.

### A1.2. Proton nuclear magnetic resonance of chitosan and *N,N,N*–trimethyl chitosan

$^1$H NMR confirmed successful methylation of TMC (See Figure A1.1). $^1$H NMR spectra were collected on a fully automated, 400 MHz Varian 400-MR (Santa Clara, CA) NMR spectrometer equipped with a 7620 sample changer and VJ-4 software. The following parameters were used: relaxation delay = 10 s, number of transients = 128, pulse angle = 90°, temperature = 26 °C. Chitosan was dissolved in $D_2O$/HCl (100/1 v/v) and TMC was dissolved in $D_2O$ at 5 mg $mL^{-1}$. Additionally, TMC was $D_2O$/HCl at 5 mg $mL^{-1}$ to confirm *N*–dimethyl chemical shift as done by Sieval and colleagues [2]. NMR spectra were zero-filled and multiplied by an exponential decay curve with a line broadening factor of 0.3 to improve signal-to-noise ratio before signal

integration. Chitosan and TMC peak assignments were made according to previously reported literature values [1,3] and internally referenced by assigning the residual hydrogen resonance of $H_2O$ to 4.76 ppm [4]. Chitosan's degree of acetylation and TMC's degree of quaternization were calculated as reported by Curti and Campana-Filho [5]. Chitosan was found to be 9% acetylated. The methylation reaction to form TMC resulted in *N*–methylation and *O*–methylation. The degree of *N*–trimethylation (DQ), *N*–dimethylation (DD), and *O*–methylation (DOM) were 71%, 18%, and 84% respectively, using the equations described below and adapted from Curti and Campana-Filho 2006:

$$DQ = \left[\frac{I_{NQ}}{9} \times \frac{1}{S}\right] \times 100$$

$$DD = \left[\frac{I_{ND}}{6} \times \frac{1}{S}\right] \times 100$$

$$DOM = \left[\frac{I_{OM}}{3} \times \frac{1}{S}\right] \times 100$$

$$S = \frac{I_{NQ}}{9} + \frac{I_{ND}}{6} + \frac{I_{NAc}}{3}$$

where $I_{NQ}$ is the integrated signal intensity from the hydrogens in the trimethylated amino group at 3.3 ppm, $I_{ND}$ is the integrated signal intensity from the hydrogens in the dimethylated amino group at 2.5 ppm, $I_{OM3}$ is the integrated signal intensity from the hydrogens in the *O*–methyl groups on the C3 position at 3.5 ppm, and $I_{NAc}$ is the integrated signal intensity from the hydrogens in the *N*–acetyl groups at 2.0 ppm. The degree of *O*–methylation at the TMC C6 position was not calculated due to unreliable peak definition. Degree of methylation values were calculated from TMC dissolved in $D_2O$.

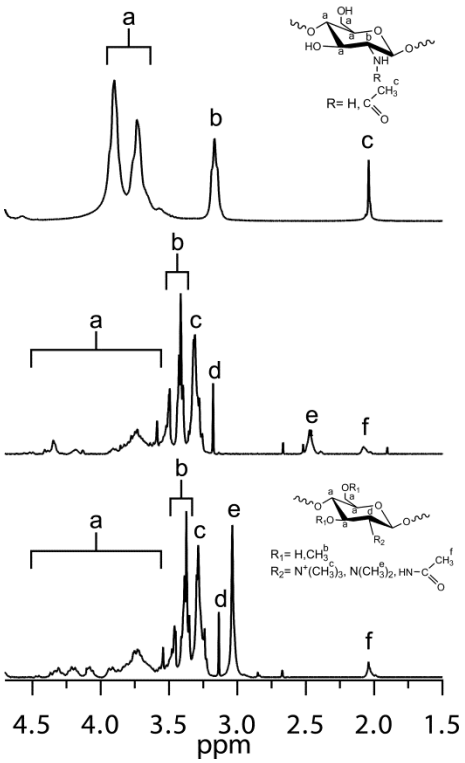


**Figure A1.1.** $^{1}$H NMR spectra of chitosan (top), TMC in $D_2O$ (middle), and TMC in $D_2O$/HCl (100/1 v/v)

## A2. Supporting information for combined delivery of growth factors and adipose-derived stem cells from an engineered periosteum to a critical-sized mouse femur defect

### A2.1. Luciferase expressing adipose-derived stem cells differentiation potential

Luciferase-expressing adipose derived stem cells (Luc–ASCs) were differentiated down osteogenic and adipogenic lineages using the appropriate differentiation media. For osteogenic differentiation, Luc–ASCs base growth media, consisting of DMEM low glucose, 15% FBS, 1% antibiotic/antimycotic and supplemented with 1× MEM vitamins and 1× MEM non–essential vitamins, was supplemented with 10 nM dexamethasone, 20 mM β-glycerophosphate, and 50 µM L-absorbic-2-phosphate. Adipogenic media was made by supplementing the Luc–ASCs

growth media with 0.5 µM dexamethasone, 0.5 µM isobutylmethylxanthine, and 50 µM indomethacin.

Luc–ASCs (Passage 3 or less) were plated at a density of 100,000 cells per well in 6-well plates in Luc–ASCs growth media. After overnight attachment, the Luc–ASCs growth media was aspirated and replaced with the appropriate media according to experimental group. Luc–ASCs were exposed to either base growth, osteogenic, or adipogenic media. The Luc–ASCs were allowed to differentiate for 21 days, replacing with the appropriate media at least 2 times per week.

Calcium staining using Alizarin Red was used to evaluate *in vitro* mineralization for osteogenesis and Oil Red O staining was used to visualize oil droplet formation for adipogenesis. For Alizarin Red staining, a 0.01 g $mL^{-1}$ stain solution was prepared. The solution pH was adjusted to between 4.1 and 4.3 using 0.1% ammonium hydroxide, and then filtered. For Oil Red O staining, a stock solution was prepared at 0.5%. Before staining, an Oil Red O working solution was prepared by mixing 3 parts 0.5% Oil Red O stock dye solution to 2 parts PBS, allowed to sit for 10 minutes, then filtered and allowed to sit for another 10 minutes before use. After 21 days of *in vitro* culture in the appropriate differentiation medium, cell media was aspirated and the cells were washed with PBS. Neutral buffered formalin (NBF, 10%) was added to each well to cover the cells for 1 hour at room temperature. The NBF was aspirated from each well; the wells to be stained with Oil Red O were washed with PBS and the wells to be stained with Alizarin were washed with DI water. The appropriate stains were then added to their respective wells and incubated for 20 minutes at room temperature. The stain was aspirated off and the wells were washed several times with either DI water (Alizarin) or PBS (Oil Red O) and imaged using light microscopy (Figure A2.1). Luc-ASCs cultured for 21 days in growth media

do not stain with either Alizarin Red or Oil Red O (Figure A2.1 A and C). Luc-ASCs cultured for 21 days in osteogenic media stain strongly with Alizarin (Figure A2.1 B), indicating mineralization. Luc-ASCs cultured for 21 days in adipogenic media show evidence of lipid accumulation by Oil Red O staining (Figure A2.1 D).

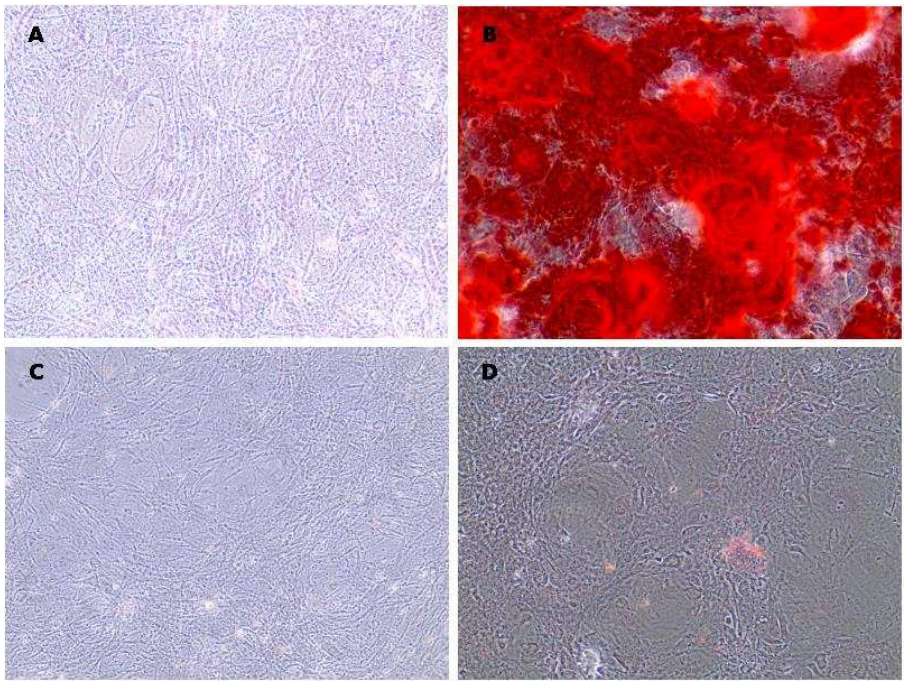


**Figure A2.1.** Images showing results of Luc-ASC exposed to osteogenic and adipogenic differentiation media for 21 days. (A) Luc-ASCs exposed to base growth media for 21 days and stained with Alizarin Red. (B) Luc-ASCs exposed to osteogenic media for 21 days and stained with Alazarin Red. (C) Luc-ASCs exposed to base growth media for 21 days and stained with Oil red O. (D) Luc-ASCs exposed to adipogenic media for 21 days and stained with Oil Red O**.**

### A2.2. Growth factor release from nanofiber scaffolds

Figure A2.2 shows results from the ELISA measurements of FGF-2 and TGF-β1 release from the nanofiber-coated and growth factor-modified allografts in vitro, for 20 days. Most of the released growth factor is eluted during the first 7 days of the release study.

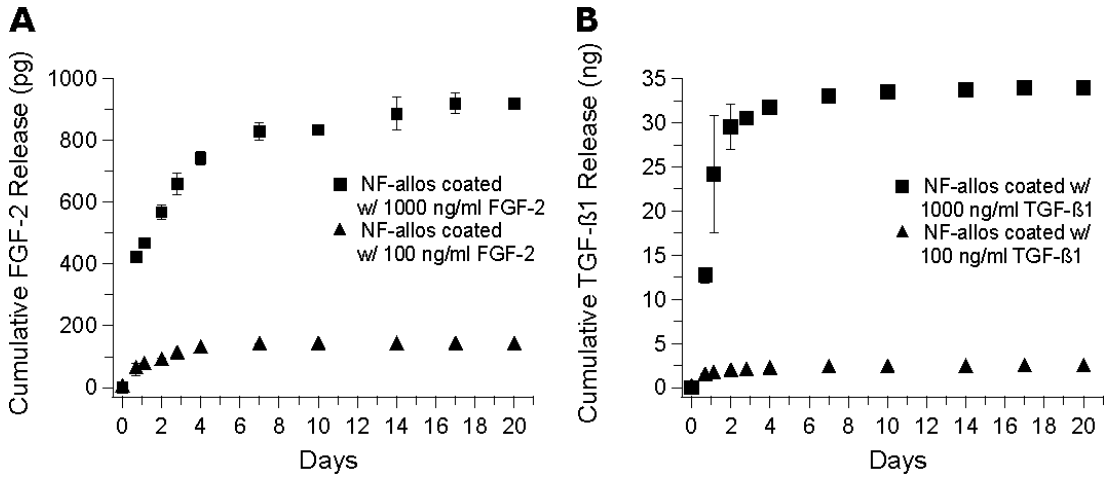


**Figure A2.2.** *In vitro* growth factor release measured over 20 days. (A) FGF-2 release profile. (B) TGF-β1 release profile.

### A2.3. Fluorescence imaging of luciferase expressing adipose-derived stem cells seeded on chitosan nanofibers

Luc-ASCs (P6) were seeded onto chitosan nanofibers coated with 7-layer PEMs of trimethylchitosan and heparin at a concentration of 500,000 cells in 30 µl. The Luc-ASCs were then cultured overnight in Luc-ASC base growth media. On the following day, Luc-ASCs media was aspirated and replaced with a 4 µM calcein-AM solution and incubated at 37 °C and 5% $CO_2$ for 30 minutes. Cells were rinsed with PBS and subsequently fixed with a 3.7 % formaldehyde solution for 15 minutes. The cells were then permeabilized with 0.5 % Tween-20 for 15 minutes and stained with a DAPI solution (1:1000) for 5 minutes. Stained Luc-ASCs on nanofibers were imaged using a Zeiss Axio Imager A.2 fluorescent microscope and appropriate filters for calcein and DAPI. Uniform cell distribution was observed on and within the fibers. A representative micrograph is shown in Figure A2.3.

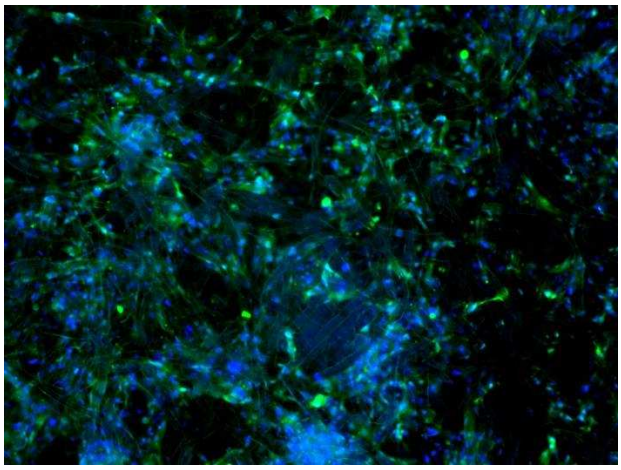

**Figure A2.3.** Luc-ASCs seeded onto chitosan NFs stained with DAPI and calcein-AM stains to show uniform seeding on nanofibers. DAPI (blue) stains cell nuclei, while calcein-AM (green) stains viable cells' cytoplasm.

## A3. Supplementary information for i*n vitro* co-delivery of growth factors from engineered periosteum promotes proliferation and inhibits differentiation of mouse adipose-derived stem cells

Table A3.1. qPCR Primer and hydrolysis probe sequences

| Target Gene | Primer or Probe | Sequence (5' to 3') |
|---|---|---|
| *Alpl* | Primer 1 | CAAGGACATCGCATATCAGCTA |
| | Primer 2 | GCCTTCTCATCCAGTTCGTAT |
| | Probe | CGCCACCCATGATCACGTCGAT |
| *Bglap* | Primer 1 | GAACAGACAAGTCCCACACAG |
| | Primer 2 | AGCAGAGTGAGCAGAAAGATG |
| | Probe | CCCAGACCTAGCAGACACCATGAG |
| *Bmp2* | Primer 1 | TGCAGATGTGAGAAACTCGTC |
| | Primer 2 | CGCAGCTTCCATCACGAA |
| | Probe | CCAGAGATGAGTGGGAAAACGGCC |
| *Col1a1* | Primer 1 | CGCAAAGAGTCTACATGTCTAGG |
| | Primer 2 | CATTGTGTATGCAGCTGACTTC |
| | Probe | CCGGAGGTCCACAAAGCTGAACA |
| *Col2a1* | Primer 1 | TCCTCTGCGATGACATTATCTG |
| | Primer 2 | CTCCTTTCTGCCCCTTTGG |
| | Probe | AGAGTGCTGTCCCATCTGCCC |
| *Pparg* | Primer 1 | CTGCTCCACACTATGAAGACAT |
| | Primer 2 | TGCAGGTTCTACTTTGATCGC |
| | Probe | AGCTGACCCAATGGTTGCTGATTACA |
| *Runx2* | Primer 1 | GTAGCCAGGTTCAACGATCTG |
| | Primer 2 | CCGTCCACTGTCACTTTAATAGC |
| | Probe | TGAAACTCTTGCCTCGTCCGCTC |
| *Sox9* | Primer 1 | CGACCCATGAACGCCTT |
| | Primer 2 | GTCTCTTCTCGCTCTCGTTC |
| | Probe | AGACCAGTACCCGCATCTGCAC |
| *Tnfsf11* | Primer 1 | TCCCGCTCCATGTTCCT |
| | Primer 2 | AGTGCTGTCTTCTGATATTCTGT |
| | Probe | AGCATCGCTCTGTTCCTGTACTTTCG |
| *Vegfa* | Primer 1 | CCGAAACCATGAACTTTCTGC |
| | Primer 2 | GACTTCTGCTCTCCTTCTGTC |
| | Probe | TGCTGTACCTCCACCATGCCAAG |
| *Ywhaz* | Primer 1 | AGAGTCGTACAAAGACAGCAC |
| | Primer 2 | AGAATGAGGCAGACAAAGGTT |
| | Probe | TCGGATACCCAAGGAGATGAAGCAGA |

Table A3.2. Average % atomic concentration of C, O, Ca, P from engineered periosteums on bone allografts [a]

| | C1s | O1s | Ca2p | P2p | C/O |
|---|---|---|---|---|---|
| Untreated Bone | 56.0 ± 4.1 | 25.4 ± 2.5 | 3.3 ± 0.7 | 2.9 ± 0.5 | 2.2 ± 0.5 |
| +PEM | 59.4 ± 0.3 | 31.2 ± 1.1 | n.d. | n.d. | 1.9 ± 0.1 |
| FD | 57.8 ± 0.0 | 34.6 ± 0.0 | n.d. | n.d. | 1.7 ± 0.0 |
| FD+PEM | 60.1 ± 0.0 | 32.8 ± 0.2 | n.d. | n.d. | 1.8 ± 0.0 |
| NF | 60.9 ± 0.4 | 33.0 ± 0.6 | n.d. | n.d. | 1.8 ± 0.1 |
| NF+PEM | 58.4 ± 0.3 | 32.7 ± 0.4 | n.d. | n.d. | 1.8 ± 0.0 |

[a]Values are average ± range. Data are from XPS high resolution spectra (n=2). n.d. = not detected.

## A4. Research protocols

This section contains the standard operating protocols used in the reseach conducted in this work. They are intended to serve as a reference material for the Kipper lab and any researcher who may find them useful in their work. May your research be fruitful.

# Cell fixing for SEM Imaging SOP Kipper Lab

Last updated 03/04/14 by Raimundo Romero

**Purpose**: To fix mammalian cells and dehydrate for SEM imaging

**Materials needed:**
Sample(s)
Sodium cacodylate
Glutaraldehyde
Sucrose
35%, 50%, 70%, 100% ethanol solutions
Hexamethyldisilazane (HMDS)
Conducting adhesive tape (carbon or copper)

**Procedure:**

1. Prep buffer solutions (0.2 M Na-cacodylate, 0.1 M sucrose buffer)
   a. Mix together 19.4 mLs of DI $H_2O$
   b. 0.68 g sucrose
   c. 0.42 g of sodium cacodylate

2. Separate into 10 and 9.4 mLs aliquots and place into 2 separate centrifuge tubes

3. Add 0.6 mLs of 30% glutaraldehyde to aliquot of 9.4 ml of buffer (This is the primary fixative; final concentration of glutaraldehyde = 1.7%)

4. Immerse samples in primary fixative for 45 mins

5. Place samples in other 10 ml portion of sodium cacodylate buffer for 10 mins

6. Dehydrate samples by immersing in an increasing graded ethanol series (35%, 50%, 70%, 100%) for 10 mins at each concentration.

7. Lastly, place samples in HMDS for 10 mins and then air dry

8. Coat samples with ~10 nm of gold before imaging and attach to Aluminum stub or sample holder with conductive adhesive tape. (Both are at SEM sample prep bench at the CIF in Chemistry.)

# CTAB RNA lysis buffer SOP — Kipper Lab

Last updated 3/02/16 by Rai Romero — **Colorado State University**

**Purpose**: To make CTAB lysis buffer for RNA extraction

**Materials needed:**

RNAse free water
PVP-40, Polyvinylpyrrolidone
CTAB, cetyltrimethylammonium bromide
NaCl, Mw= 58.44 g/mol
Tris-HCl, Mw= 157.6 g/mol
EDTA, Mw= 292.2 g/mol
β-ME, beta-mercaptoethanol

**Procedure**

Note: Ensure adequate RNAse decontamination has been performed on items used in preparation of CTAB buffer.

Making stock solutions

1. Heat water bath in Rm 367 to 65 °C.
2. Make 10% CTAB solution
    a. 5 g of CTAB
    b. 50 mls of RNase free water
3. 5 M NaCl solution
    a. 14.16 g NaCl
    b. 50 ml of RNase free water
4. 0.5 M EDTA, pH 8.0
    a. 7.31 g EDTA
    b. 50 mls of RNase free water
    c. Adjust pH to 8 w/ NaOH pellets and bring to pH= 8 w/ concentrated HCl
5. 1 M Tris-HCl, pH 8.0
    a. 7.88 g Tris-HCl
    b. 50 ml
    c. Adjust pH to 8 w/ NaOH pellets then to pH= 8 w/ concentrated HCl
6. CTAB extraction buffer working concentration (makes 10 ml)

| CTAB lysis buffer stock solns | Final lysis buffer conc. |
|---|---|
| 2 mls of 10% CTAB solution | 2% (v/v) CTAB |
| 4 ml of 5 M NaCl solution | 2 M NaCl |
| 0.4 ml of 0.5 M EDTA, pH 8.0 | 20 mM EDTA |
| 1 ml of 1 M Tris-HCl, pH 8.0 | 100 mM Tris-HCl |
| 0.2 g of PVP-40 | 2% PVP-40 |
| 2.5 ml of RNase free water | |
| 0.1 ml of β-ME | 1% (v/v) β-ME |

    a. Mix all components together except β-ME to 65 °C. (10% CTAB solution may precipitate out when stored at room temp; reheat to solubilize CTAB).

b. Add β-ME right before lysis

7. CTAB lysis buffer stock solutions can be stored at room temperature and are stable for at least 2 weeks.

| Version | Date | By | Notes |
|---|---|---|---|
| 1.1 | 3/02/16 | Rai Romero | Increased NaCl to 2 M in final working conc. |
| 1.0 | 02/04/16 | Rai Romero | |

# CTAB RNA isolation SOP — Kipper Lab

Last updated 03/02/16 by Rai Romero — **Colorado State University**

**Purpose**: To extract RNA from cells cultured on polysaccharide scaffolds

**Materials needed:**

RNAse free water
PVP-40, Polyvinylpyrrolidone
CTAB, cetyltrimethylammonium bromide
NaCl, Mw= 58.44 g/mol
Tris-HCl, Mw= 157.6 g/mol
EDTA, Mw= 292.2 g/mol
β-ME, beta-mercaptoethanol
Ammonium acetate, Mw= 77.08 g/mol
100% ethanol
100% propanol
PCR-grade RNase-free 1.5 ml centrifuge tubes
24:1 Chloroform:isoamyl alcohol (CHISAM)
1000, 200, 10 µl filter pipet tips, RNase-free
Glycoblue (Co-precipitante)
Microcentrifuge
-20 °C freezer
Ice
Nanodrop or Take3 spectrophotometer
DNA-free DNase treatment kit

**Procedure**

Background: This protocol was developed to isolate RNA from a low number of mammalian cells cultured on chitosan matrices. The protocol is based on Wang 2010 and Yu et al 2013 articles.[1,2] Initial protocol written in Romero lab notebook 9 pgs 18-20.

Note: Ensure adequate RNAse decontamination has been performed on items used in preparation of CTAB buffer.

Make CTAB lysis buffer (Refer to CTAB RNA lysis buffer SOP for detailed instructions)

| CTAB lysis buffer stock solns | Final lysis buffer conc. |
|---|---|
| 2 mls of 10% CTAB solution | 2% (v/v) CTAB |
| 4 ml of 5 M NaCl solution | 2 M NaCl |
| 0.4 ml of 0.5 M EDTA, pH 8.0 | 20 mM EDTA |
| 1 ml of 1 M Tris-HCl, pH 8.0 | 100 mM Tris-HCl |
| 0.2 g of PVP-40 | 2% PVP-40 |
| 2.5 ml of RNase free water | |
| 0.1 ml of β-ME | 1% (v/v) β-ME |

c. Mix all components together except β-ME to 65 °C. (10% CTAB solution may precipitate out when stored at room temp; reheat to solubilize CTAB).
d. Add β-ME right before lysis.

**Make 25 mls of 3 M Ammonium acetate ($NH_4C_2H_3O_2$) in RNase-free $H_2O$**

Add 5.78 g of $NH_4C_2H_3O_2$ into 25 mls of RNase-free $H_2O$.

**RNA extraction (assuming samples are in a 48 microtiter plate)**

1. Aspirate cell media.
2. Rinse cells/samples once w/ 500 µl of PBS (-Mg, -Ca)
3. Add 600 µl of pre-warmed (to 65 °C) CTAB lysis buffer to samples. Incubate at RT for 10 mins. May move samples to 1.5 microcentrifuge tubes and vortex to lyse cells.
4. If samples are still in 48 well plate, pipet vigorously to break up cells then transfer to 1.5 microcentrifuge tube
5. Add 600 µl of CHISAM (24:1). Vortex samples to mix thoroughly.
6. Centrifuge at 15,000 *g* RT for 5 mins.
7. Transfer upper clear aqueous phase (about 550 µl) to new microcentrifuge tube and add fresh 550 µl of CHISAM (24:1). Vortex to mix thoroughly.
8. Centrifuge at 15,000 *g* RT for 5 mins.
9. Transfer upper clear aqueous phase (about 500 µl) to new microcentrifuge tube.
10. Add 100 µl of 3 M $NH_4C_2H_3O_2$ to have final 0.5 M M $NH_4C_2H_3O_2$ conc. (pre-chilled on ice)
11. Add 2 µl of Glycoblue
12. Vortex to mix well
13. Add 600 µl of 100% isopropanol (pre-chilled on ice).
14. Vortex to mix well
15. Chill samples at -20 °C for 15 mins.
16. Centrifuge at 15,000 *g* RT for 15 mins.
17. Decant supernatant and wash pellet w/ 1 ml of 75% ethanol.
    a. Be careful not to lose blue pellet!
    b. Add 1 ml of EtOH and vortex until pellet is dislodged from side of microcentrifuge tube
    c. Centrifuge samples at max speed for 10 mins
18. Resuspend in 46 µl of RNase-free $H_2O$.
19. Read RNA conc. (ng/µl), 260/280 nm ratio, 260/230 nm ratio.

**DNase treatment**

1. Add 5 µl of 10X DNAse 1 Buffer and 1 µl of rDNase 1 to the RNA and mix gently
2. Incubate at 37 °C for 20-30 mins
3. Add 5 µl resuspended DNase Inactivation Reagent and mix well.
4. Incubate for 2 mins at RT, mixing occasional.
5. Centrifuge at 10,000 *g* for 1.5 mins and transfer ~45 µl RNA to a new tube.
    a. This will pellet DNase Inactivation Reagent.
    b. Carefully transfer supernatant and not transfer DNase Inactivation reagent.
6. Ensure DNA-free treated RNA comprises only about 20% and no more than 40% of RT-PCR reaction volume.
    a. 20% of 20 µl is 4 µl

b. 40% of 20 µl is 8 µl
c. May increase RT-PCR reaction volume to 50 µl to accommodate DNA-free treated RNA.

| Version | Date | By | Notes |
|---|---|---|---|
| 1.0 | 03/02/16 | Rai Romero | Original protocol |


1 Wang, L. & Stegemann, J. P. Extraction of High Quality RNA from Polysaccharide Matrices using Cetlytrimethylammonium Bromide. *Biomaterials* **31**, 1612, doi:10.1016/j.biomaterials.2009.11.024 (2010).

2 Yu, C., Young, S., Russo, V., Amsden, B. G. & Flynn, L. E. Techniques for the isolation of high-quality RNA from cells encapsulated in chitosan hydrogels. *Tissue Eng Part C Methods* **19**, 829-838, doi:10.1089/ten.TEC.2012.0693 (2013).

# Determination of degree of TMC methylation SOP Kipper Lab

Last updated 06/08/15 by Rai Romero (see Romero LN #7, pg 79)

**Purpose**: To determine the degree of quaternization, demethylation, and O-methylation in synthesized TMC

**Materials needed:**

Synthesized TMC
NMR spectra of TMC (.fid file)
ACD/NMR Processor Software (ver. 12.01)

**Procedure:**

## *NMR spectra processing*

1. Retrieve NMR spectra from e-mail or CIF NMR workstation.
2. Unzip NMR spectra files.
3. Open .fid file in ACD/NMR Processor software.
    a. This will display the spectra in the time domain (see below)

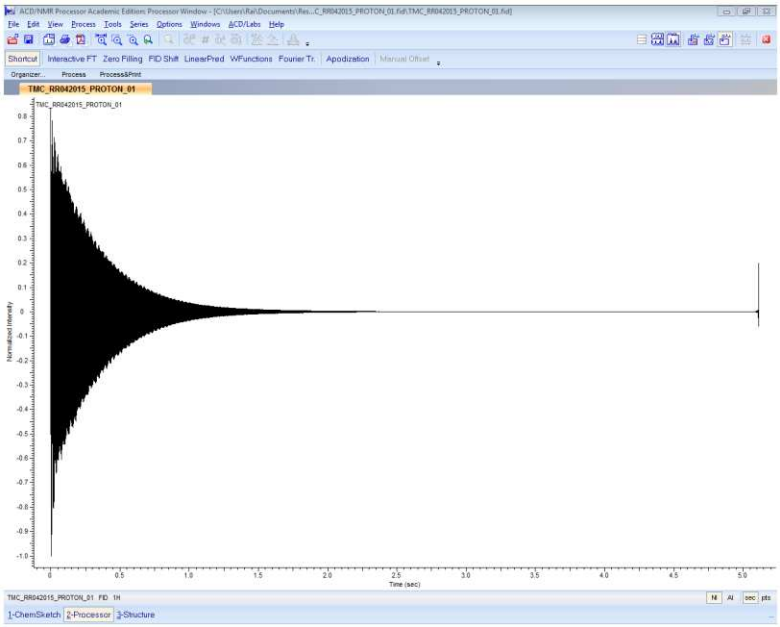

Fig. 1. TMC spectra in the time domain

4. Zero fill spectra by opening zero-fill menu (Zero-filling button).
    a. Original points count: 16384
    b. Change Points counts to 32768
    c. Press Ok.
5. Apply a exponential decay decay curve with a line broadening factor of 0.3 to improve signal-to-noise ratio.

a. Press on WFunctions button (opens Window functions dialog box)
b. LB = 0.3, exponential should be selected
c. Press ok.

6. Apply a Fourier Transform and baseline correction by pressing the shortcut button
    a. Apply fourier transform (default)
    b. Phase
        i. Method = simple
        ii. Equal phase = true
        iii. Fix Ph1 = false
    c. Baseline
        i. Range= full
        ii. Method = “SpAveraging”
        iii. BoxHalfWidth = 30
        iv. Noise factor = 5
    d. This will display the spectra in the frequency domain (see below)

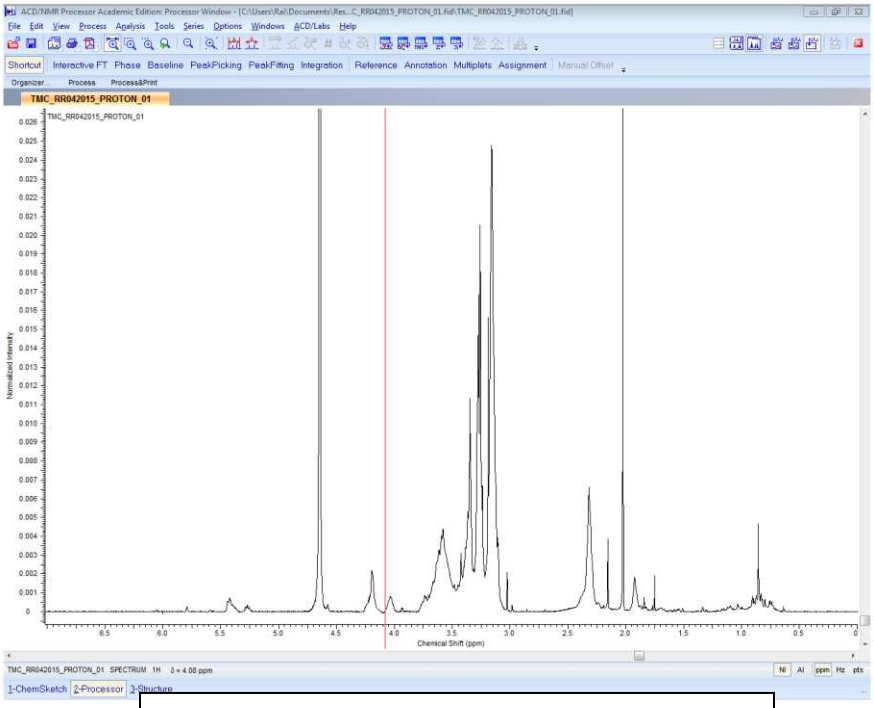


Fig. 2. TMC spectra in the frequency domain

7. Set Reference peak
    a. For $D_2O$ @ 26 °C, set to 4.76 ppm
    b. Reference > click on peak, shift to 4.76 ppm
8. Set Dark regions
    a. Analysis > Dark regions > $D_2O$ (under solvents)
9. Assign peaks of interest

| Functional group | shorthand | ppm shift |
|---|---|---|
| —$N(CH_3)_3$ | DQ | 3.3 |
| —$N(CH_3)_2$ | DD | 2.5 |
| —$OCH_3$, C3 position | $DOM_3$ | 3.5 |
| —$OCH_3$, C6 position | $DOM_6$ | 3.4 |
| —$NHCOCH_3$ | NAc | 2.0 |

10. Integrate peaks and calculate DQ, DM, $DOM_3$, and S according to Romero et al 2014, Supp. Info.

$$DQ = \left[\frac{I_{NQ}}{9} \times \frac{1}{S}\right] \times 100$$

$$DD = \left[\frac{I_{ND}}{6} \times \frac{1}{S}\right] \times 100$$

$$DOM = \left[\frac{I_{OM}}{3} \times \frac{1}{S}\right] \times 100$$

$$S = \frac{I_{NQ}}{9} + \frac{I_{ND}}{6} + \frac{I_{NAc}}{3}$$

"…where $I_{NQ}$ is the integrated signal intensity from the hydrogens in the trimethylated amino group at 3.3 ppm, $I_{ND}$ is the integrated signal intensity from the hydrogens in the dimethylated amino group at 2.5 ppm, $I_{OM3}$ is the integrated signal intensity from the hydrogens in the *O*–methyl groups on the C3 position at 3.5 ppm, and $I_{NAc}$ is the integrated signal intensity from the hydrogens in the *N*–acetyl groups at 2.0 ppm. The degree of *O*–methylation at the TMC C6 position was not calculated due to unreliable peak definition. Degree of methylation values were calculated from TMC dissolved in $D_2O$."[1]

11. Export phased spectrum as ASCII file to plot in Igor.

References

1. Romero, R.; Chubb, L.; Travers, J. K.; Gonzales, T. R.; Ehrhart, N. P.; Kipper, M. J., Coating cortical bone allografts with periosteum-mimetic scaffolds made of chitosan, trimethyl chitosan, and heparin. *Carbohydr Polym* **2015,** *122*, 144-51.

# Use of EDS on SEM SOP Kipper Lab

Last updated 08/17/12 by Rai Romero

**Purpose**: To safely and correctly use the EDS module on the SEM in the CIF in CSU's chemistry dept.

**Materials needed:**
SEM w/ EDS module
Sample
Conducting adhesive tape
**Procedure:**

1. Ensure samples are dry. Beware of surface contamination w/ gloves, forceps etc.
2. Insert samples into test chamber as one would when SEMing.
3. Set working distance (WD) to 10 mm
4. Change probe current to 10
5. On second workstation, open NSS EDS software
6. Under Prog files\Thermo Scientific\NSS, open Automation client
7. Ensure proper parameters are chosen
    a. Column setting
    b. Column Parameter Polling
        i. Time Interval: 1 sec
        ii. Check all boxes: Poll magnification, poll Acc. Voltage, and poll working dist.
8. Click on "Avg. Electron image"
9. Click "Start acquisition"
10. View compass data button toggles between elemental mappings and phases
11. Let appropriate signals be acquired in order to produce a good signal to noise ratio
12. Stop acquisition
13. Calc atomic composition

14. Export to word. In order to export next acquisition, previously exported acquisition Word window must be closed.
15. When done, turn off SEM as usual

# Electrospinning of Chitosan SOP Kipper Lab

Last updated 08/19/12 by Rai Romero

**Purpose**: To electrospin chitosan nanofibers

**Materials needed:**

Electrospinning apparatus
Grounded collector
Aluminum foil
Syringe
Needle
0.35 g of Chitosan
3.5 mL Trifluoroacetic acid (TFA)
1.5 mL Dichloromethane (DCM)
20 mL glass vial
Magnetic stir bar

**Timeline**

| Day 0 | Day 1 | Day 2 (optional) |
|---|---|---|
| **Check spinning supplies**<br>**Start mixing chitosan solution (solution spins for 24 hrs)** | **Espin chitosan solution**<br>**Neutralize chitosan NF mat** | **Further modify w/ PEMs** |

**Procedure:**

1. Add Chitosan and TFA into the vial and mix for 3 hrs
2. Add in DCM and mix for at least 21 hrs. Ensure to achieve a 70:30 mix of TFA/DCM soln.
3. Wash needle and syringe w/ 70:30 TFA/DCM soln
4. Put dissolved chitosan e-spinning soln into syringe and place on syringe pump

5. Set up proper spinning parameters on syringe pump (needle inner diameter, flow rate, needle to collector distance, voltage).
6. Ensure yellow duct tubing is put in the fume hood
7. Wrap collector with aluminum foil (makes cleaning collector easier) and connect negative alligator clip to foil
8. Clip positive alligator clip to needle and turn on DC power supply
9. Turn on syringe pump and E-spin for 3 hrs (observe for first 15 mins to ensure proper e-spinning)

# FTIR KBr Pellet SOP

# Kipper Lab

Last updated 03/12/17 by Rai Romero

**Colorado State University**

**Purpose**: To make a KBr pellet for FTIR transmission analysis

**Materials needed:**

Anhydrous KBr (found in dessicator)
Torque wrench
2 Mortar and pestle
Acetone
DI $H_2O$
Pellet press die set

**Procedure**

Background: Ensure KBr and sample are dried and have minimal residual water. Water has a strong absorption at ~3200-3400 $cm^{-1}$.

Note: Work quickly as KBr is hygroscopic!

**Making the KBr pellet**

1. Crush KBr w/ mortar and pestle
2. Weigh out 90 mg of KBr.
3. Weigh out 10 mg of sample. (Sample should only make about 0.2 to 1% of KBr mixture)
4. Mix 10 mg of sample and 90 mg of crushed KBr together in a new mortar and pestle and thoroughly mix.
5. Add ~100 mg of KBr mixture into bottom disc of die set and collar.
6. Put top disc of die set into collar and rotate 360 to evenly spread mixture onto press columns.
7. Place into manual press and finger tighten bolt onto die set
8. Use torque wrench to slowly apply pressure. Ensure bolt press and die set are aligned.
9. Torque bolt to 20 ft*lbs and hold for 30 seconds. Release and untighten press bolt
10. Remove bottom disc of die set and observe KBr pellet. A good KBr pellet will be clear towards the middle of the disc. If still opaque, repress die set using a slightly higher amount of torque (~30-40 ft*lbs).
11. Clean die press by rinsing w/ DI $H_2O$. Dry quickly with acetone and dry nitrogen gas.

| Version | Date | By | Notes |
|---|---|---|---|
| 1.1 | 03/12/17 | Rai Romero | Added clean-up step. |
| 1.0 | 04/05/16 | Rai Romero | Original protocol |

# HUVEC culture SOP Kipper Lab

Last updated 01/28/15 by Raimundo Romero

**Purpose**: To culture expand HUVEC cells from ATCC (CRL-1730)

**Materials needed:**

| | |
|---|---|
| HUVECs (ATCC; CRL-1730) | F-12K medium (Kaghan's modification) |
| Culture flasks (75 $cm^2$) | Fetal Bovine Serum (FBS) |
| Fibronectin | Heparin |
| Sterile PBS (w/o $Ca^{2+}$, $Mg^{2+}$) | Endothelial cell growth supplement (ECGS) |
| Sterile water | 100X antibiotic/antimycotic solution |
| Warm water bath | 10 and 25 ml serological pipets |
| 37 °C incubator, 5% $CO_2$ | 70% EtOH |
| Media filters | DMSO (for making cryopreservation media) |

**Background:** This SOP is loosely based on Baudin's 2007 paper, A protocol for isolation and culture of human umbilical vein endothelial cells.[1] ATCC's datasheet recommends their HUVECs grown in media consisting of F-12K medium, 0.1 mg/ml heparin, 0.03-0.05 mg/ml ECGS, 10% FBS. Add enough antibiotic/antimycotic to make 1X final concentration.

**Procedure:**

## *Preparation: Making HUVEC media (Makes 500 mls of HUVECs media)*

1. Thaw 50 ml of FBS. (takes ~10-15 mins)
2. Reconstitute 1 vial (15 mg) of ECGS w/ 1 ml of F-12K basal media. May need to vortex
3. To 500 mls of F-12K basal media, add the following
    a. 50 mls FBS
    b. 1 ml of 15 mg/ml ECGS
    c. 50 mg of heparin
    d. Add 5 mls of 100X antibiotic/antimycotic
4. Filter complete F-12K media w/ 0.22 µm media filter.
5. Warm to 37 °C in water bath. (at least 20 mins) **<u>CAREFUL:</u> DO NOT get media neck bottle wet.**

## *Preparation: Coating culture flasks w/ fibronectin solution*

1. Reconstitute 1 mg of fibronectin w/ 1 ml of sterile water. (Sigma datasheet says to dissolve at 37 °C for 30 mins). Make 75 µl aliquots and store at -20 °C for future use.
2. Dilute 75 µl of 1 mg/ml fibronectin into 3 ml of PBS (for each T-75 $cm^2$ flask)
3. Filter sterilize final fibronection solution w/ 0.22 µm syringe filters into 15 ml centrifuge tube or flask

4. Coat each 75 $cm^2$ flask with 3 mls of fibronectin solution. Swish fibronectin solution to evenly coat bottom of flask (Enough to cover bottom of flask).
5. Let flask(s) air dry for 30-40 mins at RT.
6. Leave excess fibronectin solution in flask(s)

### *Seeding HUVECs*

1. Ensure biohood is set up
    a. Ensure culture flasks are fibronectin coated and rinsed.
    b. Ensure complete F-12K media is warmed.
    c. Set aside pipets, pipet tips, centrifuge tubes, aspirator tip etc.
2. Remove HUVEC cryovial from liquid $N_2$ dewar **(USE Protective eyeware! Frozen cryovials may explode from liquid $N_2$ boil off.)**
3. Quickly thaw cryovial in water bath (~37 °C; ~2 mins) until only a small ice pellet is left. **Keep cryovial cap and threads out of water.**
4. Spray cryovial w/ 70% EtOH and move into biohood
5. Transfer cryovial contents to 9 mls of complete F-12K media and spin at ~125 *g* for 5 mins.
6. Remove supernatant and resuspend with 15 mls per cryovial and seed into a new fibronectin-coated 75 $cm^2$ flask.
7. Place culture flask in incubator (37 °C , 5% $CO_2$)

## *HUVECs Media changes*

1. Ensure biohood is set up
    a. Ensure complete F-12K media is warmed.
    b. Set aside pipets, pipet tips, centrifuge tubes, aspirator tip etc.
2. Remove culture flask from incubator and remove old media.
3. Add 20 mls of warmed complete F-12K media to each 75 $cm^2$ flask.
4. Put culture flask(s) back in incubator

## *Splitting (or subculturing) HUVECs*

1. Ensure biohood is set up
    a. Ensure culture flasks are fibronectin coated and rinsed.
    b. Ensure complete F-12K media is warmed.
    c. Set aside pipets, pipet tips, centrifuge tubes, aspirator tip etc.
2. Ensure enough culture flasks have been fibronectin-coated for splitting ratio (usually 1:3 or 1:5)
3. Thaw 0.25% trypsin-EDTA
4. Remove and discard old culture media
5. Rinse cells twice w/ 10 mls of PBS (w/o Ca, Mg)

6. Quickly rinse w/ 1 ml of 0.25% trypsin-EDTA solution. Aspirate
7. Add 3 ml of 0.25% trypsin-EDTA solution to 75 $cm^2$ culture flask
8. Let flask sit for ~5 mins and observe cells w/ inverted microscope until cells have detached
9. Add 7 mls of complete F-12K media to inhibit trypsin.
10. Spin down at ~125 *g* for 6 mins to pellet cells
11. Aspirate supernatant. Either count HUVECs (continue to counting HUVECs section) or resuspend in 10 mls of media.
12. Distribute equal volumes of cell suspension into new fibronectin coated culture flasks according to pre-chosen splitting ratio.

## *Counting HUVECs using Popat Millipore Scepter cell counter*

1. Cells should have been trypsinized and spun down according to previous section (follow up to step 10)
2. Aspirate cell media supernatant. CAREFUL NOT TO ASPIRATE CELL PELLET!!!
3. Resuspend cells in 10 mls of PBS.
4. Ensure cell solution is equally mixed. Transfer a 250 µl aliquot to a 1.5 ml microcent tube
5. Respin down cells left in 15 ml cent tube at ~125 g for 6 mins.
6. While cells are spinning down, initialize Scepter unit by inserting 60 µm sensor chip
    a. Wait until unit is initialized
    b. When ready, place end of sensor chip into 250 µl cell suspension aliquot
    c. Depress plunger
    d. Suck up cell sample by slowly letting go of plunger
    e. Calculate total cell number based on cell concentration

## *Counting HUVECs using hemacytometer and trypan blue exclusion assay*[2]

The following procedure will enable you to accurately determine the cell viability. Cell viability is calculated as the number of viable cells divided by the total number of cells within the grids on the hemacytometer. If cells take up trypan blue, they are considered non-viable.

1. Prepare (or find) a 0.4% solution of trypan blue in buffered isotonic salt solution, pH 7.2 to 7.3 (i.e., phosphate-buffered saline)
2. Add 10 µL of trypan blue stock solution to 100 µL of cells.
3. Load a hemacytometer and examine immediately under a microscope at low magnification.
4. Count the number of blue staining cells and the number of total cells. Cell viability should be at least 95% for healthy log-phase cultures.

    % viable cells = [1.00 – (Number of blue cells ÷ Number of total cells)] × 100

    To calculate the number of viable cells per mL of culture, use the formula below. Remember

to correct for the dilution factor.

Number of viable cells × $10^4$ × 0.110 mls = cells/mL culture

## *Cryopreserving HUVECs*

1. Ensure biohood is set up
    a. Set aside pipets, pipet tips, centrifuge tubes, cryovials, aspirator tip etc.
2. Make HUVEC cryopreservation media (95% complete F-12K HUVEC media, 5% (v/v) DMSO)
    a. For 10 mls, add 0.5 ml to 9.5 mls of cold complete F-12K media
3. Trypanize cells using same steps as in splitting HUVECs section
4. Count cells
5. Pipet cells into 15 ml cent tube and spin down at 125 *g* for 5 mins
6. Aspirate supernatant and resuspend HUVECs at ~1x$10^6$ cells/ml
7. Dispense 1 ml of HUVEC cell solution into cryovials
8. Ensure bottom portion of Mr. Frosty has adequate volume of 100 % isopropanol (250 ml)
9. Place tightly sealed cryovials into Mr. Frosty and put back in -80 °C to achieve near 1 °C/min cooling rate.
10. Leave undisturbed for a minimum of 4 hours. Then transfer cryovials to vapor phase liquid $N_2$ storage.

## *Calculation of g forces for centrifuge*[3]

$$g = (1.118\times10^{-5}) * R * S^2$$

Where

$g$ = relative centrifugal force = RCF

R = radius of rotor in centimeters

S = speed of centrifuge in RPM

Eppendorf Rotor sizes

| Rotor | Radius (cm) | Max RPM |
|---|---|---|
| A-4-44 | 16. 1 | 5,000 |
| A-45-xx | 9.5 | 14,000 |

*References*

1. Baudin, B.; Bruneel, A.; Bosselut, N.; Vaubourdolle, M., A protocol for isolation and culture of human umbilical vein endothelial cells. Nature Protocols 2007, 2 (3), 481-485.

2. Trypan Blue Exclusion Protocol. Life technologies. Acessed 1/28/15. http://www.lifetechnologies.com/us/en/home/references/gibco-cell-culture-basics/cell-culture-protocols/trypan-blue-exclusion.html

3. Thermo Tech Tip #40: Convert between times gravity (x g) and centrifuge rotor speed. Thermo Scientific. Acessed 1/28/15. http://www.thermofisher.co.nz/Uploads/file/Scientific/Applications/Life-Science-Research-Technologies/Convert-between-times-gravity-(x%20g)-and-centrifuge-rotor-speed-(RPM)-(Tech-Tip-40).pdf

# Luc-mASCs culture SOP Kipper Lab

Last updated 03/3/16 by Raimundo Romero

**Purpose**: To culture expand luciferase expressing ASCs isolated from mouse adipose tissue

**Materials needed:**

- DMEM, low glucose (Corning, 10-014-CM)
- Fetal Bovine Serum (FBS)
- MEM vitamin solution, (Corning, 25-020-CI)
- MEM non-essential amino acids (Corning, 25-025-CI)
- 100X antibiotic/antimycotic solution
- Culture flasks (75 $cm^2$)
- Sterile PBS (w/o $Ca^{2+}$, $Mg^{2+}$)
- Sterile water
- Warm water bath
- 37 °C incubator, 5% $CO_2$
- Media filters and sterile bottle
- 10 and 25 ml serological pipets
- 70% EtOH
- DMSO (for making cryopreservation media)

**Background:** Luc-ASCs were isolated from abdominal adipose tissue from FVB transgenic mice made to express luciferase. Adding D-luciferin (firefly) causes live cells to produce bioluminescence.

**Procedure:**

## *Preparation: Making Luc-mASCS growth media (Makes 1L of media)*

1. Growth Media formulation:
    a. 500 mLs of DMEM, low glucose (1g/L of glucose)
    b. 75 ml of FBS (15% final conc.)
    c. 10 ml 100X MEM vitamins
    d. 5 ml 100X MEM non-essential amino acids (1X final conc.)
    e. 5 ml of antibiotic/antimycotic solution (1% final conc.)
    f. Sterile filtered
2. Thaw FBS, MEM vitamin solution, & anti/anti aliquots. (takes ~15 mins)
3. Mix all reagents together in DMEM bottle
4. Filter growth media w/ 0.22 μm media filter.
5. Warm to 37 °C in water bath. (at least 20 mins) **<u>CAREFUL:</u> DO NOT get media neck bottle wet.**

## *Preparation: Making Luc-ASCS osteogenic media (Makes 500 ml of media)*

1. Osteogenic Media formulation[1]:
    a. Makes 200 ml Luc-mASCs osteogenic media (no dexamethasone supplementation)

b. 8 mLs of 0.5 M β-glycerophosphate
    i. 8 mls of ASC growth media
    ii. Add 0.8642 g of β-glycerophosphate
    iii. Add all 8 mls of 0.5 M β-glycerophosphate to 192 mls of ASC growth media
c. 1 ml of 0.05 M L-ascorbic-2-phosphate
    i. Add 0.01448 g of M L-ascorbic-2-phosphate to 1 ml of DI $H_2O$
    ii. Makes 1 ml of 0.05 M L-ascorbic-2-phosphate
    iii. Add 200 µl of 0.05 M L-ascorbic-2-phosphate to 200 mls of ASC growth media

2. Makes 200 mls of ASC osteogenic media supplemented w/ 20 mM β-glycerophosphate and 50 µM L-ascorbic acid-2-phosphate
3. Filter growth media w/ 0.22 µm media filter.
4. Warm to 37 °C in water bath. (at least 20 mins) **CAREFUL: DO NOT get media neck bottle wet.**

### *Seeding Luc-mASCs*

1. Ensure biohood is set up
    a. Ensure complete Luc-mASCs (growth or osteogenic) media is warmed.
    b. Set aside pipets, pipet tips, centrifuge tubes, aspirator tip etc.
2. Remove Luc-ASCs cryovial from liquid $N_2$ dewar **(USE Protective eyeware! Frozen cryovials may explode from liquid $N_2$ boil off.)**
3. Quickly thaw cryovial in water bath (~37 °C; ~2 mins) until only a small ice pellet is left. **Keep cryovial cap and threads out of water.**
4. Spray cryovial w/ 70% EtOH and move into biohood
5. Transfer cryovial contents to 4 mls of ASC growth media and spin at ~125 *g* for 5 mins.
6. Remove supernatant and resuspend with 5 mls per cryovial and seed into a new 25 $cm^2$ flask.
7. Place culture flask in incubator (37 °C , 5% $CO_2$)

## *Luc-mASCs Media changes*

1. Ensure biohood is set up
    a. Ensure complete Luc-mASCs media is prewarmed.
    b. Set aside pipets, pipet tips, centrifuge tubes, aspirator tip etc.
2. Remove culture flask from incubator and remove old media.
3. Add 17 mls of warmed complete Luc-mASCs media to each 75 $cm^2$ flask (5 mls for 25 $cm^2$)
4. Put culture flask(s) back in incubator

### *5. Splitting (or subculturing) Luc-mASCs*

6. Ensure biohood is set up

a. Ensure complete Luc-mASCs media is warmed.
b. Set aside pipets, pipet tips, centrifuge tubes, aspirator tip etc.

7. Thaw 0.25% trypsin-EDTA
8. Remove and discard old culture media
9. Rinse cells once w/ 4 mls of PBS (w/o Ca, Mg). Aspirate PBS
10. Add 4 ml of 0.25% trypsin-EDTA solution to 75 $cm^2$ culture flask
11. Let flask sit for ~5 mins and observe cells w/ inverted microscope until cells have detached
12. Add 8 mls of complete ASC growth media to inhibit trypsin.
13. Distribute equal volumes of cell suspension into new culture flasks according to splitting ratio.

### *Counting Luc-mASCs using Popat Millipore Scepter cell counter*

1. Cells should have been trypsinized and spun down according to previous section (follow up to step 10)
2. Aspirate cell media supernatant. CAREFUL NOT TO ASPIRATE CELL PELLET!!!
3. Resuspend cells in 10 mls of PBS.
4. Ensure cell solution is equally mixed. Transfer a 250 µl aliquot to a 1.5 ml microcent tube
5. Respin down cells left in 15 ml cent tube at ~125 g for 6 mins.
6. While cells are spinning down, initialize Scepter unit by inserting 60 µm sensor chip
    a. Wait until unit is initialized
    b. When ready, place end of sensor chip into 250 µl cell suspension aliquot
    c. Depress plunger
    d. Suck up cell sample by slowly letting go of plunger
    e. Calculate total cell number based on cell concentration

### *Counting Luc-mASCs using hemacytometer and trypan blue exclusion assay*[2]

The following procedure will enable you to accurately determine the cell viability. Cell viability is calculated as the number of viable cells divided by the total number of cells within the grids on the hemacytometer. If cells take up trypan blue, they are considered non-viable.

1. Prepare (or find) a 0.4% solution of trypan blue in buffered isotonic salt solution, pH 7.2 to 7.3 (i.e., phosphate-buffered saline)
2. Add 10 µL of trypan blue stock solution to 100 µL of cells.
3. Load a hemacytometer and examine immediately under a microscope at low magnification.
4. Count the number of blue staining cells and the number of total cells. Cell viability should be at least 95% for healthy log-phase cultures.

    % viable cells = [1.00 – (Number of blue cells ÷ Number of total cells)] × 100

    To calculate the number of viable cells per mL of culture, use the formula

below. Remember to correct for the dilution factor.

Number of viable cells × $10^4$ × 0.110 mls = cells/mL culture

## *Cryopreserving Luc-mASCs*

11. Ensure biohood is set up
    a. Set aside pipets, pipet tips, centrifuge tubes, cryovials, aspirator tip etc.
12. Make Luc-ASCs cryopreservation media (2x)
    a. 4 ml of ASC growth media
    b. 4 mls FBS
    c. 2 mls DMSO
13. Trypsinize cells using same steps as in splitting Luc-ASCs section
14. Count cells.
15. Pipet cells into 15 ml cent tube and spin down at 125 *g* for 5 mins
16. Aspirate supernatant and resuspend Luc-ASCs at ~2x$10^6$ cells/ml
17. Add equal volume of ASC freeze media, dropwise to ASCs in growth media to make final ASC conc 1x$10^6$ cells/ml
18. Ensure bottom portion of Mr. Frosty has adequate volume of 100 % isopropanol (250 ml)
19. Place tightly sealed cryovials into Mr. Frosty & put back in -80 °C to achieve near 1 °C/min cooling rate.
20. Leave undisturbed for a minimum of 4 hours. Then transfer cryovials to vapor phase liquid $N_2$ storage.

## *Calculation of g forces for centrifuge*[3]

$$g = (1.118\times10^{-5}) * R * S^2$$

Where

$g$ = relative centrifugal force = RCF

R = radius of rotor in centimeters

S = speed of centrifuge in RPM

Eppendorf Rotor sizes

| Rotor | Radius (cm) | Max RPM |
|---|---|---|
| A-4-44 | 16. 1 | 5,000 |
| A-45-xx | 9.5 | 14,000 |

| Date | Version | Update by | Notes |
|---|---|---|---|
| 3/3/16 | 1.1 | Rai Romero | Updated osteogenic media supplementation section |
| 1/27/15 | 1.0 | Rai Romero | Original protocol |

## *References*


1. Reger, RL, Tucker, AH, Wolfe, MR. Differentiation and characterization of human MSCs. Chapter 7. Methods in Molecular biology vol 449, Mesenchymal Stem Cells: Methods and Protocols. Eds D.J. Prockop, D.G. Phinney, and B.A. Bunnelt. Humana Press, Totowa, NJ.

2. Trypan Blue Exclusion Protocol. Life technologies. Acessed 1/28/15. http://www.lifetechnologies.com/us/en/home/references/gibco-cell-culture-basics/cell-culture-protocols/trypan-blue-exclusion.html

3. Thermo Tech Tip #40: Convert between times gravity (x g) and centrifuge rotor speed. Thermo Scientific. Acessed 1/28/15. http://www.thermofisher.co.nz/Uploads/file/Scientific/Applications/Life-Science-Research-Technologies/Convert-between-times-gravity-(x%20g)-and-centrifuge-rotor-speed-(RPM)-(Tech-Tip-40).pdf

# Lyophilizer pump oil change SOP Kipper Lab

Last updated 06/13/14 by Rai Romero **Colorado State University**

**Purpose**: To change the oil in the Hyvac 7 vacuum pump that runs the lyophilizer

**Materials needed:**

Welch Duoseal Pump oil, high vacuum (can be purchased at chem stockroom) cat no. 64742-65-0
Flathead screwdriver
Funnel
Beaker (for adding clean oil)
Tubing (for draining oil)
Used oil bucket and waste container
Mop & bucket, floor cleaner/degreaser
Gloves & paper towels (lots!)
Absorbent mats

**Notes:**

This can be a messy job! Wear lab coat and lab shoes.

Oil should be changed **at least** every 6 months or sooner, depending on the amount of use.

The James group has a dedicated funnel, beaker, & tubing for pump oil changes in Room 371 (Ensure funnel and beaker are clean. If not, rinse with fresh pump oil first before using.)

**Procedure:**

1. Run pump for about 30 mins in order to warm oil and make it less viscous.
2. Remove vacuum tubing on inlet port of the pump and move pump onto the counter. Inspect pump for any obvious leaks/wear & tear
3. Attach tubing to drain valve and drain oil into a used oil bucket until oil trickles out.
4. Close drain valve.
5. Add about 500 mls of clean oil and pulse in order to circulate oil
    a. Turn on pump and alternatively open and close inlet port (w/ hand) periodically to agitate oil in pump for 15 mins
6. Drain oil again.
7. Close drain valve and refill pump with oil (oil is added through the inlet port)
    a. The Hyvac 7 pump requires 1.5 qts (=1.4 L) of oil
    b. Usually the pump needs to be pulsed on and off in order to fully fill pump w/ 1.4 L of oil
    c. Oil should be added until oil level reaches the midway point of the oil level sight glass.
8. Replace pump in lyophilizer and reattach vacuum tubing to inlet. Run pump to see if it sounds normal
9. Pour old oil into used oil waste container.
10. Clean up area and mop up any spilled oil.

# Fluorescent Staining Mammalian Cells SOP Kipper Lab

Last updated 01/20/16 by Rai Romero **Colorado State University**

**Purpose**: To stain mammalian cells w/ Calcein-AM, Rhodamine phalloidin, & DAPI

**Materials needed:**

50 µg Calcein-AM lyophilized powder

DMSO, anhydrous

PBS (w/ added Ca2+ and Mg2+)

DAPI stock soln (1 mg/ml)

Rhodamine Phalloidin lyophilized powder

100% methanol

**Procedure:**

1) Reconstitute Calcein-AM stain and begin thawing DAPI stock solution **ENSURE TO THROUGHLY MIX STAINS BEFORE! At least 15 mins. Use vortexer!**
    a. Found in -20 °C Kipper freezer
    b. 25 µL of DMSO per 50 µg Calcein-AM lyophilized powder. Vortex for at least 20 mins.
    c. 8 µL of 2 µg/µL (2 mM stock soln) Calcein into 4 mLs of PBS makes 4 µM Calcein soln
    d. PROTECT FROM LIGHT! Working soln only good for day of making; freeze stock soln at -20 °C

2) Remove samples from incubator. Transfer samples to new staining multiwell plate. Return other samples to incubators

3) Rinse once w/ PBS. Aspirate PBS

4) Place Calcein-AM working soln on cells. Return to **37 °C** incubator for **35 mins**

5) Retrieve samples from incubator. Rinse twice w/ PBS

6) Fix cells w/ 3.7% formaldehyde for **15 mins @ Room temp**. Rinse w/ PBS 3x.

7) Permeabilize cells w/ 1% Triton-X soln for **3 mins**. Rinse w/ PBS 3x.

8) If adding Actin stain, make working solution at 5 µg/ mL. **Skip in not staining actin**!!!
    a. To make working soln from stock actin soln, put 16 µL of stock soln into 3.2 mLs of PBS
    b. Stock soln is 500 µL of 100% methanol into 1 vial of actin stain

c. Incubate for **25 mins @ Room temp**.

9) Make DAPI working soln
    a. Dilute DAPI stock solution 1:1000 in PBS (5 µl DAPI stock solution into 5 mls of PBS)

10) Incubate at RT for 5 mins. Aspirate staining soln, then rinse once w/ PBS. Aspirate. Cover w/ foil.

11) Image w/ microscope!

# microCT analysis SOP Kipper Lab

Last updated 3/17/15 by Rai Romero

**Purpose**: To calculate healing callus, total bone volume, pMOI

**Materials needed:**

µCT .ISQ data file

TIME

**Background:**

IMPORTANT: Contouring µCT data in the µCT software is very finicky and particular. Ensure to follow these instructions EXACTLY as stated. Otherwise, time will be lost and/or data will not be saved appropriately. Contouring is an iterative process to get the best fit. LEARN TO use the morph function in the contouring dialog box. When saving contour files, the software will always keep previous contour versions. Ensure to keep a log of the contour (.GOBJ) file and its associated analysis.

**Procedure:**

1. Change operator name to "Raimundo Romero" or appropriate operator name.
2. In control box window, click on evaluate button. (Brings up µCT evaluation program window)
3. Click File > Select measurement to open file(s) to evaluate (search=Kipper)
4. Open .ISQ file.
5. Decide which allograft will be evaluated (smaller animal number will be on the bottom of the two allos in the drawing field)
6. Click on "Delete objects of all images" button. IMPORTANT!!! Don't forget to do.

7. Zoom in on appropriate allo (Zoom>Zoom 5X). Ensure the allo/tissue is entirely in view throughout all slides to be analyzed.
8. Determine proximal junction slide number—Record #
9. Determine distal slide number—Record #
10. Select the first slide to be contoured (Proximal junction-100) in the image selection area.
11. Begin contouring by selecting the "Draw contour" symbol from the Drawing symbols toolbar on the left of the evaluation program dialog window
    a. First draw a contour in the counter-clockwise direction to outline the outside of the allograft
    b. Reselect the draw contour tool
    c. Then draw a contour in the clockwise direction to outline the inside of the tissue/allograft
    d. Double click on the contour handles in order to optimize contour fit.
    e. This automatically sets this image/slide as a brakepoint
    f. IMPORTANT: The **direction (counter-clockwise or clockwise)** and the **order (outside contour first, then inside contour)** of drawing the contours is EXTREMELY importance. Follow above directions EXACTLY or suffer hours of life wasted.
12. Select the next slide (typically selected at 10-slide intervals—less if bone changes rapidly or more if bone changes minimally). Begin contouring the next slide repeating steps 8.
    a. This second slide will then be set as another brakepoint.
13. To use the morph function

a. Open the contouring dialog box by clicking on the “C...” symbol in the drawing symbols toolbar or go to Tasks > Countouring.
    i. Set outer value = 31
    ii. Set inner value = 500
    iii. Global scaling (X/Y) = 1.00
b. Ensure 2 brakepoints have been set (should appear as 2 green boxes in the image selection area; each green box represents one slide/image with drawn contours).
c. Under selection, select Range. Note range.
d. In order to interpolate contours between 2 set points, select the next slide next to the first brakepoint. (Ex. If your first brakepoint is slide 538, highlight 539 in the image selection area.)
e. Note that the range should now be from your currently selected slide to the second brakepoint.
f. Click on the morph button to interpolate contours.
g. ALWAYS Double check the accuracy of interpolated contours. Edit as necessary.

14. Continue to contour the rest of the sample capturing the necessary ROI.
15. Save contours by selecting File > save GOBJ. DO NOT rename/edit file name in ANYWAY.
16. Evaluate for bone volume
    a. Ensure necessary ROI has been contoured
    b. Select Tasks > 3D evaluation
    c. Select “9: Midshaft evaluation”
        i. Click on “Default VOI”

ii. Adjust Z parameters.

1. Set VOI Start: to first slide of analysis
2. Z Dim: the additional number of slides to be analyzed
    a. Ex. VOI Start: 1  Z Dim: 25 means that the analysis will include slides 1 to 26 as VOI Start + Z Dim = Final slide number

iii. Set threshold (Keep the same for all bones analyzed!!!!)

1. Lower = 260
2. Upper = 1000

iv. Gausss sigma = 0.8; Gauss support = 1

d. Wait for evaluation to finish then record BV for sample.

# microCT backup SOP Kipper Lab

Last updated 12/04/14 by Rai Romero

**Purpose**: To backup raw data files from microCT server

**Materials needed:**

Magnetic tape drive

Time

**Background:**

IMPORTANT: microCT acquires data in a raw format first (.RSQ files) then transforms the data into an image file (.ISQ file) which allows viewing of cross sectional images used for data processing such as bone volume analysis, and 3D reconstructions. It is paramount to backup the .RSQ raw files FIRST as losing these files makes the data unrecoverable and would require rescanning a sample. Image files (.ISQ files) should only be backed up after evaluations are completed or when space needs to be cleared up on the microCT server. Raw and image files are backed up on separate magnetic tape drives. Use appropriate magnetic tape drive for each file type.

**Procedure:**

1. Ensure to read background section first!
2. Change operator name to “Raimundo Romero” or appropriate operator name.
3. In control box window, click on floppy disk button. (Brings up µCT backup program window)
4. Find files you want to back up by filtering/searching for files.

5. Retrieve magnetic tape on shelf in μCT room and insert into HP StorageWorks Ultrium 960 disk drive
6. Mount magnetic tape using the mount button. Note amount of free space on magnetic tape drive*

   *Free space on magnetic tape drive doesn't always correlate exactly to displayed free space. Magnetic tape drives say they can fit 800 Gb. This is for compressed data. Tapes can only fit ~380 Gb uncompressed data. Transfer will throw an error code if data cannot fit on magnetic tape. If this happens, mark the full magnetic tape with an X and change out to a tape with available free space.
7. Highlight appropriate file name.
8. Select Raw under selected measurement
9. Ensure "move to" is chosen (as opposed to "copy to") for moving raw data.
10. Ensure transfer destination selected is magnetic tape. Symbol seen in Figure 1 should be displayed.

Figure 1. Magnetic Tape
Transfer Destination

11. Click on start, which immediately begins file transfer.
12. Record which magnetic tape raw file has been transferred to.
13. Repeat as necessary.
14. Once finished, dismount magnetic tape drive using dismount button.
15. Put back magnetic tape drive on shelf.

# Murine Bone Cleaning SOP Kipper Lab

Last updated 1/30/14 by Rai Romero **Colorado State University**

**Purpose**: To effectively clean bone for subsequent surface modification

**Materials needed:**

Milipore water (enough to submerge bones)
70% EtOH
sonicator
Microcent tube or scintillation vial
26 ½ gauge needle
5 mL disposable syringe
Paper towels
Razor blade
Microcentrifuge tube float holder

**Procedure:**

1. Thaw bones at room temp
2. Agitate bones in Millipore water for 10 mins
3. Remove bone marrow tissue by running needle thru intramedullary cavity of bone and rinsing with Millipore water
4. Scrape diaphyseal surface of bone w/ razor blade
5. Put bone in microcent tube and fill w/ 70% EtOH (or put multiple bones in 20 ml vial)
6. Place in sonicator and sonicate for 3 hrs
7. Aspirate used 70% EtOH and replace w/ new soln. Vortex for 30 s.
8. Aspirate EtOH and dry under vacuum for at least 2 hrs
9. Use immediately or store in 8 °C fridge until needed. No long term storage in fridge.

# NMR of Polysaccharides SOP Kipper Lab

Last updated 05/21/15 by Rai Romero

**Purpose**: To safely and correctly use the NMR located in the CIF in CSU's chemistry dept.

**Materials needed:**

NMR tubes and cap
Vial (for solid samples)
Mini stir bar
Sample (solid or liquid)
Rubber bulb and Glass pasteur pipet
Deuterated solvent ($CDCl_3$, $D_2O$ etc.)

**Procedure:**

## *NMR tube Cleaning Procedure*

1. Remove old samples from 5 mm NMR tube.
2. Rinse 3x acetone, aspirating acetone with liquid trap .
3. Rinse 2x with Millipore water, aspirating water with liquid trap.
4. Let air dry or if in hurry perform a final rinse with $D_2O$ before sample addition.
   DO NOT USE HEAT TO DRY NMR TUBES AS THIS MAY DEFORM THE NMR TUBES!!!!

## *Solid Sample Prep:*

1. Determine appropriate solvent for solid material. Common NMR solvents are $CCl_4$, $D_2O$, $CDCl_3$.
   If unknown, try non-deuterated version of solvent FIRST! (deuterated solvents are EXPENSIVE!!!)
2. Dissolve sample with deuterated solvent in vial. (For polysaccharides, 5 mg/ml in $D_2O$ is a good starting point, acidified $D_2O$ for chitosan)

3. Ensure sample is completely dissolved (ie no chunks or particulate matter). May need

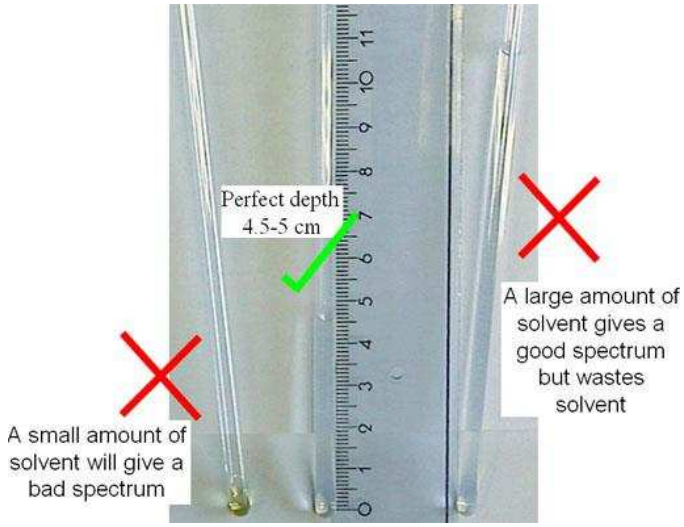


to stir overnight.
4. Add ~1 ml or at least 4-5 cm of dissolved sample into clean NMR tube.
5. Determine appropriate internal standard, if applicable.

*Loading sample for 400 Mhz robotic NMR (more detailed step-by-step procedure is available via the CIF)*

**Walkup operator login**

1. Obtain access and get trained to use CIF NMRs
2. Agilent 400 MHz robotic NMR is first come, first serve, walkup instrument
3. Login info is <your EID> and password is nmr4CSU
4. Access autosampler by pressing access request button on robot control panel.
5. Find an empty sample position in sample tray 1

**Robot Control Panel**

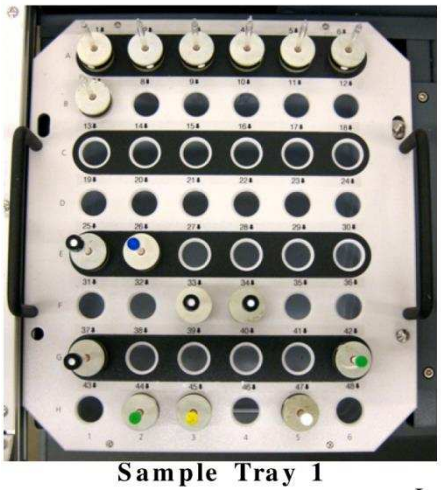
**Sample Tray 1**

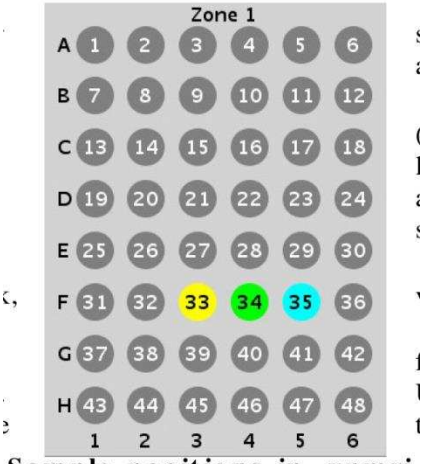

**Sample positions in vnmrj**

6. Verify sample position is empty by checking daily sample log
7. Take empty spinner turbine from tray 2 and insert NMR tube containing your sample.
8. Double check NMR tube straightness tube gauge on desk. Also check sample is centered using depth gauge.
9. **IMPORTANT:** Without removing or sliding NMR tube in spinner turbine, wipe down outside of NMR tube with ethanol using a kimwipe.
10. **DO NOT REMOVE TURBINE #96 FROM SAMPLE TRAY #2.** If it is empty, leave it empty.

Turbine # 96

*Setting up experiment/study queue in VNMRJ*

1. You must click on New Study, to start a new experiment.
2. Highlight the correct sample position in the sample position map in the VNMRJ software. (Sample position outlined with a dotted lined is currently selected sample position.)
3. Click on the correct protocol in the protocols tab panel. This adds the protocol in the study queue.
4. Double click on the protocol in the study queue to open and edit it.
5. Enter sample info in the start tab in the sample info panel.
6. Enter sample name and solvent.
7. Verify/enter correct email in Eaddr box
8. In the acquire tab in the sample info panel, study parameters can be changed.
9. For chitosan and TMC proton NMR's, the following parameters should be used:
    a. Pulse angle= 90°

b. Relaxation time (d1)= 10 s
c. Number of scans= 128
d. Acquisition time= ~2.5 s
e. Saturation mode = no
f. Room temp.

10. Once all parameters have been edited and studies have been added to the study queue, click submit in the study queue panel.
    a. To apply current studies in study queue to another sample located in a different sample position:Select new sample position.
    b. Change sample name.
    c. Double check appropriate studies are in the study queue.
    **d.** Click submit. No need to reenter study parameters.

Protocols tab panel

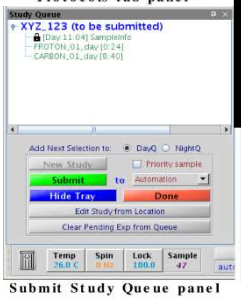

Submit Study Queue panel

Enter sample info panel

Sample Position map or Spectrum viewer

Vnmrj software interface

**Polyelectrolyte Multilayer (PEM) Assembly**

**Date:**_____

PH:

| Time (min) | Step | Start | Stop |
|---|---|---|---|
| 0 | Rinse | | |
| 5 | Chitosan | | |
| 10 | Rinse | | |
| 15 | Heparin | | |
| 20 | Rinse | | |
| 25 | Chitosan | | |
| 30 | Rinse | | |
| 35 | Heparin | | |
| 40 | Rinse | | |
| 45 | Chitosan | | |
| 50 | Rinse | | |
| 55 | Heparin | | |
| 60 | Rinse | | |
| 65 | Chitosan | | |
| 70 | Rinse | | |
| 75 | Heparin | | |
| 80 | Rinse | | |
| 85 | Chitosan | | |
| 90 | Rinse | | |
| 95 | Heparin | | |
| 100 | Rinse | | |
| 105 | Stop | | |

**Notes:**

# Polysaccharide Nanoparticle Preparation SOP Kipper Lab

Last updated 08/10/15 by Raimundo Romero

**Purpose**: To prepare nanoparticles from 2 oppositely charged polyelectrolytes

**Materials needed:**

sodium acetate
acetic acid, (concentrated/glacial)
Ultrapure water (Resistivity > 18.0 MΩ·cm)
polysaccharides (chitosan, heparin, HA, etc)

**Procedure:**

1. Prep 200 ml 0.1 M Na-acetate solution
    a. 200 ml ultrapure water
    b. 1.64 g of Na-acetate
    c. Mix until dissolved

2. Prep 200 ml 0.1 M acetic acid solution
    a. 200 ml ultrapure water
    b. 1.149 ml of glacial acetic acid
    c. Mix until homogenous

3. Calibrate pH meter, immerse in 0.1 M Na-acetate solution and titrate to pH 5 w/ 0.1 M acetic acid solution. This makes a pH 5 0. M acetate buffer solution.

4. Make 2 mg/ml solutions of each polyelectrolye in 0.1 M acetate buffer
    a. Measure 25 mls of 0.1 M acetate buffer
    b. Measure 50 mg of one polyelectrolyte
    c. Mix until dissolved (at least 2 hours)
    d. Repeat A-D for the other polyelectrolyte
5. Filter polyelectrolyte solutions with 0.22 μm PVDF syringe filters.
6. For example, to make 1:4 chitosan and heparin nanoparticles:
    a. Begin stirring 16 mls of heparin in a 100 ml beaker at 800 rpm w/ 1 in. stir bar
    b. Using one-shot addition, add 4 ml of chitosan solution
    c. Stir for 3 hours
7. Allow nanoparticle solution to sit overnight for larger particles to settle to bottom of beaker
8. Aliquot supernatant into 1.5 ml microcentrifuge tubes.
9. Centrifuge at 4500 *g* for 20 mins.
10. After centrifugation, visually confirm nanoparticle pellet on bottom of microcentrifuge tube.
11. Decant supernatant
12. Resuspend nanoparticles in 50 μl of ultrapure water or pH-buffered solution.
    a. May need to rigorously vortex in order for nanoparticles to resuspend.

# Pore Size Determination Using ImageJ SOP Kipper Lab

Last updated 08/16/12 by Rai Romero

**Purpose**: To determine pore sizes of tissue engineered scaffolds from SEM images using ImageJ

**Materials needed:**

ImageJ software (freeware; download from http://rsbweb.nih.gov/ij/download.html)

SEM images

**Procedure:**

1. Open image
2. Create duplicate of image (ctrl+shift+D)
3. Select Line tool and draw line the width of the scale bar on SEM image and measure distance in pixels
4. Set scale of image using ImageJ Set scale command (Analyze > Set scale). Check global
5. Change image type from RGB→ 8-bit ( Image > Type > 8-bit)
6. Normalize histogram (Process > Enhance contrast)
    a. Saturated pixels = 1%
    b. Check normalize
7. Subtract background (Process > Subtract Background)
    a. Determine best rolling ball radius. RECORD!!!
8. Threshold Image (Image > Adjust > Threshold)

    a. RECORD THRESHOLD LIMITS!!!!

9. Use Fill holes command (Process > Binary > Fill holes)
10. Set appropriate measurements

a. Check area, Feret's diameter, limit to threshold
b. Measure 4-5 areas of interest to get a rough estimation of areas to be measured. This will be used in order to set the lower bound of particles to be included in subsequent analysis
c. Measure major and minor axis of pores to roughly calculate area of ellipse

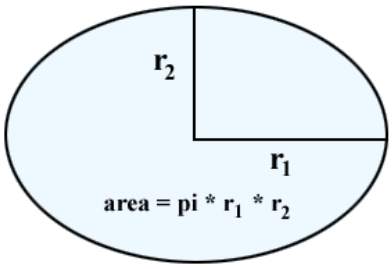


.

11. Analyze particles (Analyze > Analyze particles)

    a. Size: 10000-Infinity
    b. Circularity: 0-1
    c. Show: Outlines
    d. Checked: Display results, clear results, summarize, record starts

12. Select new window with outline mask. Invert color cheme (Image > Lookup tables > invert LUT)

13. Change toddds another color (red or green…. Etc.)

14. Invert color again and change image type to RGB. Save mask.

15. Use image calculator to overlay inverted mask onto original image (Process > Image calculator). Original image should be image 1 and the mask image 2. Select add function

    e. Check "create new window"

# Spectra-Tech Continuum IR Microscope SOP Kipper Lab

Last updated 11/16/12 by Rai Romero

**Purpose**: To acquire IR spectra using the Continuum IR microscope module in reflectance mode

**Materials needed:**

Sample (the more reflecting, the better)
Omnic Software
Standards for alignment
Glass slide
Microscope components

Fig. 1

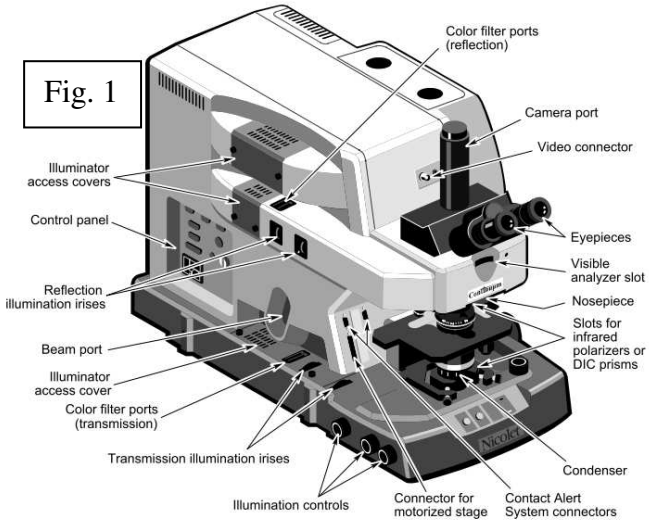


Fig. 2

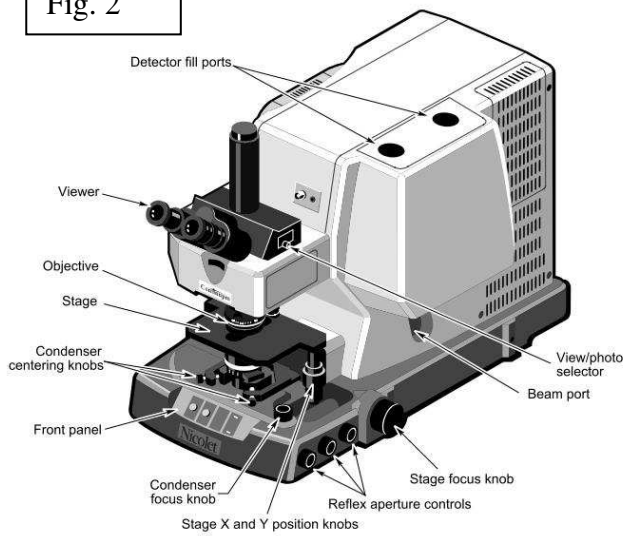

Fig. 3

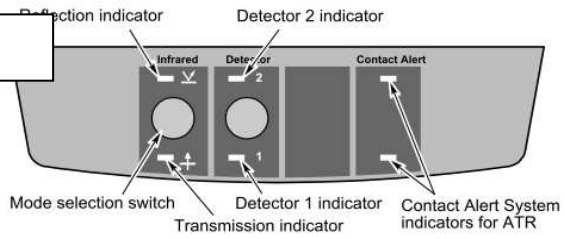


*Front panel*

**Procedure:**

1. Cool detector 1 on the IR microscope module w/ liq. $N_2$ using provided thermos. The detector is cooled w/ ~750 mL liq. $N_2$ (~26 fl. Oz). Let detector stabilize for 20 mins before analyzing samples. Once cooled, the detector should remain cold for ~18 hrs. (Nicolet Continuum User Guide p 10)

2. From Fig. 2 above, rotate the beam port knob all the way clockwise to ensure the "scope" beam path is engaged. (Note: Beam port knob is loose. Shoving it in while turning helps)

3. Open purge valve located between workstation tower and the Magna-IR AEM

4. Open Omnic software

5. In Experiment drop down menu, select appropriate experimental setup

6. To edit current experimental setup: Collect > Experimental Setup (Crtl+E)

7. Select Bench tab. Move sample on sample stage until max signal is obtained (about 0.3-0.4 for Freeze dried chitosan on allograft

8. Aperture iris wheel down (towards check mark) (From Fig. 1: reflection Illumination irises)

9. Field Iris wheel up (towards check mark) (From Fig. 1: reflection Illumination irises)

10. Reflex Aperture knob turned clockwise

11. Reflex Aperature controls (Fig. 2) allows to change the field of view

12. To collect background, use Spectra Tech Au mirror found in drawer 5.2, in wooden box labeled Spectra Tech

13. Use 10x objective to bring sample into rough focus

14. Turn nosepiece to infrared objective (big black one) and focus sample.

15. Drop plastic cover  around sample(s)

16. Acquire background spectrum and save background spectra. (Remember file location!)

17. In experimental set up, choose to “Use background from file” and find previously acquired background spectra

18. Collect sample spectra!

# Water bath cleaning Protocol — Mammalian Cell Culture Room (367)

Last updated 06/26/15 by Raimundo Romero

**Purpose**: To clean and disinfect the water baths during monthly maintenance

**Materials needed:**
Sponge
Lab Soap/detergent
Bacdown disinfectant, (Fisher cat. No. 04-355-13)
1:64 dilution (or 15.5 mls per 1000 mls of RO water)
RO water
Algicide

**Background**: As common use resources, the water baths have a high potential of contamination and the ability to ruin someone's experiment. It is imperative that the water baths are regularly cleaned and maintained appropriately. This means **NO USE of chlorine based cleaners** (such as bleach) to disinfect the water baths due to premature corrosion of the stainless steel. Also, the use of RO water is important as purer water (such as ultrapure water (defined as >18.2 MΩ*cm) will also cause premature corrosion as well.

**Procedure:**
1. Remove items inside all water baths.
2. Turn water bath off and safely empty all water baths.
    a. Locate the drain port (if water bath has one) or invert water bath over the sink to drain. Seek assistance if necessary.
3. Clean inside of water baths with lab soap and water. Rinse THOROUGHLY.
4. Disinfect water baths with Bacdown spray.
    a. Spray onto water bath. Let surface remain wet for 10 mins.
    b. Wipe and Rinse THOROUGHLY.
5. Refill water baths with RO water

| Protocol Revision History Date | Name | Changes |
|---|---|---|
| | | |
| 06/26/15 | Raimundo Romero | Wrote original protocol |

# Western Blot SOP

# Kipper Lab

Last updated 08/10/16 by Rai Romero

**Colorado State University**

**Purpose**: To run a Western blot using Nicole Ehrhart's Biorad Mini protean system

**Materials needed:**

For cell lysis
RIPA lysis buffer w/ protease inhibitors
Sonicator or sonicator wand

For Protein quantification
BCA Protein assay kit
Microplate reader
BSA standards (included in kit or make your own)

For electrophoresis
Protean Mini Gel electrophoresis unit
Protean mini gel transfer cassettes w/ sponges
Power supply
Gels
Electrophoresis Running buffer
Gel loading tips
Laemmlie Sample buffer (2x or 4x)
2-mercaptoethanol (β-ME)
Molecular weight ladder
Heat block

For wet tank transfer
Ponceau S staining solution
Empty pipet tip boxes
Razor blade
Forceps
Transfer buffer
Ice pack (that will fit in wet transfer set up)
Stir bars
Stir plate
Millipore Filter paper
PVDF membranes
100% methanol

For antibody incubation steps
Blocking buffer (Non-fat dry milk or BSA buffers)
5x TBS-T
1 x TBS-T
Primary antibodies
Secondary antibodies

For development of blots
Plastic sheet protectors
Chemiluminescence substrate solution
Chemiluminescence imager

**Procedure:**

***Cell lysis***

1. Rinse cells on allografts with PBS once before transferring to new well.
2. Adding RIPA buffer+protease inhibitors to samples. (usually add 200 ul to each well of a 48 well plate). Let sit for 5 mins on ice.
3. Pool cell lysates together (if seeing low protein expression). Pulse samples w/ sonicator wand for 2-3 secs.
4. Transfer cell lysates to 1.5 microcentrifuge tubes and spin down at 14k RPM (max speed) at 4 °C for 15 mins.
5. Proteins are located in the supernatant while cell debris should of spun down to bottom of microcentrifuge tube. Transfer supernatant to new microcentrifuge tube and proceed immediate to BCA assay for protein quantification or freeze down to -20 °C until ready to analyze.

***BCA protein assay***

1. Refer to Pierce BCA protein assay kit instructions to make BSA standards and follow assay instructions.
    a. Pipet sample (25 or 10 µl) into microplate well
    b. Add 200 µl of working reagent to each well and mix thoroughly.
    c. Cover plate and incubate at 37 °C for 30 mins.
    d. Cool plate to ET and measure absorbance at 562 nm on plate reader.
    e. Using standard ladder, quantitate protein concentration present in sample(s).

***Sample prep for loading into gels***

1. Calculate amount of protein to load into each lane (20 µg- 30 µg of total protein should be sufficient). Ensure gel lanes have sufficient volume to hold your sample!
2. Ensure MW ladder is thawed.
3. Ensure the following solutions are made up:

    a. Running buffer, 5X, 1 L
        i. 15 g Tris-base
        ii. 72 g glycine
        iii. 5 g SDS
        iv. 1 L DI H2O
    b. 2x or 4x Laemmli buffer (for protein denaturation)
4. Turn on heat block to 95 °C
5. Mix together the appropriate amount of cell lysate volume together with laemmli buffer and β-ME into microcentrifuge tube. Mix thoroughly.
6. Heat mixture on heat block at 95 °C for 5 mins to denature proteins.
7. Set up electrophoresis tank
    a. Open/prep gels and remove combs
    b. Clamp gels onto holder (short side facing inward) and insert into tank.
    c. Add running buffer to inner chamber first to check for leaks! IMPORTANT: If leaking, gel will not run!
    d. If no leaks, then fill outer electrophoresis tank w/ running buffer.
8. Load lanes of gels w/ samples, taking care not to cross-contaminate wells.
9. Attach tank cover and mate leads.
10. Run gels at 180 V (constant V) for ~45 mins (until dye front reaches near bottom of gel).
11. Turn off power supply and immediately proceed to transferring.

***Wet tank transfer***

1. Ensure sufficient transfer buffer is available.
    a. 1X Transfer buffer, 1 L
        i. 5.8 g Tris-base
        ii. 2.9 glycine
        iii. 900 ml DI H2O
        iv. 100 ml methanol
2. Remove gel from plastic casing and immerse in transfer buffer.
3. Equilibrate transfer sponge, filter paper, and gel in transfer buffer for 15 mins.
4. Prep PVDF membrane
    a. Cut PVDF membranes to same size as gels.
    b. Soak PVDF membrane with methanol for 10-20 secs, or until it changes from opaque white to uniform transluscent gray.
    c. Immerse PVDF membrane in DI H2O for 2 mins.
    d. Immerse in transfer buffer for 3 mins to equilibriate.
    e. IMPORTANT: DO NOT LET MEMBRANE DRY OUT! If it does, membrane must be re-wet.
5. Assemble transfer cassette.
    a. (-) Cathode electrode

b. Sponge
c. Filter paper
d. Gel
e. PVDF membrane
f. filter paper
g. sponge
h. (+) Anode electrode

6. Clamp transfer cassette and immerse in transfer buffer in transfer tank.
7. Add stir bar and gently stir transfer buffer.
8. Transfer conditions
9. Same day
    i. 4 °C
    ii. 100 V (voltage may need to be modified if connecting multiple transfer tanks to one power supply).
    iii. 1.5 hours
10. Overnight transfer
    i. 4 °C
    ii. 40 V (constant voltage)
    iii. Overnight (~5 pm to 9 am next day)
11. After transferring, remove membrane from transfer cassette and proceed to Ponceau S stain or immunoblotting. BE SURE TO NOTE THE SIDE OF THE MEMBRANE FACING THE GEL AND KEEP THIS SIDE FACING UP WHEN PLACING MEMBRANE INTO STAINING TRAY.

***Check successful protein transfer w/ Ponceau S stain (Adapted from Wallert and Provost Lab)***

1. Ponceau S stain can detect µg's of protein on PDVF and nitrocellulose membranes w/ a clear background and red bands.
2. Prep Ponceau S stain (0.1% (w/v) in 1% (v/v) acetic acid)
    a. 10 ml MilliQ water
    b. 0.3 ml glacial acetic acid
    c. 0.033 g Ponceau S
    d. Bring to a total of 30 ml w/ MilliQ water.
    e. Store at room temp.
3. After transfer of protein from gel to membrane, immerse membrane in a sufficient amount of Ponceau S stain for 5 mins on rocker plate. DO THIS BEFORE BLOCKING!
4. After staining, immerse membrane in sufficient 5% (v/v) acetic acid solution for 5 mins on rocker plate.
5. Remove acetic acid solution and replace with fresh 5% (v/v) acetic acid solution. Let sit for 5 mins on rocker plate.
6. Confirm proteins were transferred onto PVDF membranes by appearance of red bands.

7. Transfer membrane into water for 3 washes of 5 mins.
8. Remove membrane and block as normal.

***Immuno-blot/Immuno-stain protocol (Adapted from Brad Charles immune-blot protocol)***

1. Ensure sufficient solutions are available
    a. TBS-T (Tris buffered saline, Tween-20 0.05%), 1 L
        i. 800 ml DI H2O
        ii. 6.057 g Tris (50 mM )
        iii. 29.22 g NaCl
        iv. Adjust to pH 7.4 and add water to make 1 L
        v. Add 500 µl of Tween-20.
    b. Blocking buffer (100 ml)
        i. 5 g nonfat dry milk (NFDM)
        ii. 100 ml of TBS-T
        iii. Allow sufficient time to dissolve (takes about 1 hr).
2. With membrane in staining tray, add sufficient blocking buffer to cover membrane. Place onto rocker plate and block for 1 hour at RT.
    a. Many Blocking buffer buffers can be used. Common blocking buffers include 5% NFDM, 5% BSA, or a combination of both as well as commercial formulations. The best blocking buffer will be dependent on application as well as the antibodies used. Experiments should be conducted to optimize appropriate blocking buffer.
3. Pour off blocking buffer and rinse 3 times w/ TBS-T for 5 mins each. Replace TBS-T w/ each rinse step.
4. Make up primary (1°) antibody (Ab) solution using TBS-T or 0.5% NFDM in TBS-T as diluent. Use manufactuer's recommended dilution as a starting point but experimentally verify. Common dilutions range from 1:1000 to 1: 10,0000.
5. Incubate membrane w/ 1° Ab solution overnight at 4 °C or 1-2 hours at RT.
6. Pour off 1° Ab solution and rinse 3 times w/ TBS-T for 5 mins each. Replace TBS-T w/ each rinse step.
7. Make up secondary (2°) antibody (Ab) solution using TBS-T or 0.5% NFDM in TBS-T as diluent. Use manufactuer's recommended dilution as a starting point but experimentally verify. Common dilutions range from 1:10,0000 to 1:50,000.
8. Incubate for 1 hour at RT on rocker plate.
9. Pour off 2° Ab solution and rinse 3 times w/ TBS-T for 5 mins each. Replace TBS-T w/ each rinse step.
10. Proceed to imaging.

***Immuno-blot imaging (w/ specific instructions for Dr. Dawn Duval's Chemidoc XRS+ instrument)***

1. Assuming chemiluminescence based detection, make up substrate working solution.
2. Coat membrane w/ substrate solution and sandwich between plastic sheet protector to ensure uniform coating of membrane solution with substrate solution. (used ~400 µl of substrate solution for xx $cm^2$ of membrane.
3. Blot away excess substrate solution.
4. Turn on Chemidoc camera (black box on top of computer)
5. Open image tab software → new or open protocol
6. Application → Select → blots → colormetric
7. Hit run protocol
8. Allow time for camera to warm
9. Once warm, hit cancel
10. Use colormetric protocol:
    a. Bring membrane into focus
    b. Snap photo of MW ladder(s) and ensure correct membrane position.
11. Application → select → blot → chemi
12. Ensure no filter is on camera (top of imaging unit)
13. Setup protocol for image exposer
    a. Signal accumulation mode click setup
    b. First image time (sec): 5
    c. Last image time (sec): 300
    d. Total # of images: 100
14. Run protocol "chemi"
15. Merge MW and chemi pics.
16. Remove membrane from Chemidoc and shut down instrument.

***Stripping and re-probing of membrane***

1. Rinse off chemiluminescence substrate solution w/ 3 rinses of TBS-T. 5 mins each rinse.
2. Immerse membrane into stripping buffer (I used Thermo Restore WB stripping buffer) for 20 mins at RT.
3. Confirm no residual HRP activity is present by reimaging membrane w/ substrate solution.
4. Block membrane using sufficient blocking buffer.
5. After confirming HRP deactivation, re-probe membrane with 1° Ab and 2° Ab solutions following the steps from the immunoblotting section and reimage membrane. Repeat as necessary.

| Version | Date | By | Notes |
|---|---|---|---|
| 1.0 | 04/21/14 | Rai Romero | Original protocol |

# XPS Use SOP Kipper Lab

Last updated 01/06/15 by Rai Romero

**Purpose**: To safely and correctly use the XPS located in the CIF in CSU's chemistry dept.

**Materials needed:**

XPS
Sample
Conducting adhesive tape

**Procedure:**

1. Ensure samples are dry. Beware of surface contamination w/ gloves, forceps etc.
2. Mount non conducting samples w/ conductive double sided tape (Carbon or copper tape is fine)
3. Ensure to remember & record sample treatments when attaching to sample holder
4. On Auto valve control console, press "Backfill intro" to break vacuum of sample introduction chamber
5. Insert sample holder w/ special U shaped clamp
6. Cover and press "Pump intro" on auto valve control console to pump down sample introduction chamber
7. nderneath and to the right of the XPS computer workstation, press on button for $H_2O$ pump
8. Wait until vacuum reaches 2.9 E-8 torr
9. Turn on light in test chamber
10. Press "intro sample" on auto valve control console
11. Ensure stage controls (x,y,z, rotation dials) are aligned properly (black marks on dial) and that stage holder in test chamber is rotated properly so that small wall of stage holder points toward sample and the insertion rod

12. LOWLY proceed to insert samples holder into test chamber. Ensure to take note of positions of brass clips and DO NOT BENT THEM!!!

13. Turn on monitor and align sample w/ gun. Once sample is aligned, zoom in w/ camera all the way.

14. Create a new directory. (Sample setup > Dir) Box that is highlighted will have new folder created in it.

15. Go to sample set up. Enter file name

16. Go to ESCA/ISS menu > setup align

17. Check that C1s peak is visible and at 285 eV

18. Turn on ion gun or neutralizer if C1s is not at 285 eV to neutralize charging

19. Acquire setup > setup survey

20. Enter 0 eV for lower limit, range 1200 eV

21. Under resolution, click surv.

22. Ensure x ray anode is Al monochromated 7 mm filament or leave on default

23. Acquisition time 5 min

24. Hit acquire

25. Use Multipack software to observe survey spectra. By clicking Acq in multipack, the last acquired spectrum will be presented. Peak identification along with mass percents can be extracted. Save survey spectrum

26. Back In XPS software, go to Acquire setup > setup multi (this is for a multiplex acquisition i.e. to collect multiple HRES spectra)

27. Click add region and add appropriate peaks; Set up high resolution (HRES)
    a. Sweeps: 4
    b. Peak/noise ratio (if present): ~250
    c. Multipak's HRES notation is odd. S1 peak refers to S2p peak, N1 for N1s etc.

28. Click on "Next Menu" and set acquisition time.

29. Click acquire

30. Let the acquisition run. Acquire HRES spectra in Multipak and save.

31. Save using File> Save current file as  option. (NOT save current spectrum as; this only saves usually O1s envelope and will NOT save the other envelopes)

32. Once done with XPS analysis, align XPS stage in order to retract sample stage. Ensure the small wall of stage holder is facing towards the retractor.

33. Open test chamber valve by pressing intro sample button on auto valve control console

34. CAREFULLY and SLOWLY insert rectractor to remove sample stage. Once sample stage is on retractor lower the z-control of stage holder.

35. Slowly pull out rectractor until test chamber valve closes. Remove sample stage with U clamp. Remove samples and clean stage.

REFERENCES


1. de Britto D, Assis OBG. A novel method for obtaining a quaternary salt of chitosan. Carbohydrate Polymers 2007;69(2):305-310.
2. Sieval AB, Thanou, M., Kotze, A.F., Verhoef, J.C., Brussee, J., Junginger, H.E. Preparation and NMR characterization of highly substituted N-trimethyl chitosan chloride. Carbohydrate Polymers 1998;36(2–3):157–165.
3. de Britto D, Celi Goy R, Campana Filho SP, Assis OBG. Quaternary Salts of Chitosan: History, Antimicrobial Features, and Prospects. International Journal of Carbohydrate Chemistry 2011;2011:12.
4. Gottlieb HE, Kotlyar V, Nudelman A. NMR Chemical Shifts of Common Laboratory Solvents as Trace Impurities. Journal of Organic Chemistry 1997;62(21):7512-7515.
5. Curti E, Campana-Filho SP. Viscosity Behavior of Chitosan and N,N,N-Trimethylchitosan Chloride Salts in Acid-Free Aqueous Solution. Journal of Macromolecular Science, Part A: Pure and Applied Chemistry, Vol. 43, No. 3, 2006: pp. 555–572 2006;43(3):555-572.
6. Hellemans J, Mortier G, De Paepe A, Speleman F, Vandesompele J. qBase relative quantification framework and software for management and automated analysis of real-time quantitative PCR data. Genome Biology 2007;8(2).

CIRRICULUM VITAE

# Raimundo Romero

raromero@engr.colostate.edu

## Education

Ph.D. Candidate, Bioengineering — Expected December 2017
*Colorado State University*

B.S. in Chemistry, Cum laude — June 2011
*Pacific Union College*

## Research Experience

**Ph.D. Thesis** — Aug. 2011–Present

*School of Biomedical Engineering, Colorado State* University

**Thesis Title:** Engineering a Biomimetic Periosteum on Cortical Bone Allografts for the Reconstruction of Critical-Sized Bone Defects in Mice

## Research Collaborations

Dr. Nicole P. Ehrhart and Dr. Ruth Rose, *Colorado State University*
Clinical collaborators on Ph.D. research project.

Dr. Salman Khetani and Christine Lee, *University of Illinois at Chicago*
Used glycosaminoglycan and chitosan polyelectrolyte multilayers to deliver TGF-β to hepatocytes in a co-culture model.

Dr. Ketul Popat and Dr. Melissa Reynolds, *Colorado State University*
Used nitric oxide releasing polyelectrolyte multilayers coated on titanium nanotubes to characterize human platelet response.

## Awards & Honors

| | |
|---|---|
| 2016 | **Outstanding Graduate Student Award**, *School of Biomedical Engineering, Colorado State University.* |
| 2015 | **Student Travel Achievement Recognition Award, Honorable Mention,** *Society for Biomaterials* |
| 2011 | **American Institute of Chemists Student Award,** in recognition of demonstrated ability, leadership, and professional promise. *Pacific Union College.* |
| 2011, 2009 | **Biology Department Employee of the Year Award,** *Pacific Union College*. |
| 2010 | **Hispanic Scholarship Fund General Scholarship,** in recognition of academic achievement. *Hispanic Scholarship Fund* |
| 2009 | **Peter E. Hare Chemistry Scholarship,** in recognition of academic achievement. *Pacific Union College*. |

**Areas of Expertise: (detailed on pg. 4)**

1. Materials engineering, characterization, & analysis
2. Mammalian cell culture
3. Natural polymers processing and chemical synthesis
4. Molecular biology techniques and assays (ELISA, Western Blotting, qPCR)
5. Small animal (mice) handling/techniques

**Thesis Experience Highlights:**

- 2 first author and 1 co-first author publications,
- Increased project budget by 13.3% with grant idea, development, and application
- Co-inventor on 2 patent applications, 1 patent awarded
- Honorable Mention, Student Travel Achievement Recognition Award, SFB Annual Meeting 2015

**Funding**

2015 **School of Biomedical Engineering Travel Grant $500**
*School of Biomedical Engineering, Colorado State University*

2014 **Bioscience Discovery Evaluation Grant Program $40,000 "**Co-culture of Endothelial and Mesenchymal Cells to Vascularize Bone Allografts"
***Assisted in grant idea generation and writing***
*Colorado State University Ventures and the State of Colorado*

2013 **Shrake-Culler Scholarship $2500,** Awarded for demonstrating a passion for higher education, an outstanding work ethic, and a successful academic record.
*Colorado State University.*

2011 **Alliances for Graduate Education and the Professoriate (AGEP) Fellowship**. One year fellowship covering tuition and salary.
*Colorado State University*

**Research Interests**

Stem Cell-biomaterial interactions
Engineered stem cell microenvironments
Polysaccharide biomaterials
Non-invasive imaging techniques
Stem cells for Bone Tissue engineering
Learning Analytics

**Professional Society Memberships**

Biomedical Engineering Society
Society for Biomaterials
SPIE
Society for Learning Analytics Research

**Patents and Pending Patent Applications**

1. International Patent WO 2014/169281 A1. M.J. Kipper., K.C. Popat, M.M. Reynolds, V. Leszczak, **R. Romero**.
2. U.S. Patent Application 2015/0086602 A1 M.J.Kipper, N.P. Ehrhart, **R. Romero**, T. Gonzalez.

**Publications**

1. Lin, C., **Romero, R.**, Sorokina, L.V., Ballinger, K.R., Place, L.W., Kipper, M.J. Khetani, S.R. "A Polyelectrolyte Multilayer Platform for Investigating Growth Factor Delivery Modes in Human Liver Cultures". 2017. *Accepted.*
2. Walker, R.S.*, **Romero, R.***, Staver, J.M.*, Zang, Y., Reynolds, M.M., Popat, K.C., Kipper, M.J. "Glycocalyx-Inspired, Nitric Oxide-Releasing Surfaces Reduce Platelet Adhesion and Activation on Titanium". *ACS Biomaterials Science and Engineering.* 2017. *3*(1). 68-77. ***These authors contributed equally to this work.**
3. **Romero, R.**, Travers, J.K., Asbury, E., Pennybaker, A., Chubb, L., Rose, R., Ehrhart, N.P., Kipper, M.J. "Combined delivery of FGF–2, TGF–β1, and adipose-derived stem cells from an engineered periosteum to a critical-sized mouse femur defect ". *J Biomed Mater Res Part A*. 2017. (105A). 900-911.
4. **Romero, R.**, Chubb, L., Travers, J.K., Gonzalez, T., Ehrhart, N.P., Kipper, M.J. "Coating Cortical Bone Allografts with Periosteum-Mimetic Scaffolds made of Chitosan, Trimethyl Chitosan and Heparin" *Carbohydrate Polymers.* 2015. (122). 144-151.

## Conference Presentations

1. **Romero, R.**, Chubb, L.S., Travers, J.K., Rose, R., Pennybaker, A., Asbury, E., Ehrhart, N.P., Kipper, M.J. "Assessing an Engineered Periosteum in Reconstructing a Critical-Sized Femur Defect in Mice". Biomedical Engineering Society Annual Meeting 2015. Tampa,FL. Oct. 9, 2015. Poster presentation.
2. **Romero, R.**, Chubb, L.S., Travers, J.K., Rose, R., Pennybaker, A., Asbury, E., Ehrhart, N.P., Kipper, M.J. "Bridging the Gap: Assessing an Engineered Biomimetic Periosteum on Bone Allografts for the Reconstruction of Large Segmental Bone Defects in Mice". Society for Biomaterials 2015 Annual Meeting. Charlotte, NC. April 16, 2015. **Oral presentation.**
3. **Romero, R.**, Chubb, L.S., Asbury, E., Pennybaker, A., Travers, J.K., Ehrhart, N.P., Kipper, M.J. "Assessing the Osteoinductivity of Engineered Biomimetic Periosteum on Cortical Bone Allografts". Biomedical Engineering Society Annual Meeting 2014. San Antonio, TX. Oct. 24, 2014. Poster presentation.
4. **Romero, R.**, Menard, Z., Chubb, L.S., Ehrhart, N.P., Kipper, M.J. "Engineering a Biomimetic Periosteum for Cortical Bone Allografts: Incorporation of Heparin-Binding Growth Factors into Chitosan-Based Tissue Engineering Scaffolds". Society for Biomaterials Annual Meeting 2014. Denver, CO. April 16, 2014. Poster presentation.
5. **Romero, R.,** Chubb, L.S., Ehrhart, N.P., and Kipper, M.J. "Smart Cortical Bone Allografts for Critical-Sized Defects: Engineering a Biomimetic Periosteum". Biomedical Engineering Society Annual Meeting 2013. Seattle, WA. Sept. 27, 2013. Poster presentation.
6. **Romero, R.**, Ehrhart, N.P., Kipper, M.J. "Surface Modified Chitosan Tissue Engineering Scaffolds for a Biomimetic Periosteum on Cortical Bone Allografts". Society for Biomaterials 2013 Annual Meeting. Boston, MA. April 11, 2013. Poster presentation.

## Invited Talks

1. "Revitalizing Bone: Co-delivery of growth factors and stem cells via an engineered periosteum". Pacific Union College, Department of Chemistry, Angwin, CA. May 19, 2016.
2. "Engineering a Biomimetic Periosteum: An Interdisciplinary Project". Pacific Union College, Department of Chemistry, Angwin, CA. May 22, 2014.

## Research Techniques

***Material Characterization/Analysis***

- SEM
- XPS
- FTIR (transmission, ATR)
- $^{1}$H NMR
- AFM
- Spinning spindle viscometry

***Polymer fabrication and synthesis***

- Electrospinning
- Layer-by-layer deposition
- Surface chemistry modifications
- Methylation of chitosan

***Image based acquisition***

- Epi & inverted fluorescence microscopy
- Light microscopy
- Bioluminesence imaging (IVIS-100)
- Micro-CT
- Radiography (mice)

***Mammalian Cell Culture***

- Mammalian cell maintenance & expansion
- Adipose-derived stem cell isolation
- HUVEC cell culture

***Molecular Biology***

- ELISA
- Western Blotting
- qPCR

***Animal Handling and techniques***

- Small animal handling and care
- Inhaled anesthetic delivery
- SQ, dermal, IP injections
- Bone & adipose tissue harvest

***Histology***

- Tissue prep for paraffin embedding
- H&E staining analysis

**Service**

College of Engineering Curriculum Committee Graduate Student Member (FA 2016, FA/SP 2017)

Colorado State University Scott Building Safety Inspection Member (FA 2014 & 2015)

CSU School of Biomedical Engineering Student Panel (SP 2012, SP 2015, SP 2016, FA 2016)

**Research Supervision**

**Undergraduates:**

John K. Travers, Emilie Asbury, Atherly Pennybaker Chemical and Biological Engineering

Joseph Staver, Chemistry

**Teaching Experience**

**Co-Instructor** (CBE160, Intro to MATLAB for Chemical and Biological Engineers)
*Colorado State University,* Fall 2016, Spring 2017
**Accomplishments:**

- Independently instructed 4 course sections totaling ≥ 70 students.
- Prepared weekly lectures, quizzes, and assignments to highlight concepts in learning MATLAB
- Obtained Graduate Teaching Certificate and created a teaching portfolio (expected Dec. 2017)

**Teaching Experience, continued**

**Graduate Teaching Assistant** (CHEM 108, Fundamentals of Chemistry Laboratory)
*Colorado State University,* Spring 2015
**Accomplishments:**

- Instructed 3 laboratory sections comprised of 68 students
- Conducted mid-semester poll to elicit student feedback and adjusted lab policies accordingly
- Prepared weekly pre-lab lectures to highlight theory of laboratory exercise, explain lab procedures, and demonstrate proper use of laboratory equipment.

**Responsibilities:**

- Supervised students to perform laboratory experiments in a timely and safe manner
- Assisted students in learning difficult concepts in lab and at weekly office hours
- Used a learning management system (Canvas) to post announcements and grades for students

**Head Teaching Assistant** (CHEM 111,112,113, General Chemistry).
*Pacific Union College,* 2008-2011
**Accomplishments:**

- Promoted twice in 2 years
- Ensured weekly lab preparations for 136 students were done to efficiently run labs

**Responsibilities:**

- Managed a team of 8 teaching assistants on a weekly basis
- Wrote weekly lab quizzes
- Supervised 7 lab sections consisting of a total 160 students
- Grading and grade input into course management software (Blackboard).

**Head Teaching Assistant for Introductory Chemistry** (CHEM 101).
*Pacific Union College,* Summer 2011
**Responsibilities:**

- Supervised 1 lab section consisting of a total 20 students in a safe and timely manner
- Grading and grade input into course management software (Blackboard).

**Outreach**

**Biomedical Engineering Track Instructor**.
*Northrop Grunman STEM Summer Camp*, July 18-22, 2016

- Introduced biomedical engineering concepts to 13 middle and high school students
- Mentored campers by discussing various biomedical engineering areas.
- Developed curriculum to emphasize engineering problem solving in a biomedical context.

**Teaching Assistant for Honors Science Camp**.
*Leoni Meadows Christian Summer Camp (Grizzly Flats, CA*), June 2010, 2011

- Designed, organized, and implemented a one-week (15 hours) of introductory chemistry lab curriculum appropriate for junior and senior high school students.
- Ensured age-appropriate activities and proper safety protocols were followed.
- Mentored campers by discussing various pre-professional career tracks.
- Assisted with introductory biology lab activities.